ION TRANSPORT AND CHARGE COMPENSATION IN CONDUCTING POLYMERS

ABDULRAHMAN ALBETAR

Ion Transport and Charge Compensation in Conducting Polymers

By

Abdulrahman Albetar

A thesis submitted to the School of Graduate Studies
in partial fulfilment of the requirements
for the degree of Doctor of Philosophy

Department of Chemistry

Memorial University of Newfoundland

St. John's, Newfoundland, Canada A1B 3X7

July 2012

بِسْمِ اللَّهِ الرَّحْمَٰنِ الرَّحِيمِ

In the name of God, the most gracious, the most merciful

Praise be to God, the Cherisher and Sustainer of the worlds

Abstract

Ion Transport and Charge Compensation in Conducting Polymers

The ion transport properties and the accompanied charge compensation mechanisms of electrochemically prepared conducting polymers have been investigated by cyclic voltammetry and impedance spectroscopy. The conducting polymers considered in this work are polypyrrole and polyfluorenone in which p-doping and n-doping were probed, respectively, in various electrolyte solutions. Both polymers were prepared by anodic coupling polymerization using various techniques: potentiodynamic, potentiostatic, and galvanostatic. Chemical modifications of the two polymers have been achieved under optimized conditions to obtain high quality, stability, and interesting electrochemical properties, such as charge capacity and electroactivity, of the deposited films. These modifications can facilitate the understanding of ion transport in conducting polymers in order to enhance their use in many potential applications, such as batteries, fuel cells, flexible displays, and other electrochemical devices. The surface morphology and elemental analysis for the polymer films were characterized by scanning electron microscopy and energy dispersive X-ray emission, respectively.

The rate and mode of ion transport in conducting polymers have been controlled using dopant anions of various sizes and charges during film deposition. Cyclic

voltammetry and impedance spectroscopy have been used to probe the mode of ion transport (anion or cation transport) using scan rate dependence and potential dependence, respectively. An enhanced anion transport rate was achieved using large univalent dopant anions, while an enhanced cation transport rate was achieved using a polyanion electrolyte during film deposition. Polypyrrole film modifications have been achieved chemically using various additives during film deposition and electrochemically by overoxidation at mild potentials before film degradation. Deactivation and reactivation of the polyfluorenone films were investigated by cyclic voltammetry in which deactivation was achieved for modified and unmodified films by continuous cycling during n-doping. However, reactivation of a deactivated film was only achieved following modification with a steric stabilizer, polyethylene glycol, by polarizing the film at positive potentials.

Acknowledgements

I would like to express gratitude to my supervisor Dr. Peter Pickup for his guidance, encouragement, and patience throughout my degree. I really appreciate his discipline, leadership, and boundless knowledge. I would like also to thank my supervisory committee members Dr. Raymond Poirier and Dr. Yuming Zhao for their assistance and guidance.

I would like to thank the Center for Chemical Analysis, Research and Training (C-CART) at Memorial University for facilitating the use of instrumentation. Special thanks to Mr. Michael Shaffer for the SEM measurements.

I would never forget the support from my parents and the help from my wife to finish my degree. My wife did a lot to raise the kids in my absence. The hope from the two beautiful flowers (Ammar and Juna) is highly recognisable.

Financial support from King Fahd University of Petroleum and Minerals, Chemistry Department at Memorial University, and NSERC are gratefully acknowledged.

Contents

List of Figures

List of Tables

Glossary

Symbol	Meaning
A	electrode area (cm^2)
A^-	anion
AAS	atomic absorption spectroscopy
ARS	Alizarin Red S
BFEE	boron trifluoride ethyl etherate
C^+	cation
CE	counter electrode
C_L	layer capacitance
C_{lf}	low-frequency capacitance
C_{lim}	limiting capacitance
C_s	series capacitance
CV	cyclic voltammogram
d	film thickness
E	potential (V)
e^-	electron
EDX	energy dispersive X-ray
EIS	electrochemical impedance spectroscopy
E_{pa}	anodic peak potential
E_{pc}	cathodic peak potential
f	frequency in hertz
F	Faraday constant (96,485 C mol^{-1})
FcOH	1-(Ferrocenyl)ethanol
FO	fluoreno-9-one
GCE	glassy carbon electrode
GS	galvanostatic
i_{pa}	anodic peak current (A)
i_{pc}	cathodic peak current (A)

ITO	indium tin oxide
m	mass (g)
M	molar mass
n	number of electron
NaPSS	poly(sodium 4-styrenesulfonate)
n_{pol}	number of electron consumed during polymerization
OP	overoxidation peak
PD	potentiodynamic
PEG	polyethylene glycol
PFO	polyfluorenone
PPy	polypyrrole
PPy-Fc	ferrocene-doped polypyrrole
PS	potentiostatic
Py	pyrrole
Q_{cv}	charge under cyclic voltammogram (C)
Q_{pol}	polymerization charge (C)
R_{CT}	charge transfer resistance (ohm)
R_e	electronic resistance (ohm)
RE	reference electrode
R_i	ionic resistance (ohm)
R_s	solution resistance (ohm)
SCE	saturated calomel electrode
SEM	scanning electron microscopy
TEAP	tetraethylammonium perchlorate
WE	working electrode
Z_{im}	imaginary impedance (ohm)
Z_{re}	real impedance (ohm)
ν	scan rate ($V\ s^{-1}$)
σ_{ion}	ionic conductivity ($S\ cm^{-1}$)
ω	angular frequency in radians per second

Chapter 1

Introduction

1.1 Background

1.1.1 Organic semiconductors

The concept that organic molecules can conduct electricity under certain conditions led scientists to think about exploiting their properties in many potential applications. Intrinsic semiconductivity of organic molecules can be observed in highly conjugated single molecules as well as in short and long conjugated polymer chains (1). Polycyclic aromatic compounds, such as pentacene, anthracene, and rubrene are single molecules with natural semiconductivity. Polyacetylene and its derivatives, however, are conjugated chains with semiconducting properties. Both of these types of molecules show interesting properties and can be used for optoelectronics devices, such as organic light-emitting diodes (OLEDs), organic field-effect transistors (OFETs), and other display devices (2; 3; 4).

The electronic conductivity of organic molecules resembles that of inorganic semiconductors where doping is required to generate higher conductivity; the concept of doping is significantly different in each type though. Like inorganic semiconductors,

the intrinsic conductivity of organic molecules lies in magnitude between conductors and insulators at about 10^{-9} S cm^{-1}, which can be improved by doping to reach values as high as 10^{5} S cm^{-1}, approaching that of copper (ca. 10^{6} S cm^{-1}). In contrast to conductors, current in semiconductors can be carried either by electrons or holes. These two modes of conduction arise from the doping process, where the former results from doping with electrons or negative charges (so-called n-doping) and the latter is due to doping with holes or positive charges (so-called p-doping) (5; 6).

Organic semiconductors can be divided in general into two main groups: charge-transfer complexes, and conjugated polymers (7). Charge-transfer complexes exist when a charge is partially transferred from an electron donor molecule to an electron acceptor molecule or between two parts of a large molecule to form electron donor-electron acceptor complexes. This type of complex exhibits interesting optical and electrical properties due to overlap between molecular orbitals. On the other hand, conjugated polymers, which have a backbone of alternating single and double bonds, can show high conductivity and interesting optical properties due to *delocalised π-electrons* throughout the conjugated system. This type of molecule can combine the properties of inorganic compounds like electrical conductivity and the properties of organic compounds, such as processibility, and flexibility. There are, however, still some deficiencies such as stability that need to be improved (8; 9). As a background for this thesis, the next sections focus on conducting polymers CPs (or more precisely called intrinsic conducting polymers ICPs), which are conjugated polymers in origin.

1.1.2 Conducting polymers

Intrinsically conducting polymers have a long history. In 1862, polyaniline (PAn) was electrochemically synthesised by the anodic oxidation of aniline in a dilute sulphuric acid solution. The product of the electrochemical synthesis was a blue-black powder that was insoluble in many solvents (10). Later on, in 1977, polyacetylene (PA) was discovered to be a conductor when doped with iodine (11). This discovery was considered to be the birth of conducting polymers due to the breakthrough in electric conductivity.

Although polyacetylene (11) and polysulfurnitride (7) were the first reported conducting polymers, the instability of the former and the explosive nature of the latter limit their popularity. Since then, many polymers have been investigated for potential applications as electronic conductors, including polypyrrole (PPy) (12), polythiophene (PTh) (13), polyaniline (PAn) (14), polyparaphenylene (PPP) (7), and their derivatives (15). Today, due to the variety of relevant applications, the field of conducting polymers is one of the most active areas of research in materials sciences (7; 14; 16; 17). However, due to the complexity inherent to the nature of conducting polymers, much has to be done in order to improve the physical properties of conducting polymers, which are of great interest to materials engineering.

1.2 Electrochemistry of conducting polymers

The electrochemistry of conducting polymers is a central part for many syntheses, characterizations, and applications of materials used in electrochemical devices. Understanding the electrochemistry of conducting polymers helps to overcome the kinetic limitations and thermodynamic restrictions inherent to the nature of conducting polymers.

The complexity in electrochemistry of conducting polymers resulted primarily from the various processes that occur while doping and undoping, such as conductivity changes with potentials, multiple redox potentials result in broad redox waves, and ion-exchange properties. Secondly, conducting polymers can also have localized redox centers, metallic or organic, which influence the main redox wave of the polymer, and so a large potential dependence is expected. Thirdly, the synthetic parameters significantly affect the electrochemical behaviour. Thus, characterization of conducting polymers is a key step toward improving their performance for future devices. One step toward approaching this aim is to have the polymers coated onto electrode surfaces, so-called polymer-coated electrodes, which are suitable for electrochemical characterizations.

1.2.1 Polymer-coated electrodes

Polymer-coated electrodes have been the subject of extensive research over the last few decades due to their suitability for electrochemical characterizations and applications (18). The first polymer-coated electrode was reported in 1979 where superior electrochemical behaviour with good stability was observed for a polypyrrole-

platinum coated electrode (19). This finding opened the door for research to study conducting polymers at interfaces which revealed the complex nature of the electrochemistry involved. Furthermore, many enhancements for electrochemical devices can be achieved when metal, carbon, or inorganic electrodes are coated with organic polymers.

There are several techniques used to produce polymer-coated electrodes. The simplest way is to cast a polymer solution into an electrode surface or dip the electrode surface into the polymer solution (20). Other techniques such as metastable polymerization (21), and electropolymerization (22) start with monomer species which are polymerized at the electrode surface under certain conditions, such as solvent evaporation or at deposition potential. Photopolymerization is also used to coat electrode surfaces under UV light irradiation (23). More recently, *in situ* photopolymerization has been used to produce polypyrrole within mesoporous TiO_2 surface (24).

1.2.2 Electropolymerization and deposition of conducting polymers

1.2.2.1 The concept

Electropolymerization of an electroactive monomer can be done in two distinct ways; anodic electropolymerization known as oxidative coupling, and cathodic electropolymerization known as reductive coupling. Oxidative coupling is the most widely used way to produce conducting polymers, where oxidation of the monomer is followed by coupling steps until the polymer deposits onto the electrode surface (7).

Polymers produced in this way are in their oxidized state, and so anions from the electrolyte solution are incorporated as counterions to maintain electroneutrality. Thus, polymer formation and its oxidation (i.e. doping) take place at the same time (17). Many conducting polymers are prepared in this way including: polypyrroles, polythiophenes, and polyanilines.

Producing conducting polymers by reductive coupling is much less common. The first reductive electropolymerization was performed with 2,5-dichlorobenzonitrile where the electron withdrawing cyano group stabilizes the negative charge on the aromatic ring (25). A famous group of polymers produced under reductive conditions are poly(*p*-phenylenevinylenes) (PPVs) via the poly(*p*-xylylenes) (PPXs) (26; 27). However, the mechanism of electrochemical polymerization by reductive coupling is still not fully understood. Presumably, producing radical anions is the first step which initiates a chain propagation step (25). To maintain electroneutrality of the polymer film, two anions, e.g. Br^-, are removed per monomer unit, instead of cation insertion. The process continues as such until the polymer is deposited onto the electrode surface. Catalytic currents can be observed by using cathodic mediators (e.g. anthracene) which are used to reduce the reduction potential. The radical anion of the mediator, which has a lower reduction potential, is first produced and then it reacts with the monomer of the substrate to produce a radical anion of the substrate plus the original mediator (28).

1.2.2.2 Mechanism of anodic electropolymerization

To date, the exact details of electropolymerization mechanisms are still somewhat controversial (29; 30; 31). Diaz was the first to propose an $E(CCE)_n$ mechanism for the electrochemical formation of conducting polymers (32). According to Diaz's mechanism, monomers are oxidized at the electrode surface; oxidized monomers dimerize to form dication dimers, which are deprotonated to form neutral dimers; neutral dimers are then oxidized and coupled with radical cation monomers to form trimers and so on. As such, the growth will continue as an electrochemically driven chain propagation process. In general, Diaz's mechanism includes four steps; the first step is electrochemical followed by two chemical steps; the last step is electrochemical oxidation of the dimers which takes place more easily than the monomer due to their longer conjugation lengths (17).

There are three main concerns with Diaz's mechanism. First, the rate constant for coupling between radical cations of the monomer is much higher than that between the monomer and oligomers (33; 34). Second, the deprotonation step becomes insignificant for longer chain length due to resonance stabilization of the conjugated system (29; 35). Third, there was an early concern about radical cation-radical cation (RR) coupling being not favourable due to strong Columbic repulsion. According to the findings in reference (36), equally charged small molecules are able to dimerize at diffusion-controlled rates, and so the concept of RR coupling is now well accepted (30). Despite the first two concerns, Diaz's mechanism is widely accepted with some

modifications (37; 38). First, as the chain length increases, the coupling between charged oligomers and monomer radical cations decreases. However, coupling of oligomers with each other will also take place in addition to the normal chain propagation (39). Second, deprotonation can be enhanced by addition of a base, such as water. According to the findings in references (40; 41), addition of 1% water to an acetonitrile polymerization solution will enhance the rate of polymerization and improve the adherence and the morphology of the polymer film, which is the so-called water effect. Medium size oligomers will not grow by coupling with monomers or dimers except in the presence of proton acceptor, i.e. base.

Electropolymerization of CPs can be achieved according to the modified mechanism as follows (17; 20): first, oxidation and coupling of monomers; second, nucleation and growth within the diffusion layer; and last, solid state formation by cross polymerization at the electrode surface. As such, nucleation is a key step for electropolymerization, which is the focus of the next subsection.

1.2.2.3 Origin of the nucleation process

Like metal electrodeposition onto a foreign substance, an overpotential is required to start electropolymerization onto electrode surfaces, which is indicated by a nucleation loop in cyclic voltammetry. As a result, understanding of nucleation conditions is a key step to grow conducting polymer films electrochemically. However, the origin of the nucleation process for conducting polymers is not fully understood.

A nucleation loop usually appears in the first cycle as an increased current in the reverse scan resembling metal electrodeposition. However, metal electrodeposition is different from electropolymerization in that the former has only one redox step, while the latter has multiple redox steps for each bond formation which is indicated by the current rising with each new cycle. As a result, the comparison between these two processes is not suitable (17).

Nucleation during electropolymerization was first described by Pletcher (42; 43). It has been characterized as redox catalysis or autocatalysis which induces monomer oxidation (44). There are two kinds of nucleation; instantaneous where the number of nuclei is constant, and progressive where nuclei are generated continuously. The layer growth can be in three different ways; one dimensional (1D) where nuclei grow in one direction, two dimensional (2D) where nuclei grow preferably parallel to the electrode surface in two directions, and three dimensional (3D) where nuclei grow in three directions with no preference (17; 45; 46; 47).

In contrast, a new analysis indicates the existence of two different effects that can be confused with nucleation; trace-crossing effects where the current is maximum before the switching potential, and loop effects where the current is maximum after the switching potential. Neither is necessarily a result of nucleation processes but can be due to a homogenous *comproportionation* reaction in which charged oligomers react with neutral monomers. This possible origin of the so-called nucleation loop makes better sense because the loop or the crossing which normally appears in the first cycle

can also appear in subsequent cycles during electropolymerization as reported in reference (48).

1.2.2.4 Stoichiometry of electropolymerization

Since the coupling steps for conducting polymers result from activation of two species, the polymer formation process needs two electrons per molecule (2 F for one mole) plus the charge for partial oxidation of the polymer (ca. 0.3 F). Thus, the electrochemical stoichiometry per reacting monomer is 2.07 to 2.6 F. The stoichiometric equation therefore for the electropolymerization process of a monomer (HMH) is (17);

$$n\,(HMH) \rightarrow H(M)_nH^{(nx)+} + (2n-2)\,H^+ + (2n-2+nx)\,e^- \qquad [1.1]$$

Where **n** is the number of repeating units, and **x** is the doping level of the polymer. As such, **(2n-2)** electrons are used for the polymer formation process (only one electron from each end). The same number of protons is removed. In addition, **nx** electrons are used for partial oxidation, and so the final polymer chains have a positive oxidation state of **nx** which is compensated by counterions from the electrolyte solution. Generally, **x** has values of 0.25 to 0.4, which means every third to fourth unit needs one counterion charge to maintain electroneutrality.

The doping level of the polymer (degree of oxidation or average number of holes per monomer unit) is a function of potential, i.e. x(E). Doping levels can be affected by synthesis parameters, such as the applied charging potential, solvent, and supporting electrolyte. They can vary significantly from much lower than the typical value of 0.33 to as high as 1, where every unit bears a positive charge after doping. Such high doping

levels require high electrode potentials to overcome the Columbic repulsive forces. A doping level of 1 can be only achieved for a very high stable system, such as poly(4,4`-dimethoxybithiophene) (17). The doping level can be estimated from the charge under the anodic wave for p-doping, $Q_{ox}(E)$, integrated to the set potential **(E)** (20);

$$\mathbf{x(E)} = \frac{\mathbf{Q_{ox}(E)}}{\mathbf{n_{monomer}\, F}} \qquad \textbf{[1.2]}$$

Where $n_{monomer}$ is the moles of monomer units in the film, which can be estimated from the mass of the film and can be used to estimate the film thickness ***d*** (20);

$$d = \frac{n_{monomer}\, M}{\rho\, A} \qquad \textbf{[1.3]}$$

Where ***M*** is the molar mass of the monomer unit, ρ is the density of the undoped film, and ***A*** is the electrode area.

1.2.2.5 Electropolymerization techniques

Various electropolymerization techniques can be employed to control the structure and morphology of the deposited film. Varying the counterion in the electrolyte solution and changing the electrochemical conditions such as formation potential or current, result in significant alteration of the deposited film (49; 50; 51; 52; 53). In general, polymer films can be deposited electrochemically onto an electrode surface by three different techniques; potentiostatic (at constant potential), potentiodynamic (potential scanning), or galvanostatic (at constant current). These techniques are also known as chronoamperometry, cyclic voltammetry, and chronopotentiometry, respectively.

Each one of these techniques has its own advantage. The film thickness can be controlled by the polymerization charge density (Q in C cm^{-2}) using the galvanostatic technique. The film crystallinity and surface morphology can be controlled by the polymerization potential using the potentiodynamic technique. The surface porosity has been found to increase with switching potential for potentiodynamic polymerization (54). The film oxidation state can be controlled by the potentiostatic technique where the electrode potential can be held at a certain value during polymer deposition. The molecular weight distribution has also been found to be a function of the applied potential. As the applied potential increases, the molecular weight of the polymer increases to a maximum value before overoxidation occurs (7; 55).

Polymer films deposited onto an electrode surface by electrochemical polymerization consist of a mixture of conjugated chain lengths (46). The average conjugation length, estimated by UV-Vis spectroscopy, can be controlled by the formation potential, and the polymerization temperature. It has been reported that low formation potentials produce polypyrrole with short chain lengths between 8 to 12 units, and higher formation potentials lead to longer chain lengths between 32 to 64 units (56). At very high potentials, cross-linked polymer chains are produced with a dramatic decrease in conductivity (57). Obviously, low formation potentials decrease the oxidation levels of the intermediate species and low polymerization temperatures slow down the coupling reactions, which result in shorter chain lengths.

One of the drawbacks of polymer films deposited electrochemically can be that the film morphology is not homogenous (i.e. varies across the film). The deposition rate increases as the concentration of radical cations builds up in the diffusion layer. As such, layers close to polymer/solution interface are more porous than those close to the electrode/polymer interface (20).

1.2.3 Kinetics in conducting polymers

1.2.3.1 Ion transport in conducting polymers

Because the redox mechanism of conducting polymers involves both electrons and ions (16), they can be considered as electronic and ionic conductors. However, since the mobility of ions is generally much lower than electrons, ion transport is usually the rate determining step and therefore limits the switching rate between conducting and nonconducting states (58). Obviously, fast ion transport facilitates the switching process which is desired for many applications. Understanding and improving the mobility of ions are therefore crucial steps for CPs to be used for many devices. Much research has been focused on enhancing ion transport and understanding the kinetic limitations of ion mobility between the polymer chains (59; 60; 61; 62; 63; 64). Much of this work concentrates on the factors that result in changing the morphology of the polymer films to elucidate the kinetic limitations and improve the understanding of ion transport rates.

There are many factors that can affect the electrochemical behaviour of conducting polymers, e.g. ion transport and redox potential (65; 66; 67), including effects of the solvent (68), dopant ion (69), formation electrolyte (70; 71; 72), and

polymerization potential (73). To date, many researchers have been trying to elucidate the diverse mechanisms of ion transport by various experiments (74); nevertheless, the comprehensive mechanism is still under debate.

An important insight into ion transport was provided by Ren and Pickup (75). They found that based on the structure of the polymer film, the rate and the type of the mobile ions can be varied as follows. First, the ionic conductivity of polypyrrole films can result from two different ion types. Anion transport is mainly responsible for ionic conductivity if small counterions are incorporated into the polymer matrix, such as ClO_4^-, whereas cation transport is mainly responsible for the ionic conductivity if polyanion counterions are incorporated into the polymer matrix, such as poly(styrenesulfonate) (PSS^-). However, the original anion dominated mode for ionic conductivity can be restored if a dication is present in the electrolyte solution. In other words, the counterions incorporated into the polymer film control the charge compensation process. Second, the mobility of the ions is significantly different in each mode. As a result of different degrees of ion pairing between mobile and fixed charges, cation transport inside polymer/polyanion composite is much faster than anion transport inside polymer/anion composites. Third, the ionic conductivity of polymer/anion films increases with oxidation level; however, for polymer/polyanion composite films, ionic conductivity decreases with oxidation level. This was explained by the fact that the mobile ion concentration increases in the first case with oxidation and decreases in the second case with oxidation.

With relation to these findings, it has been found that both anions and cations are involved in n-doping as well as in p-doping processes for poly(3,4-ethylenedioxythiophene) (76). Further, a recent contribution to ion transport indicates that the use of divalent anions like SO_4^{2-}, CO_3^{2-} or $C_2O_4^{2-}$ for PPy switching involves mixed anion/cation transfers with cation dominance (77). In contrast to delocalized monovalent anions and localized multivalent anions in the PPy matrix, divalent anions have partial localization within the PPy matrix. While localization of dopant ions inside the polymer matrix changes the doping process from normal doping to self doping, partial localization of the dopant ions involves both types of doping. As such, mixed ion transport has its own unique applications where partial switching is required (76).

Self-doped conjugated polymers are an important class of conducting polymers, where charged functional groups are covalently bound to the polymer backbone or physically trapped inside the polymer chains. Polymers modified with negatively charged groups (e.g. sulfonate, SO_3^-) behave as self-doped polymers due to immobilization of the charged functional groups by covalent bonds. On the other hand, polymers deposited from a polyanion electrolyte (e.g. polystyrene sulfonate, PSS) behave as self-doped polymers due to immobilization of the large counterions inside their chains. There are ongoing interests to control ion transport inside the polymer chains by modification of the polymer backbone, and so it has been shown that the concept of self-doped polymers can be extended to n-doped polymers (78).

Many electrochemical applications, such as sensors and electrocatalysis, are strongly related to the morphology of the electroactive materials. There are different models to relate morphology to ion permeability. The voltammetric response of ion transfer in a polymer film can be used to probe the structure of the film (59). The relationship between the ionic conductivity of polypyrrole films and the electrolyte conductivity was explained by a two-phase model consisting of permselective polymer and pores/channel filled with electrolyte (79).

Many researchers have tried to enhance electronic and ionic conductivities by synthesizing new polymers with low band gap and/or fabricating existing polymers to reduce the band gap, which can be estimated from the difference of anodic p-doping and cathodic n-doping peak potentials (80; 81; 82; 83). This can be done by adding electron withdrawing and/or electron donating groups to the polymer backbone which can help to stabilize the charge of the doped form. The former can help to stabilize n-type conductors by lowering the energy level of the conduction band, while the latter can help to stabilize p-type conductors by elevating the energy level of the valence band. Adding both groups, i.e. electron donating and electron withdrawing, to the same polymer backbone can reduce the band gap of the polymer more effectively by lowering the conduction band and elevating the valence band (84).

1.2.3.2 Effect of formation electrolyte

A supporting electrolyte is needed for two different processes. First, while forming the polymer electrochemically counterions are inserted from the formation

electrolyte into polymer matrix to compensate polymer backbone charges. Second, while switching between doped and undoped states counterions are inserted from the doping electrolyte into polymer matrix to compensate for the redox process. In both cases the net charge of the polymer film should be zero to fulfill the electroneutrality condition. Understanding the role of the formation electrolyte is a key step for improving the kinetic limitations due to the fact that formation electrolyte can influence the morphology of polymer films significantly.

It is worth noting that the produced polymer film can hold up to 40% of its weight as incorporated ions or salt. Many properties therefore of conducting polymers are electrolyte dependent. The effect of the formation electrolyte can change the electronic conductivity of the polymer film by multiple orders of magnitude (85; 86). Further, the interactions between dopant ions and polymer backbone charges can restrict the movement of ions, which can create kinetic limitations. The electrolyte concentration used for polymer formation can also affect physical properties, such as electrochemical deformation, of the polymer film (87). In addition the electrolyte type can affect the structure (88), and thus the electrochemical response of the polymer (89; 90; 91; 92).

The supporting electrolyte can also affect the flux of the solvent during redox switching. For n-doping processes, the identity of the dopant cation controls solvent transport. For example, for tetraethyl ammonium (TEA^+) insertion, solvent and ions

move in opposite directions, while they move in the same direction for tetrapropyle ammonium (TPA^+) insertion (69).

Switching the polymer between doped and undoped states involves ions movement across the solution/polymer interface (93). In the normal doping process, the mobile ions are anions for p-doping and cations for n-doping. However, if the polymer chains contain in their structure negatively bound charged functional groups (14), the polymer behaves as self-doped. As a result of the localized anionic sites in the polymer chains, cations are the mobile ions, i.e. cations are expelled upon p-doping instead of anions being inserted. Self-doped polymers are an important class of conducting polymers because of enhancement of ion transport rates by decreasing ion pairing (75).

1.3 Doping of conducting polymers

Reduction or oxidation of conducting polymers, either chemically or electrochemically, results in doping where counter charges are inserted into the polymer film to compensate for the polymer backbone charges. In the case of a chemical process, the redox doping reagent can be either an electron acceptor or an electron donor. While the former results in doping the conducting polymers with positive charges (i.e. p-doping), the latter results in doping the conducting polymers with negative charges (i.e. n-doping). Similarly, the electrochemical route of doping can be achieved by applying an anodic current causing oxidation, or p-doping, or by applying a cathodic current causing reduction, or n-doping. Because most studies on conducting polymers have focused on

polymers which are not stable in their reduced form, n-doping has been much less studied than p-doping. The most famous example of a polymer that can be n-doped is polythiophene. The cation used to maintain the electroneutrality of the reduced polymer has limited mobility inside the polymer film due to kinetic restrictions.

The simplest case for the voltammetric response of a doping process is for a redox thin film involving one-electron transfer, where the cathodic and anodic waves are identical with the current **i** proportional to scan rate **ν**, as described by equation 1.4 (17).

$$i = \frac{n^2F^2A\Gamma_T\nu\, exp\theta}{RT(1+exp\theta)^2} \qquad \textbf{[1.4]}$$

Where Γ_T is the total surface coverage of reduced and oxidized states (i.e. $\Gamma_R + \Gamma_O$), $\theta = (nF/RT)(E-E^\circ)$, **n** is the number of electrons transferred, **F** is the Faraday constant (96485 C mol^{-1}), **A** is the area of the electrode, **ν** is the potential scan rate, and **R** is the gas constant (8.314 J $(mol\ K)^{-1}$).

As the film thickness increases, the current response to a potential scan can be delayed due to slow ion transport or electron transfer kinetic. Thus, the current **i** can become proportional to the square root of the scan rate $\nu^{1/2}$, and a separation between the anodic and cathodic waves may be observed.

The voltammetric responses of conducting polymer films are different from those of the simple redox film discussed above, as indicated by the complex shapes of their voltammograms. A characteristic feature of voltammetric waves for conducting polymers is *hysteresis* (94), or separation between the anodic and cathodic waves, which has been attributed to many factors, such as slow heterogeneous charge transfer (17),

conformational changes during doping (95), interactions between oxidized chains (20), or N-shaped free energy curves resulting from phase transitions (96). It has also been recently attributed to the stability of the charged intermediates (56). Another characteristic feature is that the current does not decay to zero after doping, but resembles a pure capacitance, which has been attributed to charging of the double layer at polymer/solution interface (20).

Another feature is the first cycle effect which describes the large difference in wave shapes that are observed between the first cycle and subsequent cycles. It is also called a memory effect due to the fact that the electrochemical response depends on previous events. It has been attributed to many factors, such as polymer chains rearrangement, solvent expulsion, and structural relaxation (17; 97). All of which indicate that the interactions between the polymer chains and the incorporated species are different in the first cycle than in subsequent cycles. This effect could be used to advantage in molecular memory (MM) devices based on redox charge storage, which has been studied for use in memory devices such as dynamic random access memory (DRAM). There are many advantages for MM versus DRAM, such as higher charge density, lower cost, and longer retention time (98).

Doping a conducting polymer at a potential beyond its stability range results in overoxidation of the polymer film. This generally causes a loss of conjugation, conductivity, and electroactivity. For p-doping, a nucleophile can attack the positive centers of the polymer chains, resulting in chemical addition reactions indicated by

chemically irreversible waves. On the other hand, overoxidation can be used for advantage. Since addition reactions via overoxidation result in modification of the original polymer chain, the products of overoxidation can have new properties like permselectivity toward specific ions. For example, polypyrrole films can be used in many applications after overoxidation, such as electroanalysis, and sensors (20).

There are two different electronic states that arise during doping which enhance the conductivity in conducting polymers. Polaron and bipolaron are two states that appear as intragap between the conduction and valence bands. Polarons are the main states generated at low doping levels, while bipolarons are the main states generated at high doping levels (99). Further, the electronic conductivity has a potential dependence, where the maximum conductivity is inherent to the polymer films when the charges are injected or withdrawn (100).

1.4 Energy bands of conducting polymers

The molecular orbitals of the monomers used to produce conducting polymers are significantly changed by polymerization. The highest occupied molecular orbital (HOMO) splits into a band of non-degenerate levels called the π band, or valence band. Similarly, the lowest unoccupied molecular orbital (LUMO) splits into another band of non-degenerate levels called the π^* band, or conduction band. The gap between these two bands, called band gap (E_g), is typically $\geq$ 2 eV, and decreases with increasing conjugation length. It can be electrochemically estimated as mentioned previously. After

doping, oxidation or reduction, new levels are created within the band gap, and so the energy levels get closer to each other. Thus, the mobile charge carriers, electrons or holes, move faster between electronic bands, and hence the electronic conductivity increases. Moreover, the existence of charged particles within the polymer can cause distortion of the polymer chain geometry which changes the band structure and enhance the electronic conductivity further (20).

Polarons and bipolarons are usually created above the valence band by p-doping. At low doping levels, where polarons serves as charge carriers, electronic conductivity is proportional to the concentration of the charge carriers. However, at higher doping levels, where bipolarons serve as the charge carriers, the electronic conductivity drops significantly as the valence band becomes emptied by p-doping (20).

Although conducting polymers have some common properties with inorganic solids and redox polymers, there is a demand for a reliable model to account for the unique behaviour of conducting polymers (101). For example, a model primarily based on potential gradient (i.e. migration) has to be considered for conducting polymers rather than that based on concentration gradient (i.e. diffusion) which has been used for redox polymers (75). Treatment of ion transport solely as diffusion can result in a significant error.

On the other hand, the use of solid state models to describe conducting polymer behaviours is not very appropriate due to features like solvation and structural changes which do not occur for the rigid solid state (20).

1.5 Polymers and solvents used in this work

1.5.1 Polypyrrole

Since the first electrochemical synthesis of polypyrrole (PPy) in 1979 (19), PPy has attracted the attention of many researchers due to its stability and processibility as a positive electrode material (102). However, using PPy as a negative electrode material is unlikely (103) due to its unstable reduced form. PPy films are typically produced by anodic electropolymerization, with conductivities of 10 – 100 S cm^{-1}. Thus, PPy films can be deposited electrochemically as polycations with dopant anions such as ClO_4^- or polyanions such as PSS^-.

Although PPy deposition and doping have been extensively studied, the electrochemical mechanism of the polymerization is still debated. During PPy formation, the pyrrole units are linked primarily at the α-α′ positions. β-position coupling is also possible, however, α-position coupling predominates. Every three to four pyrrole units carry one positive charge as indicated by the concentration of incorporated counterions; polypyrrole has a composition of ca. $C_4H_3N\text{-}(BF_4)_{0.25}$ if polymerized from CH_3CN containing Et_4NBF_4 as a supporting electrolyte. The charge consumed during polymerization is ca. 2.3 electrons per pyrrole unit (37).

While the neutral polypyrrole is a poor conductor, it is relatively easy to be oxidized (p-doped) and switched to the p-conducting state. The π-electrons of polypyrrole have a low ionization energy due to the extended conjugated π system which allows the removal of electrons from the valence band at low potentials (103).

Polypyrrole can be electrochemically deposited from aqueous or non-aqueous solutions. Ionic media is required in both cases to deposit a CP film onto electrode surfaces. Inorganic salts or acids can be used as aqueous media to furnish conductive solution. For non-aqueous media, a supporting electrolyte (e.g. Et_4NBF_4) or ionic cosolvent is required to enhance the conductivity of the solution. Furthermore, it has been found that the stability and conductivity of conducting polymer films have been significantly altered using a steric stabilizer, such as polyethylene glycol (PEG), with a Lewis acid as additives to the main solvent (104).

1.5.2 Polyfluorenone

The first polyfluorenone (PFO) films were deposited electrochemically in 2004, when oxidative coupling of flouren-9-one molecules in Bu_4NBF_4/dichloromethane (CH_2Cl_2) solution was used to deposit PFO films onto platinum electrodes (105). Films of PFO with reasonable quality were produced for electrochemical characterization; however, the stability of the films on electrode surfaces needs to be reconsidered for improvement. Subsequently, in 2006, PFO films were deposited onto platinum electrodes by oxidative coupling in boron trifluoride ethyl etherate (BFEE) at lower polymerization potentials (106). These films show better quality for electrochemical characterization; however, the stability of the films on electrode surfaces is still a concern. The work in this thesis shows that the stability of the PFO films can be enhanced by adding a steric stabilizer (i.e. PEG) to the formation solution.

The ability of PFO to be n- and p-doped has made it an interesting polymer for ion transport characterization. Obviously, ion transport for PFO is more complicated than PPy where both cations and anions significantly contribute to the redox processes. While the reduced state (n-doped) of PFO is highly stable due to the electron deficient conjugated chain, the oxidized form (p-doped) can still be produced and probed. This makes PFO a good choice for cathodic electrode materials for many potential applications as n-type conductors. However, the kinetic restrictions resulting from charge trapping in polymer films result in loss of reversibility as the dopant cation size increases. Thus, the use of steric stabilizers like polyethylene glycol (PEG) is important to improve the electrochemical reversibility, as shown in this work.

PFO has been copolymerised with thiophene, which gives stable copolymer films (107). The copolymer films have been electrochemically characterized and the band gap (E_g) has been electrochemically estimated from their potential peaks, which is in agreement with the optical band gap (108).

A remarkable stability and reversibility has been shown for electrodes coated with copolymers of fluorenone with an alkyl thiophene group (109). A decrease in ionic conductivity resulted from partial trapping of negatively charged ions when the polymer was cycled over a positive potential window. A further decrease in ionic conductivity was observed if the polymer film was first cycled to negative potentials before cycling to positive potentials. The decrease in ionic conductivity was attributed to partial loss of electrochemical activity with cycling due to ion pairing and charge trapping effects.

1.5.3 Boron trifluoride ethyl etherate

Boron trifluoride ethyl etherate (BFEE) can be used as a medium with (110) or without (106) a cosolvent to facilitate electrochemical syntheses. It is a strong Lewis acid which lowers the formation potential for many conducting polymers because it facilitates the oxidation process. However, pure BFEE can damage the aromaticity of some conducting polymers due to overoxidation which results in additive polymerization. As a result, cosolvent is often used to reduce its activity and protect the aromaticity of conducting polymers. For PPy formation from BFEE, isopropyl alcohol (104) or acetonitrile, as done in this work, can be used to improve the film quality.

1.6 Characterizations of conducting polymers

Cyclic voltammetry (CV) and electrochemical impedance spectroscopy (EIS) are the most used techniques for electrochemical characterizations of polymer films. CV is also used for electrochemical synthesis of conducting polymers as mentioned previously. The thermodynamics of polymer films can be studied in general by CV where all qualitative aspects of chemical and electrochemical reactions can be identified. During polymer formation the current increase with cycling is a direct measure of the thickness of the electroactive polymer layer on the electrode surface, and so relative growth rates can be established (48). The kinetics of the electrochemistry of polymer films, on the other hand, can best be studied by EIS where quantitative measurements can be obtained for electron and ion transport. It has been used to characterize different PTh

coated electrodes (58) as well as to probe PPy/carbon black composite electrodes at various doping levels (111).

Electrochemical quartz crystal microbalance (EQCM) techniques can be used with cyclic voltammetry or potential step techniques to observe net mass changes and ion transport rates during electrochemical deposition by measuring the resonance frequency shift which is linearly related to mass changes. It can be also used to monitor ion exchange during the redox processes of polymer films (112; 113; 114; 115). A mass decrease, for example, is observed by EQCM for polypyrrole films, which is clear evidence for anion removal from the film under reduction. Low mobility of the counterions can result in switching of the mobile ions as shown by EQCM as a mass increase. The mass increase attributed to cation insertion is observed at the end of the reduction wave, and so mixed ion transport for a reduction process is clearly illustrated by EQCM (20). This transient cation insertion was also observed by CV for polypyrrole, but is not yet fully understood (75).

1.7 Applications of conducting polymers

Redox switching between the conducting and nonconducting states of conducting polymers is a crucial property in many applications. As a result of redox switching many properties can be altered, such as electronic conductivity, polymer ionic strength, polymer ion permeability, and optical properties (116).

There are many applications for conducting polymers in electrochemical devices including rechargeable battery electrodes (103; 117), supercapacitors (118), electrochromic display materials (119), molecular electronic devices, biosensors (7), electroanalysis, and electrocatalysis (120). In addition, conducting polymers can be used as corrosion protection layers when deposited onto metal surface, where the metal oxide layer becomes thicker due to a redox reaction with the conducting polymer. Finally, conducting polymers can be used in artificial muscles where high doping level can cause up to a 30% increase of polymer volume (16).

1.8 Objectives

The main objective of this work was to understand the kinetic limitations of ion transport in conducting polymers. Improving ion mobility in polymer films by changing morphology and electrolyte counterions are the main approach to facilitate doping processes. Both n-doping and p-doping have been characterized throughout the thesis work.

In the first part of the thesis, dopant anions of various size/charge including electroactive species were incorporated into polypyrrole films and characterized to facilitate the understanding of ion transport mechanisms. In the second part, polyfluorenone films deposited from BFEE, with and without a steric stabilizer, were investigated during n-doping for deactivation/reactivation processes.

References

1. A. Virkar, S. Mannsfeld, Z. Bao, N. Stingelin, *Adv. Mater.* 22 (2010) 3857.

2. Y. Yamashita, Sci. Technol. *Adv. Mater.* 10 (2009) 1.

3. M. He, *J. Am. Chem. Soc.* 131 (2009) 11930.

4. A. Heeger, *Chem. Soc. Rev.* 39 (2010) 2354.

5. J. Anthony, A. Facchetti, M. Heeney, S. Marder, X. Zhan, *Adv. Mater.* 22 (2010) 3876.

6. L. Chua, J. Zaumseil, J. Chang, E. Ou, P. Ho, H. Sirringhaus, R. Friend, *Nature* 434 (2005) 194.

7. M. Gerard, A. Chaubey, B. Malhotra, *Biosen. Bioelectron.* 17 (2002) 345.

8. J. Clark, G. Lanzani, *Nat. Photonics* 4 (2010) 438.

9. H. Yan, Z. Chen, Y. Zheng, C. Newman, J. Quinn, F. Dotz, M. Kastler, A. Facchetti, *Nature* 457 (2009) 679.

10. H. Letheby, *J. Chem. Soc.* 15 (1862) 161.

11. H. Shirakawa, E. Louis, A. MacDiarmid, C. Chiang, A. Heeger, *J. Chem. Soc. Chem. Commun.* (1977) 578.

12. J. Stejskala, M. Omastova, S. Fedorovac, J. Prokes, M. Trchova, *Polymer* 44 (2003) 1353.

13. J. Roncali, *Chem. Rev.* 92 (1992) 711.

14. A. Malinauskas, *J. Power Sources* 126 (2004) 214.

15. E. Naudin, H. Ho, L. Breau, D. Bélanger, In Conducting Polymers and Polymer Electrolytes, Chapter 4, ACS Symposium Series 832 (2002) 52.

16. G. Inzelt, M. Pineri , J. Schultze, M. Vorotyntsev, *Electrochim. Acta* 45 (2000) 2403.

17. J. Heinze, B. Frontana-Uribe, S. Ludwigs, *Chem. Rev.* 110 (2010) 4724.

18. M. Kaneko, D. Wohrle, *Adv. Polym. Sci.* 84 (1988) 141.

19. A. Diaz, K. Kanazawa, G. Gardini, *J. Chem. Soc. Commun.* (1979) 635.

20. P. Pickup, In Modern Aspects of Electrochemistry, ed. B. Conway, J. Bockris, R. White, Plenum, New York 33 (1999) 549.

21. E. Bravo-Grimaldo, S. Hachey, C. Cameron, M. Freund, *Macromolecules* 40 (2007) 7166.

22. S. Ritter, R. Noftle, *Chem. Mater.* 4 (1992) 872.

23. R. de Barros, M. Areias, W. de Azevedo, *Synth. Met*. 160 (2010) 61.

24. N. Strandwitz, Y. Nonoguchi, S. Boettcher, G. Stucky, *Langmuir* 26 (2010) 5319.

25. S. Tanaka, T. Iso, *J. Chem. Soc. Chem. Commun.* (1994) 1071.

26. P. Damlin, C. Kvarnstrom, H. Neugebauer, A. Ivaska, *Synth. Met*. 123 (2001) 141.

27. N. Alpatova, G. Girina, *Russ. J. Electrochem.* 42 (2006) 670.

28. J. Utley, J. Gruber, *J. Mater. Chem.* 12 (2002) 1613.

29. J. Heinze, H. John, M. Dietrich, P. Tschuncky, *Synth. Met.* 119 (2001) 49.

30. C. Andrieux, P. Audebert, P. Hapiot, J. Saveant, *J. Phys. Chem*. 95 (1991) 10158.

31. P. Narula, R. Noftle, *J. Electroanal. Chem.* 464 (1999) 123.

32. E. Genies, G. Bidan, A. Diaz, *J. Electroanal. Chem.* 149 (1983) 101.

33. C. Andrieux, P. Audebert, P. Hapiot, J. Saveant, *J. Am. Chem. Soc.* 112 (1990) 2439.

34. P. Hapiot, P. Audebert and K. Monnier, J.-M. Pernautt and P. Garcia, *Chem. Mater.* 6 (1994) 1549.

35. G. Hansen, R. Henriksen, F. Kamounaha, *Electrochim. Acta* 50 (2005) 4936.

36. H. El-Desoky, J. Heinze, M. Ghoneim, *Electrochem. Commun.* 3 (2001) 697.

37. S. Sadki, P. Schottland, N. Brodiec, G. Sabouraud, *Chem. Soc. Rev.* 29 (2000) 283.

38. R. John, G. Wallace, *J. Electroanal. Chem.* 306 (1991) 157.

39. A. Smie, A. Synowczyk , J. Heinze, R. Alle, P. Tschuncky, G. Gotz, P. Bauerle, *J. Electroanal. Chem.* 452 (1998) 87.

40. A. Downard, D. Pletcher, *J. Electroanal. Chem.* 206 (1986) 139.

41. G. Zotti, G. Schiavon, A. Berlin, G. Pagani, *Electrochim. Acta* 34 (1989) 881.

42. H. Randriamahazaka, G. Sini, F. Van, *J. Phys. Chem. C* 111 (2007) 4553.

43. S. Asavapiriyanont, G. Chandler, G. Gunawardena, D. Pletcher, *J. Electroanal. Chem.* 177 (1984) 229.

44. C. Andrieux, J. Dumas-Bouchiat, J. Saveant, *J. Electroanal. Chem.* 87 (1978) 39.

45. M. Chmielewski, M. Grzeszczuk, J. Kalenik, A. Kepas-Suwara, *J. Electroanal. Chem.* 647 (2010) 169.

46. J. Lukkari, M. Alanko, V. Pitkiinen, K. Kleemola, J. Kankare, *J. Phys. Chem.* 98 (1994) 8525.

47. D. Raymond, D. Harrison, *J. Electroanal. Chem.* 361 (1993) 65.

48. J. Heinze, A. Rasche, M. Pagels, B. Geschke, *J. Phys. Chem.* B 111 (2007) 989.

49. M. Skompska, *Electrochim. Acta* 45 (2000) 3841.

50. K. Meerholz, J. Heinze, *Electrochim. Acta* 41 (1996) 1839.

51. B. Parakhonskiy, D. Andreeva, H. Mohwald, D. Shchukin, *Langmuir* 25 (2009) 4780.

52. G. Zottia, S. Cattarina, N. Comissoa, *J. Electroanal. Chem.* 239 (1988) 387.

53. V. Abalyaeva, O. Efimov, *Russ. J. Electrochem.* 46 (2010) 571.

54. L. Niu, C. Kvarnstrom, K. Froberg, A. Ivaska, *Synth. Met.* 122 (2001) 425.

55. W. Yen, T. Jing, *Macromolecules* 26 (1993) 457.

56. C. Bof Bufon, J. Vollmer, T. Heinzel, P. Espindola, H. John, J. Heinze, *J. Phys. Chem. B* 109 (2005) 19191.

57. K. Meerholz, J. Heinze, *Synth. Met.* 55-57 (1993) 5040.

58. H. Ding, Z. Pan, L. Pigani, R. Seeber, C. Zanardi, *Electrochim. Acta* 46 (2001) 2721.

59. G. Duffitt, P. Pickup, *J. Chem. Soc. Faraday Trans.* 88 (1992) 1417.

60. C. Baker, Y. Qiu, J. Reynolds, *J. Phys. Chem.* 95 (1991) 4446.

61. C. Elliott, A. Kopelove, W. Albery, Z. Chen, *J. Phys. Chem.* 95 (1991) 1743.

62. K. Kanamura, S. Yonezawa, S. Yoshioka, Z. Takehara, *J. Phys. Chem.* 95 (1991) 7939.

63. A. Hillman, M. Mohamoud, *Electrochim. Acta* 51 (2006) 6018.

64. A. Hillman, S. Daisley, S. Bruckenstein, *Electrochem. Commun.* 9 (2007) 1316.

65. P. Topart, M. Noel, *Anal. Chem.* 66 (1994) 2926.

66. H. Yang, J. Kwak, *J. Phys. Chem.* B 101 (1997) 774.

67. G. Li, M.Sc. Thesis, Memorial University of Newfoundland, 1999.

68. H. Lee, H. Yang, J. Kwak, *J. Phys. Chem. B* 103 (1999) 6030.

69. A. Hillman, S. Daisley, S. Bruckenstein, *Electrochim. Acta* 53 (2008) 3763.

70. N. Sakmeche, S. Aeiyach, J. Aaron, M. Jouini, J. Lacroix, P. Lacaze, *Langmuir* 15 (1999) 2566.

71. H. Lee, H. Yang, J. Kwak, *Electrochem. Commun.* 4 (2002) 128.

72. P. Aubert, L. Groenendaal, F. Louwet, L. Lutsen, D. Vanderzande, G. Zotti, *Synth. Met.* 126 (2002) 193.

73. X. Du, Z. Wang, *Electrochim. Acta* 48 (2003) 1713.

74. M. Akieh, W. Price, J. Bobacka, A. Ivaska, S. Ralph, *Synth. Met.* 159 (2009) 2590.

75. X. Ren, P. Pickup, *J. Phys. Chem.* 97 (1993) 5356.

76. L. Niu, C. Kvarnstrom, A. Ivaska, *J. Electroanal. Chem.* 569 (2004) 151.

77. S. Bruckenstein, J. Chen, I. Jureviciute, A. Hillman, *Electrochim. Acta* 54 (2009) 3516.

78. N. Zhang, R. Wu, Q. Li, K. Pakbaz, C. 0. Yoon, F. Wudl, *Chem. Mater.* 5 (1993) 1598.

79. X. Ren, P. Pickup, *J. Electroanal. Chem.* 396 (1995) 359.

80. H. Huang, P. Pickup, *Chem. Mater.* 11 (1999) 1541.

81. C. Kean, P. Pickup, *Chem. Commun.* (2001) 815.

82. K. Loganathan, P. Pickup, *Electrochim. Acta* 51 (2005) 41.

83. S. Tarkuc, Y. Udum, L. Toppare, *J. Electroanal. Chem.* 643 (2010) 89.

84. C. Cheng, M. Lonergan, *J. Am. Chem. Soc.* 126 (2004) 10536.

85. X. Ren, PhD Thesis, Memorial University of Newfoundland, 1993.

86. G. Tourillon, F. Garnier, *J. Phys. Chem.* 87 (1983) 2289.

87. S. Chu, P. Kilmartin, S. Jing, G. Bowmaker, R. Cooney, J. Travas-Sejdic, *Synth. Met.* 158 (2008) 38.

88. S. Demoustier-Champagne, P. Stavaux, *Chem. Mater.* 11 (1999) 829.

89. H. Okamoto, T. Kotaka, *Polymer* 40 (1999) 407.

90. D. Kaplin, S. Qutubuddin, *Polymer* 36 (1995) 1275.

91. M. Levi, C. Lopez, E. Vieil, M. Vorotyntsev, *Electrochim. Acta* 42 (1997) 757.

92. A. Melato, M. Mendonça, L. Abrantes, *J. Solid State Electrochem.* 13 (2009) 417.

93. M. Vorotyntsev, E. Vieil, J. Heinze, *J. Electroanal. Chem.* 450 (1998) 121.

94. R. Hass, J. Garcia-Canadas, G. Garcia-Belmonte, *J. Electroanal. Chem.* 577 (2005) 99.

95. G. Inzelt, *Chem. Biochem. Eng. Q.* 21 (2007) 1.

96. S. Feldberga, I. Rubinsteinb, *J. Electroanal. Chem.* 240 (1988) 1.

97. B. Villeret, M. Nechtschein, *Phys. Rev. Lett.* 63 (1989) 1285.

98. S. Barman, F. Deng, R. McCreery, *J. Am. Chem. Soc.* 130 (2008) 11073.

99. Y. Furukawa, *J. Phys. Chem.* 100 (1996) 15644.

100. D. Ofer, R. Crooks, M. Wrighton, *J. Am. Chem. Soc.* 112 (1990) 7869.

101. L. Tolbert, *Acc. Chem. Res.* 25 (1992) 561.

102. L. Wang, X. Li, Y. Yang, *React. Funct. Polym.* 47 (2001) 125.

103. P. Novak, K. Muller, K. Santhanam, O. Haas, *Chem. Rev.* 97 (1997) 207.

104. J. Xu, G. Shi, L. Qu, J. Zhang, *Synth. Met.* 135–136 (2003) 221.

105. A. Cihaner, S. Tirkes, A. Onal, *J. Electroanal. Chem.* 568 (2004) 151.

106. S. Zhang, G. Nie, X. Han, J. Xu, M. Li, T. Cai, *Electrochim. Acta* 51 (2006) 5738.

107. K. Loganathan, P. Pickup, *Electrochim. Acta* 52 (2007) 4685.

108. K. Loganathan, F. Huang, P. G. Pickup, *Electrochim. Acta* 52 (2006) 15.

109. M. Levi, R. Demadrille, E. Markevich, Y. Gofer, A. Pron, D. Aurbach, *Electrochem. Commun.* 8 (2006) 993.

110. W. Zhou, J. Xu, Y. Du, P. Yang, *J. Appl. Polym. Sci.* 117 (2010) 2688.

111. R. Moghaddam, P. Pickup, *Phys. Chem. Chem. Phys.* 12 (2010) 4733.

112. I. Efimov, S. Winkels, J. Schultze, *J. Electroanal. Chem.* 499 (2001) 169.

113. R. Borjast, D. Buttry, *Chem. Mater.* 3 (1991) 872.

114. C. Kvarnstrom, R. Bilger, A. Ivaska, J. Heinze, *Electrochim. Acta* 43 (1998) 355.

115. A. Bund, A. Baba, S. Berg, D. Johannsmann, J. Lubben, Z. Wang, W. Knoll, *J. Phys. Chem. B* 107 (2003) 6743.

116. K. Lee, A. Heeger, *Synth. Met.* 128 (2002) 279.

117. C. Dalmolin, S. Biaggio, R. Rocha-Filho, N. Bocchi, *Synth. Met.* 160 (2010) 173.

118. J-Y Kim, K. H. Kim, K. B. Kim, *J. Power Sources* 176 (2008) 396.

119. S. Mokrane, L. Makhloufi, N. Alonso-Vante, *J. Solid State Electrochem.* 12 (2008) 569.

120. A. Malinauskas, *Synth. Met.* 107 (1999) 75.

Chapter 2

Experimental

2.1 Chemicals and Reagents

Two monomers were used to prepare the polymer-coated electrodes: pyrrole and fluoren-9-one. Pyrrole (Py, Aldrich, 98%) was purified on a dry aluminum oxide column. Fluoren-9-one (FO, Aldrich, 98%) was recrystallized from n-hexane and dried under vacuum overnight.

The solvents over the work of this thesis were used as received. Acetonitrile (CH_3CN, Aldrich, HPLC grade, 99.8%), dichloromethane (CH_2Cl_2, ACP Chemicals INC.), boron trifluoride ethyl etherate (BFEE; Aldrich, 46% BF_3 basis), and isopropyl alcohol (IPA, Sigma-Aldrich, 99.5%) were used for film deposition. All aqueous solutions were prepared with deionized water.

The supporting electrolytes and reagents were electrochemical grade and were used as received. The electrolytes that were used in CH_3CN:

tetrabutylammonium hexafluorophosphate (Bu_4NPF_6; Fluka)

tetrabutylammonium perchlorate (Bu_4NClO_4; Fluka)

tetraethylammonium tetrafluoroborate ($TEABF_4$; Alfa Aesar)

tetraethylammonium perchlorate (TEAP; Alfa Aesar)

The reagents and electrolytes that were used in aqueous solutions:

poly(sodium 4-styrenesulfonate) (NaPSS, Aldrich, MW ca. 70 000 g mol^{-1})

sodium perchlorate ($NaClO_4$, Alfa Aesar, 98%)

Alizarin Red S (ARS, synonym 3,4-dihydroxy-9,10-dioxo-2-anthracenesulfonic acid sodium salt, Sigma-Aldrich, $C_{14}H_7NaO_7S$, MW 342.26 g mol^{-1})

sodium sulfate (Na_2SO_4, J.T. Baker Chemicals, 99.9%)

trisodium orthophosphate (Na_3PO_4, BDH Chemicals)

sodium chloride (NaCl, ACP Chemicals, 99%)

lithium perchlorate ($LiClO_4$, Aldrich, 95+%)

The reagents that were used as additive to the polymerization solution for polymer film modification are:

polyethylene glycol (PEG, Fluka, analytical grade, MW av. 200, 400, or 1000),

1-(ferrocenyl)ethanol (FcOH, Fluka, 97%, MW 230.08 g mol^{-1})

Chemical structures of some of these compounds are shown in Figure 2.1.

2.2 Electrochemistry

Electrochemical experiments were carried out in conventional three-compartment glass cells under a nitrogen atmosphere at 23 ± 2 °C. A glassy carbon (GC) disc electrode (0.071 cm^2) or a Pt electrode (0.0045 cm^2) was used as the working

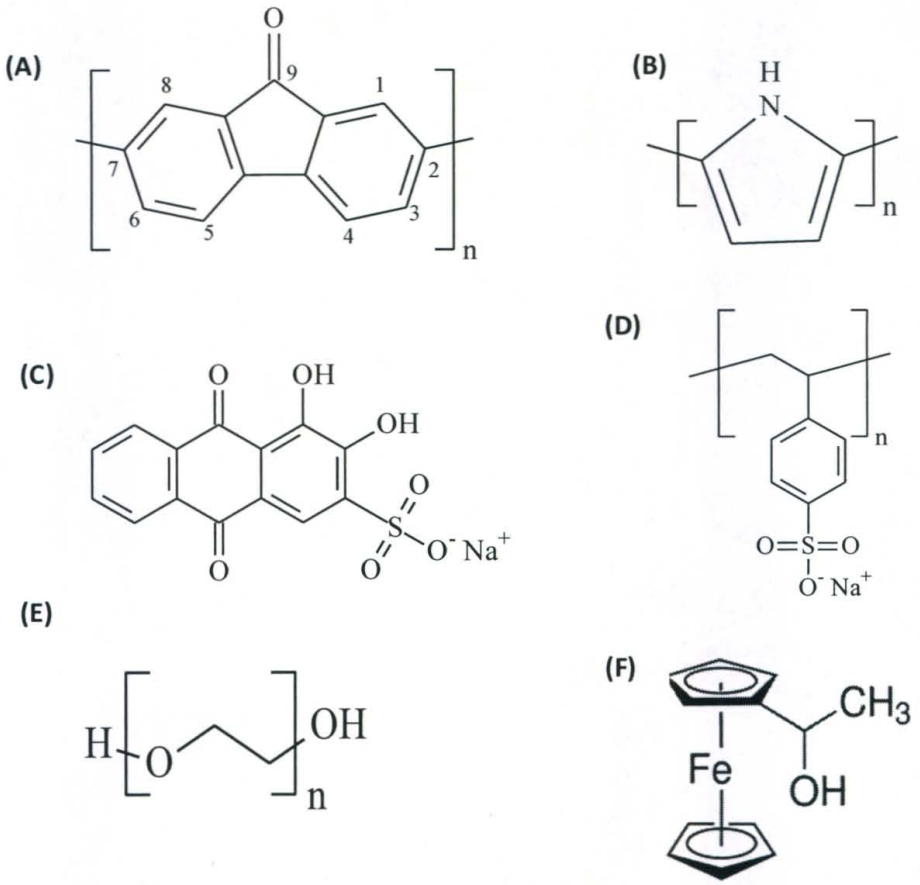

Figure 2.1 Chemical structures for **A.** polyfluorenone, **B.** polypyrrole, **C.** Alizarin Red S, **D.** poly (sodium 4-styrenesulfonate), **E.** polyethylene glycol, **F.** 1-(ferrocenyl)ethanol

electrode. A Pt wire and a saturated calomel electrode (SCE) were used as counter electrode and reference electrode, respectively. All potentials were quoted with respect to the SCE which was tested in ferrocene solution, Figure 2.2.

2.3 Electrodeposition of polymer films

Polypyrrole films were deposited from aqueous and non-aqueous solutions. In typical experiments for aqueous solution deposition, polypyrrole films were deposited from 0.1 M Py in an aqueous solution containing 0.5 M electrolyte, such as $NaClO_4$. For the non-aqueous deposition, polypyrrole films were deposited from 0.1 M Py and 20% BFEE in CH_3CN or IPA as the main solvent. In the case of incorporating a modifier into the polymer film, various concentrations of the modifier were also added to the polymerization solution, such as 10 mM of FcOH and 1% PEG.

Polypyrrole films were deposited on glassy carbon (GC) electrodes with a surface area of 0.071 cm^2. The deposition charge was typically 0.018 C (0.25 C cm^{-2}) for galvanostatic polymerization. For potentiostatic and potentiodynamic polymerization, deposition conditions of holding potential at 1.0 V (for 1, 2, or 3 minutes) and scan rate of 0.1 V s^{-1} (between -0.2 V and 1.2 V) were used for deposition onto the electrode surface, respectively.

Polyfluorenone films were deposited electrochemically on Pt working electrodes from 30 mM FO in BFEE potentiodynamically between 0.7 V and 2.0 V for various numbers of cycles at 0.1 V s^{-1}. For potentiostatic deposition, the potential was held at

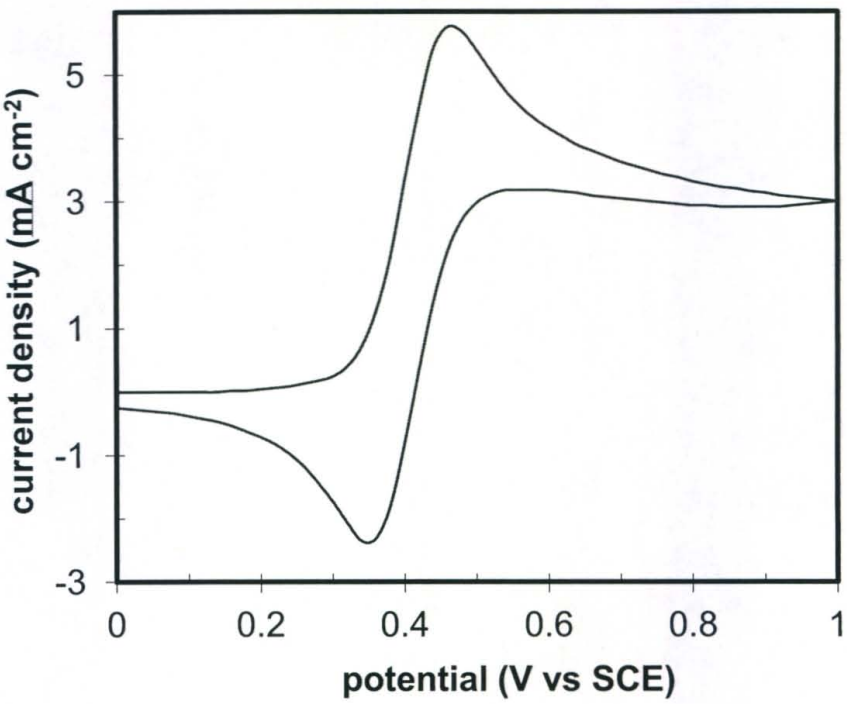

Fig. 2.2 Ferrocene cyclic voltammogram (10 mM) in CH_3CN containing 0.1 M Et_4NBF_4 at scan rate of 0.05 V s^{-1}.

1.6 V for one minute. For galvanostatic deposition, the current was held at 0.01 mA for one minute (0.06 mC). In the case where CH_2Cl_2 was used as the main solvent, a supporting electrolyte, such as Bu_4NBF_4, was added with concentration of 0.1 M. The deposition from CH_2Cl_2 was conducted potentiodynamically between 1.0 V and 2.8 V for various numbers of cycles at 0.1 V s^{-1}.

2.4 Equipment and Instrumentation

The cyclic voltammetry experiments were carried out using HA-301 Potentiostat/Galvanostat and HB-III function generator. The electrochemical and impedance measurments were carried out using a Model 273A EG&G Potentiostat/Galvanostat and Model 5210 Lock-in Amplifier with Power-Suite commercial software. The measurements were performed over the range of 10 kHz to 0.5 Hz with an ac amplitude of 10 mV at various dc potentials. A logarithmic scale was chosen over 20 points from high to low frequency. Impedance spectra were collected in the order of decreasing electrode potential, unless otherwise stated.

Scanning electron microscopy (SEM) imges and energy dispersive X-ray (EDX) spectra were obtained with a FEI Quanta 400 Enviromental SEM (ESEM) used in high-vacuum mode, and equiped with a Bruker XFlash 4010 SDD X-ray detector for acquiring elemental X-ray spectra with high effeciency, which can be used for qualitative elemental identification and semiquantitative analysis for any specific spot on the sample. The acceleration voltage was 20 keV, and the tungsten thermal emitter was

biased for 80 μA emission current. The beam current (i.e. spot size) was adjusted for necessary resolving power. The Everhart-Thornley SE detector was used when necessary for imaging, and the working distance was 10 mm.

A Perkin Elmer AD-2Z model microbalance was used to measure the deposited mass of the polymers on Pt wires.

The UV-Vis spectra were recorded by an Agilent HP8453A UV-Visible diode array spectrophotometer, using tungsten and deuterium lamps for a 190 - 1100 nm spectral range. The instrument is precise within ± 0.5 nm. The flame atomic absorption instrument is a Varian SpectrAA 50 and an iron lamp was used.

Chapter 3

Ion Transport Properties of Polypyrrole Films in Aqueous Electrolytes

3.1 Introduction

Ion transport in conducting polymers has attracted considerable interest due to its importance in many potential applications, such as batteries, flexible displays, and other electrochemical devices (1; 2; 3; 4; 5). The ion transport properties of composite polymer films, such as polypyrrole doped with polystyrene sulfonate (PPy/PSS), can be used in ion exchangers for softening drinking water (6). Such useful electrochemical behaviour of these types of films offers a competitive way for softening and regeneration processes without the need for any chemical additives. Under reduction conditions, the negative charges of the composite polymer film are compensated by cation uptake from the water resulting in Ca^{2+} and Mg^{2+} removal, i.e. softening process. Under oxidation conditions, the cations are released into a different solution, i.e. regeneration of the polymer film.

Different polymer compositions have different ways to fulfill the charge compensation or electroneutrality condition. Electron transport takes place across the electrode/polymer interface under a potential difference (i.e. oxidation or reduction). As a result, ion transport takes place to compensate or neutralize the polymer film charges as follows. Conducting polymer films made by oxidative polymerization are in their oxidized state, existing as polycations with dopant anions. Reducing these films in an electrolyte solution results in either releasing the dopant anions incorporated during the electropolymerization or insertion of cations from the electrolyte solution to neutralize the electrogenerated negative charges of the polymer film. When the polymer film is subsequently re-oxidized, the cations already inserted can be released or anions from the electrolyte solution can be inserted to neutralize the electrogenerated positive charges of the polymer film. In such ways, transport of just anions or just cations can contribute to the charge compensation process. Simultaneous movement of anions and cations can also contribute in such processes, i.e. mixed ion transport (6; 7; 8).

There are many factors that can influence the ion transport properties, such as counterion mobility inside the polymer film, morphology of the polymer film, and ion pair formation (i.e. association between ions of opposite charges). Counterion mobility in polymer films can be predicted to some extent from the size of the mobile ion, where small ions tend to have high mobility, medium ions have low mobility, and large ions are generally immobile (9; 10). The electrostatic interactions between counterions and polymer chain charges can also affect the mobility but it is not easy to predict its degree.

Ion transport rates have been studied extensively in conducting polymer films (11; 12; 13). Determination of the ion transport rates can be achieved by measuring the rate of the electrochemical switching between doped and undoped states (i.e. conducting and non-conducting states, respectively) of the polymer film, which can also reveal important insights into the morphologies of these materials (14). Understanding the ion transport properties and how they vary from one polymer film to another is a central part toward enhancing the electrochemical switching rates of conducting polymers. The electrochemical switching between doped and undoped states requires charge compensation, which involves both electron and ion transport across the electrode/polymer and polymer/solution interfaces, respectively (12; 15; 16; 17).

The ion transport properties are very complicated as revealed by many studies, and strongly depend on the polymerization conditions employed, such as the degree of oxidation of the polymer film, and the electrolyte nature and concentration (7; 18). Ion transport is also strongly influenced by the structure of the polymer film which can be altered by the dopant anions, and so different modes of ion transport can be observed based on the film structure (19). Polymer films doped with small anions (e.g. Cl^-) exhibit dominant anion transport during the switching process. On the other hand, polymer films doped with larger dopant anions (e.g. ClO_4^-) exhibit cation transport in addition to anion transport, which results in swelling of the polymer films. The original polymer film can be regenerated by polarizing at positive potentials to eject the trapped cations. Equations 3.1 and 3.2 describe anion and cation transport, respectively.

$$(PPy)^{+}A^{-} + e^{-} \rightleftharpoons (PPy)^{0} + A^{-} \quad [3.1]$$

$$(PPy)^{+}A_L^{-} + C^{+} + e^{-} \rightleftharpoons (PPy)^{0}A_L^{-}C^{+} \quad [3.2]$$

Where **PPy** represents a segment of a polymer chain for polypyrrole or any conducting polymer, e^- is an electron, A^- is a dopant anion, A_L^- is a large dopant anion, and C^+ is a small cation from the electrolyte solution. From Equation 3.1, the fast mobility of the anions results in a charge compensation mechanism preserved by only anion transport. However, if the anions are immobilized inside the polymer matrix due to their large size or high electrostatic interactions with the positive charges on the polymer chains, the charge compensation mechanism involves both anion and cation transport (Equations 3.1 and 3.2). As ions transport into/out of the polymer film, a change in volume is observed, which can be used in many potential applications, such as soft actuators and artificial muscles (20; 21; 22).

Ion exchange can accompany ion transport if the polymer film is deposited from one electrolyte solution, and then placed in a different electrolyte solution (i.e. redoped from different electrolyte). In general, ion exchange is just an equilibration process that occurs when an ionomer or a membrane containing charged species is placed in a solution containing different counterions, and so such processes are primarily under thermodynamic control. However, the exchange process can be strongly influenced by the mobility of both ions. Over typical timescales employed, full and partial exchange processes are expected at high and low mobility of ions, respectively. An electrochemically driven exchange of ions, or simply driven ion exchange, can therefore

occur if the film is subjected to potential cycling or potential bias, and so the film can be under kinetic control. It has been reported that ion exchange mechanisms depend on the type and size of the dopant anion (7; 23). Typically, ion exchange processes take place between dopant anions in the polymer films and anions of the external electrolyte solution (3; 24). However, polymer chains with localized negative charges, such as sulfonated polyaniline, have different modes of ion exchange (25). Cation exchange is found to be the dominant process for these polymer films. Equations 3.3 and 3.4 describe the two possible ion exchange processes;

$$(PPy)^{+}A_1^{-} + A_{2(sol)}^{-} \rightleftharpoons (PPy)^{+}A_2^{-} + A_{1(sol)}^{-} \quad [3.3]$$

$$(PPy/A_1)^{-}C_1^{+} + C_{2(sol)}^{+} \rightleftharpoons (PPy/A_1)^{-}C_2^{+} + C_{1(sol)}^{+} \quad [3.4]$$

Equation 3.3 can be used to describe oxidized polymer films doped with small anions, and so the high mobility of the dopant anions results in anion exchange. Equation 3.4 can be used to describe reduced polymer films incorporating large dopant anions, where immobility of these anions results in cation exchange.

There are various other techniques that can be used to probe insertion and expulsion of the mobile ions, including the use of an electrochemical quartz crystal microbalance (EQCM) (26), which can be used to monitor ion and solvent movement into/out of the polymer film directly. Cyclic voltammetry and impedance spectroscopy can also be used to probe ion transport indirectly (27). It has been found that insertion of the mobile ions is associated with a larger potential drop compared with their expulsion, and so anion insertion is associated with anodic peak shifts to more positive

potentials as the scan rate is increased. In contrast, cation insertion is associated with a cathodic peak shift to less positive potentials. However, a better diagnostic tool for insertion and expulsion of the mobile ions is impedance spectroscopy, where ionic conductivity is directly related to the mobile ion concentration in the polymer film. Ionic conductivity measured as a function of oxidation levels increases with increasing oxidation level if the mobile ions are anions. In contrast, ionic conductivity deceases with increasing oxidation level if cations are the mobile ions (28).

The objective of the work described in this chapter was to study the ion transport properties of five polypyrrole films in aqueous solutions by using dopant anions of various sizes and charges. The study aims to enhance ion transport in polymer matrices and facilitate the doping process of conducting polymers, understand the charge compensation mechanisms and charge trapping effects, and understand the kinetic limitations caused by steric effects and ion-polymer interactions.

3.2 Experimental

3.2.1 Electrochemistry

Electrochemical experiments were carried out in conventional three-compartment glass cells under a nitrogen atmosphere at 23 ± 2 °C. A glassy carbon (GC) disc working electrode of 0.071 cm^2, a Pt wire counter electrode, and a saturated calomel electrode (SCE) reference electrode were used. All potentials are quoted with

respect to the SCE. All cyclic voltammograms and impedance measurements were taken under nitrogen gas.

3.2.2 Chemicals

Pyrrole (Py, Aldrich, 98%) was purified on a dry aluminum oxide column. Acetonitrile (CH_3CN, Aldrich, HPLC grade), poly(sodium 4-styrenesulfonate) (NaPSS, Aldrich, MW ca. 70 000 g mol^{-1}), sodium perchlorate ($NaClO_4$, Alfa Aesar, 98%), Alizarin Red S (ARS, synonym 3,4-dihydroxy-9,10-dioxo-2-anthracenesulfonic acid sodium salt, Sigma-Aldrich, $C_{14}H_7NaO_7S$, MW 342.26 g mol^{-1}), sodium sulfate (Na_2SO_4, J.T. Baker Chemicals, 99.9%), trisodium orthophosphate (Na_3PO_4, BDH Chemicals), sodium chloride (NaCl, ACP Chemicals, 99%), and lithium perchlorate ($LiClO_4$, Aldrich, 95+%) were used as received unless otherwise stated. All solutions were prepared with deionized water. The chemical structures of ARS and NaPSS are shown in Figure 3.1.

3.2.3 Electrodeposition of polymer films

Polypyrrole (PPy) films were prepared electrochemically at a constant current density of 4.2 mA cm^{-2}, which correspond to a 0.3 mA deposition rate. A polymerization charge of 0.018 C was used for all films in this work, which gives a charge density of 0.25 C cm^{-2} for GC electrodes with an area of 0.071 cm^2. The five types of PPy film were deposited from different electrolytes as follows:

PPy/ClO_4^- represents PPy films prepared from 0.1 M Py + 0.5 M $NaClO_4$,

PPy/ARS represents PPy films prepared from 0.1 M Py + 0.006 M Alizarin Red S (ARS),

PPy/SO_4^{2-} represents PPy films prepared from 0.1 M Py + 0.5 M Na_2SO_4,

PPy/PO_4^{3-} represents PPy films prepared from 0.1 M Py + 0.5 M Na_3PO_4, and

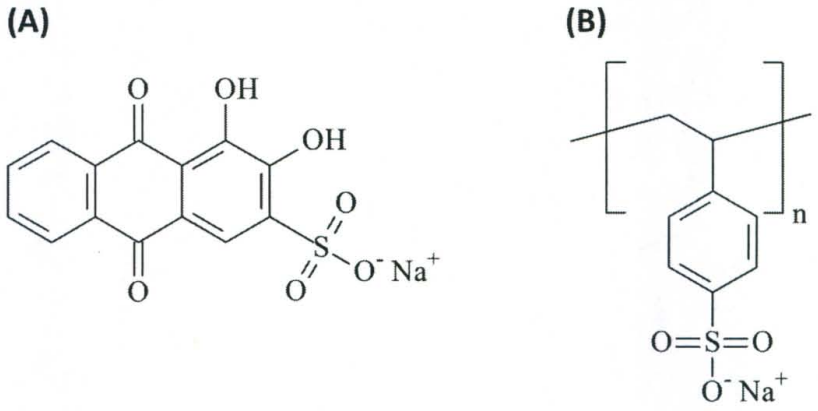

Fig. 3.1 Chemical structures for **A.** Alizarin Red S (ARS), **B.** poly (sodium 4-styrenesulfonate) (NaPSS)

PPy/PSS represents PPy films prepared from 0.1 M Py + 0.5 M poly(sodium 4-styrenesulfonate) (NaPSS).

A concentration of 2 mg mL^{-1} (ca. 0.006 M) was used for ARS due to its lower solubility in H_2O compared with the other used electrolytes.

3.2.4 Equipment

The electrochemical and impedance measurments were carried out using a Model 273A EG&G Potentiostat/Galvanostat and Model 5210 Lock-in Amplifier with Power-Suite commercial software. The measurements were performed over the range

of 10 kHz to 0.5 Hz with an ac amplitude of 10 mV at various dc potentials. A logarithmic scale was chosen over 20 points from high to low frequency. Impedance spectra were collected in the order of decreasing electrode potential from +0.2 V to -0.2 V at 0.1 V intervals, unless otherwise stated.

Scanning electron microscopy (SEM) imges and energy dispersive X-ray (EDX) spectra were obtained with a FEI Quanta 400 Enviromental SEM (ESEM) used in high-vacuum mode (i.e. not ESEM mode), and equiped with a Bruker XFlash 4010 SDD X-ray detector for acquiring elemental X-ray spectra with high effeciency, which can be used for qualitative elemental identification and semiquantitative analysis for any specific spot on the sample. The acceleration voltage was 20 keV, and the tungsten thermal emitter was biased for 80 μA emission current. The beam current (i.e. spot size) was adjusted for necessary resolving power. The Everhart-Thornley SE detector was used when necessary for imaging, and the working distance was 10 mm.

A Perkin Elmer AD-2Z model microbalance was used to measure the deposited mass of the polymers on Pt wires.

3.2.5 Ionic conductivity and capacitance

The impedance spectra for the ionic conductivity measurements were recorded in the order of decreasing potential. Each polymer film was used in only one type of electrolyte solution to avoid influences from its previous history. The ionic conductivity of the film (σ_{ion}) was calculated from:

$$\sigma_{ion} = d/(A * R_{ion}) \qquad [3.5]$$

Where **A** is the area of the electrode, **d** is the film thickness, and R_{ion} is the ionic resistance of the film, which is given by:

$$R_{ion} = 3(R_{low} - R_{high}) \quad [3.6]$$

where R_{low} is the real axis intercept of the almost vertical low-frequency region and R_{high} is the real axis intercept of high-frequency region (28; 29). Figure 3.2 illustrates how these values are taken from a Nyquist plot (imaginary impedance versus real impedance) for PPy/ClO_4^- in 0.2 M NaCl at -0.1 V.

The polymer film capacitance, or layer capacitance (C_L), were calculated using

$$C_L = \frac{-1}{\omega Z_{im}} \quad [3.7]$$

Where C_L has a unit of farad (F), ($\omega = 2\pi f$) is the angular frequency in radians per second, **f** is the frequency in hertz, and Z_{im} is the imaginary impedance in ohm. At the lowest frequency, C_L corresponds to the limiting capacitance of the polymer layer, because the redox reaction starts at the polymer/solution interface at high frequency and grows into the polymer film as the frequency decreases (28). The plots of series capacitance versus real impedance (Z_{re}) presented here are a convenient way to estimate and compare the limiting capacitances for different polymer films.

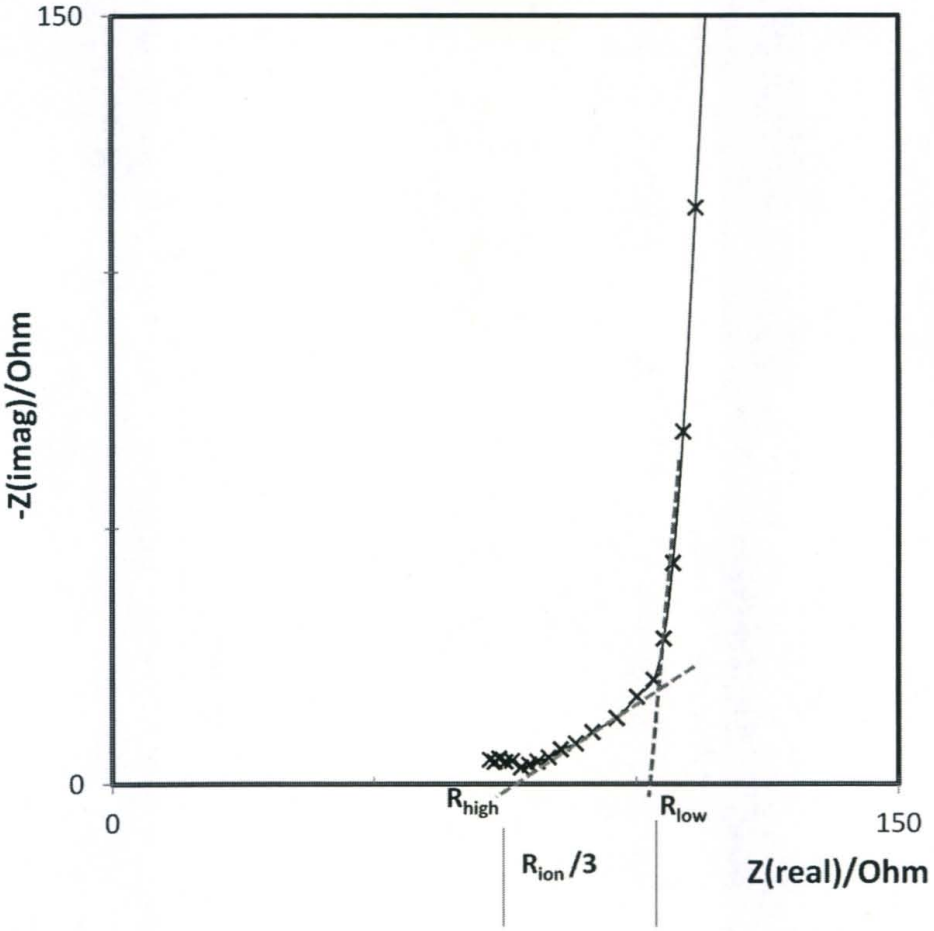

Fig. 3.2 Imaginary impedance versus real impedance plot for PPy/ClO_4^- measured at -0.1 V (vs. SCE) in 0.2 M NaCl.

3.3 Results and Discussion

3.3.1 Film characterization

3.3.1.1 Film thickness and mass

The polymerization conditions for all the polymer films used in this work are given in Table 3.1. The deposition rate and the polymerization charge were kept constant for each film, namely 0.3 mA and 0.018 C, respectively. The current and charge densities for the films deposited on glassy carbon (GC) electrodes with 0.071 cm^2 surface area were also kept constant at 4.2 mA cm^{-2} and 0.25 C cm^{-2}, respectively. A platinum wire with a diameter of 0.1 mm was used to determine the deposited masses for polymerization charges of 0.018 C. The weight of the platinum wire was measured before and after electrodeposition of the polymers by using a microbalance.

The film thickness was measured on GC electrodes and on Pt wires by using scanning electron microscopy (SEM). For GC electrode measurements, the films were scratched and tilted by 45° in order to measure the height of the grooves. The actual height was calculated by using the trigonometry equation for a right angle triangle, i.e. $\sin(45^\circ) = H_1/H_2$, where H_1 is the measured height and H_2 is the actual height, i.e. the opposite side over the hypotenuse, (Figure 3.3). For the Pt wire measurements, the width difference of the coated and uncoated parts of the wire divided by two gives the polymer film thickness. Figure 3.4 shows PPy/ClO_4^- films (A) on GC electrode and (B) on Pt wire. The dry film thickness of PPy/ClO_4^- on the GC electrode was found to be 1.05 μm, which agrees well with the result from reference (11). The conversion factor of 0.24

Table 3.1 Electropolymerization conditions and characterization of PPy films.

Film	[Py] (M)	Q_{pol} (C cm^{-2})[a]	E (V)[b]	d (μm)[c]	m_{expt} (μg)[d]	m_{theor} (μg)[e]	density (g cm^{-3})[f]
PPy/ClO_4	0.1	0.25	0.65	1.05	12	7.7	1.61
PPy/ARS	0.1	0.25	0.95	0.90	10	13	1.56
PPy/SO_4	0.1	0.25	0.65	1.14	10	6.4	1.24
PPy/PO_4	0.1	0.25	2.65[g]	0.21	2.5	6.0	1.68
PPy/PSS	0.1	0.25	0.65	1.39	13	9.7	1.32

[a] polymerization charge
[b] measured potential of steady state values during polymerization
[c] film thickness measured by using SEM on GC electrodes
[d] experimental mass deposited for 0.018 C polymerization charge on Pt wire
[e] theoretical mass calculated by using equation 3.8
[f] polymer layer density calculated using m_{expt}
[g] such a high potential value indicates a high resistance of the film due to a low doping level of trivalent anions

C cm^{-2} = 1.0 μm gave a value of 1.04 μm for polymerization charge of 0.25 C cm^{-2}. The skirt-like structure shown for the polymer layer at the interface between the coated and uncoated areas was observed for all polymer films grown on Pt wires. This behaviour is believed to be due to the surface-induced polymerization indicating that most of the polymer nucleation process occurs at the surface of the solution or at the interface between the solution and air.

The deposited mass was determined from the mass difference of a Pt wire (ca. length of 1 cm and diameter of 0.1 mm) before and after a deposition charge of 0.018 C

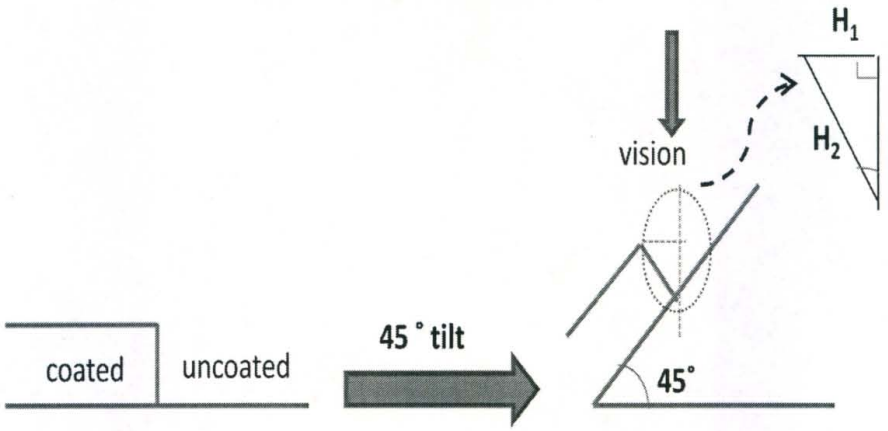

Fig. 3.3 Film thickness was measured on GC electrode by using sin (45°) = H_1/H_2, where H_1 is the measured height and H_2 is the actual height.

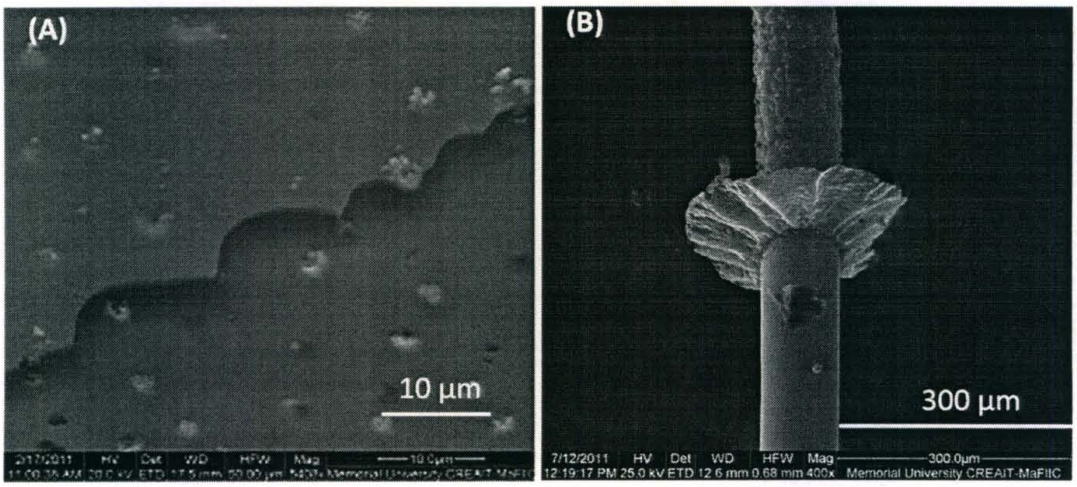

Fig. 3.4 SEM images for PPy/ClO_4^- films **A.** on GC electrode, the film is scratched and tilted by 45° to measure film thickness, **B.** on Pt wire at the junction of coated and uncoated part (skirt-like shape).

in the corresponding solution. The deposited mass was linearly proportional with the polymerization charge, i.e. mass deposition is additive. For example, the deposited masses for 0.018 C, 0.036 C, and 0.054 C polymerization charges were 12 μg, 25 μg, and 38 μg respectively for the PPy/ClO_4^- films.

The theoretical masses for 0.018 C deposition charges were calculated by using Faraday's law, Equation 3.8. The variations between the theoretical and experimental values are due to the propagation error resulting from subtracting two values with uncertainties of ±2 μg, and so the total error is ca. ±3 μg.

$$m = \frac{Q}{F}\frac{[MM_{Py}+(MM_{an}\, n_{doping}/Z_{an})]}{(2+n_{doping})} \qquad [3.8]$$

Where **m** is the deposited mass of the polymer in grams, **Q** is the polymerization charge (0.018 C), $\mathbf{MM_{Py}}$ is the molar mass of pyrrole in the polymer chain (65.1 g mol^{-1}), $\mathbf{MM_{an}}$ is the molar mass of the anion used for electropolymerization, $\mathbf{n_{doping}}$ is the number of electrons used for the doping process (i.e. doping level), $\mathbf{Z_{an}}$ is the charge of the anion, **F** is the Faraday constant (96,485 C mol^{-1}), and $\mathbf{2+n_{doping}}$ is the number of electrons consumed during polymerization (typically 2.3, 2 electrons for the coupling step and 0.3 electron for the partial reversible oxidation or doping).

Although the charge density used for deposition of all films was the same (i.e. 0.25 C cm^{-2}), the film thickness and the deposited mass varied for the different electrolyte solutions. The relationship between the film thicknesses and deposited masses is shown in Figure 3.5. All the films fall into an average value of 1 μm thickness

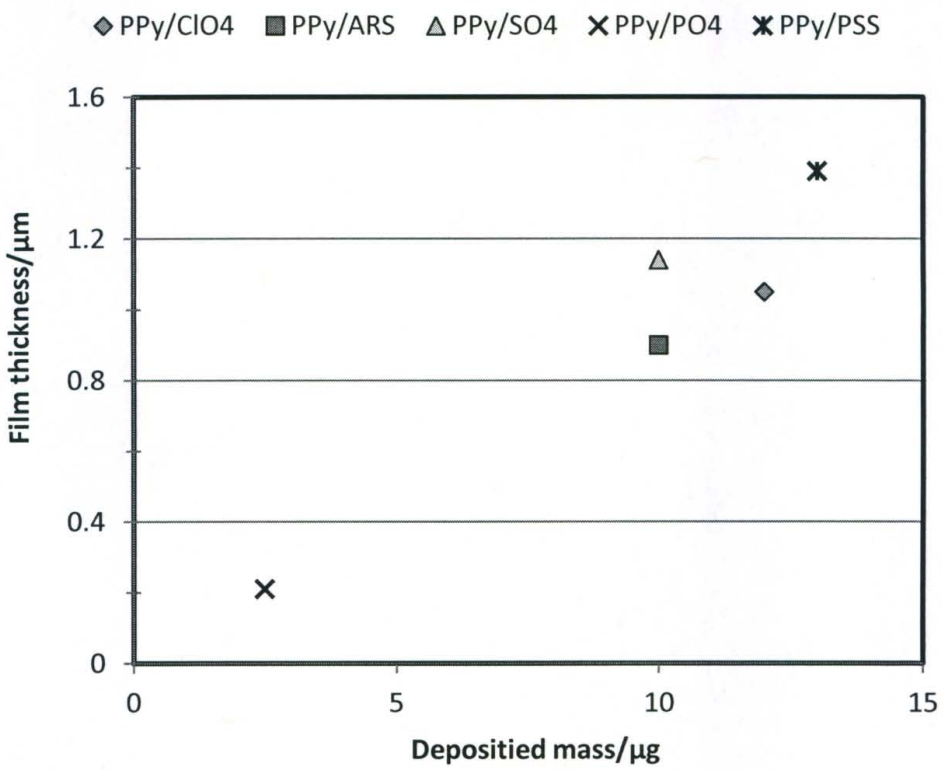

Fig. 3.5 Relationship between the film thickness and deposited mass of PPy films.

and 11 μg deposited mass, except for PPy/PO_4^{3-} which has significantly lower values indicating low polymerization efficiency with the trivalent anions.

3.3.1.2 Film morphology and composition

Scanning electron microscopy (SEM) and energy dispersive x-ray spectroscopy (EDX) have been used to probe the surface morphology and elemental composition of the polymer films. Aluminum (Al) was observed in some EDX spectra for the polymer films. The source of Al in the EDX spectra came from aluminum oxide (Al_2O_3) which was used for polishing the GC electrode surface, and indicates that Al_2O_3 was trapped into the carbon layer.

Figure 3.6 shows SEM images of the polymer films deposited on Pt wires. The polymer films doped with ClO_4^-, ARS, SO_4^{2-}, PO_4^{3-}, and PSS are shown from (A) to (E), respectively. PPy/ClO_4^- shows an uneven surface with large granules. ARS shows a porous surface with very small granules. PPy/SO_4^{2-} shows very few granules of medium size; an extended polymer layer is shown at the bottom of the image which was grown at the interface between the coated and uncoated areas of the wire. PPy/PO_4^{3-} shows aggregation areas in some parts of the film revealing that the presence of the trivalent anions was responsible for the dense nature of the polymer chains as shown in Table 3.1. PPy/PSS shows a smooth surface of the composite film indicating that the two polymer matrices of opposite charges combine in highly ordered structure. Comparing the SEM images for the polymer films with different anions, it can be concluded that the

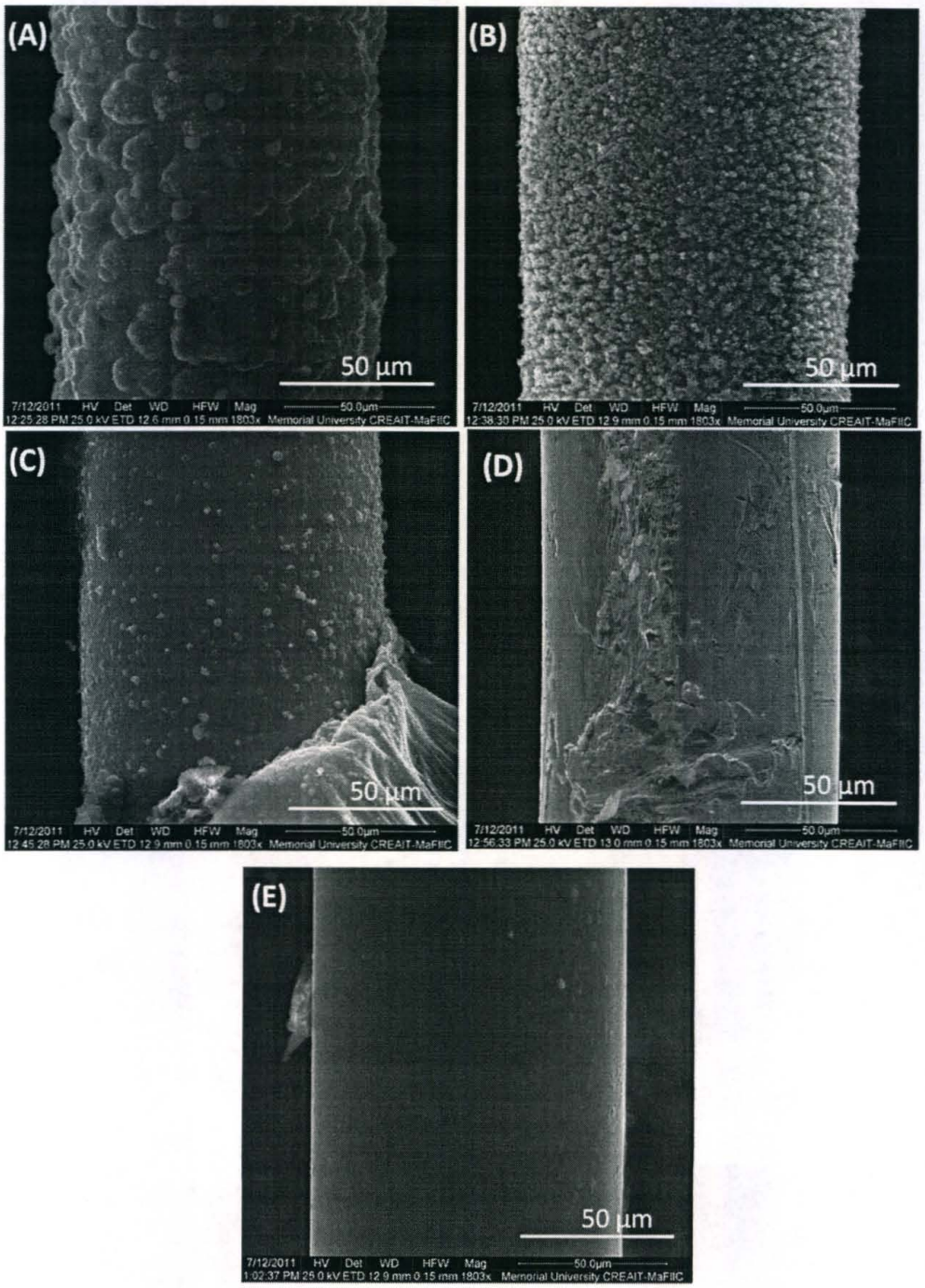

Fig. 3.6 SEM images for PPy films on Pt wires: **A.** PPy/ClO_4 **B.** PPy/ARS **C.** PPy/SO_4 **D.** PPy/PO_4 and **E.** PPy/PSS.

surface of each film is significantly influenced by the dopant anions used for the electropolymerization.

The morphology on GC electrodes is shown in Figure 3.7 for (A) PPy/SO_4^{2-} and (B) PPy/ARS. Both of them show ring morphology, where the former shows bigger rings of various sizes and the latter shows smaller rings of equal sizes. When the surface of the PPy/ARS is tilted by 45°, its enlarged SEM image showed an interesting volcano morphology with an uneven surface (Figure 3.7-C). This type of morphology could be responsible for its enhanced ion transport behaviour described below.

Figure 3.8 shows SEM images of four PPy/ClO_4^- films on GC electrodes prepared in the same way and then equilibrated in $NaClO_4$ as follows: (A) as-prepared, (B) potential cycled between +0.5 V and -1.0 V at 0.1 V s^{-1}, (C) polarized at +0.2 V for one minute, and (D) polarized at -0.2 V for one minute. The different equilibration conditions resulted in distinct morphologies indicating that the polymer films restructure as a result of gaining or losing different electrolyte ions. The as-prepared and 0.2 V polarized films (A and C) show similar morphologies with granules of various sizes, which indicates that the deposited film is in its oxidized state. However, cycling the film between its oxidized and reduced states results in a smooth morphology; reducing the film at -0.2 V results in a morphology with bigger granules. These changes in the surface morphology of the polymer films reveal ion transport influences the structure of the film.

Figures 3.9 and 3.10 show EDX spectra of polymer films on GC electrodes. The films had been cycled three times between 0.5 V and -1.0 V in $NaClO_4$ at 0.1 V s^{-1} before

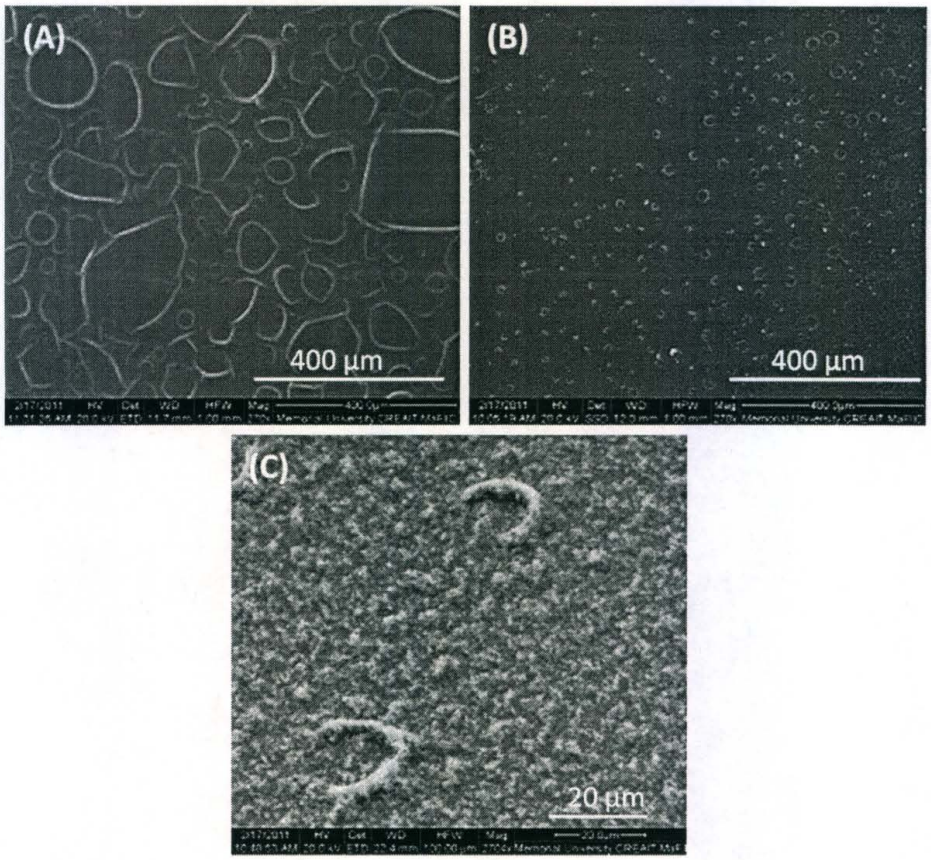

Fig. 3.7 SEM images for PPy films on GC electrodes for **A.** PPy/SO_4^{2-} **B.** PPy/ARS, and **C.** Magnified image of PPy/ARS tilted by 45˚.

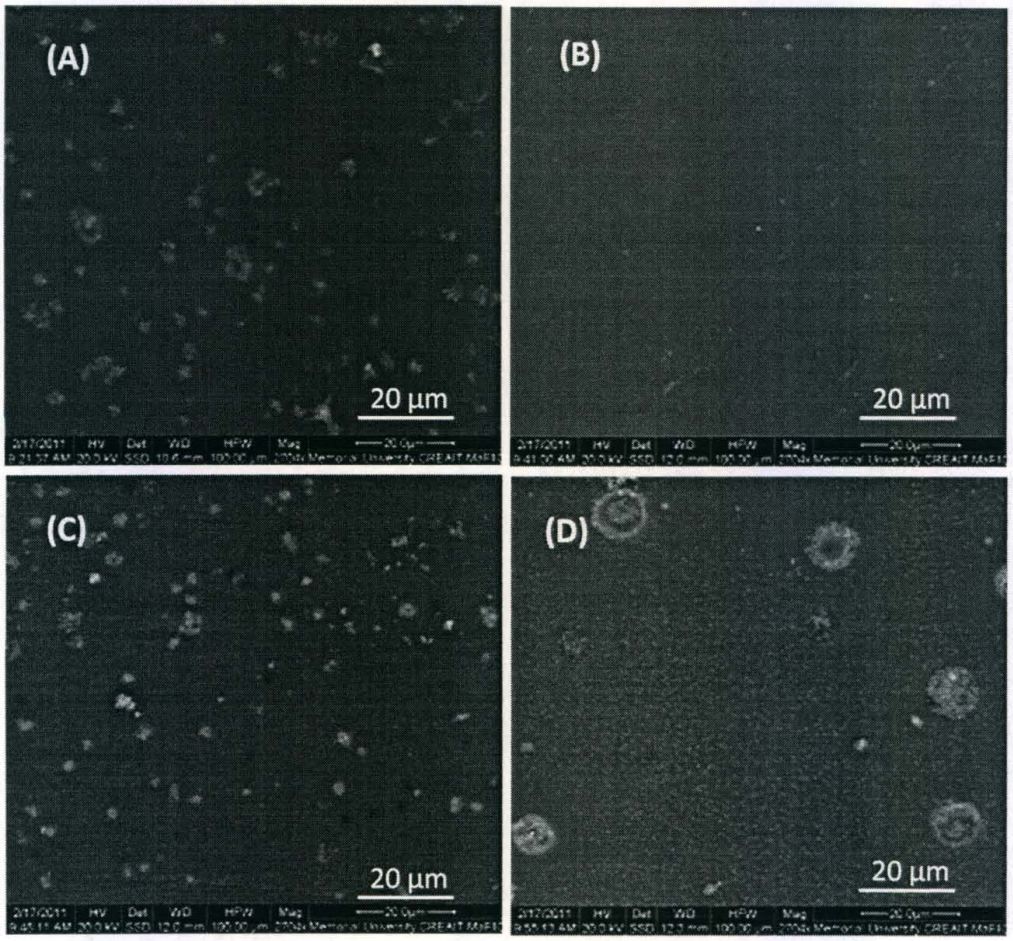

Fig. 3.8 SEM images for PPy/ClO_4^- films prepared in the same way on GC electrodes and then polarized in $NaClO_4$; **A.** as-prepared, **B.** cycled, **C.** polarized at +0.2 V, and **D.** polarized at -0.2 V.

the measurements to bring the films to the same conditions. PPy/PSS shows the highest sulfur content due to immobilized polystyrene sulfonate (PSS) in the polymer matrix. PPy/ARS also shows some content of sulfur, but the high amount of chlorine indicates anion exchange between ARS and ClO_4^-, i.e. high Cl/S ratio. From Figure 3.10, the PPy/PO_4^{3-} film shows various amounts of phosphorus at different locations of the film indicating that the dopant anions (i.e. PO_4^{3-}) are unevenly distributed over the film, which can be attributed to the low doping level. Sulfur was detected in PPy/PO_4^{3-}, presumably this is related to the presence of Al_2O_3, i.e. impurity. Table 3.2 summarizes the SEM and EDX data.

From Table 3.2, the high amount of Cl^- and Na^+ in PPy/ARS and PPy/SO_4^{2-} after cycling in $NaClO_4$ indicates mixed ion transport behaviour described below. The high Na^+/Cl^- ratio in PPy/PO_4^{3-} indicates cation transport mechanism which also indicated by the impedance results described below.

Table 3.2 Surface morphology and elemental compositions for PPy films.

		Content (eV)[a]			
Film	**Morphology[b]**	**Na**	**S**	**Cl**	**P**
PPy/ClO_4^-	large granules	0.5	---	2.0	---
PPy/ARS	porous	4.5	2.5	4.8	---
PPy/SO_4^{2-}	few granules	2.3	2.2	3.5	---
PPy/PO_4^{3-}	aggregation	6+[c]	2.3	---	4+[c]
PPy/PSS	smooth	0.9	4.8	1.7	---

[a] the concentration of the content is described as count per second (CPS) with eV unit.
[b] on Pt wires
[c] vary with different positions

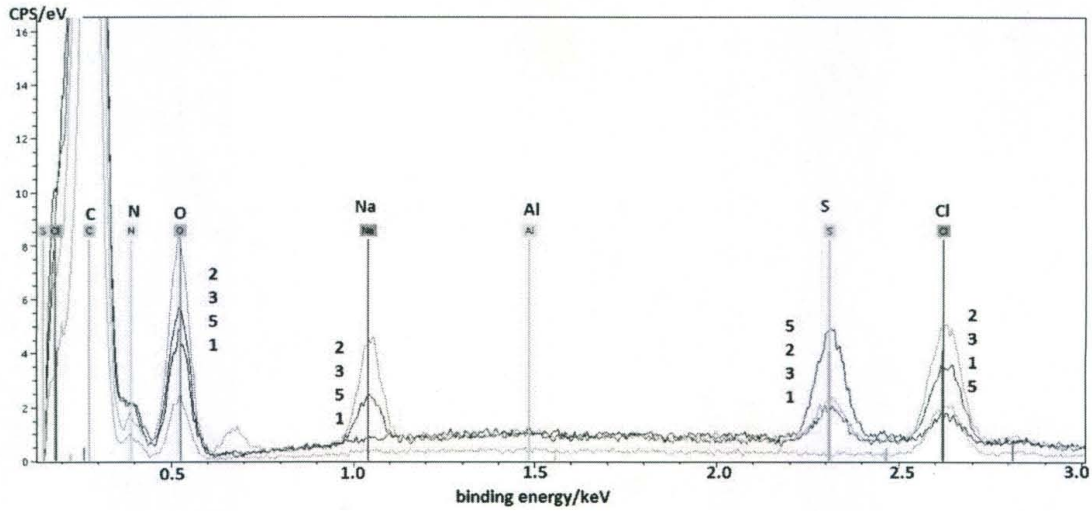

Fig. 3.9 EDX spectra for PPy films on GC electrodes; films were cycled three times in 0.2 M $NaClO_4$ before the measurements were taken; **1.** PPy/ClO_4, **2.** PPy/ARS, **3.** PPy/SO_4, and **5.** PPy/PSS.

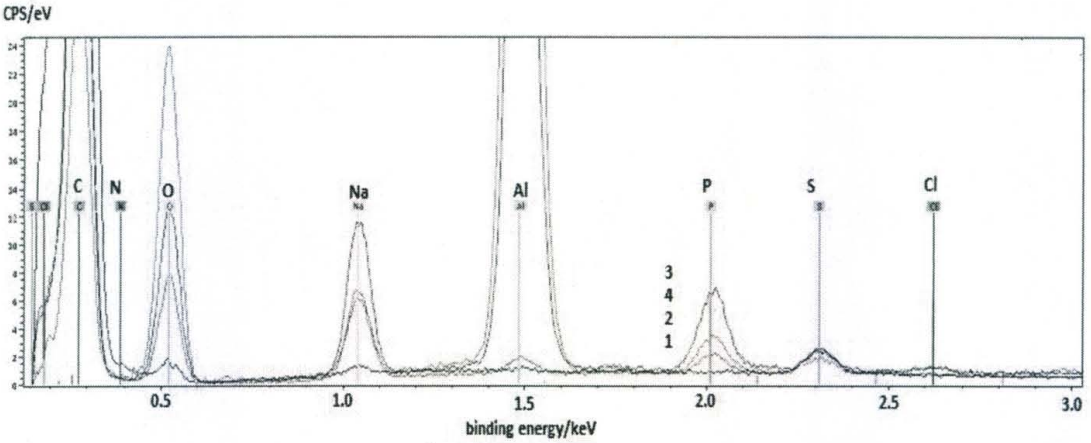

Fig. 3.10 EDX spectra for PPy/PO_4^{3-} film on a GC electrode showing various phosphate amounts at different positions of the film (1,2,3, and 4 are different positions where measurements were taken). Films were cycled three times in 0.2 M $NaClO_4$ before the measurements were taken.

3.3.2 Cyclic voltammetry

Cyclic voltammetry was used to probe the ion transport properties of the polypyrrole (PPy) films, which reveals useful thermodynamic and kinetic information. Because cyclic voltammetry is a dynamic technique (i.e. describes changes over time), kinetic information can be extracted from the voltammograms in addition to thermodynamic information. The thermodynamic properties, such as the formal potential (E°), can be determined from reversible peaks where the ratio of the cathodic peak current (i_{pc}) to anodic peak current (i_{pa}) equals one. The kinetics of electron transfer and the nature of any chemical process coupled with the electron transfer can be determined from semi-reversible peaks (i.e. $i_{pc}/i_{pa} > 1$).

Counterions can be inserted into a polymer matrix during the electropolymerization to compensate for the partial reversible oxidation of the polymer, because the potential used for polymerization of the monomers is sufficient for doping to occur. They can also be inserted during the switching process to balance the electrogenerated charges on the polymer backbone, i.e. switching between doped and undoped states. Co-ions can be inserted into a polymer matrix during the switching process if the counterions are fully or partially bound to the polymer chains, i.e. self-doped polymers. In the case where polymers are formed by oxidative coupling, such as polypyrrole, the counterions are anions and the co-ions are cations.

The typical voltammograms of PPy films show electrochemical hysteresis between the anodic and cathodic peaks with the former being sharper than the latter.

Such hysteresis has been attributed to difficulty in oxidizing the reduced form (i.e. insulating), which requires an overpotential. Such an overpotential has a kinetic origin and results in a rapid oxidation process shown as a sharp anodic peak at a more positive potential. There are two processes that occur during such oxidation; electron transfer at the polymer/electrode interface and anion transport at the polymer/solution interface. The latter involves a nucleation type process as the anions move from the solution phase to the solid phase (30).

Herein, five different PPy films were chosen based on the size and charge of their dopant anions. The PPy films used in this work can be divided into two groups. First, PPy films prepared with ClO_4^-, ARS, and PSS represent small, medium, and large dopant anions, respectively. Second, PPy films prepared with ClO_4^-, SO_4^{2-}, and PO_4^{3-} represent uni-, di-, and tri-valent dopant anions, respectively. Cyclic voltammograms (CVs) of PPy films were very stable to cycling between +0.5 V and -1.0 V at various scan rates in the electrolyte solutions used in this work.

3.3.2.1 Influence of size and charge of dopant anions

Figure 3.11 shows second cycle voltammograms at 0.1 V s^{-1} for PPy films deposited with various dopant anions, and then redoped (i.e. placed in different electrolyte for measurement) in 0.2 M NaCl. Since the first cycle of a voltammogram is usually influenced by the previous history of the film, the second cycle is shown here to illustrate the steady state behaviour. The distinct voltammograms of these PPy films

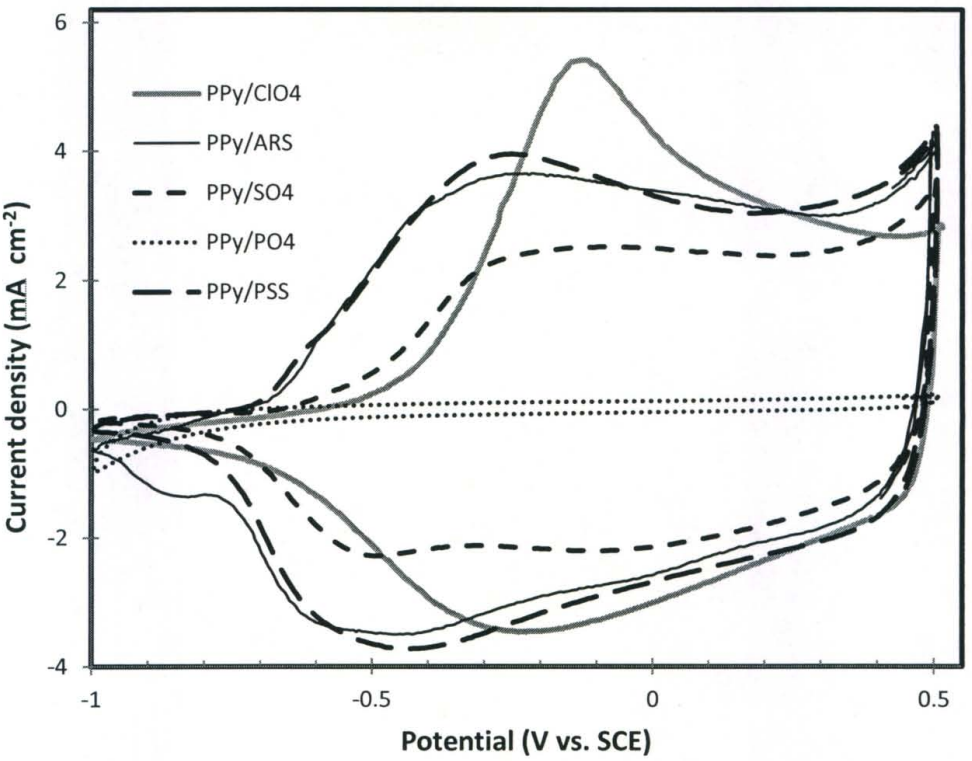

Fig. 3.11 Cyclic voltammograms (2^{nd} cycles) at 0.1 V s^{-1} of the five PPy films in 0.2 M NaCl.

reveal significant differences in the ion transport properties of each film, suggesting that charge compensation follows different mechanisms for each film. PPy/ClO_4^- exhibited a typical CV for PPy films, characterized by a broad cathodic peak and sharper anodic peak at ca. -0.2 V. PPy/ARS and PPy/PSS exhibited similar characteristic CVs indicating similar ion transport properties for each film presumably due to localization of the dopant anions. The film with the divalent anion (i.e. PPy/SO_4^{2-}) shows a CV characterized by two cathodic peaks at ca. 0 V and -0.5 V. The film of the trivalent anion (i.e. PPy/PO_4^{3-}) shows a featureless CV with a small cathodic peak at ca. -0.9 V.

From Figure 3.11, it is clearly shown that the size and the charge of the dopant anion incorporated into the polymer films during polymerization significantly influence the electrochemical behaviour of the films even though they were all redoped in the same electrolyte solution. In another word, although ion exchange processes may take place in these films to form PPy/Cl^-, the original dopant anion of each film affects the ion transport properties of the film to a significant extent. These distinct properties were further probed by cyclic voltammetry and impedance spectroscopy to elucidate the key factors behind such behaviours.

3.3.2.2 Transient cation insertion

It has been reported that the irreversible cathodic peak at ca. -0.8 V that appears in addition to the main redox peak at ca. -0.2 V for polypyrrole films doped with ClO_4^- (i.e. PPy/ClO_4^-) is due to transient cation insertion. However, there is no comprehensive

understanding for such peaks (28). The presence and absence of such peaks provide valuable kinetic information which helps to understand the ion transport properties.

Figure 3.12 shows the first cycles of voltammograms for PPy/ClO_4^- films in 0.2 M electrolytes ($NaClO_4$ and NaCl) at 0.1 V s^{-1}. Both films were prepared in the same way and the starting potential was 0.5 V. It can be seen that an irreversible cathodic peak for PPy/ClO_4^- at ca. -0.8 V appears in $NaClO_4$ but not in NaCl. Typically, the charge compensation mechanism of a PPy film is maintained by anion transport during the electrochemical switching between the oxidized (doped) and reduced (undoped) states. However, cations can be involved in the switching process under certain conditions, such as localization of large dopant anions in polymer matrices. In such cases, cations from the external electrolyte solutions can become the mobile ions for the electrochemical switching between doped and undoped states. In addition, cation transport can partially be involved in the switching process if the dopant anions have low mobility due to a kinetic factor, such as steric effects or ion-polymer interactions. The cation insertion is shown here as a reduction peak at -0.8 V indicating that anion transport is unable to fulfill the charge compensation due to low mobility of ClO_4^- inside the PPy matrix. This explanation has been proven by redoping PPy/ClO_4^- in NaCl solution, which results in disappearance of the reduction peak. Thus, the smaller counterions (Cl^-) can better maintain the charge compensation compared with ClO_4^- due to its fast mobility inside the PPy matrix (Figure 3.12). It is believed that the ion exchange process shown in Equation 3.9 occurs once the film is exposed to NaCl solution (31; 19).

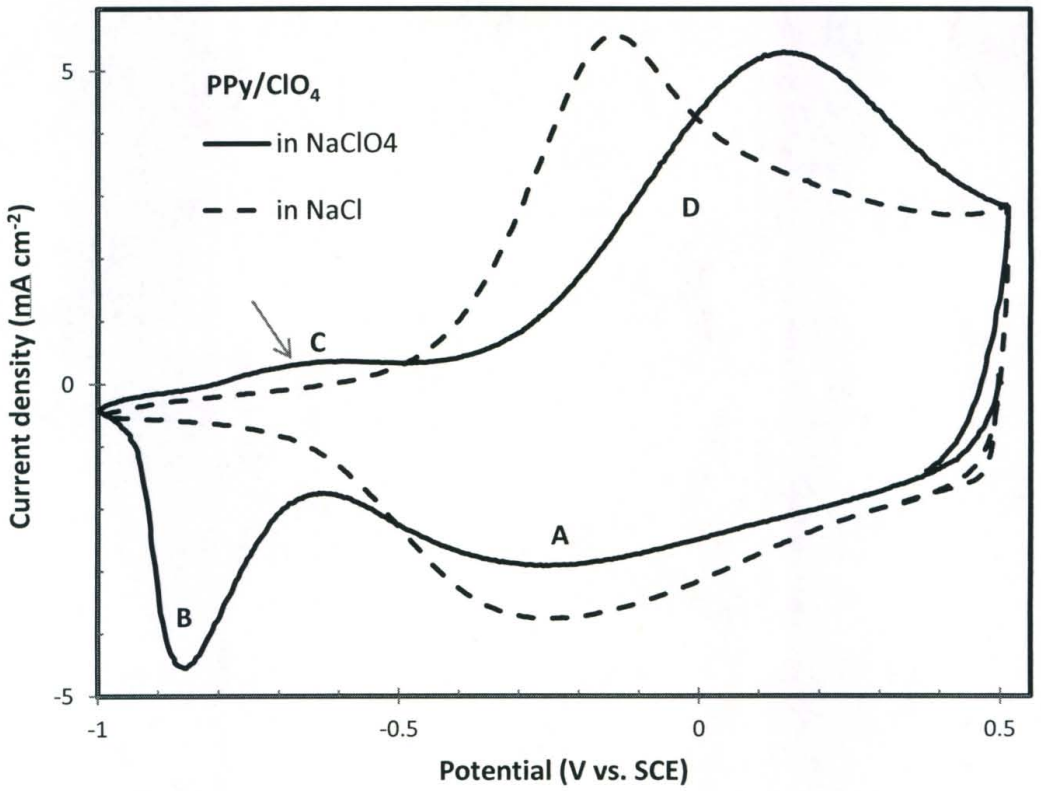

Fig. 3.12 Cyclic voltammograms (1st cycles) at 0.1 V s^{-1} for PPy/ClO_4^- films in 0.2 M electrolytes as indicated. Both films were prepared in the same way. Initial potential 0.5 V.

$$PPy\text{-}ClO_4^- + Cl^-_{(sol)} \rightarrow PPy\text{-}Cl^- + ClO_4^-_{(sol)} \quad [3.9]$$

There are two main factors affecting the mobility of the counterions inside polymer matrices, namely the size of the counterion and its interactions with the polymer charges. Comparing ClO_4^- versus Cl^-, ClO_4^- has a radius of 0.236 nm with a polyatomic tetrahedral structure and Cl^- has a radius of 0.181 nm with a spherical structure. The different charge distributions for these two anions result in different interactions with the polymer charges. The hard anion (Cl^-) has weak interactions with the soft oxidized pyrrole units. However, the perchlorate ion has stronger interactions with the PPy chains since the structure and size of the perchlorate ion make it appropriate to hydrogen bond with four pyrrole units, between the oxygen of ClO_4^- and the hydrogen of the pyrrole N-H group (32). Thus, ClO_4^- has lower mobility than Cl^- inside the PPy matrix, which can explain why the hysteresis for the PPy/ClO_4^- films is more pronounced in $NaClO_4$ compared with NaCl (Figure 3.12).

Two ion transport processes can take place for PPy/ClO_4^- films in NaCl, after the film becomes PPy/Cl^- by spontaneous ion exchange. From Figure 3.12, **A** is anion expulsion (Cl^-) and **D** is anion insertion (Cl^-). The proposed electrochemical equations for these two processes can be represented by;

$$\textbf{A. } (PPy)^+ Cl^- + e^- \rightarrow (PPy)^0 + Cl^- \quad [3.10]$$

$$\textbf{D. } (PPy)^0 + Cl^- \rightarrow (PPy)^+ Cl^- + e^- \quad [3.11]$$

In contrast, four distinct ion transport processes can take place for PPy/ClO_4^- films in $NaClO_4$, indicated in Figure 3.12 as: **A**, anion expulsion (ClO_4^-); **B**, cation insertion

(Na^+); **C**, cation expulsion (Na^+); and **D**, anion insertion (ClO_4^-). The proposed electrochemical equations for these processes can be represented by;

$$\textbf{A. } (PPy)^+(ClO_4^-) + e^- \rightarrow (PPy)^{(1-x)+}(ClO_4^-)_{(1-x)} + x(ClO_4^-) \quad [3.12]$$

$$\textbf{B. } (PPy)^+ ClO_4^- + Na^+ + e^- \rightarrow (PPy)^0 ClO_4^- Na^+ \quad [3.13]$$

$$\textbf{C. } (PPy)^0 ClO_4^- Na^+ \rightarrow (PPy)^+ ClO_4^- + Na^+ + e^- \quad [3.14]$$

$$\textbf{D. } (PPy)^0 ClO_4^- Na^+ + ClO_4^- \rightarrow (PPy)^+(ClO_4^-)_2 Na^+ + e^- \quad [3.15]$$

Where **PPy** represents a segment of a polymer chain for polypyrrole or any conducting polymer; and **x** (from 0 to 1) represents the oxidation level and indicates that some dopant anions stay in the polymer matrix. Equation **A** is written for any charge ratio, but the other equations are taken for **x** equals zero for simplicity.

A and **D** are anion transport; **B** and **C** are cation transport. The slow Na^+ ejection resulting in charge trapping is due to ion pair formation with the original dopant anions. Thus, both Na^+ and ClO_4^- stay inside the PPy matrix as non-exchange electrolyte. In addition, the film has two main structures for the reduced form (31), i.e. partially reduced form $(PPy)^{(1-x)+}(ClO_4^-)_{(1-x)}$ and fully reduced form $(PPy)^0 ClO_4^- Na^+$. It can be noticed from Figure 3.12 that the cathodic peak associated with anion expulsion (peak **A**) is bigger in NaCl than $NaClO_4$. This indicates that the film is partially reduced in $NaClO_4$, and becomes fully reduced after cation insertion.

The second reduction peak has been further probed by cycling PPy/ClO_4^- between 0.5 V and -1.0 V in $NaClO_4$ which results in deactivation of the cathodic peak

associated with Na^+ insertion (Figure 3.13). This peak was regenerated by polarizing at 0.5 V for 5 minutes. The CV after the polarization shows a peak shift to less negative potential indicating restructuring or relaxation of the polymer chains during the potential cycling (10; 33).

In contrast to PPy/ClO_4^-, PPy/ARS exhibited no or very little transient cation insertion in either NaCl or $NaClO_4$, which indicates enhanced anion transport (Figure 3.14). This behaviour can be attributed to the porous morphology as shown by the SEM results (Figures 3.6-B and 3.7-C). The multi redox peaks in $NaClO_4$ suggest contributions from various ions during the potential scan. Presumably, the large dopant anions incorporated during the electropolymerization have a significant influence on the structure of the polymer film causing the enhanced ion transport, while large counterions inserted into the polymer film after the deposition of the film can hinder ion transport (i.e. the case of PPy/ClO_4^- in $NaClO_4$). As a result, it can be concluded from the results of CVs and EDX spectra that a large dopant anion (e.g. ARS) with weak ion-polymer interactions can undergo partial ion-exchange with counterions from the external electrolyte solution (Figure 3.9 for EDX spectra).

It has been shown that PPy films doped with univalent anions (i.e. ClO_4^-) exhibit transient cation insertion in order to overcome the slow mobility of the counterions (28). However, when the same film is redoped with smaller counterions (e.g. Cl^-), the film maintains its electroneutrality without the need for cation uptake due to the fast mobility of the counterions. In contrast, polymer films doped with larger dopant anions

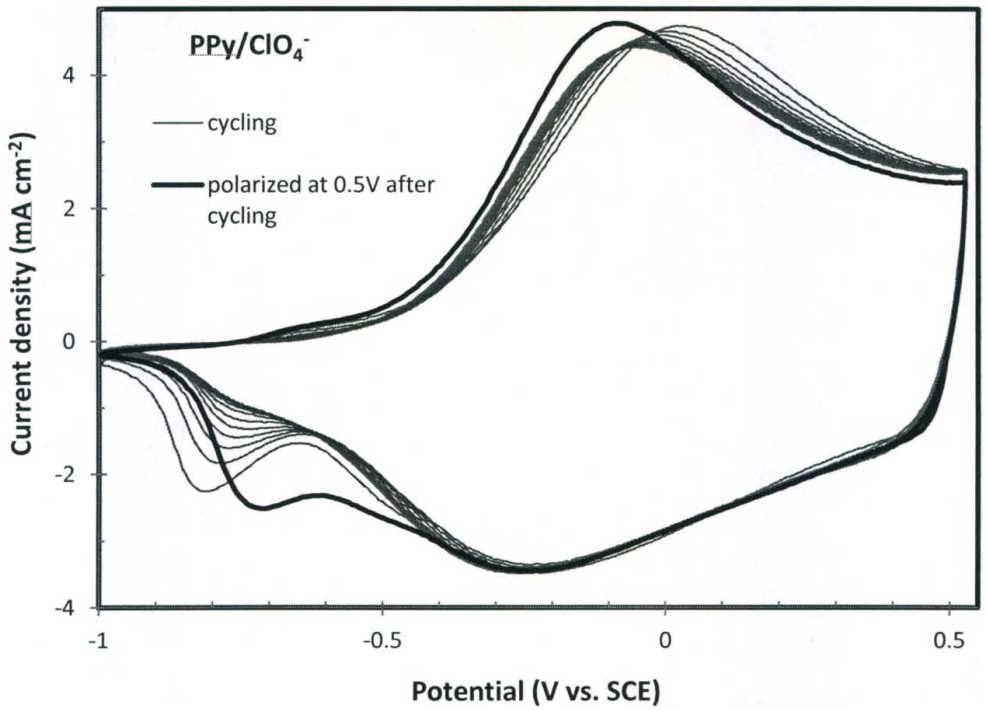

Fig. 3.13 Cyclic voltammograms at 0.1 V s^{-1} for PPy/ClO_4^- films in 0.2 M $NaClO_4$. The film was first cycled ten times between 0.5 V and -1.0 V (thin line), then polarized at 0.5 V for 5 minutes to remove any trapped charges, finally a CV was taken again with the same settings (thick line).

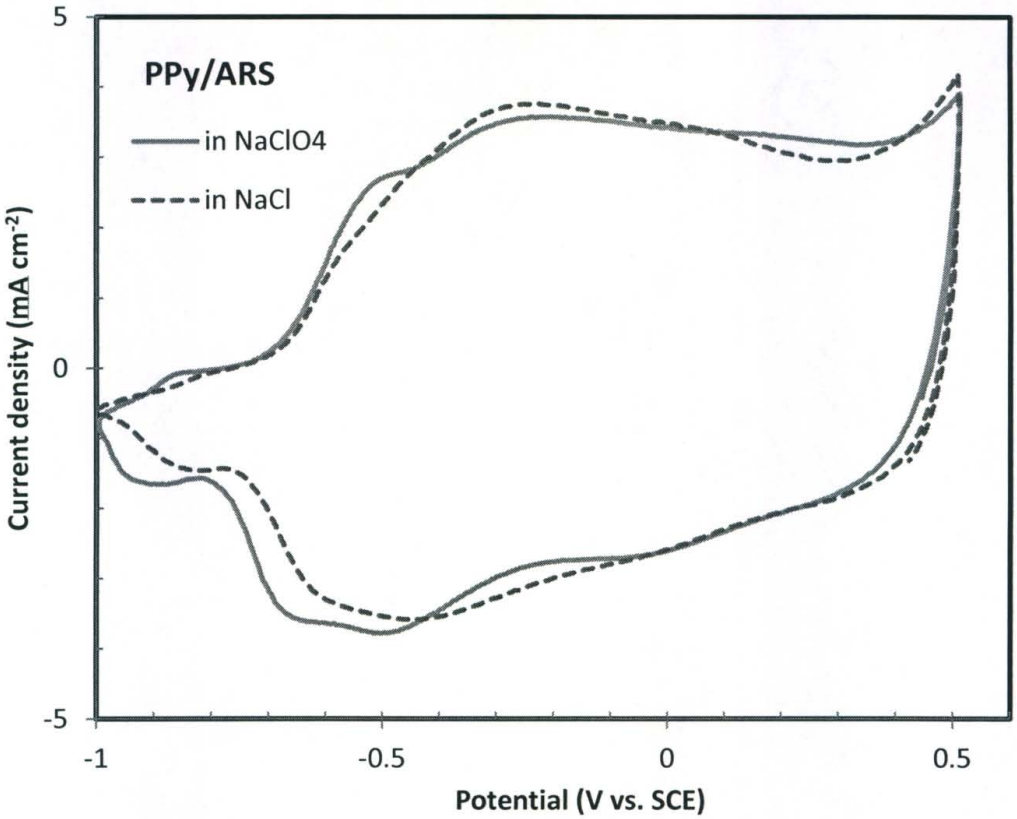

Fig. 3.14 Cyclic voltammograms (2nd cycles) at 0.1 V s^{-1} for PPy/ARS films in 0.2 M electrolytes as indicated. Both films were prepared in the same way. Initial potential 0.5 V.

(e.g. ARS, weak ion-polymer interactions) during the electropolymerization exhibit porous morphology and enhanced ion transport.

3.3.2.3 Overpotential on the first scan

Figure 3.15 shows CVs of PPy/SO_4^{2-} films for the first three consecutive cycles in two different electrolytes, namely NaCl and $NaClO_4$. In both cases, the first cycle started at +0.5 V in the cathodic direction was different from the subsequent cycles with sharp cathodic peaks at ca. -0.7 V to -0.9 V. Another feature of the first cycle is the absence of the main cathodic wave at ca. -0.2 V which can be seen in the subsequent cycles.

Large overpotentials are generally observed on the first cathodic scan, which cause the cathodic peak to be shifted to more negative potentials with usually large currents. It has been reported that such overpotentials result in cation uptake causing a large increase in the ionic conductivity and structural changes of the polymer chains (34; 35; 36). A large overpotential was clearly observed for the PPy films doped with divalent anions (e.g. SO_4^{2-}) owing to ion-polymer interactions which hinder the mobility of the dopant anions. Such hindrance results in absence of the main reduction wave on the first cycle. However, after re-oxidation takes place in the NaCl electrolyte, the overpotential disappears in the subsequent cycles and the main reduction peak appears. The ion-polymer interactions for the divalent anions are stronger than for univalent anions, because the divalent anions are surrounded by more monomer units to balance their charge. Typically, every three to five pyrrole units can hold one negative charge, and so six to ten pyrrole units can hold either two univalent anions or one divalent

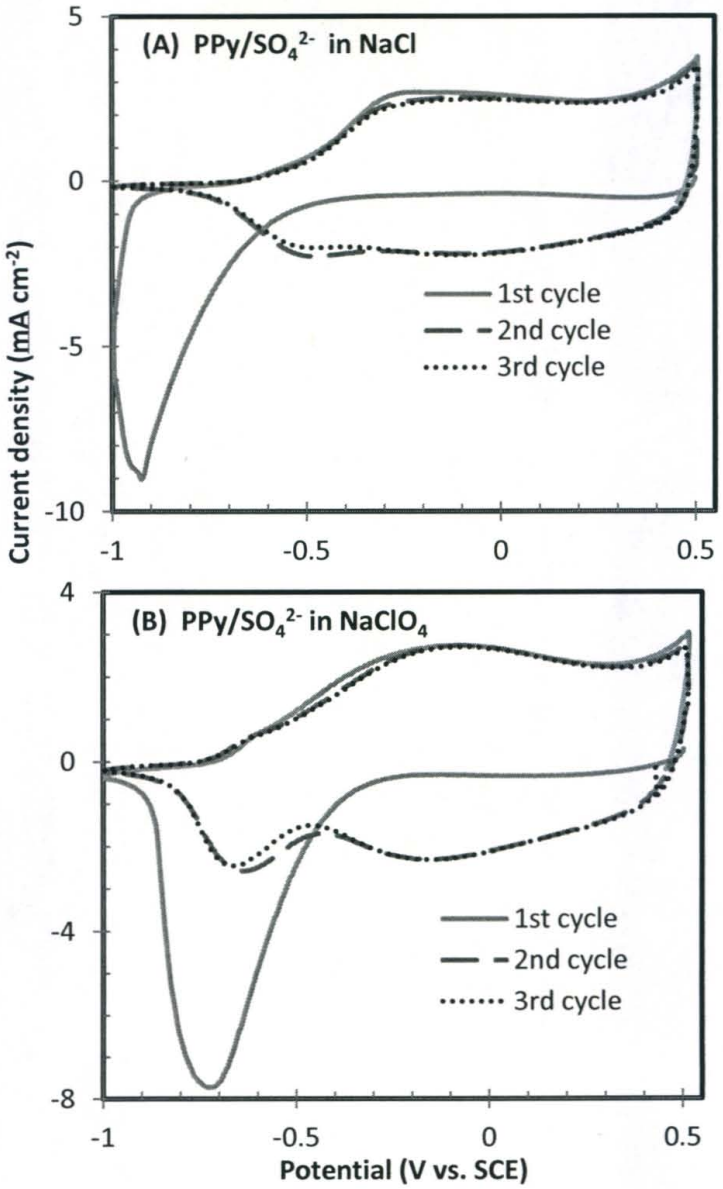

Fig. 3.15 The first three cycles of PPy/SO_4^{2-} voltammograms at 0.1 V s^{-1} in 0.2 M of; **A.** NaCl, **B.** $NaClO_4$. Initial potential 0.5 V.

anion. Thus, divalent anions are bound more strongly to the polymer matrix than univalent anions.

When PPy/SO_4^{2-} is redoped in NaCl solution, a slow ion exchange process is expected to take place where the univalent anions replace the divalent anions (i.e. Equation 3.16 has small equilibrium constant, K_{eq}). This is because SO_4^{2-} is bound strongly to the PPy matrix, and so the ion exchange is presumably slow. The absence of the main reduction wave at -0.2 V on the first scan indicates that SO_4^{2-} was not expelled. In addition, the appearance of a new reduction peak at a lower potential (ca. -0.8V) indicates that the electroneutrality of the film was preserved by cation uptake from the electrolyte solution. As a result, the original dopant anions form ion pairs with the electrolyte cations and stay inside the polymer matrix as a non-exchange electrolyte (i.e. $Na_2SO_4(aq)$). This can be concluded because the cation uptake peak at ca. -0.8 V has no counterpart peak (i.e. irreversible peak) indicating that the cations are trapped in the film due to the ion pair formation.

$$(PPy)^{2+}SO_4^{2-} + 2\,Cl^- \rightleftharpoons (PPy)^{2+}(Cl^-)_2 + SO_4^{2-} \qquad [3.16]$$

The ion transport process during the first cycle for PPy/SO_4^{2-} is believed to take place in NaCl solution according to Equations 3.17 and 3.18. For the subsequent cycles, only Cl^- insertion and expulsion are taking place, Equation 3.19.

$$(PPy)^{2+}SO_4^{2-} + 2x\,Na^+ + 2x\,e^- \rightarrow (PPy)^0(SO_4^{2-})_{(1-x)}(Na^+)_{2x} + x\,(SO_4^{2-}) \qquad [3.17]$$

$$(PPy)^0(SO_4^{2-})_{(1-x)}\,(Na^+)_{2x} + 2\,Cl^- \rightarrow (PPy)^{2+}(Cl^-)_2\text{-}(Na_2SO_4)_{pore} + 2x\,e^- \qquad [3.18]$$

$$(PPy)^0\text{-}(Na_2SO_4)_{pore} + 2\,Cl^- \rightleftharpoons (PPy)^{2+}(Cl^-)_2\text{-}(Na_2SO_4)_{pore} + 2\,e^- \qquad [3.19]$$

There is only partial ion exchange taking place as indicated by equation 3.17 where **x** indicates the amount of the original dopant anions which are removed. In contrast, the film becomes $\mathbf{(PPy)^{2+}(ClO_4)_2^{2-}\text{-}(Na_2SO_4)_{pore}}$ after the first scan in $NaClO_4$ solution and the ion transport will follow the same electrochemical behaviour with transient cation insertion (i.e. cation uptake at low potential) to overcome the low mobility of the counterions (i.e. ClO_4^-). This can be concluded from the presence of the second reduction wave at ca. -0.6 V in $NaClO_4$ for the subsequent cycles. In both cases, ion-polymer interactions for the divalent anions result in an overpotential on the first scan, causing cation uptake from the electrolyte solution.

3.3.2.4 Scan rate dependence

Further insight into the ion transport properties of the polymer films can be obtained from scan rate dependence experiments. Changing the scan rate while taking CV measurements over a fixed potential window was used to test the thermodynamic and kinetic control of each peak. Under thermodynamic control, the peak shape should not change with changing scan rate. However, the peak shape is changed with changing scan rate under kinetic control. Since the electroactive material (i.e. the polymer film) is immobilized on the electrode surface, the charged species (i.e. electrolyte ions) in the solution are responsible for any mode of mass transport (i.e. diffusion and/or migration).

The results of scan rate dependence experiments are shown in Figure 3.16 for four films doped with different anions, namely ClO_4^-, ARS, SO_4^{2-}, and PSS^-. The trivalent anion (i.e. PO_4^{3-}) has been excluded due to the high film resistance, causing very low

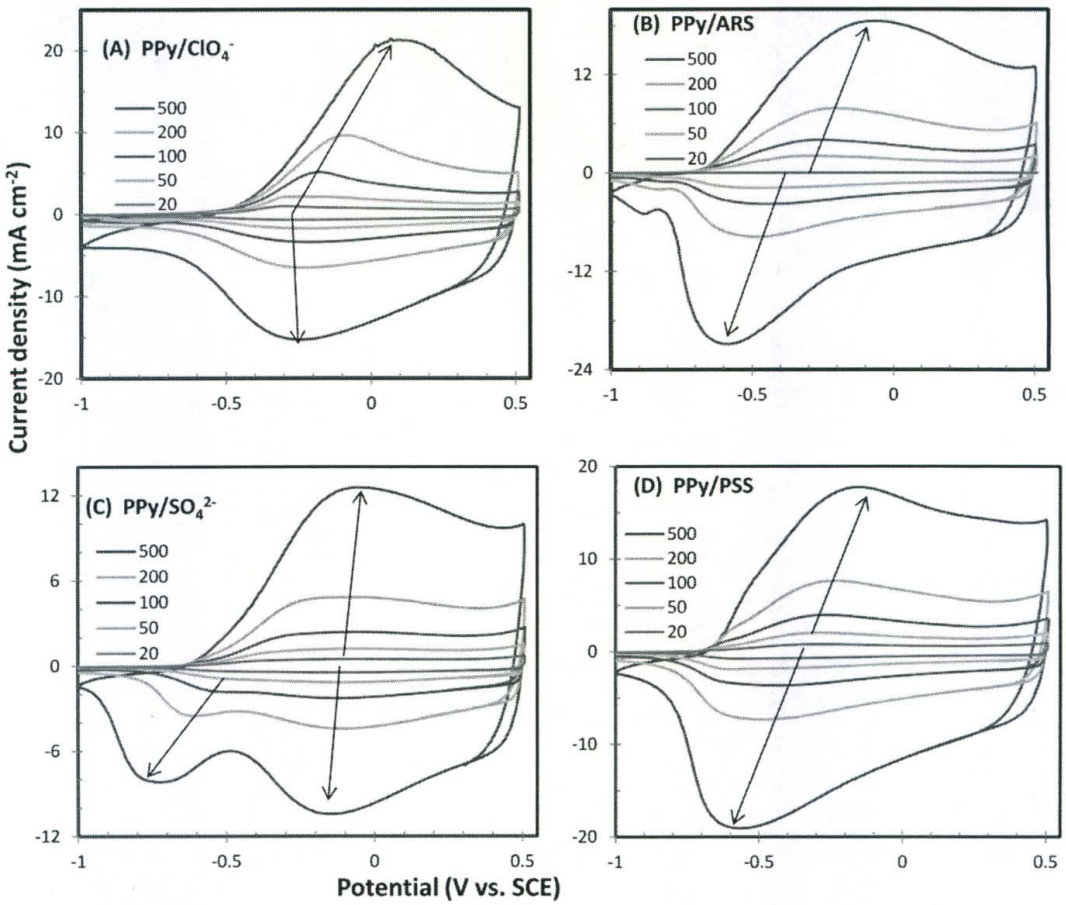

Fig. 3.16 Cyclic voltammograms of four PPy films in 0.2 M NaCl at various scan rates; **A.** PPy/ClO_4^-, **B.** PPy/ARS, **C.** PPy/SO_4^{2-}, **D.** PPy/PSS. Scan rates in mV s^{-1} are indicated.

currents. Each film was tested in NaCl over five scan rates from high to low rate, namely 0.5, 0.2, 0.1, 0.05, and 0.02 V s^{-1}. The first cycle of the as-prepared films has been excluded in each case to show the steady state behaviour.

The peak separations in Figure 3.16 increase with increasing scan rate as a result of the anodic peaks shifting to more positive potentials and the cathodic peaks shifting to more negative potentials. However, the cathodic peak of PPy/ClO_4^- very slightly shifted to more positive potentials with increasing scan rate. Both PPy/ARS and PPy/PSS films exhibited similar peak shifts with scan rate. In contrast, the PPy/SO_4^{2-} film exhibited two cathodic peaks in NaCl. The main cathodic and anodic peaks at ca. -0.2 V were almost constant with increasing scan rate. However, the second cathodic peak at ca. -0.8 V became more pronounced at higher scan rates and was significantly shifted to more negative potentials with increasing scan rate.

It can be seen that ion insertion from the solution into the polymer films is associated with higher film resistance than ion expulsion as indicated by the peak shifts. The film is in its reduced (neutral) state at the beginning of ion insertion at about -0.6 V, which is non-conducting and has very low ionic conductivity because it is undoped. The film resistance in this case is high and causes the anodic peak shifts with increasing scan rate. In contrast, the film is in its oxidized state at the beginning of ion expulsion at about +0.5V, and so the film resistance is at its minimum value (i.e. conducting state). Thus, there are no peak shifts with increasing scan rate if the peak corresponds to ion expulsion (28). In the case where mixed ion transport is involved (e.g. PPy/ARS and

PPy/PSS), peak shifts are observed in both peaks indicating that there is ion insertion in both cases.

Figures 3.17 and 3.18 summarize the changes of the peak potentials (E_p) and the peak currents (i_p) with scan rate, respectively. These changes are indicative of various rates and modes of ion transport in the polymer films. Plots for the anodic peaks and cathodic peaks versus scan rate are shown separately. From Figure 3.17, it can be noticed that the peak shifts for the polymer films exhibited different slopes as follows. The anodic peak for PPy/ClO_4^- is more sensitive to scan rate than the cathodic peak, where the former has a high slope and the latter is almost unchanged. Based on the previous discussion, such behaviour can be attributed to anion transport. Both PPy/ARS and PPy/PSS films exhibited similar dependences on scan rate where the cathodic and anodic peaks are significantly shifted away from each other indicating ion transport has both contributions of anions and cations at the same potentials. However, in the case of PPy/SO_4^{2-} where two cathodic peaks are present at two distinct potentials, the ion transport process revealed anion and cation contributions but at different potentials. The peak corresponding to anion insertion exhibited very little shift compared with cation insertion indicating low anion insertion presumably due to the electroactive centers on the polymer backbone being blocked by the original dopant anions (SO_4^{2-}), and so cation insertion occurs to compensate for the localized divalent anions.

From Figure 3.18, the current of the anodic and cathodic peaks increases linearly with increasing scan rate in all cases indicating that the peaks are under thermodynamic

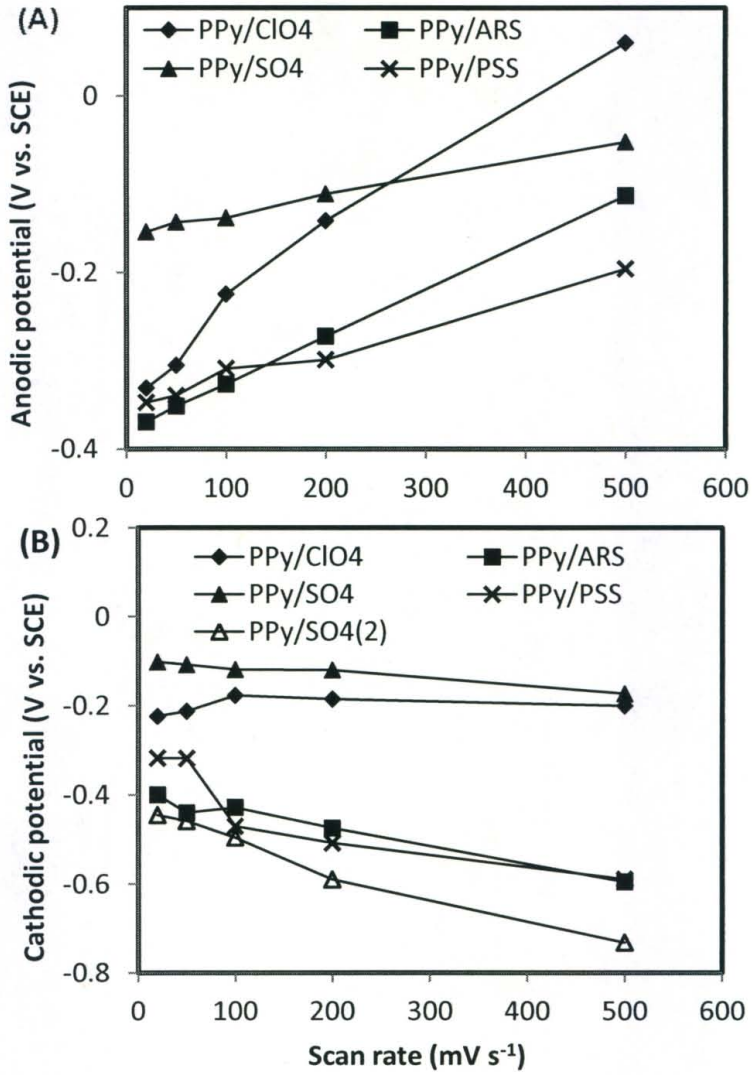

Fig. 3.17 Peak potentials versus scan rates for PPy films; **A.** anodic potential, **B.** cathodic potential. PPy/SO_4(2) represents the second cathodic peak at ca. -0.7 V of PPy/SO_4^{2-} film.

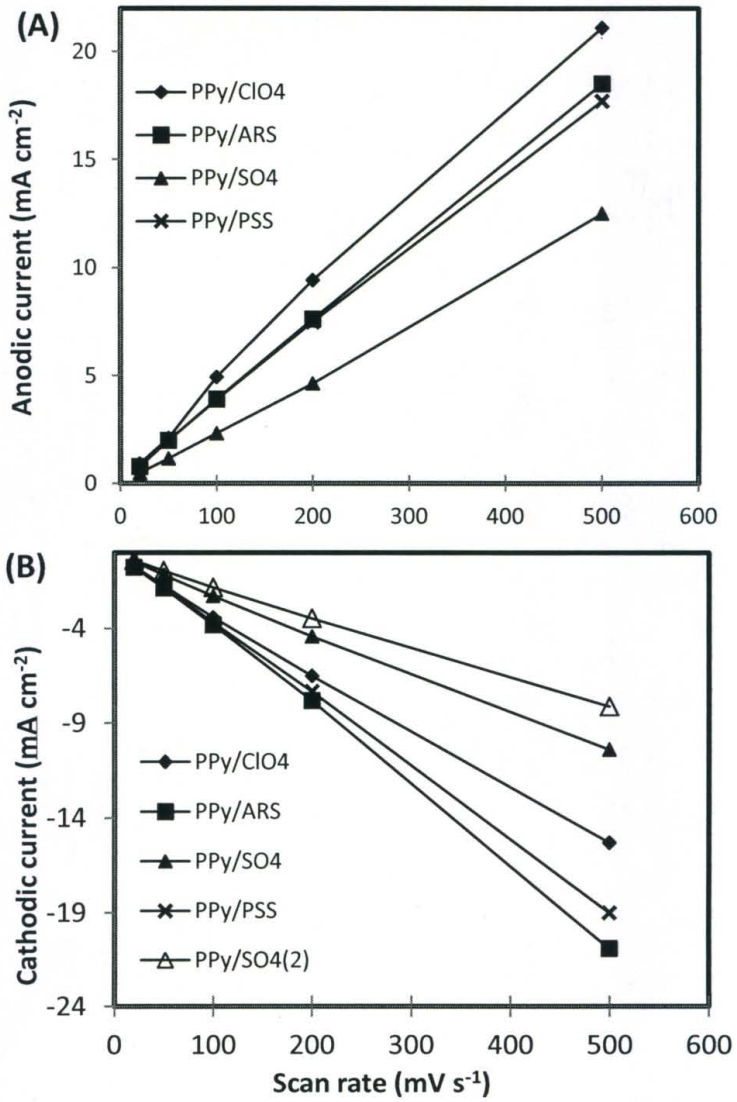

Fig. 3.18 Peak current versus scan rates for PPy films; A. anodic current, B. cathodic current. $PPy/SO_4(2)$ represents the second cathodic peak at ca.-0.7 V for PPy/SO_4^{2-} film.

control. As scan rate increases, electrolyte ions travel faster to maintain the electroneutrality of the film, causing bigger currents. Thus, the way the potential varies with time affects the way the current varies with time. PPy/ClO_4^- shows the highest increase in the anodic current indicating dominance of anion contributions in the redox process. In contrast, PPy/ARS and PPy/PSS show the highest increase in the cathodic current indicating dominance of cation contributions compared with the other films. However, such indication is not quantitative enough to find the dominance of ion transport in each case. The ion transport properties for the five PPy films are described more quantitatively in the next section by using impedance spectroscopy.

3.3.3 Impedance spectroscopy

Impedance spectroscopy is a powerful technique to probe charge transport in polymer-coated electrodes quantitatively (37). The impedance (vector Z = rotating vectors E/I) is measured at a fixed frequency or as a function of frequency and one can assume a linear behaviour of current versus potential. Ionic and solution resistances can be identified from Nyquist plots, and so the ionic conductivity can be calculated based on Equations 3.5 and 3.6 (38). Nyquist plots are a way of showing a frequency response by plotting imaginary impedance versus real impedance. From Nyquist plots, three processes can be identified as the frequency is swept from high to low values: electron transfer across the electrode/polymer interface at high frequencies, ion transport processes within the polymer layer at medium frequencies, and capacitive charging

behaviour at low frequencies (39). Since the electron transport for PPy films is very fast, the charge transfer resistance (R_{CT}) is negligible, causing the absence of a semicircle at high frequencies in the Nyquist plots.

Nyquist and capacitance plots are the most useful depictions of the polymer film impedances, and so they are shown here for comparative studies of the polymer films. Impedance measurements were recorded for oxidized (i.e. doped and so conducting) states of the polymer films between +0.2 V and -0.2 V, unless otherwise stated. High potential values were avoided to prevent overoxidation of the polymer films, which damages the conjugation of the polymer chains causing them to become non-conducting. Results were recorded in the order of decreasing potential values for any potential dependence experiment to have consistent measurements. Because current sensitivity is changed automatically while taking the impedance measurements, some points show inconsistent values compared with others.

3.3.3.1 Potential dependence

Figures 3.19 and 3.20 show Nyquist plots for the polymer films' impedance measured in 0.2 M NaCl at various potentials from +0.2 V to -0.2 V. All polymer films were equilibrated under potential cycling conditions in 0.2 M NaCl before the impedance measurements were taken to bring the films to the same ion equilibrium conditions. The results of these two figures indicate that the ion transport properties of the polymer films exhibited significant potential dependence, which are summarized in Figure 3.21.

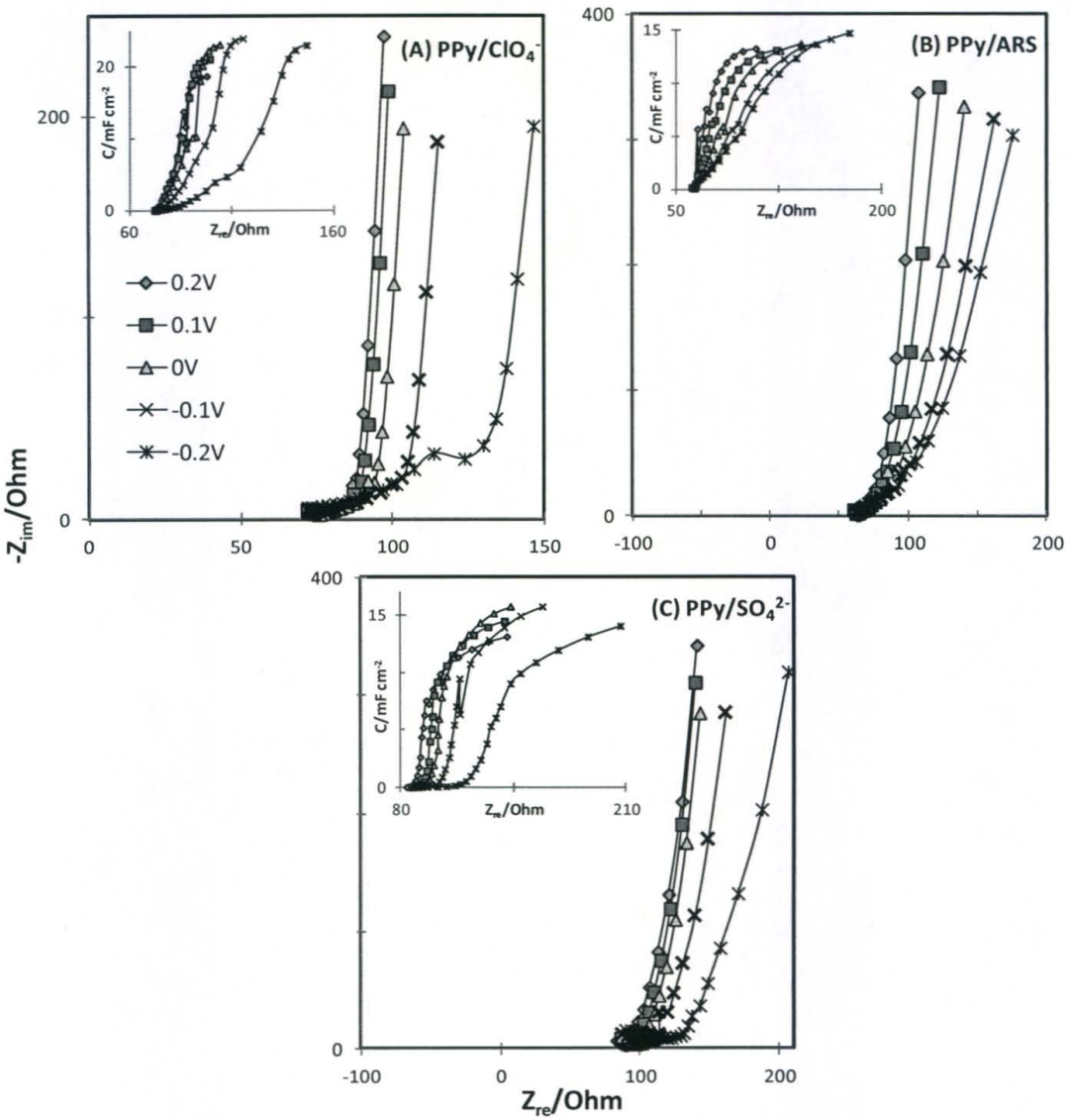

Fig. 3.19 Nyquist plots for PPy films equilibrated under cycling conditions in 0.2 M NaCl, and measured at different potentials as indicated. **A.** PPy/ClO_4^-, **B.** PPy/ARS, **C.** PPy/SO_4^{2-}. Inset series capacitance versus real impedance.

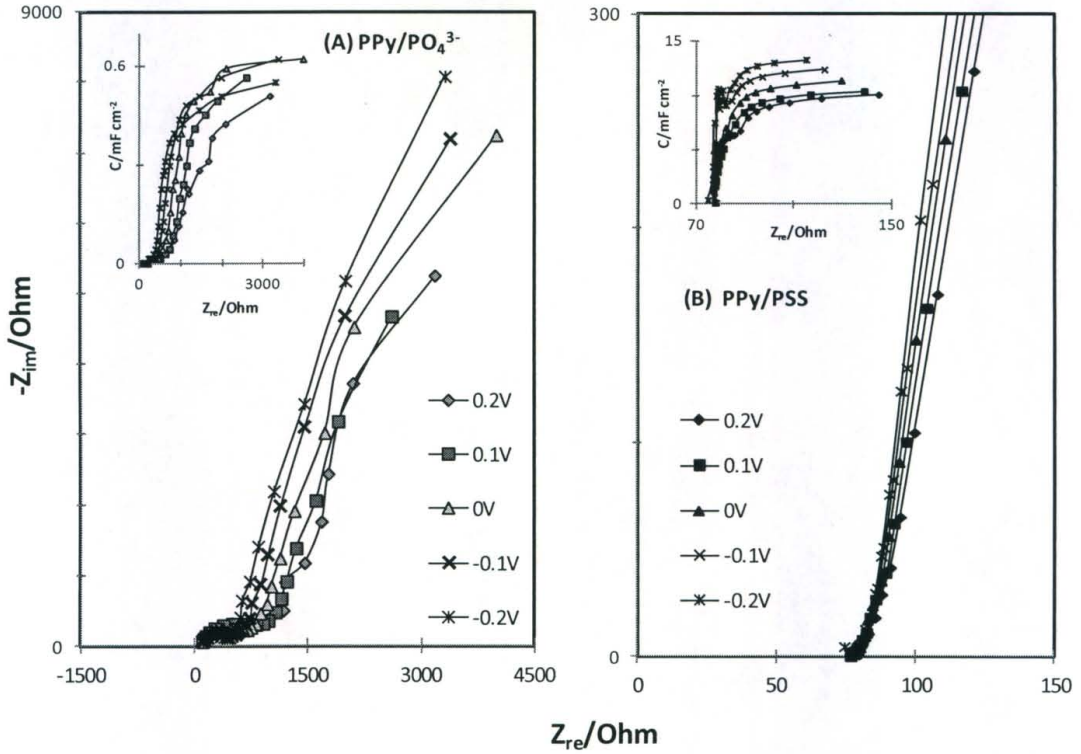

Fig. 3.20 Nyquist plots for **A.** PPy/PO_4^{3-}, **B.** PPy/PSS films equilibrated under cycling conditions in 0.2 M NaCl, and measured at different potentials as indicated. Inset series capacitance versus real impedance.

Figure 3.21 summarizes the ionic conductivities exhibited by the polymer films at various oxidation levels which increase as the potential is increased. The ionic conductivities of PPy/ClO_4^-, PPy/ARS, and PPy/SO_4^{2-} increased with increasing electrode potentials, while the ionic conductivities for PPy/PO_4^{3-} and PPy/PSS decreased with increasing electrode potentials. The ionic conductivity of the polymer film with trivalent anions (i.e. PPy/PO_4^{3-}) was multiplied by a factor of one thousand to fit with the scale of the other films.

The ionic conductivities are directly related to the mobile ion concentrations in the polymer films. As the mobile ion concentration in the film increases, the ionic conductivity increases and vice versa. The charge carried by the mobile ions can therefore be inferred from how ionic conductivities changes with potential, i.e. oxidation levels (14; 28). For an oxidation process (i.e. p-doping), anion transport is indicated by an increasing ionic conductivity at higher potentials, where the mobile ion concentration (i.e. anion) increases with oxidation. On the other hand, cation transport is indicated by a decreasing ionic conductivity at higher potentials, where the mobile ion concentration (i.e. cation) decreases with oxidation. It is also worthy to note that the electroneutrality of the oxidation process for polymer films can be maintained either by anion insertion and/or by cation expulsion. The former is associated with an ionic conductivity increase while the latter is associated with an ionic conductivity decrease. The redox process can therefore be accomplished by mixed ion transport and dominated by either anion or cation transport which influences the net ionic conductivity of the film.

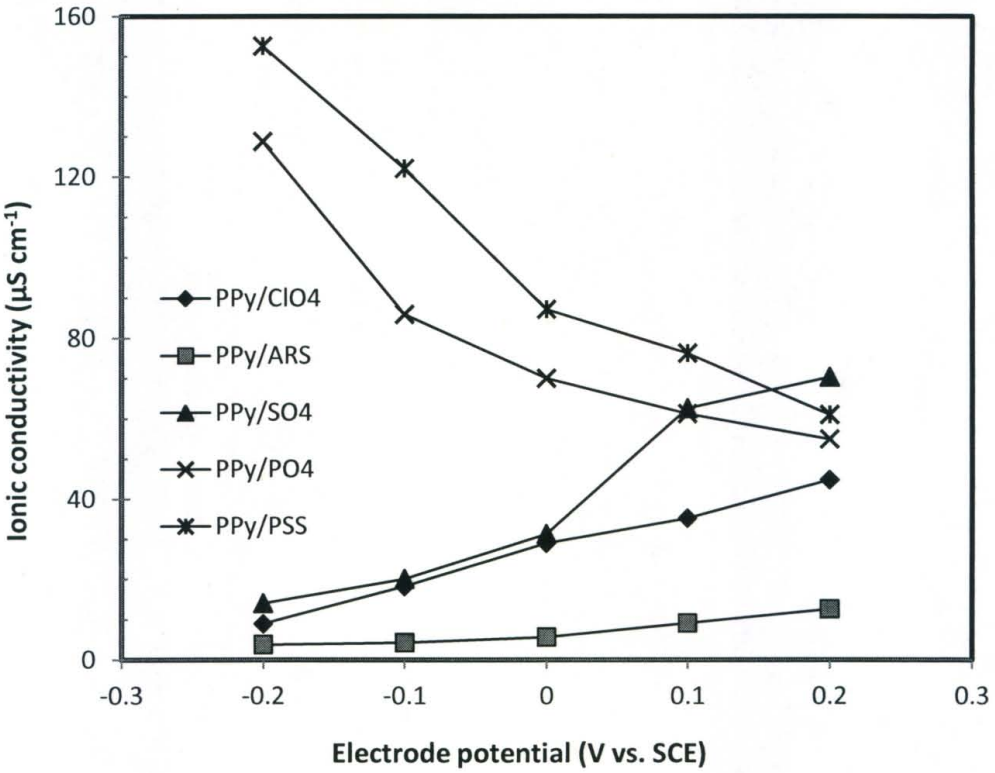

Fig. 3.21 Ionic conductivity versus electrode polarization potential measured in 0.2 M NaCl. The ionic conductivity of the polymer film with trivalent anions (i.e. PPy/PO_4^{3-}) is multiplied by a factor of one thousand to fit with the scale for the other films.

The real impedance (Z_{re}) should be constant at low frequency (i.e. capacitive behaviour). However, inhomogeneity of the polymer films results in Z_{re} continuing to increase at low frequency (34) which is observed particularly for the polymer film doped with trivalent anions (i.e. PPy/PO_4^{3-}).

Capacitance plots (series capacitance versus real impedance) are shown in the insets of Figures 3.19 and 3.20 for comparison with their impedance plots. They illustrate the rate and the way of reaching the limiting capacitance for each polymer film. The rate can be inferred from the slope of rising where the steeply rising or bigger slope indicates the higher conductivity, and so the absence of charge transfer resistance. However, the zero slope or constant capacitance values indicate the presence of significant charge transfer resistance. The way of reaching the limiting capacitance can be inferred as the frequency decreases where the redox reaction encompasses the whole polymer layer at the lowest frequencies. Thus, the low-frequency capacitance can be seen as equilibrium charge storage in the polymer layer where charge insertion and expulsion are in equilibrium as the AC potential wave oscillating between the cathodic and anodic directions (40). The limiting capacitance is also proportional with accessible electroactive centers, and so for polymer films with same polymerization charges the higher limiting capacitance is the more accessible electroactive centers. Interestingly, the offset of rising capacitance for PPy/SO_4^{2-} exhibited zero slope with constant capacitance at -0.2 V indicating significant charge transfer resistance presumably due to low concentration of the mobile ions at such a potential.

From the insets of Figures 3.19 and 3.20, it can be noticed that each polymer film has a different rising capacitance, and so the rate of reaching the limiting capacitance varies. The highest rates can be seen at +0.2 V for PPy/ClO_4^-, PPy/ARS, and PPy/SO_4^{2-} indicating that p-doping is facilitated at higher levels of oxidation. In contrast, for PPy/PSS and PPy/PO_4^{3-} the rate was highest at -0.2 V indicating that p-doping of the self-doped polymer (i.e. PPy/PSS) is facilitated at lower levels of oxidation. The polymer film with trivalent anion (i.e. PPy/PO_4^{3-}) exhibited as self-doped polymer regarding the rate of reaching the limiting capacitance. These results also confirm the one in Figure 3.21 where ionic conductivity is related to the rate of reaching the limiting capacitance.

Figure 3.22 shows the limiting capacitance versus the electrode potential for each polymer film, which refers to accessible electroactive centers at each oxidation level. The capacitance of the polymer film with trivalent anions (i.e. PPy/PO_4^{3-}) was multiplied by a factor of ten to fit with the scale of the other film. It can be seen that the accessible electroactive centers had their maximum values at -0.1 V for PPy/ClO_4^-, PPy/SO_4^{2-}, and PPy/PO_4^{3-}, while for PPy/PSS and PPy/ARS increased as the polymer films reduced and reached the neutral state.

It has been shown that anion transport is indicated by increasing ionic conductivities at higher oxidation levels, while cation transport is indicated by decreasing ionic conductivities at higher oxidation levels. The rate of reaching the limiting capacitance is facilitated at higher oxidation levels for the polymer films with anion transport properties, but at lower oxidation levels for the polymer films with

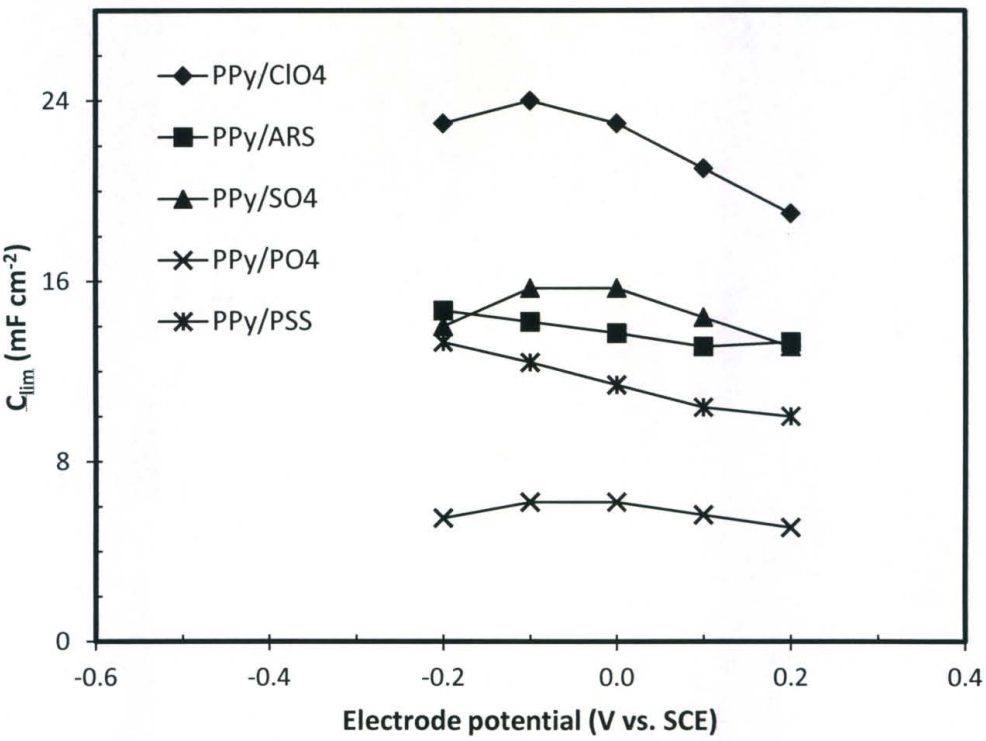

Fig. 3.22 Limiting capacitance versus electrode potential for the PPy films. The capacitance of PPy/PO_4^{3-} is multiplied by a factor of ten to fit with the scale for the other films.

cation transport properties. In addition, the way of reaching the limiting capacitance is significantly influenced by the nature and mobility of the dopant anions used for polymerization and deposition of the polymer films.

3.3.3.2 Ionic conductivity with different electrolytes

Impedance spectroscopy was used to measure the ionic conductivities of the polymer films at +0.2 V in three different 0.2 M electrolyte solutions (i.e. NaCl, $NaClO_4$, and $LiClO_4$). These electrolytes were chosen based on their ions' size, and so the influence of counterions and co-ions is illustrated for the comparative study. Figure 3.23 shows Nyquist plots measured at +0.2 V for the polymer films (i.e. PPy/ClO_4^-, PPy/ARS, and PPy/SO_4^{2-}) equilibrated under potential cycling conditions in the corresponding electrolyte solution. It can be seen that the solution resistance (R_s), offset of the impedance spectrum, of each film was sensitive to the both electrolyte ions but to different degrees. Table 3.3 summarizes the ionic conductivities for the five polymer films calculated at a constant film thickness of 1 μm.

Table 3.3 Ionic conductivities measured at +0.2 V for polymer films.

	Ionic conductivity (μS cm^{-1})				
Electrolyte (0.2 M)	**PPy/ClO_4**	**PPy/ARS**	**PPy/SO_4**	**PPy/PO_4**	**PPy/PSS**
NaCl	39.1	42.7	31.3	1.3	67.1
$NaClO_4$	5.9	36.1	29.3	1.2	---
$LiClO_4$	11.7	39.1	39.1	2.8	---

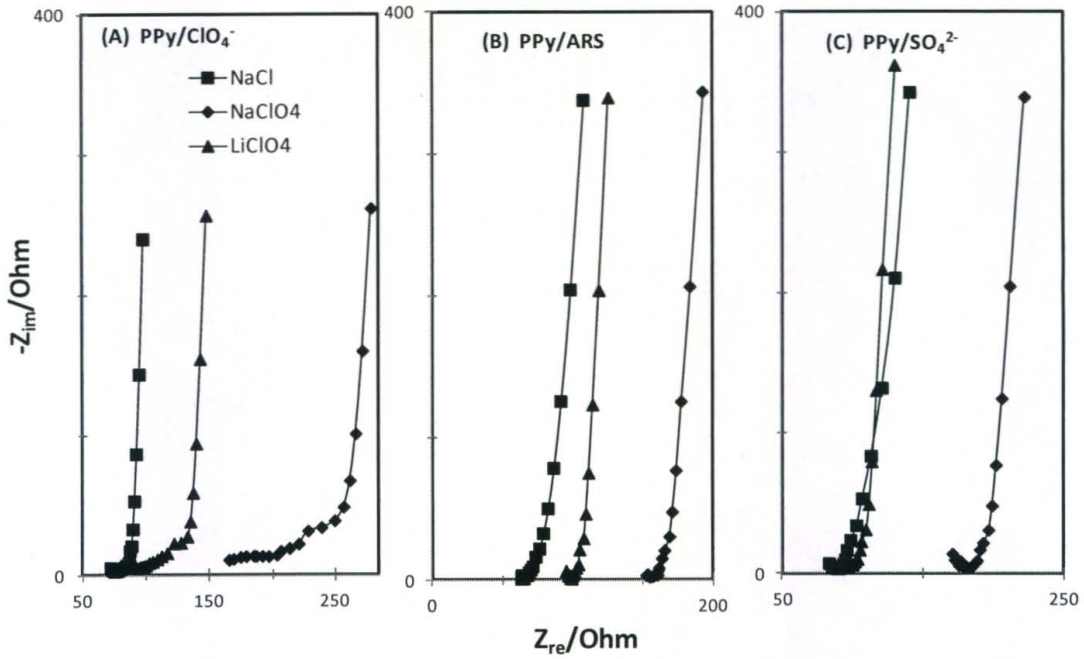

Fig. 3.23 Nyquist plots measured at 0.2 V for three PPy films in three different electrolytes (0.2 M) as indicated; **A.** PPy/ClO_4^-, **B.** PPy/ARS, **C.** PPy/SO_4^{2-}. The films were equilibrated under cycling conditions in the corresponding solution before the measurements were taken.

The dependence of ionic conductivity on the electrolyte ions reveals kinetic limitations about the mobile ions. As can be seen from Table 3.3, the polymer films with univalent small anions (i.e. PPy/ClO_4^-) exhibited enhanced ion transport in NaCl solution. However, the ionic conductivity decreased by a factor of seven in $NaClO_4$, where the perchlorate ion is almost three times more massive than the chloride ion. This indicates that the electrostatic interactions between the anions and polymer chains play a significant role besides the steric effects. In $LiClO_4$, the ionic conductivity increased by a factor of two compared with $NaClO_4$, where Li^+ is almost three times less massive than Na^+. Thus, the ionic conductivity of PPy/ClO_4^- is influenced by both electrolyte ions, but more significantly by counterions indicating anion transport properties.

For the polymer films with univalent large anions or divalent anions (i.e. PPy/ARS and PPy/SO_4^{2-}), the ionic conductivity is not significantly affected by changing the electrolyte ions, and so almost steady values of ionic conductivities were observed while changing the electrolyte ions. This indicates that these polymer films exhibited mixed ion transport properties, and so both ions compensate for each other to overcome any kinetic limitation. This behaviour can be attributed to the partially localized dopant anions which act as anionic sites besides the cationic sites of the polymer chains.

For PPy/PO_4^{3-}, it has been shown from potential dependence experiments that such films exhibit cation transport properties similar to PPy/PSS films, and so the change of co-ions influences the ionic conductivity more than the counterions. For PPy/PSS, the ionic conductivity is expected to be significantly influenced by co-ions due to the fully

localized dopant anions which act as anionic sites. However, due to uncharacteristic impedance behaviours or bad experimental results in $NaClO_4$ and $LiClO_4$, it was not possible to get accurate values for comparison.

The low ionic conductivity of PPy/PO_4^{3-} can be attributed to the compact agglomerate nature and low doping level of the films as shown by SEM and EDX images, respectively. Interestingly, the ionic conductivity of PPy/PSS is significantly bigger than for any other film in NaCl electrolyte. This behaviour has been attributed to the large dissociation constant between the mobile ions (i.e. Na^+) and the sulfonate groups (SO_3^-) of the polyanion electrolyte, which is believed to be due to strong solvation after dissociation compared with the positive charges on the polypyrrole chains. These positive charges have diffuse nature causing polarisable chains, and so strong interactions with the mobile ions are expected (28; 41).

The capacitance plots for the polymer films (i.e. PPy/ClO_4^-, PPy/ARS, PPy/SO_4^{2-}, and PPy/PO_4^{3-}) are shown in Figure 3.24 and were measured under the same conditions of Figure 3.23. These plots show the limiting capacitance level and the slope of the rising capacitance for each film in the three different electrolytes. The limiting capacitance level indicated by the maximum capacitance reached at low frequencies reveals how many electroactive centers are accessible to the electrolyte ion charges and the slope of the rising capacitance shows how easily (i.e. fast) these centers are occupied with the charges, and so steeply rising curves indicate high ion mobility (i.e. short charging time) (40). It can be seen that the limiting capacitance level was not greatly influenced by the

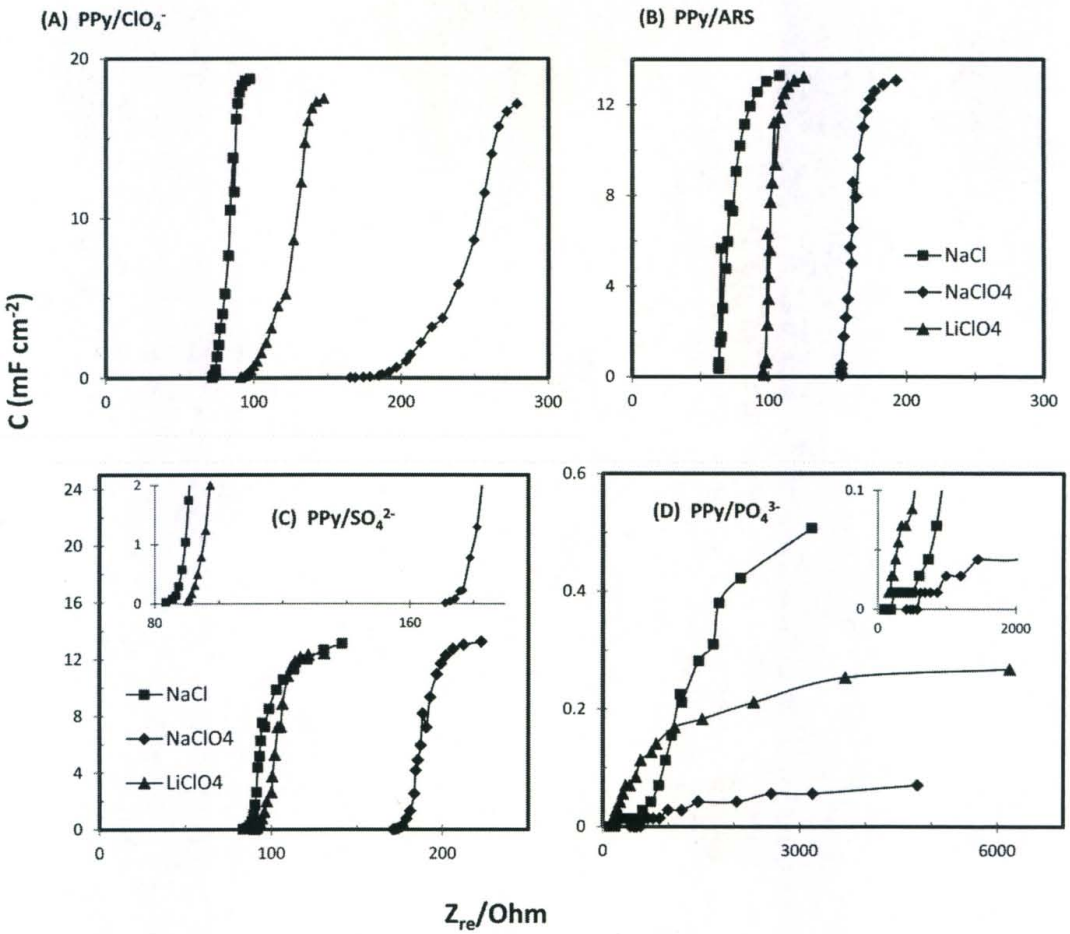

Fig. 3.24 Capacitance plots measured at 0.2 V for PPy films in three different electrolytes as indicated; **A.** PPy/ClO_4^-, **B.** PPY/ARS, **C.** PPy/SO_4^{2-}, **D.** PPy/PO_4^{3-}. Enlarged plots of the high frequency regions are inset (same axes for the inset plots). The films were equilibrated under cycling conditions in the corresponding solution before the measurements were taken.

external electrolyte ions when the polymer films were doped with univalent or divalent anions (i.e. ClO_4^-, ARS, SO_4^{2-}). However, the slope of the rising portion was influenced by the electrolyte ions as shown clearly for PPy/ClO_4^-. The mobility of ions inside the polymer matrix in the electrolyte solutions is in the order of $NaClO_4$ < $LiClO_4$ < NaCl, confirming the results in Table 3.3 for the ionic conductivities. Thus, the ion mobility is influenced by both counterions (Cl^- and ClO_4^-) and co-ions (Li^+ and Na^+).

For PPy/ARS, the slope of the rising portion was almost the same in each electrolyte indicating that the ion mobility exhibits similar values as also shown in Table 3.3. Similar results are shown for PPy/SO_4^{2-} with little slope distinction in different electrolytes in the order of $NaClO_4$ < NaCl < $LiClO_4$. For PPy/PO_4^{3-}, the slopes of the rising portions indicate that the ion mobility in the three electrolytes increases in the order of $NaClO_4$ < NaCl < $LiClO_4$ as magnified in the inset of Figure 3.24(D). However, the limiting capacitance level (i.e. the number of electroactive centers which are accessible to ion charges) of the film exhibited its maximum value in NaCl where both counterions and co-ions can be easily accommodated due to their smaller sizes.

It has been shown that the dependence of ionic conductivity on ion transport properties for the polymer films can be divided into three groups: anion transport where the ionic conductivity is most influenced by the counterions (i.e. the case for PPy/ClO_4^-), mixed ion transport where the ionic conductivity is fairly constant (i.e. the case for PPy/ARS and PPy/SO_4^{2-}), and cation transport where the ionic conductivity is most influenced by the co-ions (i.e. the case for PPy/PO_4^{3-}).

3.3.3.3 Influence of the initial oxidation state of the film

One of the crucial points for conducting polymers, which still needs to be resolved, is the dependence of ion transport properties on the initial degree of oxidation of the polymer film. For that reason, the polymer films were equilibrated at different conditions in order to vary their oxidation states. Impedance measurements were taken at +0.2 V after the films deposition without any further treatment for the as-prepared film. The cycled films were cycled between 0.5 V and -1.0 V for three times at 0.1 V s^{-1} in NaCl. The polarized films were held at a specified potential for one minute, except otherwise stated, in NaCl. All films were deposited under the same conditions, and so all should have same amount of electroactive materials.

The polymer films that are considered here are PPy/ClO_4^- and PPy/PSS. The Nyquist plots and the capacitance plots for PPy/ClO_4^- and PPy/PSS are shown in Figures 3.25 and 3.26, respectively. For PPy/ClO_4^-, four equilibration conditions were tested at +0.2 V. It can be seen that the as-prepared film was in a highly conducting state and exhibited a high capacitive nature indicating that the film was deposited with a high concentration of mobile ions. The cycled film exhibited a medium conductivity between the two polarized films. The -0.2 V polarized film exhibited the lowest conducting state and lowest capacitive nature as well indicating that the film loses a significant amount of the mobile ions after polarizing at such low potential. The low concentration of mobile ions can be seen from the limiting capacitance level at low frequencies. In addition, the capacitance plots show the way of reaching the limiting capacitance which reflects about

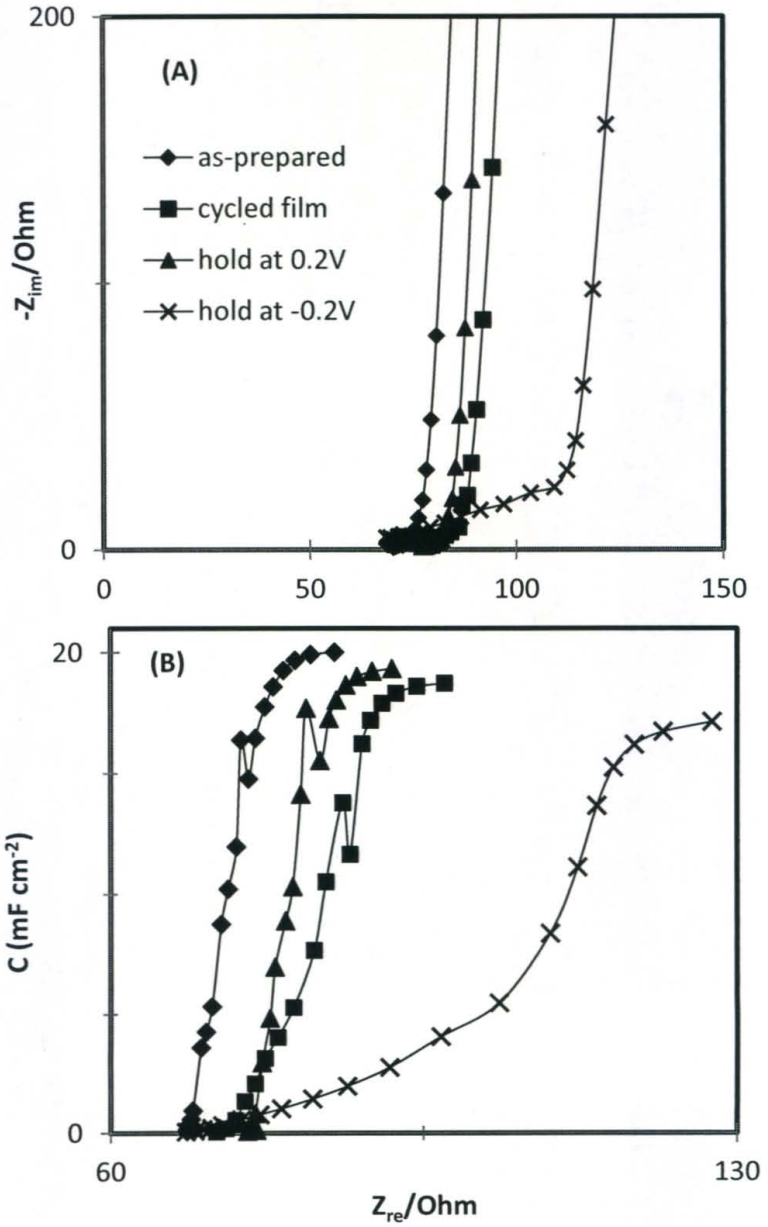

Fig. 3.25 (A) Nyquist plots and **(B)** capacitance plots for PPy/ClO_4^-. The films were equilibrated under different conditions in 0.2 M NaCl as indicated, and then measured at 0.2 V.

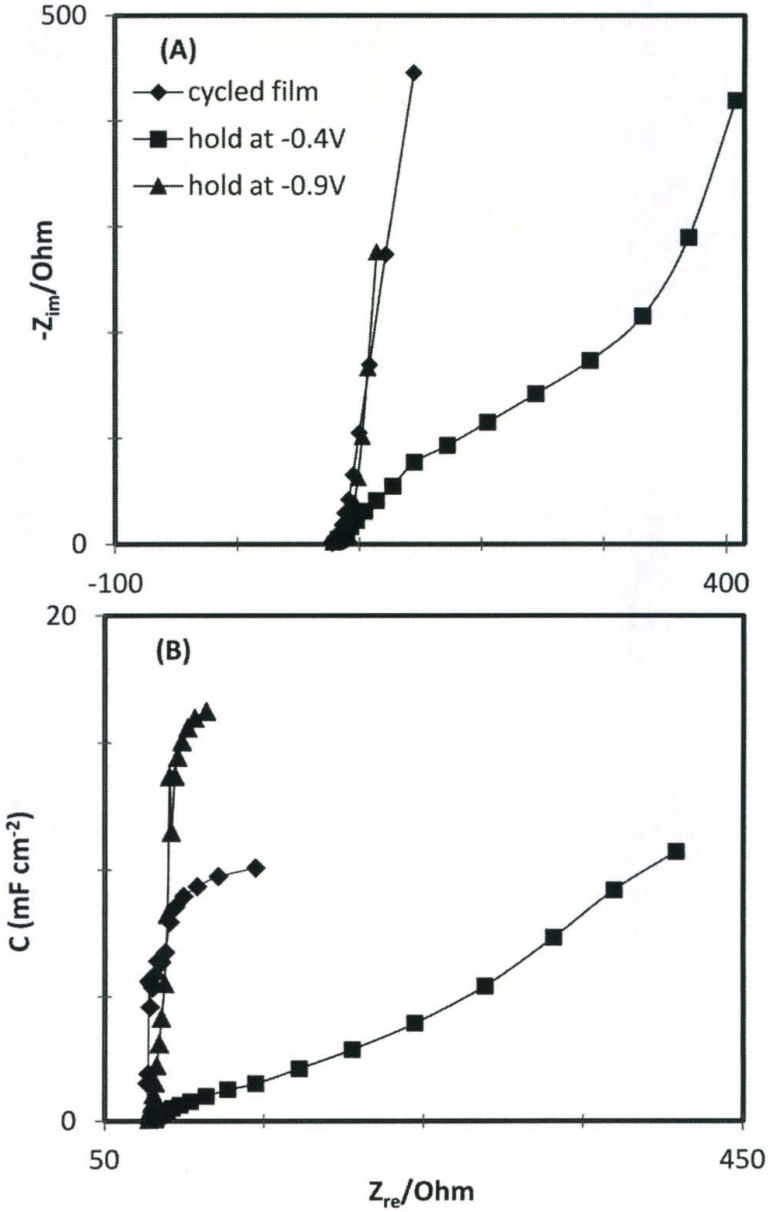

Fig. 3.26 (A) Nyquist plots and **(B)** capacitance plots for PPy/PSS. The films were equilibrated under various conditions in 0.2 M NaCl as indicated, and then measured at 0.2 V.

charging time of the film. It can be seen that most of the films exhibited the same slope to reach the limiting capacitance, while the -0.2 V polarized film exhibited two different slopes. Because the higher slope of rising indicates higher conductivity, it can be concluded that such film exhibited higher conductivity at lower frequencies.

The capacitance plots show that the steepest slope of rising was for the as-prepared film. This can be attributed to a high doping level (i.e. high oxidation state) that can be achieved by the electrochemical polymerization. The least steep slope of rising for the -0.2 V polarized film indicates that the film approaches its neutral (non-conducting) state by polarizing at low potentials. It can be seen that as the slope of rising became less steep, the lower limiting capacitance level. The low level of limiting capacitance indicates a lower number of electroactive centers that can be reached, and thus a lower oxidation (doping) state is expected for the lower capacitance levels.

For PPy/PSS, three equilibration conditions were tested at +0.2 V. It should be noticed that some equilibration conditions showed uncharacteristic behaviours or bad experimental results, and so they are not used here. Figure 3.26(A) shows high ionic conductivity for the cycled film and the -0.9 V polarized film. However, it can be seen from the capacitance plots that these two films exhibited distinct limiting capacitance levels where the -0.9 V polarized film had significantly higher capacitance level. This can be attributed to a solely cation transport mechanism which occurs while the film is reduced at such low potential. On the other hand, the -0.4 V polarized film exhibited slow ionic conductivity indicating low cation insertion occurs at this potential. It can also

be seen that the slope of rising became significantly less steep at such an oxidation state indicating low ion mobility (i.e. long charging time). It can be concluded that high ionic conductivity and more electroactive centers can be achieved after reducing the film at -0.9 V.

3.4 Conclusions

Five polypyrrole films have been electrochemically synthesized from five different electrolytes with anions of varying size and charge. Scanning electron microscopy (SEM) and energy dispersive X-ray spectroscopy (EDX) reveal distinct morphologies and elemental compositions, respectively. It was found that the morphologies of the polymer films can be changed electrochemically.

The polymer films show significant differences in their ion transport properties and charge compensation mechanisms due to the different dopant anions incorporated during the polymerization. The kinetic limitations resulting from the size and charge of the dopant anions can be overcome by redoping the film in a different electrolyte with smaller ions (e.g. NaCl). The low mobility of counterions resulting from steric effects or ion-polymer interactions influences the ion transport properties of the polymer films causing cation uptake from the electrolyte solution. Both of the resulting overpotential and transient cation insertion have kinetic rather than thermodynamic origins, where the restricted anion transport is overcome by cation uptake. The scan rate dependence indicates that the main redox peak of each film is under thermodynamic control. In

addition, the peaks corresponding to ion insertion shift with increasing scan rate because the films exhibit high resistance at the beginning of ion insertion.

The polymer films doped with univalent aromatic anions (i.e. PPy/ARS) show enhanced rates of ion transport (i.e. both anion and cation) after redoping with a smaller anions (e.g. in NaCl), which is attributed to the porous morphology caused by the aromatic anions. PPy/PSS shows an enhanced rate of cation transport, which is attributed to the large dissociation constant between the mobile ions and fixed polyanion charges.

The ion transport properties of the polymer films exhibited significant potential dependence as indicated by the ionic conductivity measurements in NaCl electrolyte. Ionic conductivities measured as a function of oxidation levels can be used to identify the mode of ion transport within the polymer films. In addition, the limiting capacitance and ion mobility can quantitatively be identified by using capacitance plots. It was found that these ion transport properties are significantly influenced by the dopant anions used for polymerization and deposition of the polymer films. It can be concluded that the ion transport properties of the self-doped films are significantly influenced by the initial oxidation state compared with the normal doped films. Valuable information can be taken from the dependence of ion transport properties on the oxidation state of the conducting polymers which can be used for many potential applications in electrochemical devices.

References

1. P. Holzhauer, K. Bouzek, *J. Appl. Electrochem.* 36 (2006) 703.

2. N. Levy, M. Levi, D. Aurbach, R. Demadrille, A. Pron, *J. Phys. Chem. C* 114 (2010) 16823.

3. M. Akieh, S. Ralph, J. Bobacka, A. Ivaska, *J. Membr. Sci.* 354 (2010) 162.

4. H. Varela, R. Bruno, R. Torresi, *Polymer* 44 (2003) 5369.

5. E. Smela, *Adv. Mater.* 15 (2003) 481.

6. C. Weidlich, K. Mangold, K. Juttner, *Electrochim. Acta* 50 (2005) 5247.

7. S. Li, Y. Qiu, X. Guo, *J. Appl. Polym. Sci.* 114 (2009) 2307.

8. V. Misoska, J. Ding, J. Davey, W. Price, S. Ralph, G. Wallance, *Polymer* 42 (2001) 8571.

9. M. Vorotyntsev, E. Vieil, J. Heinze, *J. Electroanal. Chem.* 450 (1998) 121.

10. U. Johanson, M. Marandi, T. Tamm, J. Tamm, *Electrochim. Acta* 50 (2005) 1523.

11. H. Mao, J. Ochmanska, C. Paulse, P. Pickup, *Faraday Discuss. Chem. Soc.* 88 (1989) 165.

12. S. Bruckenstein, J. Chen, I. Jureviciute, A. Hillman, *Electrochim. Acta* 54 (2009) 3516.

13. H. Yang, H. Lee, Y. Kim, J. Kwak, *J. Electrochem. Soc.* 147 (2000) 4239.

14. X. Ren, P. Pickup, *J. Electroanal. Chem.* 396 (1995) 359.

15. M. Akieh, W. Price, J. Bobacka, A. Ivaska, S. Ralph, *Synth. Met.* 159 (2009) 2590.

16. G. Maia, R. Torresi, E. Ticianelli, F. Nart, *J. Phys. Chem.* 100 (1996) 15910.

17. S. El Sana, C. Gabrielli, H. Perrot, *Russ. J. Electrochem.* 40 (2004) 267.

18. G. Inzelt, V. Kertesz, A. Nyback, *J. Solid State Electrochem.* 3 (1999) 251.

19. T. Raudsepp, M. Marandi, T. Tamm, V. Sammelselg, J. Tamm, *Electrochem. Commun.* 12 (2010) 1180.

20. A. Emamgholizadeh, M. Khoshroo, A. Omrani, A. Rostami, *J. Appl. Polym. Sci.* 117 (2010) 3107.

21. K. Yamato, K. Kaneto, *Anal. Chim. Acta* 568 (2006) 133.

22. P. Metz, G. Alici, G. Spinks, *Sens. Actuators* A 130 (2006) 1.

23. C. Barbero, M. Miras, E. Calvo, R. Kotz, O. Haas, *Langmuir* 18 (2002) 2756.

24. C. Gautier, O. Alévêque, F. Seladji, M. Dias, T. Breton, E. Levillain, *Electrochem. Commun.* 12 (2010) 79.

25. H. Varela, S. Maranhao, R. Mello, E. Ticianelli, R. Torresi, *Synth. Met.* 122 (2001) 321.

26. J. Huang, D. Kekuda, C. Chu, K. Ho, *J. Mater. Chem.* 19 (2009) 3704.

27. J. Rubinson, Y. Kayinamura, *Chem. Soc. Rev.* 38 (2009) 3339.

28. X. Ren, P. Pickup, *J. Phys. Chem.* 97 (1993) 5356.

29. G. Li, P. Pickup, *J. Phys. Chem. B* 103 (1999) 10143.

30. W. Albery, Z. Chen, B. Horrocks, A. Mount, D. Bloor, A. Monkman, C. Elliott, *Faraday Discuss. Chem. Soc.* 88 (1989) 247.

31. C. Jin, F. Yang, W. Yang, *J. Appl. Polym. Sci.* 101 (2006) 2518.

32. X. Ren, P. Pickup, *Can. J. Chem.* 75 (1997) 1518.

33. Y. Cohen, M. Levi, D. Aurbach, *Langmuir* 19 (2003) 9804.

34. G. Duffitt, P. Pickup, *J. Chem. Soc. Faraday Trans.* 88 (1992) 1417.

35. J. Tamm, A. Alumaa , A. Hallik, V. Sammelselg, *J. Electroanal. Chem.* 448 (1998) 25.

36. Y. Li, *Electrochim. Acta* 42 (1997) 203.

37. J. Kim, T. Amemiya, D. Tryk, K. Hashimoto, A. Fujishima, *J. Electroanal. Chem.* 416 (1996) 113.

38. S. Mondal, K. Prasad, N. Munichandraiah, *Synth. Met.* 148 (2005) 275.

39. C. Ehrenbeck, K. Juttner, *Electrochim. Acta* 41 (1996) 511.

40. R. Moghaddam, P. Pickup, *Phys. Chem. Chem. Phys.* 12 (2010) 4733.

41. A. Romero, J. Cascales, T. Otero, *J. Phys. Chem. B* 109 (2005) 907.

Chapter 4

Ion Transport in Modified Polypyrrole Films

4.1 Approach and importance

Conducting polymers can be utilized to incorporate and immobilize different species in their matrices, i.e. modified polymer films. It has been found that modified polymer films can possess interesting chemical, electrical, and magnetic properties (1). Conducting polymers, such as polypyrrole (PPy), polythiophene (PTh), and polyaniline (PAn), have been utilized to incorporate ferrocenes (two cyclopentadiene rings with Fe) and other metallocene complexes (two cyclopentadiene rings with a transition metal e.g. Ru, Co, Ni) (2). Ferrocene-containing polypyrrole (PPy-Fc) was exploited to increase the sensitivity of carbon monoxide gas sensors, i.e. electrocatalysis applications (3). A paramagnetic property of conducting polymers was shown for polypyrrole doped with a ferrocene derivative, i.e. p-ferrocenyl benzene sulfonic acid (4). A platinum coated electrode with polypyrrole containing ferrocene sulfonate (PPy-$FcSO_3$) was shown to electrocatalyse the hydrogen gas evolution reaction in strong acid solutions (5).

Polymer-coated electrodes with electroactive species containing a redox center can work as electron-transfer mediators to regenerate redox enzymes, e.g. glucose oxidase, without the need for additive reagents, i.e. reagentless. Such electrodes have applications in biosensors with high selectivity and sensitivity (6). It was also shown that conducting polymer composites with ferrocene groups as dopant molecules possess increased charge capacity due to the additional electroactivity of the dopant molecules. These composite materials can be used as electrode materials for rechargeable batteries (7; 8).

Conducting polymer films can also be modified with large molecules, such as steric stabilizers and surfactants. It was shown that such modification can influence the physical properties of the polymer films, such as morphology, mechanical strength, conductivity, and solubility. The large molecules can act as counterions and can stabilize the polymerization process by reducing the natural repulsion of the radical cations (9; 10).

It is an interesting property of conducting polymers that electroactive and non-electroactive species can be incorporated into their matrices, and both can significantly influence the ion transport properties of the film. The focus of the work in this chapter was to study ion transport of a variety of modified polymer films by cyclic voltammetry and impedance spectroscopy where the electroactive dopant ions can be monitored during the insertion and ejection into/out of polymer films.

Electroactive species can be incorporated into conducting polymers either during or after the electrodeposition process (4; 11). In both cases, the electroactive species should possess a charge. The incorporation process during the electrodeposition of conducting polymers requires negative charged species if the polymer is deposited by oxidative polymerization; and positive charged species if the polymer is deposited by cathodic polymerization. As such, the electroactive species will be incorporated as counterions. However, incorporation after the electrodeposition of the conducting polymer involves ion exchange between the counterions of the polymer film and the external electrolyte ions of a monomer-free solution. For maximum incorporation of the desired species, the monomer-free solution should not contain any other charged species which could compete with the desired species.

Non-ionic species can be incorporated into polymer matrices by activation with a Lewis acid, such as boron trifluoride ethyl etherate (BFEE). Non-ionic species containing an electron-donating group, such as a hydroxyl group, can form a complex with the Lewis acid making charged species which are suitable for incorporation into polymer matrices (12).

4.2 Modification of polypyrrole films with a ferrocene derivative

1-(Ferrocenyl)ethanol (FcOH) is a ferrocene derivative with an ethyl alcohol group attached to one of the cyclopentadienyl rings (Figure 4.1). It is also known as α-methylferrocenemethanol. Ferrocene and its derivatives (e.g. FcOH) exhibit useful

electrochemical behaviour characterized by a reversible one electron Fe(III/II) redox couple. In the present case, the ethanol group attached to ferrocene was chosen to produce a negatively charged ion which can act as dopant anions for polypyrrole electrodeposition. The non-ionic molecule FcOH can be activated by using a Lewis acid, such as boron trifluoride diethyl etherate (BFEE). Figure 4.2 shows that the lone pair of the oxygen of the hydroxyl group attacks the empty orbital of boron of the Lewis acid. Following deprotonation, the net charge of the formed complex is negative.

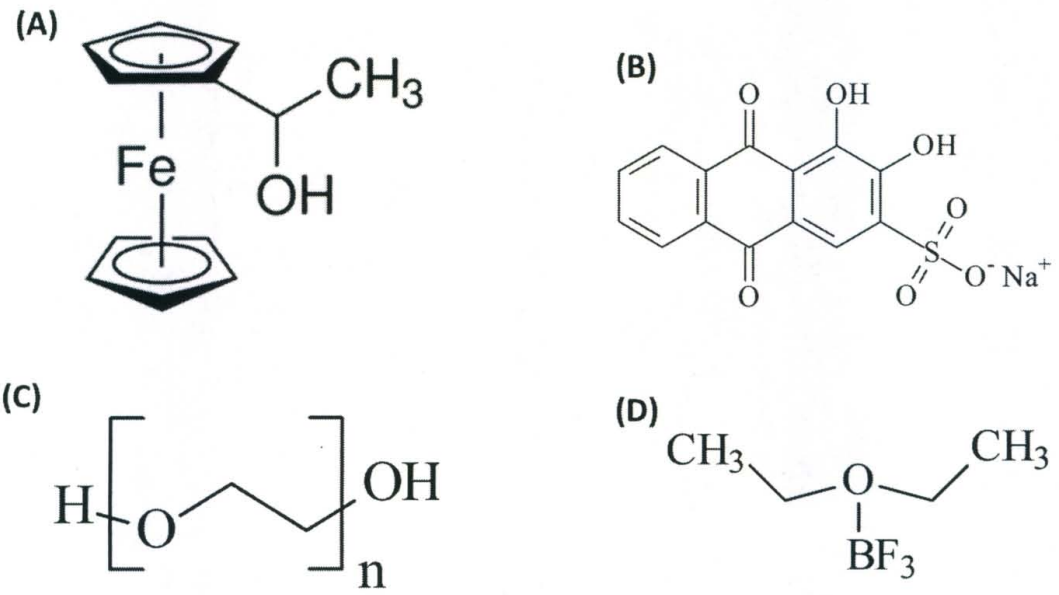

Fig. 4.1 Chemical structures of **A.** 1-(ferrocenyl)ethanol (FcOH); **B.** Alizarin Red S (ARS); **C.** polyethylene glycol (PEG); **D.** boron trifluoride ethyl etherate (BFEE).

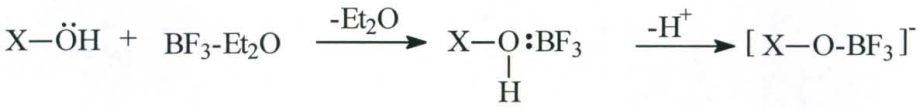

Fig. 4.2 Complex formation between a hydroxyl group and BFEE (X is a substituent group).

4.2.1 Preparation of ferrocene-modified polymer films

The system used to produce ferrocene-containing polypyrrole coated electrodes (PPy-Fc) utilized the Lewis acid solution (i.e. BFEE) as a conducting medium and to activate the hydroxyl group of FcOH. Acetonitrile (CH_3CN) was used as a co-solvent, except where otherwise stated. Figure 4.3 shows voltammograms for the electrochemical polymerization of Py in the presence of FcOH. Three non-consecutive cycles (1^{st}, 4^{th}, and 8^{th}) are shown; the first cycle signifies the nucleation process which indicates the starting of the electrodeposition of the film on the electrode surface as a result of a phase change from solution to solid; the fourth and eighth cycles signify that the current increased as an indication of film growth with cycling. The current of the initially reversible peak at ca. 0.4 V assigned to FcOH also increased with cycling, which indicates that the FcOH concentration at the electrode surface increases during the electrodeposition. The peak separation increased linearly with cycling which can be attributed to the solution resistance (R) and the current (i) increase with film deposition (i.e. $\Delta E = 59\ mV + iR$).

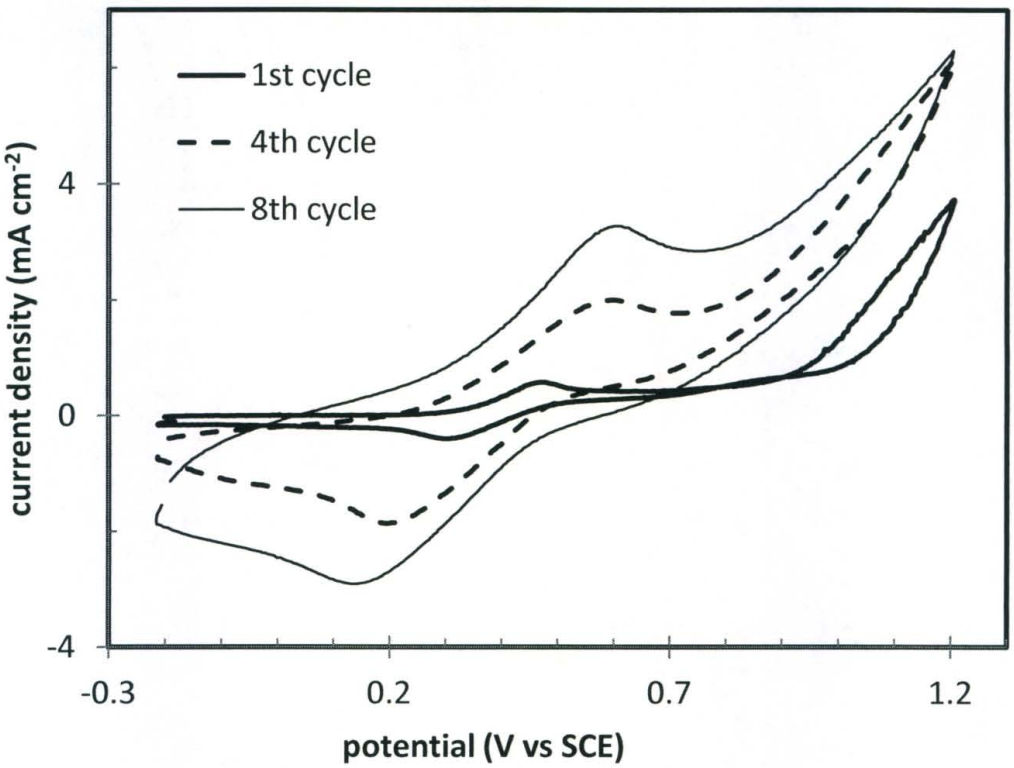

Fig. 4.3 Electropolymerization of pyrrole on a GC electrode (0.071 cm^2) from 0.1 M Py, 10 mM FcOH, and 20% BFEE in CH_3CN. The deposition rate was 0.1 V s^{-1}. The starting potential was -0.2 V and the switching potential was 1.2 V.

Three polymerization techniques were used to prepare PPy-Fc coated electrodes, namely potentiodynamic (PD), potentiostatic (PS), and galvanostatic (GS). Figure 4.4 shows voltammograms of electrodes modified by each technique, which are characterized by reversible couples at -0.10 V assigned to PPy redox and at +0.15 V assigned to FcOH redox, i.e. Fe(III/II). The shift of the FcOH redox peak toward less positive potentials relative to Figure 4.3 is due to the change in solvent, i.e. water vs. CH_3CN, where the film is better solvated in water solution indicated by its facile electrochemistry. It can be seen that the three techniques successfully incorporated FcOH into the PPy matrices. However, the polymerization charge for each film was different, and so the voltammograms cannot be used for quantitative comparison. Each technique has its own advantage over the others. The polymerization charge can be best controlled by the galvanostatic technique which can be used to control the film thickness. The insertion of FcOH during the electrochemical polymerization can be observed and monitored during potentiodynamic polymerization which shows that the amount of FcOH increases during film growth on the electrode surface (Figures 4.3). The potentiostatic technique is useful to avoid overoxidation of the conjugated system of the polymer films as the formation potential is fixed at a certain value. A more compact film is expected to be produced by this technique indicated by the small peaks at -0.5 V and -0.8 V, caused by charge trapping, which are a characteristic of dense film ion transport properties (see Chapter 3).

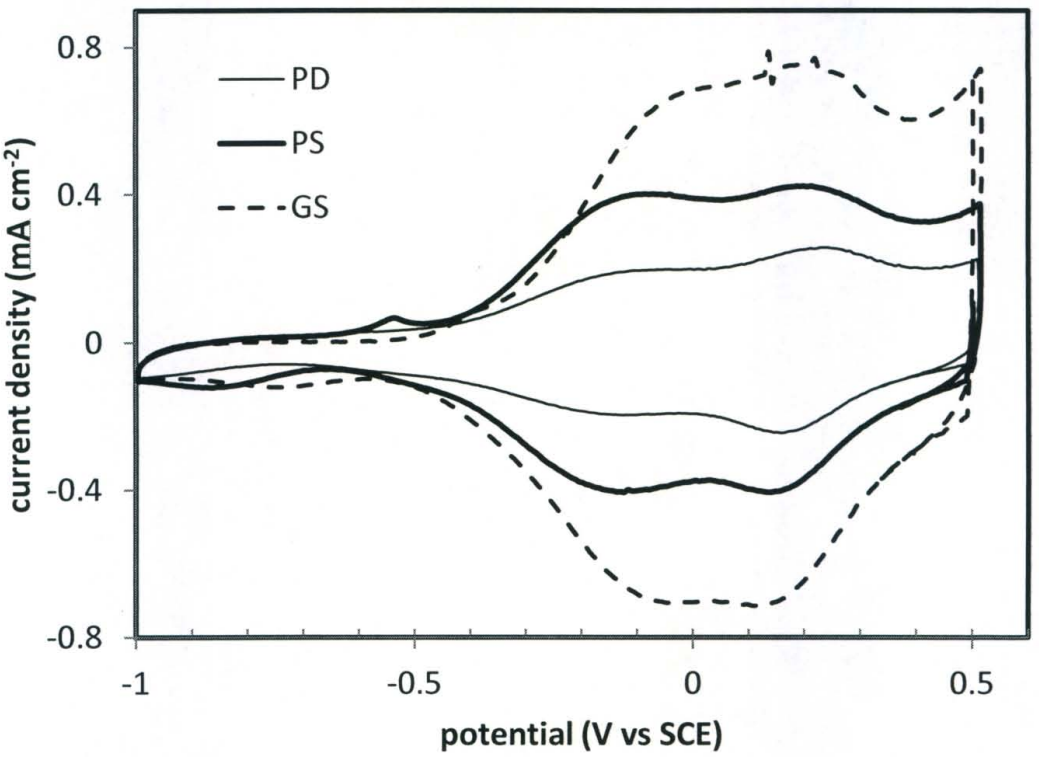

Fig. 4.4 Cyclic voltammograms of PPy-Fc coated electrodes prepared by using different techniques as follows; GC: galvanostatic, PS: potentiostatic, PD: potentiodynamic. The measurements were taken in 0.5 M $NaClO_4$ electrolyte solution at a scan rate of 0.1 V s^{-1}. The polymer films were deposited on GC electrodes from 0.1 M Py, 10 mM FcOH, and 20% BFEE in CH_3CN under the following deposition condition; GS: 0.3 mA (0.018 C), PS: 1.0 V for 1 minute, PD: 0.1 V s^{-1} (5 cycles between -0.2 V and 1.2 V).

The three polymerization techniques were tested for various polymerization charges. Figures 4.5, 4.6, and 4.7 show cyclic voltammograms of PPy-Fc films prepared by potentiodynamic, potentiostatic, and galvanostatic techniques, respectively. The films prepared potentiodynamically exhibited current responses that were proportional to the number of cycles used for deposition. The redox waves for PPy ($E_p \approx 0.0$ to -0.2 V) and FcOH ($E_p \approx 0.15$ to 0.20 V) experienced similar current increases with increasing number of polymerization cycles. However, the films produced with more polymerization cycles (from 10 and 15 cycles) exhibited greater current increases for the FcOH redox wave. This behaviour was even more pronounced for the films prepared by potentiostatic polymerization, where sharp oxidation peaks can be seen for the films prepared with longer polymerization times (2 and 3 minutes). The films grown galvanostatically exhibited more consistent current increases with polymerization charge for both redox waves. The origin of the disproportionate increases for the anodic FcOH wave is believed to be charge trapping and was found to be difficult to control.

The three techniques gave linear relationships between the polymerization charge and the area under the voltammogram which reflects the amount of the deposited material, i.e. both PPy and FcOH. The polymerization charge can roughly be estimated by integration of the area under the oxidation peak for the potentiodynamic technique due to current variation during the film electrodeposition. In contrast, the galvanostatic technique produces films with polymerization charges that can easily be calculated, where the current is kept constant throughout the electrodeposition. The

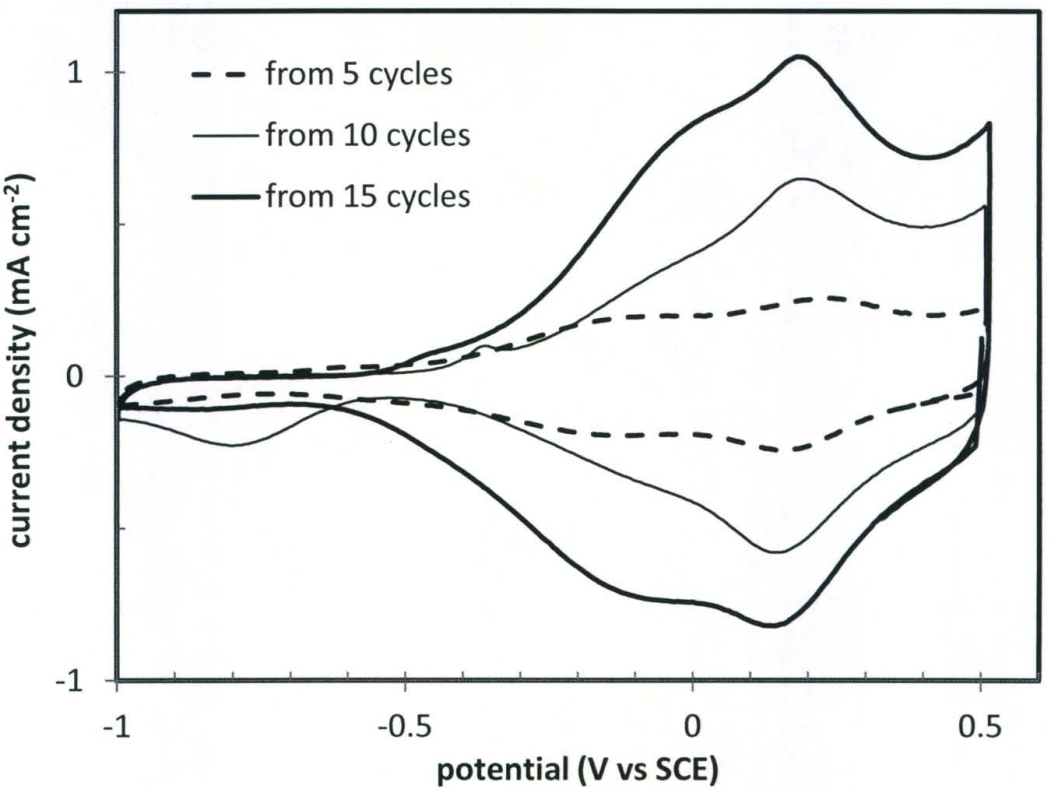

Fig. 4.5 Cyclic voltammograms of PPy-Fc films in 0.5 M $NaClO_4$ at 0.1 V s^{-1} with different polymerization cycles as indicated. The polymer films were deposited on GC electrodes from 0.1 M Py, 10 mM FcOH, 20% BFEE in CH_3CN by potentiodynamic polymerization at a scan rate of 0.1 V s^{-1} between -0.2 V and 1.2 V.

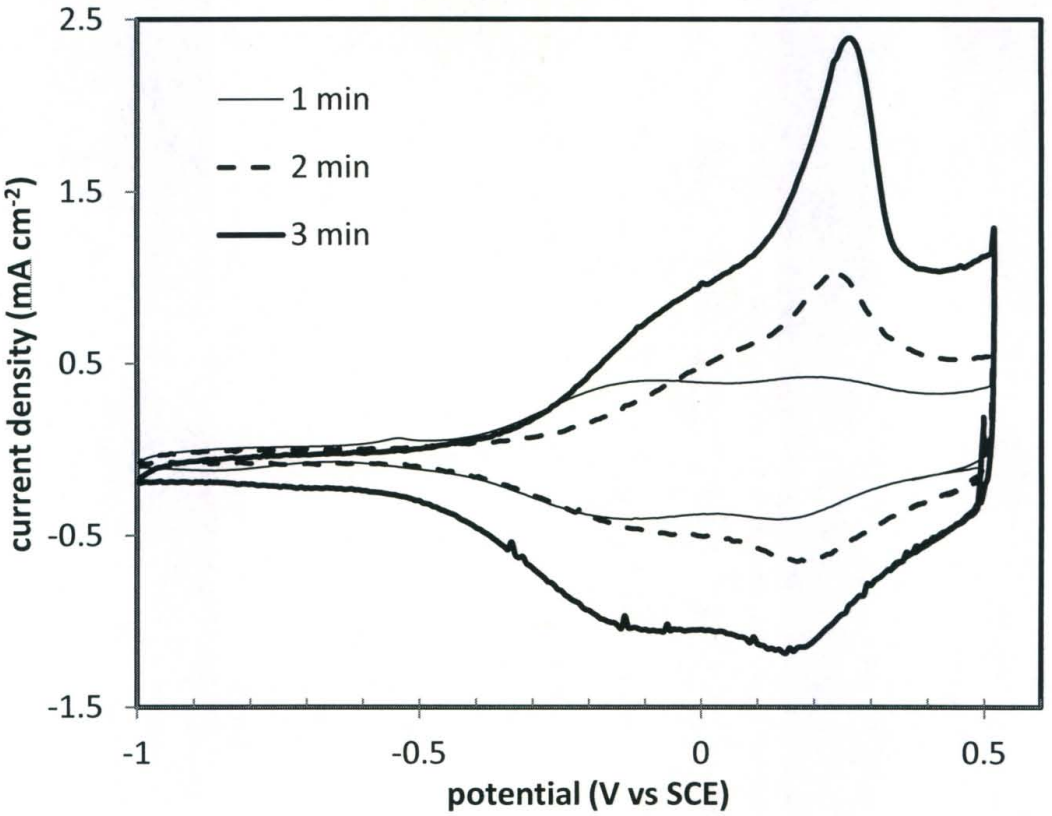

Fig. 4.6 Cyclic voltammograms of PPy-Fc films in 0.5 M $NaClO_4$ at 0.1 V s^{-1} with different polymerization time as indicated. The polymer films were deposited on GC electrodes from 0.1 M Py, 10 mM FcOH, 20% BFEE in CH_3CN by potentiostatic polymerization at 0.1 V.

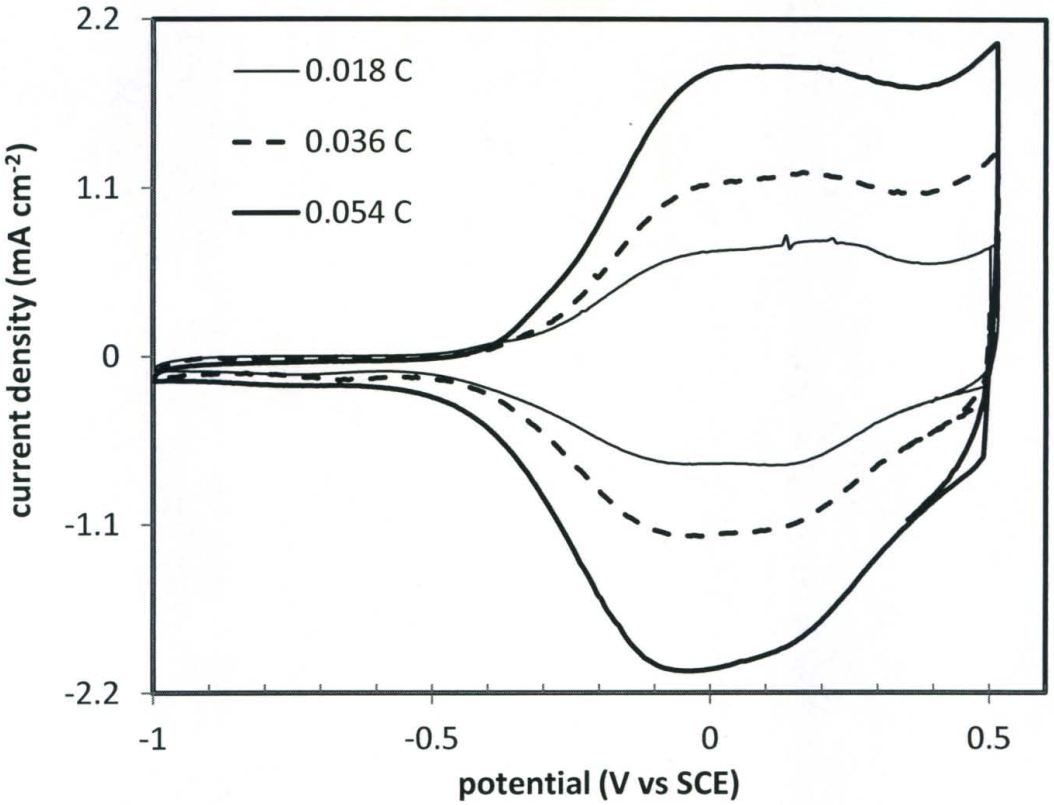

Fig. 4.7 Cyclic voltammograms of PPy-Fc films in 0.5 M $NaClO_4$ at 0.1 V s^{-1} with different polymerization charges as indicated. The polymer films were deposited on GC electrodes from 0.1 M Py, 10 mM FcOH, 20% BFEE in CH_3CN by galvanostatic polymerization at a deposition rate of 0.3 mA.

charge used for film deposition (Q) can therefore be calculated from **(Q = i * t)** where **i** is the current in ampere and **t** is the deposition time in seconds. For the potentiostatic technique, the produced current can be integrated over the time interval to find the deposition charge.

Modification of a polymer film with electroactive species (e.g. a ferrocene derivative) can also be achieved after electrodeposition onto an electrode surface. Electroactive species can be incorporated into the polymer film after electrodeposition by potential cycling in a monomer free solution containing the electroactive species which can act as counterions to maintain the electroneutrality of the film. The exchange of counterions can be enhanced by cycling the film between doped and undoped states, in this way. In addition, the incorporation by ion-exchange can be achieved by polarizing the film at a fixed potential, at which counterion charges are required to maintain electroneutrality. However, the incorporation cannot be achieved to a significant level if the polymer film is not porous enough to allow for entry of the electroactive species.

Figure 4.8 shows cyclic voltammograms for PPy films after cycling in FcOH solution, compared with an as-prepared film. Although there were small peaks at ca. 0.2 V indicating incorporation of FcOH, much greater incorporation was obtained with a more porous PPy film doped with a large aromatic molecule, i.e. PPy/ARS. This film was characterized in Chapter 3 and found to be highly porous. After electrodeposition of PPy/ARS onto the electrode surface, the film was polarized at 0.6 V in FcOH containing BFEE/CH_3CN solution. The polymer film became polycationic and FcOH is believed to

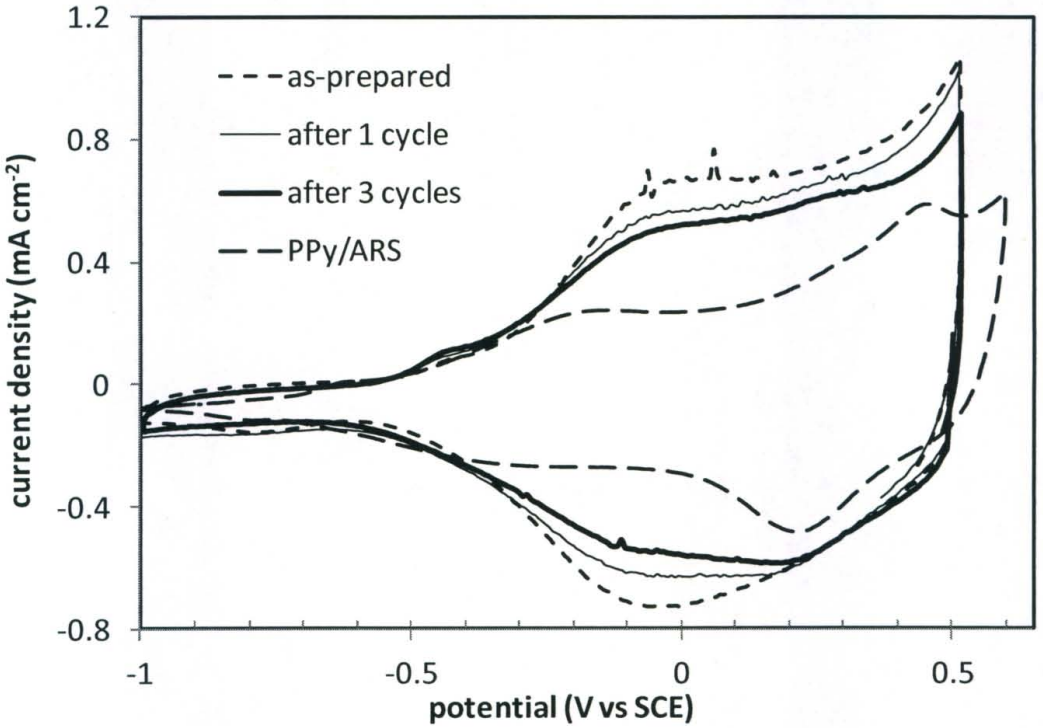

Fig. 4.8 Cyclic voltammograms of PPy-Fc films in 0.5 M $NaClO_4$ at 0.1 V s^{-1}. The polymer films were deposited from 0.1 M Py, 20% BFEE in CH_3CN at 0.3 mA with a deposition charge of 0.018 C. The films were cycled before the measurements in FcOH solution (10 mM FcOH, 20% BFEE in CH_3CN between 0.5 V and -1.0 V for the indicated number of cycles. PPy/ARS was deposited from 0.1 M Py, 6 mM ARS aqueous solution and then polarized at 0.6 V (3 minutes) in FcOH solution before the measurement in 0.2 M NaCl. The current for PPy/ARS was divided by a factor of ten.

possess a negative charge after complex formation with BFEE (see Figure 4.2), and thus FcOH can contribute to the ion transport needed to maintain the electroneutrality of the polymer film. The redox waves can clearly be seen at ca. -0.2 V and ca. 0.3 V for PPy and FcOH electrochemistry, respectively. Note the change in the scale of Figure 4.8.

4.2.2 Investigation of electropolymerization conditions

Different FcOH concentrations can be incorporated into PPy films during the electrodeposition of the film from different solution concentrations as shown in Figure 4.9. Two polymer films were grown from two different FcOH concentrations (i.e. 10 mM and 15 mM) and the CVs of these films were compared with a polymer film grown in the absence of FcOH, i.e. an unmodified polymer film. Obviously, the ion transport properties of the films were significantly influenced by the FcOH concentration inside the polymer matrix. It can be seen that the polypyrrole oxidation peak of the film prepared with 15 mM FcOH was significantly shifted to more positive potentials, but the FcOH oxidation peak, i.e. Fe(III/II), was shifted to a lower degree. This can be attributed to ion transport being impeded by the high concentration of FcOH inside the polymer film. It is also probable that the polymer chains were restructured by the introduced electroactive species, as suggested by the distinct electrochemical behaviour of the polymer after incorporation.

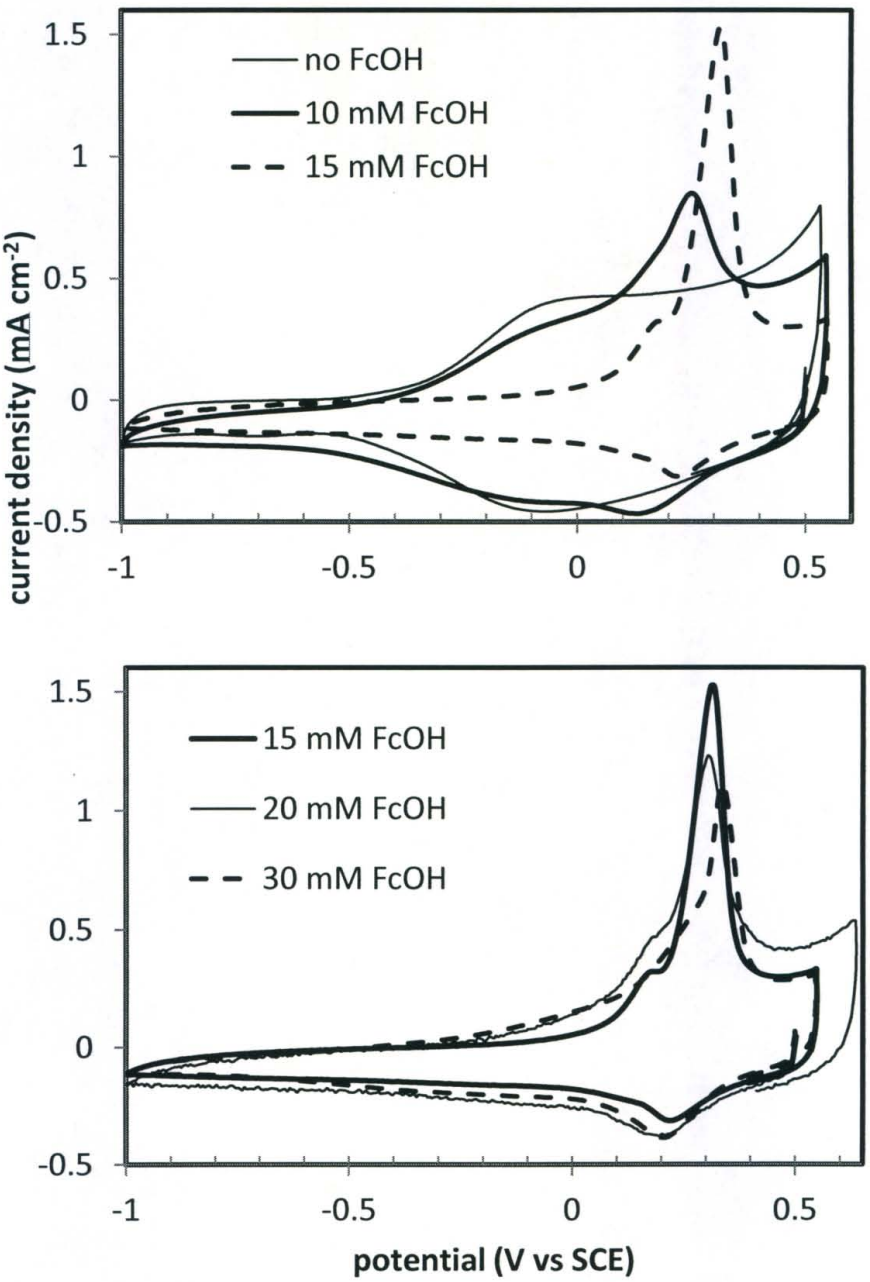

Fig. 4.9 Cyclic voltammograms of PPy and PPy-Fc films prepared with different concentrations of FcOH as indicated (A and B). The CVs were taken in 0.5 M $NaClO_4$ at 0.05 V s^{-1}. The films were deposited on GC electrodes from 0.1 M Py, the indicated concentration of FcOH, 20% BFEE in CH_3CN at a deposition charge of 0.018 C.

Presumably, as the FcOH concentration in the formation solution increases, the FcOH concentration inside the polymer matrix increases to a certain extent. However, Figure 4.9(B) shows that the films deposited from the solutions containing ≥ 15 mM FcOH exhibited similar electrochemical behaviour with variable charge trapping which affects the maxima of the oxidation peaks. It can also be noticed that the oxidation peak of PPy starts to disappear at 20 mM FcOH, and disappears completely at 30 mM FcOH. At such high concentrations of FcOH, the redox properties of the polymer film became silent and the redox wave of FcOH prevailed.

Figure 4.10 shows cyclic voltammograms for PPy-Fc films deposited by constant current polymerization from the same solution at different deposition rates. The electropolymerization conditions of PPy-Fc films deposited at different rates are summarized in Table 4.1. The deposition charge was kept constant for all films (i.e. 0.018 C). It can be seen that the deposition rate has a significant influence on the electrochemical behaviour of the film. For the film deposited at the slowest deposition rate (0.05 mA), the film exhibited typical "dense film" behaviour where the anion transport limitation is overcome by cation insertion. A small reduction peak can therefore be seen at ca. -0.9 V which is attributed to Na^+ insertion. This film shows a clear reversible wave for FcOH at ca. 0.2 V, but a less reversible wave for PPy which can be seen at ca. -0.2 V. The films deposited at 0.08 mA and 0.3 mA exhibited similar redox waves with more area under the peak for the former. This behaviour can be attributed to partial overoxidation of the conjugated system for the film deposited at 0.3 mA where

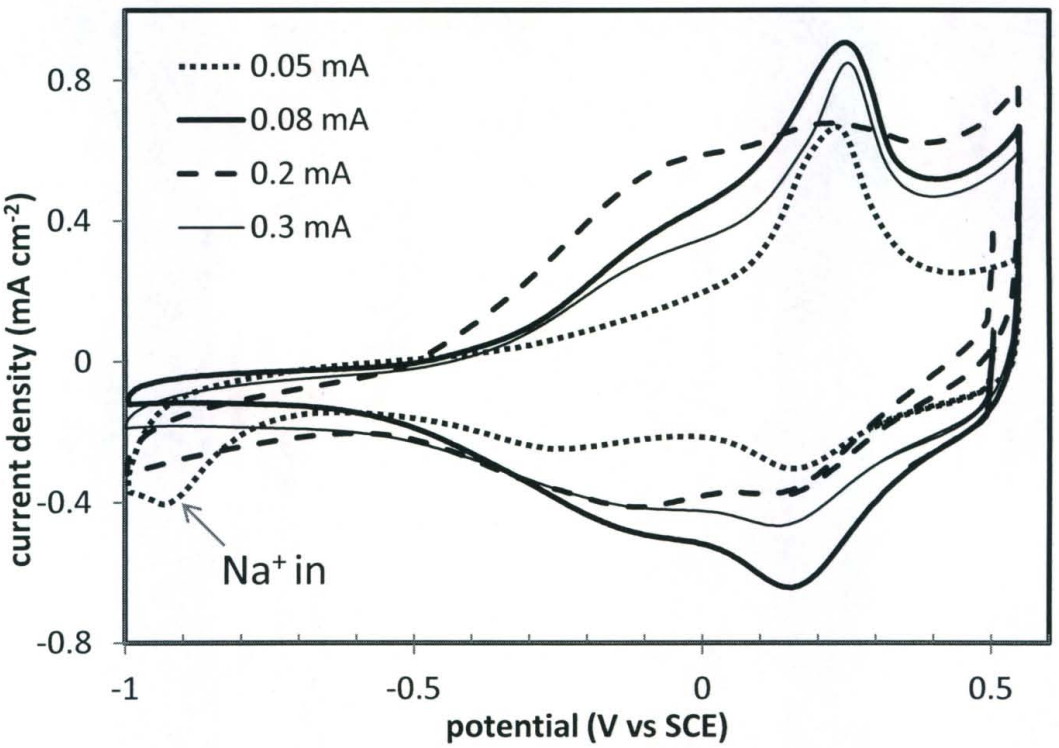

Fig. 4.10 Cyclic voltammograms of PPy-Fc films prepared by galvanostatic polymerization at different deposition rates as indicated. The CVs were measured in 0.5 M $NaClO_4$ at 0.05 V s^{-1}. The films were deposited on GC electrodes from 0.1 M Py, 10 mM FcOH, 20% BFEE in CH_3CN with a deposition charge of 0.018 C (0.25 C cm^{-2}).

the formation potential rose to 1.3 V at such deposition rate, see Table 4.1. The film polymerized at 0.2 mA exhibited small peaks for FcOH compared with the other films. The charges associated with FcOH incorporation have a major influence on the FcOH wave, as considered in more details in the next section. It can be concluded that the film polymerized at 0.08 mA shows optimized electrochemical behaviour where the waves for PPy and FcOH can clearly be identified.

Table 4.1 Electropolymerization conditions for deposition of PPy-Fc films at various deposition rates

deposition rate (mA)[a]	deposition time (sec)	measured potential (V)	deposition charge (mC)[b]
0.05	360	0.7	18.0
0.08	225	1.0	18.0
0.10	180	1.0	18.0
0.20	90	1.2	18.0
0.30	60	1.3	18.0

[a] constant current applied for electropolymerization of pyrrole
[b] electrodeposition of polypyrrole onto a GC electrode of 0.071 cm^2, corresponding to a charge density of 0.25 C cm^{-2}

4.2.3 Film characterization by UV-Vis and atomic absorption spectroscopy

The UV-Vis absorption spectra were measured for modified (PPy-Fc) and unmodified (PPy) polymer films. Figure 4.11 shows absorption spectra of the polymer films deposited on indium tin oxide (ITO) electrodes (a conducting and transparent glass coated with tin-doped indium oxide) from BFEE/CH_3CN by constant current polymerization (0.18 C). Two absorption bands can be identified for the PPy film at 330 nm and 460 nm. In contrast, two bands at 460 nm and 650 nm and one shoulder at 330 nm can be identified for the PPy-Fc film. The band and shoulder at 330 nm can be assigned to π-π^* transition of the polymer conjugated system (3; 13; 14). The band at 460 nm can be assigned to a bipolaron conducting state of PPy (13). The existence of FcOH in the modified polymer film could be responsible for changing the 330 nm band to a shoulder due to disturbing the conjugated system. The band at 650 nm can be assigned to ferrocenium, indicating the effective modification of PPy with FcOH (3). The increased absorption at lower wavelengths is due to metal oxide (ITO) of the electrode surface.

Atomic absorption spectroscopy (AAS) was used for quantitative determination of iron (Fe) in the electrochemically deposited polymer films. The polymer films were deposited on ITO electrodes to collect measurable amounts of the polymer material (mass production). After the films were peeled from the ITO electrodes, they were dissolved in 5 mL aqua regia (HNO_3 : HCl, 1:3), and then diluted to 25 mL with 50 % HCl solution.

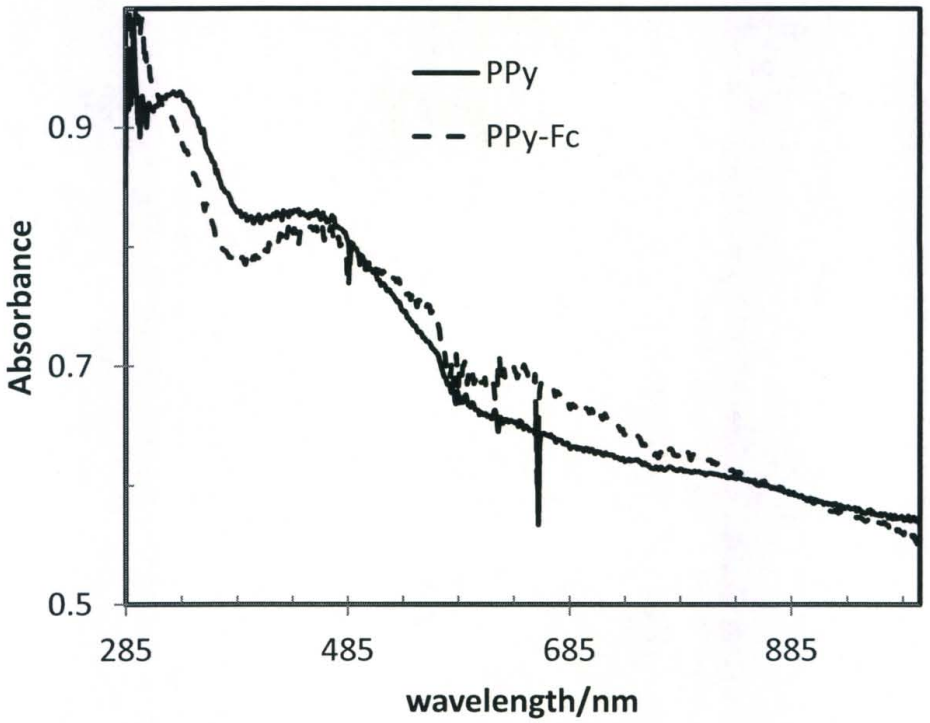

Fig. 4.11 UV-Vis spectra of PPy and PPy-Fc films on ITO electrodes. The films were deposited from 0.1 M Py, 10 mM FcOH for PPy-Fc, 10% BFEE in CH_3CN with deposition charges of 0.18 C.

Table 4.2 Polymer films used for Fe AAS

	[Py] (M)[a]	[FcOH] (mM)[a]	BFEE (mL)[b]	CH_3CN (mL)	Q (C)[c]	m (mg)[d]	[Fe] (ppm)[e]	% Fe[f]
Film 1	0.1	10	1	9	1.44	0.44	0.07	0.4
Film 2	0.5	20	1	9	4.32	1.10	0.35	0.8

[a] concentration in the deposition solution
[b] boron trifluoride ethyl etherate
[c] polymerization charge in coulomb
[d] total mass of the polymer film
[e] iron concentration from calibration curve (ppm or mg/L)
[f] percentage of iron in the polymer film by mass

The polymer films were deposited from two different solutions on ITO electrodes as shown in Table 4.2. The concentration of Fe in the films was determined by AAS after calibration with five Fe standard solutions. The data show that the concentration of Fe was proportional to the FcOH concentration used to deposit the films. It can be concluded that FcOH can be incorporated into the polymer film by using electrochemical deposition.

The number of moles of Py and FcOH, mole ratio of Py to FcOH, and number of electron per Py unit consumed during polymerization (n_{pol}) of each film are shown in Table 4.3. The mole ratio (Py:FcOH) was calculated by assuming that each polymer film consisted of PPy (65 g mol^{-1} of Py ring) and FcOH (230.1 g mol^{-1}) only. The ratio indicates that FcOH incorporation increased linearly with its concentration in the polymerization

Table 4.3 Properties of the polymer films from AAS measurements

	µmole of Py[a]	µmole of FcOH[a]	Py:FcOH[b]	n_{pol}[c]
Film 1	6.6	0.032	214	2.26
Film 2	16.5	0.15	106	2.71

[a] number of mole of Py and FcOH in the films
[b] mole ratio
[c] number of electron consumed per Py unit during polymerization

solution. The number of electron consumed per Py unit (n_{pol}) was calculated by using Equation 4.1.

$$n_{pol} = Q_{pol} M_{Py}/m_{Py}F \qquad [4.1]$$

where Q_{pol} is the polymerization charge, M_{Py} is the molar mass of Py, m_{Py} is the mass of Py in the film, and **F** is Faraday constant (96485 C mol^{-1}). The value of n_{pol} = 2.26 for Film 1 is a typical value for polymerization of Py (15), where two electrons are consumed per Py unit and 0.26 electrons are consumed for the partial oxidation (doping) for each Py unit. This value indicates that every four Py units carry one positive charge. In contrast, value of n_{poly} = 2.71 for Film 2 indicates some inefficiency in the deposition where some charge is consumed to oxidize FcOH both in the film and solution.

4.2.4 Monitoring the ion transport processes

One of the crucial points for incorporation of electroactive species into the polymer matrix is to monitor and control the insertion and ejection processes which in

turn influence ion transport of the polymer film. Many efforts were made to understand the nature of the interactions between PPy and FcOH in our PPy-Fc films. It is demonstrated in the preceding sections that FcOH insertion can be observed during the film growth and during the film cycling in a FcOH solution. Several methods were also employed to expel FcOH out of the film, such as cycling in aqueous and non-aqueous solutions, polarizing the film at positive and negative potentials, use of a steric stabilizer, and overoxidation of the film, which are the subject of this section and the next chapter. The experiments in this chapter helped in understanding the nature of interactions, but none of them was able to fully expel the FcOH from the film. This can be attributed to physical trapping of FcOH inside the polymer matrix, formation of a complex between the FcOH and the π electrons of PPy, and/or covalent bonding between the FcOH and PPy chains.

Cycling conducting polymer films in electrolyte solutions results in ion exchange between the film and solution until a steady state behaviour is reached. Figure 4.12 shows cycling the PPy-Fc films between 0.5 V and -1.0 V in aqueous and non-aqueous solutions. During cycling, charges trapped into the film during the electrodeposition were released at different potentials. It can also be seen that FcOH was not significantly expelled by cycling in either solution. The redox wave for FcOH can therefore be seen at the end of the cycling process. In the aqueous solution, a decrease in both anodic and cathodic peaks can be noticed with continuous cycling, however, the former experienced more decrease than the latter probably due to higher concentration of

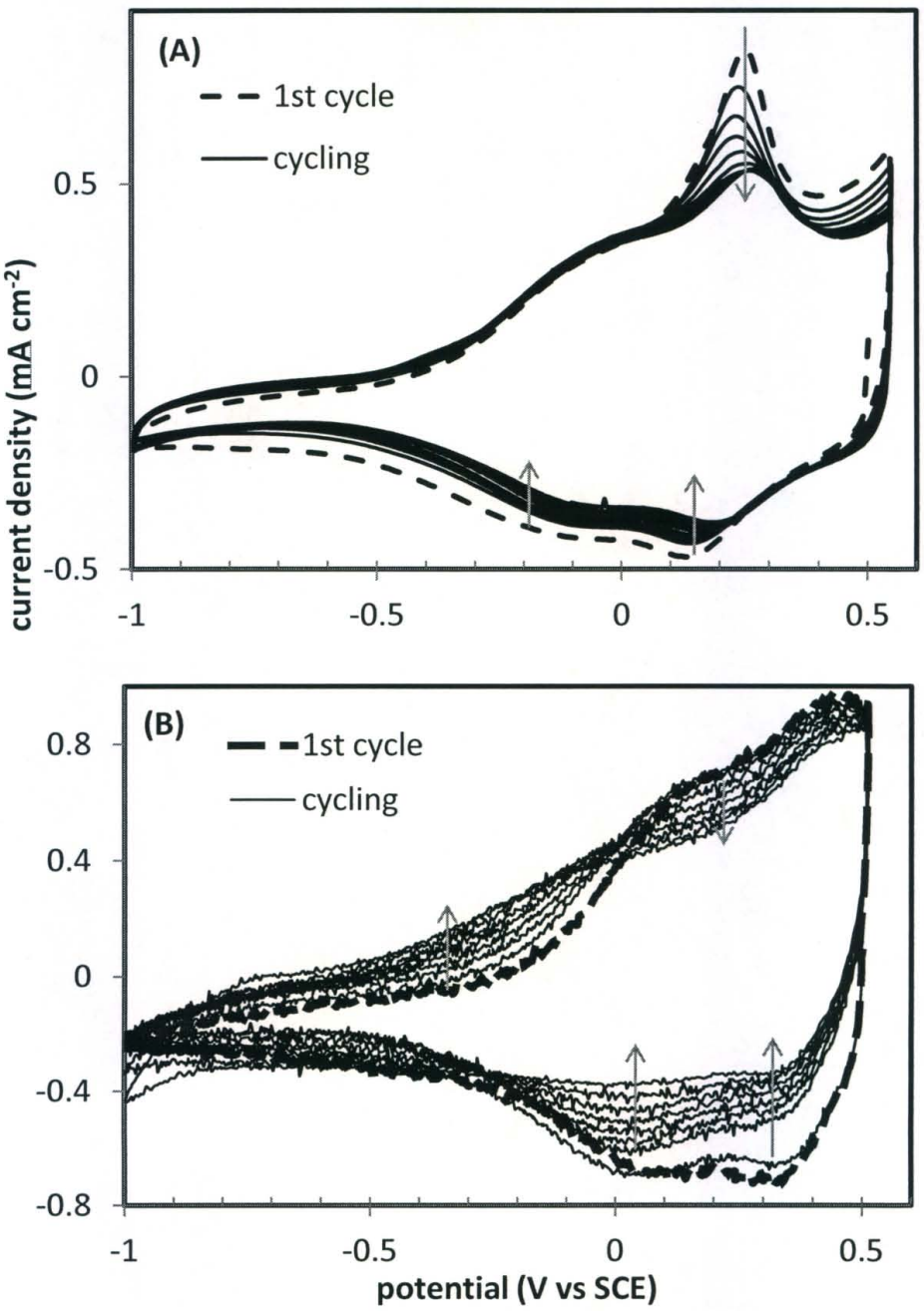

Fig. 4.12 Cycling of PPy-Fc films in **A.** 0.5 M $NaClO_4$ at 0.05 V s^{-1}; **B.** CH_3CN with 0.1 M Et_4NClO_4 at 0.1 V s^{-1}. The films were deposited on GC electrodes from 0.1 M Py, FcOH (**A.** 10 mM, **B.** 20 mM), 20% BFEE in CH_3CN with deposition charges of 0.018 C (0.25 C cm^{-2}).

Fe(II) than Fe(III) in the polymer matrix. A small peak shift in the positive direction can be noticed for both peaks which may indicate polymer chain restructuring. In the non-aqueous solution, the FcOH redox peaks can be seen at ca. 0.4 V which is consistent with Figure 4.3 for FcOH in the non-aqueous solution. The PPy redox peaks experienced also a small shift to positive potentials seen at ca. 0.05 V. Both PPy and FcOH redox waves decreased with cycling, however, the charging current (below -0.1 V) increased during the anodic scan and decreased during the cathodic scan which may attributed to cation transport of the reduced form. The current changes were tested by hydrolysis in aqueous solution (dipping in aqueous solution for about one minute). Figure 4.13 shows CVs in non-aqueous solution of a PPy-Fc film before and after hydrolysis. It can be seen that the film exhibited lower cation insertion currents (below -0.3 V) after hydrolysis and more facile anion insertion (-0.3 V to +0.3 V on the anodic scan), which can be attributed to a better solvation after hydrolysis.

Polarizing the polymer film at a fixed positive potential causes the film to be in an oxidized doped state and drives the redox reaction of FcOH to Fe(III), i.e. $Fe^{2+} \rightarrow Fe^{3+} + e^-$. In contrast, polarizing the film at a fixed negative potential causes the film to be in a reduced undoped state and drives the redox reaction of FcOH to Fe(II). i.e. $Fe^{3+} + e^- \rightarrow Fe^{2+}$. Figure 4.14 shows voltammograms of a PPy-Fc film at three different conditions: as-prepared, polarized at 0.3 V, and polarized at -0.2 V. The anodic peak of FcOH decreased significantly with polarization at 0.3 V indicating less Fe(II) to be oxidized, but the PPy redox wave was not or very little affected by such polarization.

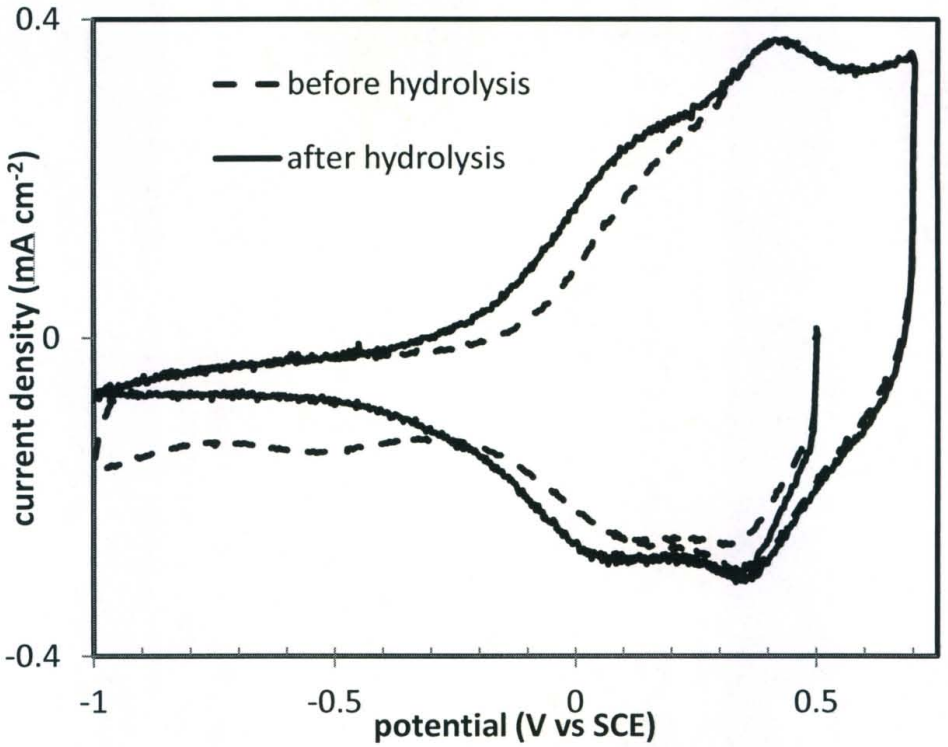

Fig. 4.13 Cyclic voltammograms of a PPy-Fc film in CH_3CN with 0.1 M Et_4NClO_4 at 0.05 V s^{-1} before and after hydrolysis (dipping in an aqueous solution for about one minute). The film was deposited on a GC electrode from 0.1 M Py, 15 mM FcOH, 20% BFEE in CH_3CN with a deposition charge of 0.018 C (0.25 C cm^{-2}).

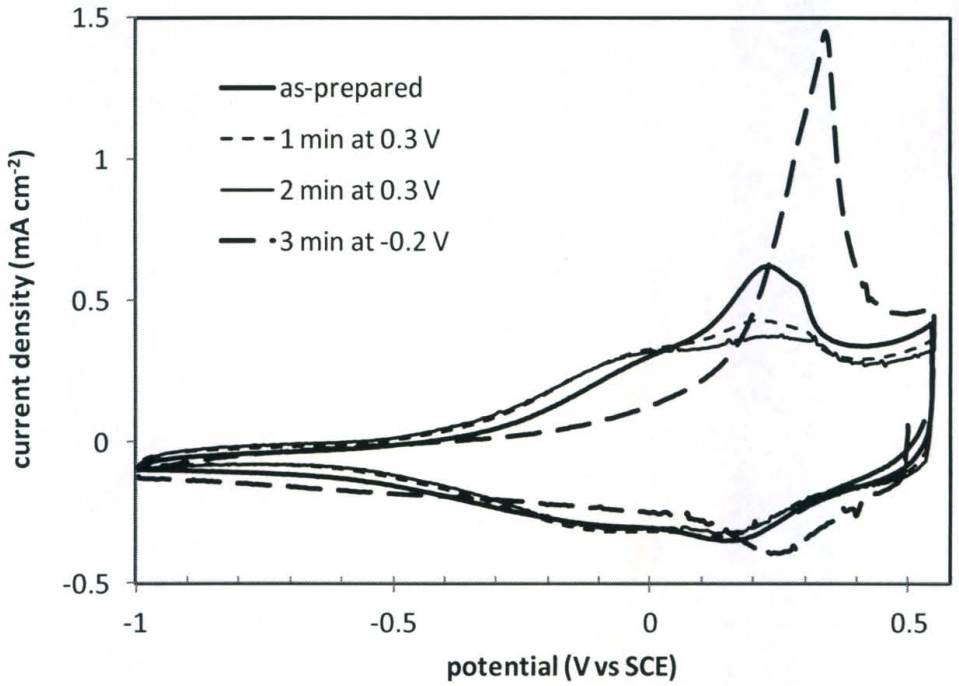

Fig. 4.14 Cyclic voltammograms of PPy-Fc films in 0.5 M $NaClO_4$ at 0.05 V s^{-1}. The films were polarized at different potentials for the indicated time. The films were deposited on GC electrodes from 0.1 M Py, 10 mM FcOH, 20% BFEE in CH_3CN with deposition charges of 0.018 C (0.25 C cm^{-2}). The -0.2 V polarized film is a different film made at the same conditions.

Shifting the PPy anodic peak to less positive potentials indicates facile electrochemical switching to the conducting state. On the other hand, a high anodic peak spike with peak shift to more positive potentials was observed after polarizing the film at -0.2 V indicating more Fe(II) to be oxidized. The PPy redox wave almost disappeared, probably due to the non-conducting neutral state (very low counterion concentration in the polymer matrix) which requires an overpotential to switch the film to the conducting state. In both cases, the cathodic peak (i.e. undoping) did not change significantly indicating insignificant loss of FcOH.

Using a steric stabilizer, such as polyethylene glycol 400 (PEG-400), during the electrochemical deposition of the polymer film can increase the porosity of the film and facilitate the transport of larger molecules and ions. Large molecules, such as FcOH, could potentially move freely into/out of the polymer film. PPy-Fc coated electrodes were therefore prepared in the presence of 1% or 2% PEG-400. The activation and insertion of PEG molecules into the polymer film follow the same reaction steps as shown in Figure 4.2. The modified films (i.e. PPy-Fc-PEG) showed enhanced electrochemical activity in both aqueous and non-aqueous solutions. Figure 4.15 shows cycling of PPy-Fc-PEG in aqueous solution where the anodic peak decreased with cycling more than the cathodic peak. There are clear FcOH peaks showing significant incorporation of FcOH into the film. However, removal of FcOH from the polymer film during cycling was insignificant as indicated by the almost constant charge under the Fe(III) reduction peak. The trapped charges released during oxidation of Fe(II) were

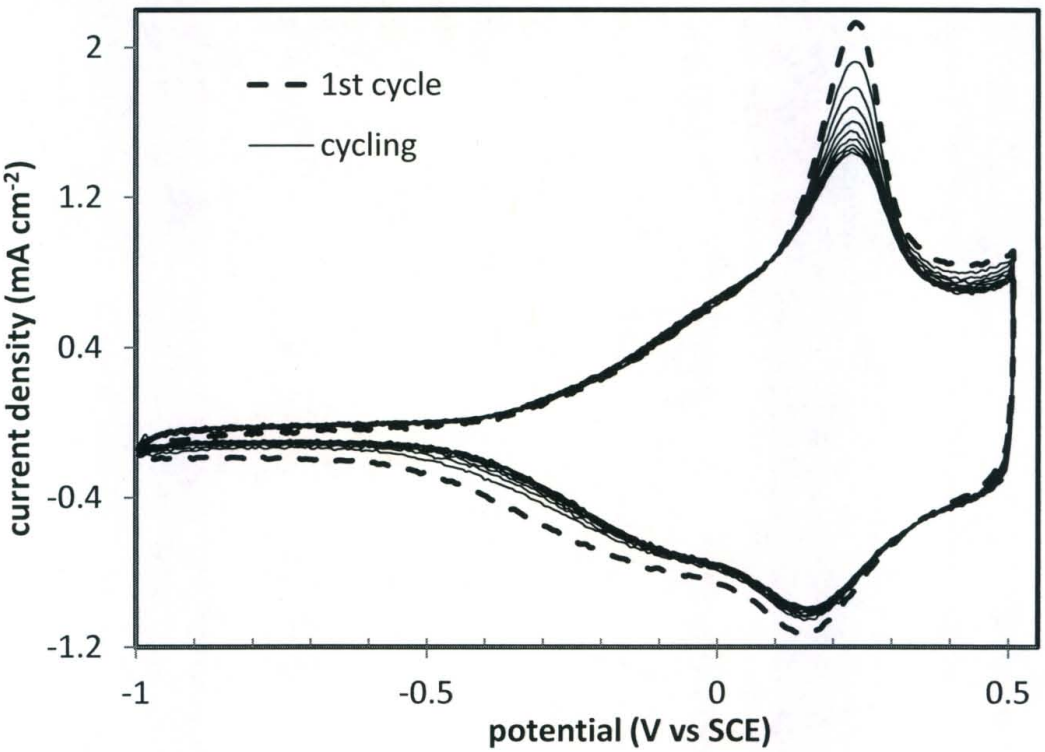

Fig. 4.15 Cycling of a PPy-Fc-PEG film in 0.5 M $NaClO_4$ at 0.1 V s^{-1}. The film was deposited on a GC electrode from 0.1 M Py, 20 mM FcOH, 20% BFEE, 1% PEG-400 in CH_3CN system with a deposition charge of 0.018 C (0.25 C cm^{-2}).

significantly reduced with cycling. In the non-aqueous solution, the charging current (below 0 V) of the PPy-Fc-PEG film was reduced compared with the PPy-Fc film (Figure 4.16). Facile anion transport and electron transport can also be noticed for the PPy and FcOH redox waves, respectively at 0.1 V and 0.35 V, after modifying the film with PEG. However, in both cases there is no indication for FcOH complete removal indicating strong interactions between FcOH and the polymer chains. The influence of steric stabilizers on the electrochemical activity of the polymer films is described in more details later in this chapter.

4.2.5 Influence of counterions

The influence of counterions on the ion transport properties of PPy-Fc films was studied in three different solutions (i.e. NaCl, $NaClO_4$, and ARS) and compared with the unmodified PPy film. These films were made in the same way in the presence (i.e. for PPy-Fc) and absence (i.e. for PPy) of FcOH. The ion transport properties of PPy films depend mainly on anion transport. All the solutions used to test ion transport have the same co-ion (i.e. Na^+), but the counterions differs in size as follows; small (Cl^-), medium (ClO_4^-), and large (ARS), see Figure 4.2 for the structure of ARS. Figure 4.17 shows CVs of PPy and PPy-Fc films in three different electrolyte solutions. It can be seen that the highest electrochemical activity, and so the highest ion mobility, for PPy-Fc is in $NaClO_4$, but for PPy it is in NaCl. It is obvious that Cl^- exhibited high mobility due to its small size, but for ClO_4^- to exhibit higher mobility than Cl^- in PPy-Fc is an anomalous behaviour. The

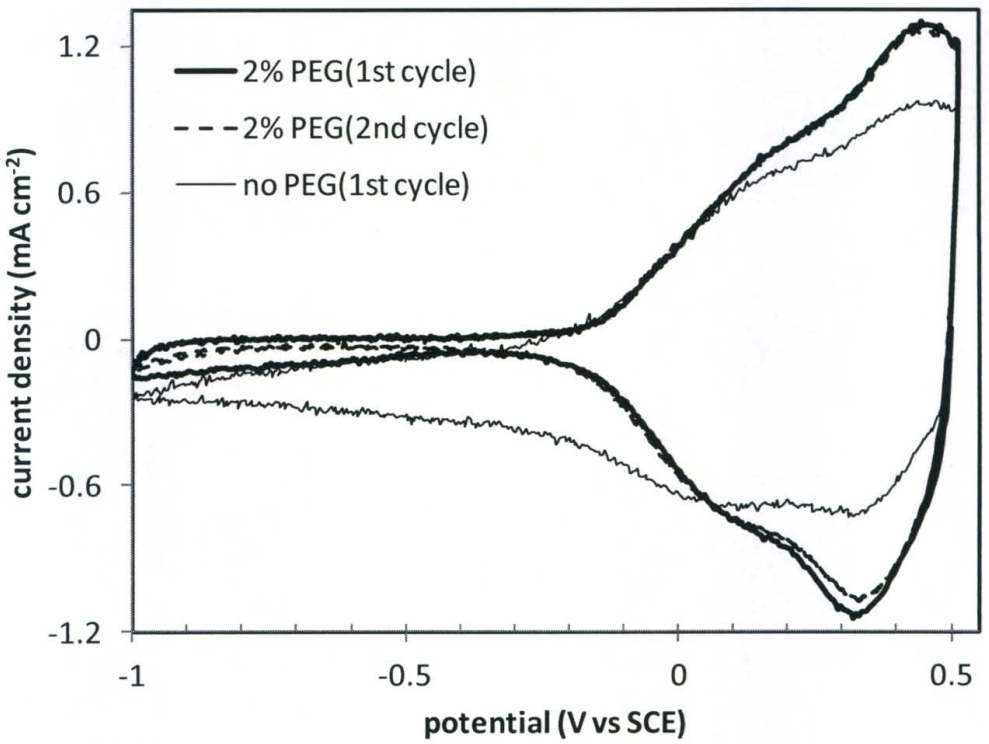

Fig. 4.16 Cyclic voltammograms of PPy-Fc films with/out PEG-400 in CH_3CN with 0.1 M Et_4NClO_4 at 0.1 V s^{-1}. The films were deposited on GC electrodes from 0.1 M Py, 20 mM FcOH, 20% BFEE, 2% PEG-400 in CH_3CN system with deposition charges of 0.018 C (0.25 C cm^{-2}).

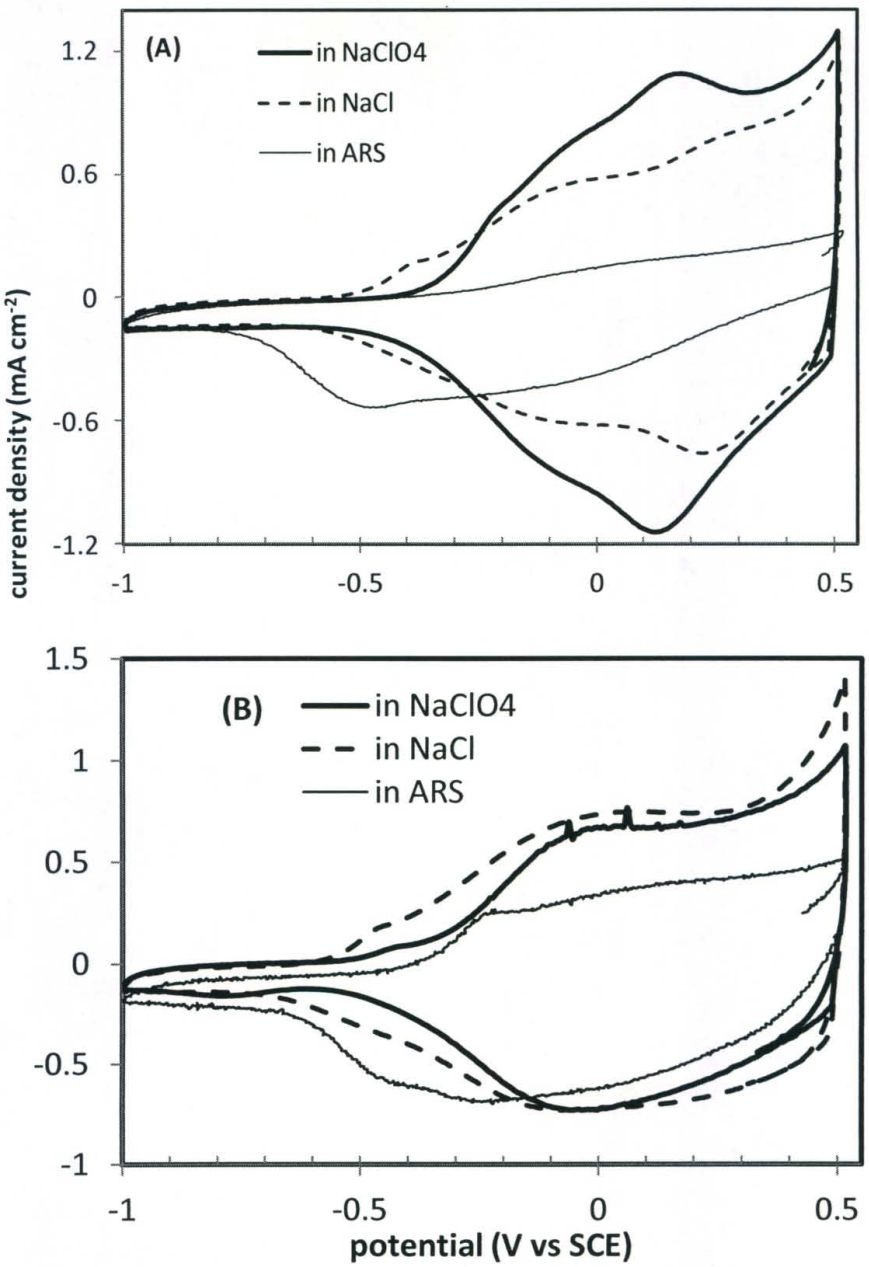

Fig. 4.17 Cyclic voltammograms of **A.** PPy-Fc; **B.** PPy films at 0.1 V s^{-1} in various electrolyte solutions as indicated. The films were deposited on GC electrodes from 0.1 M Py, 10 mM FcOH, 20% BFEE in CH_3CN with a deposition charge of 0.018 C (0.25 C cm^{-2}).

unexpected behaviour of some mobile ions was observed in PPy matrices and was attributed to various ion-polymer interactions (16). In this case, where Cl^- has lower ion mobility than ClO_4^- in PPy-Fc, the unexpected behaviour can be attributed to the additional intermolecular interactions in the modified polymer film (i.e. PPy-Fc) which affected by the smaller ion more due to its electronic distribution (i.e. hard ion). Thus, polymer film modifications can change the ion transport properties of the polymer film due to the additional intermolecular interactions, i.e. thermodynamic origin. Finally, it can be seen that both polymer films exhibited low electrochemical activity in ARS, where the counterions are too large to move into/out of the polymer film.

4.2.6 Impedance spectroscopy

The modified polymer films (PPy-Fc) were investigated by electrochemical impedance spectroscopy (EIS) which can be used to probe the electronic and ionic properties of the doped and undoped states of conducting polymers. The impedance results for PPy-Fc are compared with those of an unmodified polymer film (PPy) to observe the influence of the modifier group on the ion transport properties of the polymer film. Figure 4.18 shows impedance plots for PPy and PPy-Fc films in 0.5 M $NaClO_4$ at various potentials representing decreasing oxidation levels (i.e. 0.2 V, 0.1 V, 0 V, and -0.1 V). Both polymer films were deposited from BFEE/CH_3CN on GC electrodes at constant current with deposition charges of 0.018 C (i.e. 0.25 C cm^{-2}). The impedance measurements were taken after cycling in $NaClO_4$ solution (two cycles between 0.5 V

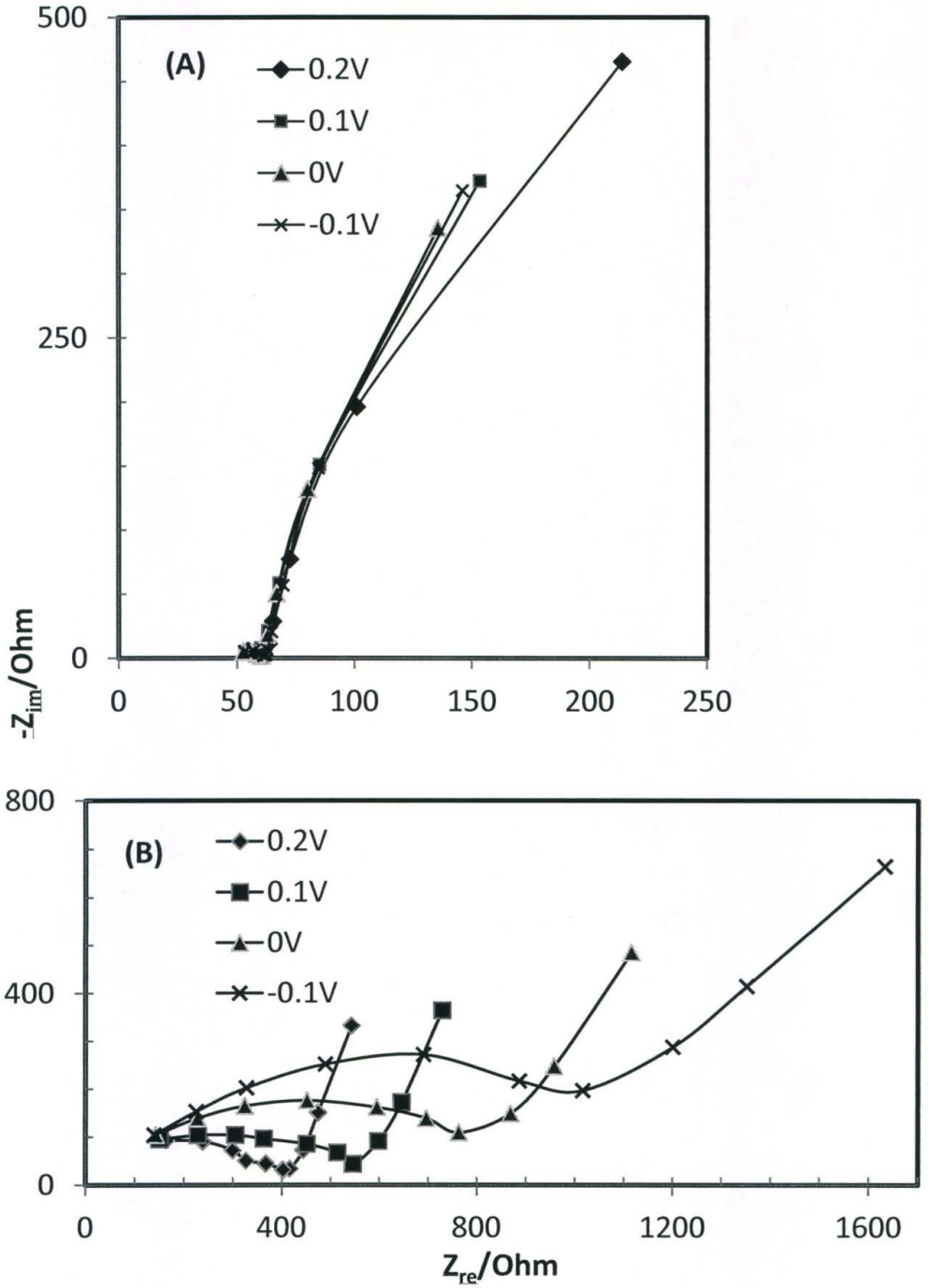

Fig. 4.18 Impedance plots of **A.** PPy, **B.** PPy-Fc films measured in 0.5 M $NaClO_4$ at the indicated potentials. The films were cycled twice in $NaClO_4$ between 0.5 V and -1.0 V before measurements. The films were deposited on GC electrodes from 0.1 M Py, 20 mM FcOH (B), 20% BFEE in CH_3CN with deposition charges of 0.018 C.

and -1.0 V at 0.1 V s^{-1}) to bring the films to the same conditioned state. The impedance behaviour of the PPy film was largely potential independent over the tested range with negligible charge transfer resistance (R_{CT}). In contrast, the PPy-Fc film exhibited potential dependent behaviour with significant charge transfer resistances that increased at lower potentials (i.e. lower oxidation states). It can also be seen that the PPy film exhibited faster ion transport in $NaClO_4$, indicated by very small Warburg lines (almost negligible) which represent the ionic resistance inside the polymer matrix.

Figure 4.19 compares the impedance and series capacitance (C_s) behaviours for PPy and PPy-Fc at 0.2 V. The appearance of a charge transfer resistance can be attributed to the presence of the large immobilized group (FcOH) inside the polymer matrix, which reduces the mobility of the ClO_4^- counterions. It can also be seen that the immobilization of such groups can increase the charge capacity of the polymer film (Figure 4.19-B). Three features can be identified from the capacitance plots of PPy-Fc; the zero slope at high frequency indicating a significant charge transfer resistance, the high slope at medium frequency indicating high ionic conductivity of the polymer layer, and the almost horizontal slope at low frequency, where the redox reaction encompasses the whole polymer layer, indicating the limiting capacitance of the polymer layer. This behaviour is not completely shown in the plot, and so it was called low-frequency capacitance (C_{lf}).

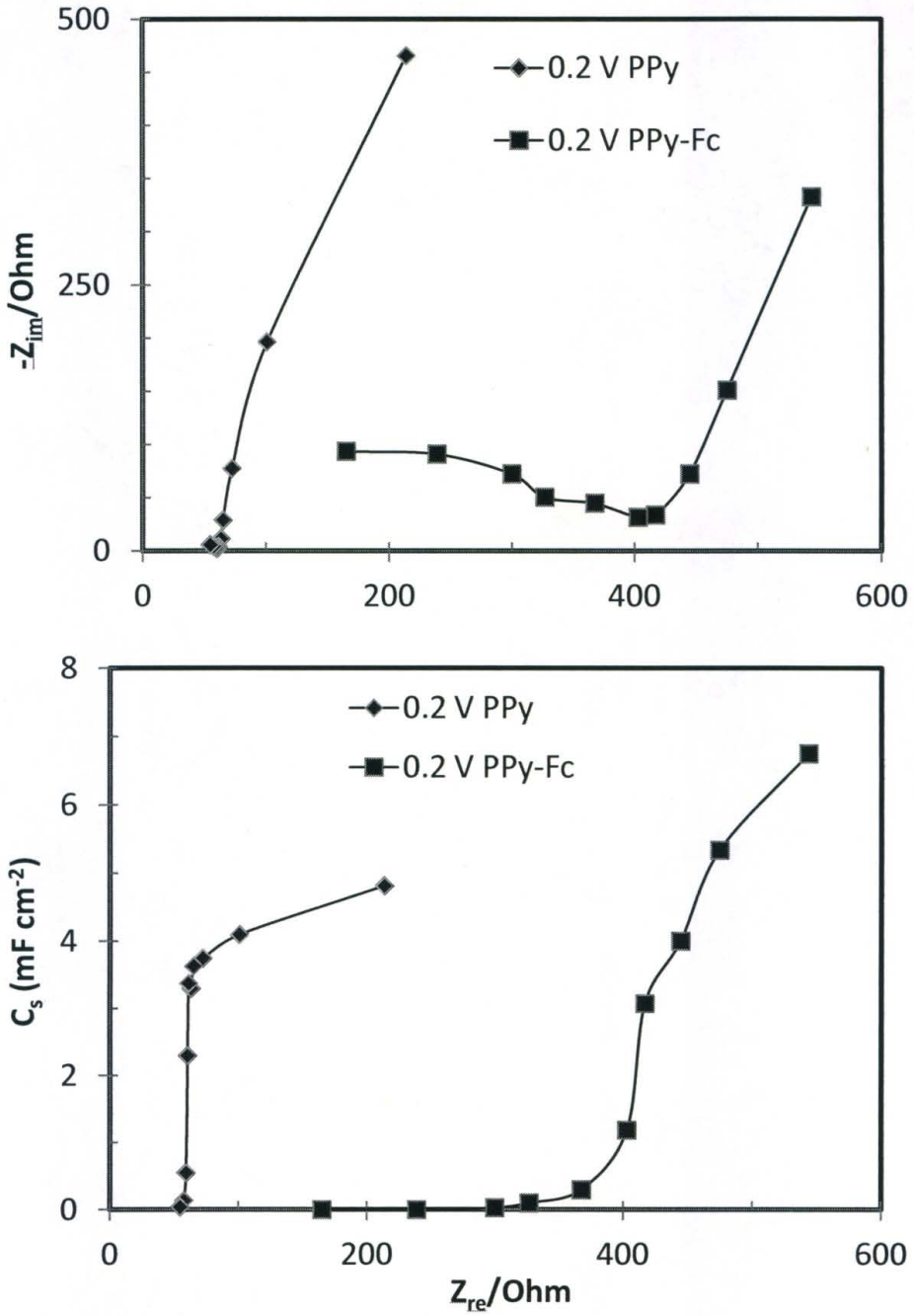

Fig. 4.19 **A.** Impedance and **B.** series capacitance plots for PPy and PPy-Fc films measured in 0.5 M $NaClO_4$ at 0.2 V. The films were cycled twice in $NaClO_4$ between 0.5 V and -1.0 V before measurements. The films were deposited on GC electrodes from 0.1 M Py, 20 mM FcOH for PPy-Fc, 20% BFEE in CH_3CN with deposition charges of 0.018 C.

Table 4.4 summarizes properties taken from impedance and capacitance plots. The two polymer films (PPy and PPy-Fc) are compared at four different oxidation states. It should be noticed that the two films were deposited at the same deposition charge (0.018 C) on GC electrodes and cycled in $NaClO_4$ electrolyte solution before the measurements were taken. It can be seen that the charge transfer resistance (R_{CT}) and the ionic resistance (R_i) were much larger for the PPy-Fc film due to restricted ion mobility resulting from FcOH immobilization. R_{CT} and R_i for the PPy film are almost constant and independent of potential indicating that the contribution of electron transport was insignificant due to fast electron transport over the potential range. It can also be seen that as the oxidation state of PPy-Fc increases (i.e. from -0.1 V to 0.2 V), R_{CT} and R_i decrease indicating higher conductivity at higher doping levels. The low frequency capacitance (C_{lf}) was highest at 0 V and 0.2 V for PPy and PPy-Fc films, respectively. This can be attributed to the maximum level of electroactive centers that were accessible at different oxidation states due to different ion transport mechanisms. The uncompensated solution resistance (R_s) was constant for both films indicating that its value is independent of potential.

Table 4.4 Properties of PPy and PPy-Fc films in 0.5 M $NaClO_4$

polymer film[a]	E[b] (V)	R_s[c]	R_s'[d]	R_{low}[e]	R_{high}[f]	R_{CT}[g]	R_i[h]	C_{lf} (mF cm^{-2})[i]
PPy	0.2	54	62	61	57	8	12	4.8
PPy	0.1	53	62	61	57	9	12	6.0
PPy	0	53	62	61	57	9	12	6.7
PPy	-0.1	53	62	62	57	9	15	6.1
PPy-Fc	0.2	55	403	417	380	348	111	6.7
PPy-Fc	0.1	55	546	546	500	491	138	6.2
PPy-Fc	0	55	770	763	600	715	489	4.6
PPy-Fc	-0.1	55	1000	NA	700	945	NA	3.4

NA: not available

[a] polymer films were deposited on GC electrodes with deposition charge of 0.018 C (0.25 C cm^{-2}) from CH_3CN/BFEE.

[b] potential bias for impedance measurements (versus SCE)

[c] uncompensated solution resistance (all resistances were measured in ohm)

[d] real axis intercept (Z_{re}) of low-frequency semi-circle

[e] real axis intercept (Z_{re}) of low-frequency region of impedance plot

[f] real axis intercept (Z_{re}) of high-frequency Warburg line

[g] charge transfer resistance ($R_{CT} = R_s' - R_s$)

[h] ionic resistance, $R_i = 3\ (R_{low} - R_{high})$

[i] capacitance taken at the lowest frequency

4.3 Modification of polypyrrole films with steric stabilizers

Steric stabilizers are macromolecules used to stabilize polymer systems by dispersion of their chains. It was reported that the conductivity and mechanical stability of polypyrrole films can be enhanced by using a steric stabilizer, such as polyethylene glycol (PEG), during the electrodeposition (12). PEG is a non-ionic compound, but can be activated to gain a negative charge by using BFEE as shown in Figure 4.2.

The influence of steric stabilizers on the electrochemical behaviour of the polymer films (i.e. PPy and PPy-Fc) is described in this section. Ferrocene-containing polymer films grown in the presence of polyethylene glycol (i.e. PPy-Fc-PEG) of different molecular weights were investigated for enhanced electrochemical activity and compared with PPy and PPy-Fc films in aqueous electrolytes. Figure 4.20 shows cyclic voltammograms of PPy-Fc-PEG prepared in the presence of 1% PEG-400. The films were deposited from BFEE/CH_3CN by using three different techniques: galvanostatic (GS), potentiostatic (PS), and potentiodynamic (PD). All of the techniques were successful to deposit PPy-Fc in the presence of PEG-400 and both waves of PPy and FcOH can be clearly identified in the three voltammograms. The enhanced electrochemical activity of each film can be compared with its counterpart film grown without PEG (see Figure 4.4). A comparison of polymer films grown with different concentration of PEG-400 is shown in Figure 4.21. A film grown without PEG (i.e. PPy-Fc) is also shown in the figure as a reference point. The highest electrochemical activity for the polymer films can be seen for the film grown from 1% PEG-400.

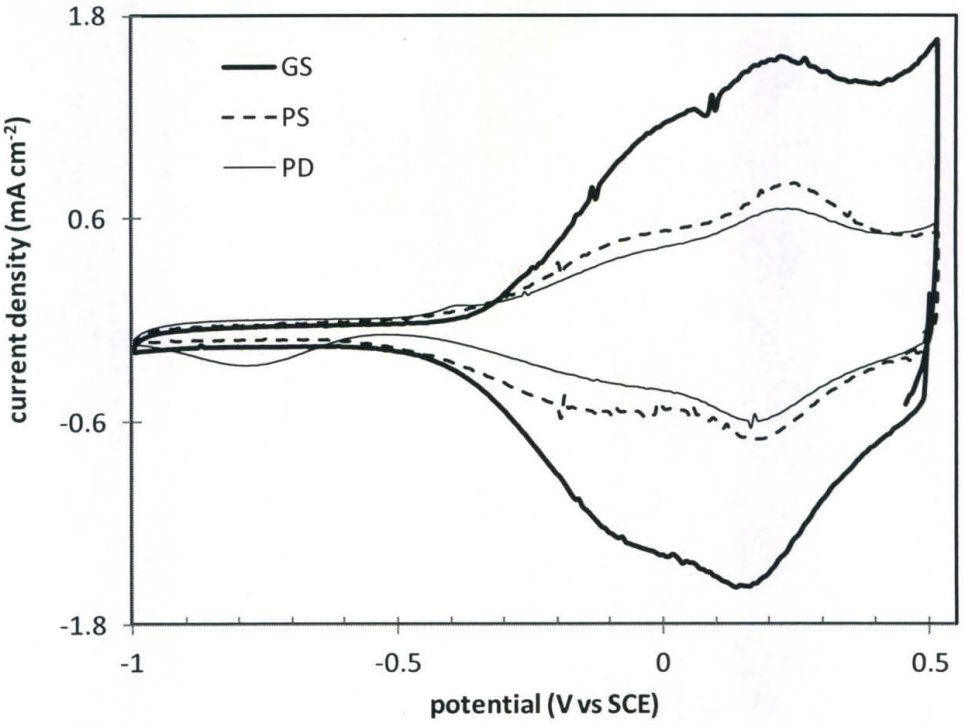

Fig. 4.20 Cyclic voltammograms of PPy-Fc films prepared in the presence of 1% PEG-400 and deposited by using various techniques as follows; GC: galvanostatic, PS: potentiostatic, PD: potentiodynamic. The measurements were taken in 0.5 M $NaClO_4$ electrolyte solution at scan rate of 0.1 V s^{-1}. The polymer films were deposited on GC electrodes from 0.1 M Py, 10 mM FcOH, and 20% BFEE in CH_3CN under the following deposition condition; GS: 0.3 mA (0.018 C), PS: 1.0 V for 1 min., PD: 0.1 V s^{-1} (5 cycles between -0.2 V and 1.2 V).

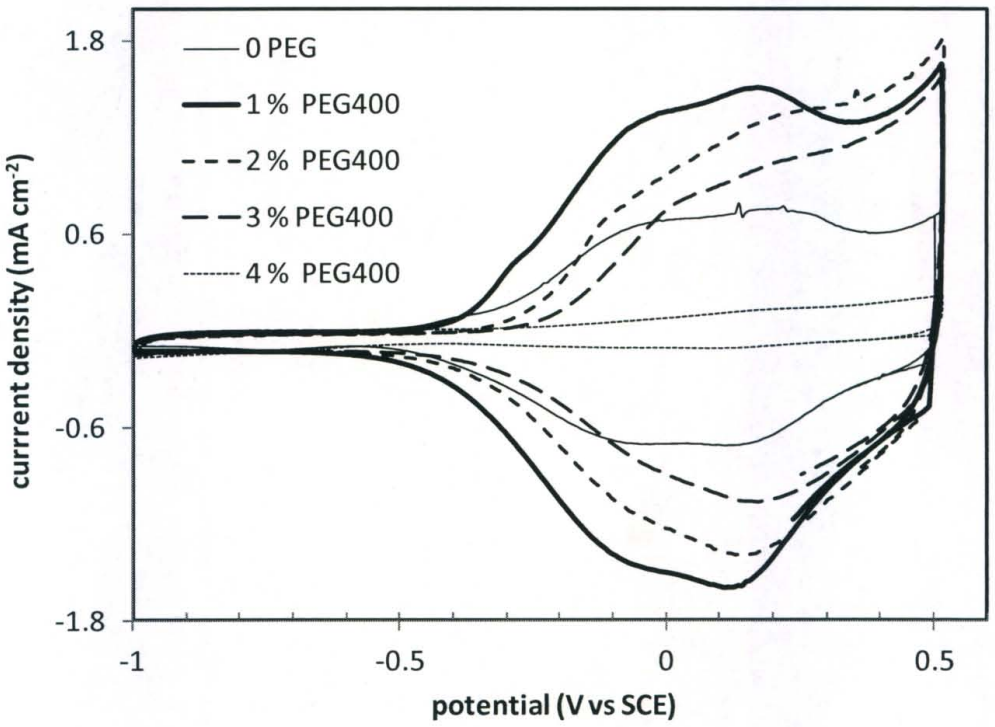

Fig. 4.21 Cyclic voltammograms of PPy-Fc films prepared in the presence of various concentrations of polyethylene glycol 400 (PEG-400). The measurements were taken in 0.5 M $NaClO_4$ at 0.1 V s^{-1}. The polymer films were deposited on GC electrodes from 0.1 M Py, 10 mM FcOH, 20% BFEE, PEG-400 in CH_3CN with deposition charges of 0.018 C (0.25 C cm^{-2}).

However, the activity was gradually decreased with increasing PEG-400 concentration above 1%, and a sharp activity decrease with 4% PEG-400 was observed.

The influence of PEG can be explained by dispersion effects. After the activation of PEG with BFEE, it can be involved in charge compensation of the forming polycation film. The incorporation of PEG into the polymer matrix can decrease the agglomeration of the polymer chains, and thus the electroactive centers become more accessible to counterions. The electrochemical activity of the polymer films can therefore be enhanced by using PEG during the electrodeposition. However, the polymerization efficiency might be affected if the deposition charge is partially consumed in oxidizing the hydroxyl group of PEG, which could be a significant factor in the case of high concentrations of PEG.

The base polymer film (i.e. PPy) was also modified with PEG (i.e. PPy-PEG) and compared with an unmodified PPy film. Figure 4.22 shows cyclic voltammograms of polymer films prepared in the presence of 1% PEG-400 (i.e. PPy-PEG) and grown at different polymerization charges (i.e. 0.018 C, 0.036 C, and 0.054 C). These modified films were compared with an unmodified PPy film grown at 0.018 C. It can be seen that the electrochemical activity of the polymer film can be significantly enhanced with the use of 1% PEG-400 and the activity increased almost linearly with the polymerization charge.

To understand the effect of the modifier length, PEGs with different molecular weights including its monomer (i.e. ethylene glycol, EG) were investigated for the

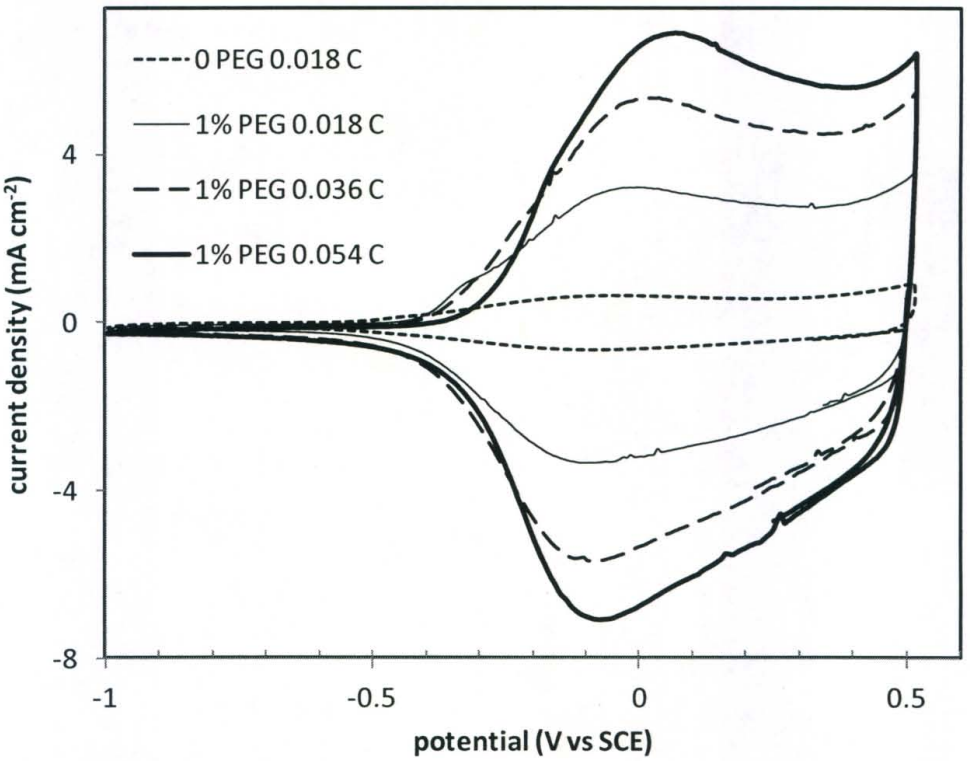

Fig. 4.22 Cyclic voltammograms of PPy films prepared with/out 1% PEG-400. The measurements were taken in 0.5 M $NaClO_4$ at 0.1 V s^{-1}. The polymer films were deposited on GC electrodes from 0.1 M Py, 20% BFEE in CH_3CN by galvanostatic polymerization with various deposition charges as indicated.

electrochemical activity of the modified polymer films. Figure 4.23 shows cyclic voltammograms of polymer films prepared in the presence of 1% of EG, PEG-200, PEG-400, and PEG-1000 and compared with an unmodified polymer film (PPy). The numbers beside PEG (i.e. 200, 400, 1000) represent the average molecular weights of the used steric stabilizer.

All of the modified films exhibited higher activities than the unmodified film, but to various degrees. The molecular weight influenced the electrochemical activity of the modified polymer films in the following order: PEG-1000 ≥ EG > PEG-400 > PEG-200. The origin of this sequence might be explained in terms of the polymerization efficiency which is enhanced with higher molecular weights of the steric stabilizers. However, EG is not a polymer and so PPy-EG has a different effect which influences its properties. Probably, EG works as a small mobile modifier to reduce the electrostatic repulsion during the deposition of the forming polycation. In contrast, PEGs produce porous composite polymer films. This conclusion can be supported by the oxidation potential offset of PPy-PEG1000 which was shifted to less positive potentials on the anodic scan, i.e. facile electrochemical switching for a porous polymer composite electrode.

Figures 4.24 to 4.27 show CVs of PPy films prepared in the presence of various concentrations of EG, PEG-200, PEG-400, and PEG-1000, respectively. The optimal concentration of the modifier was 1% which results in the highest activity over the tested range. It can be seen that the activity of all films decreased at modifier

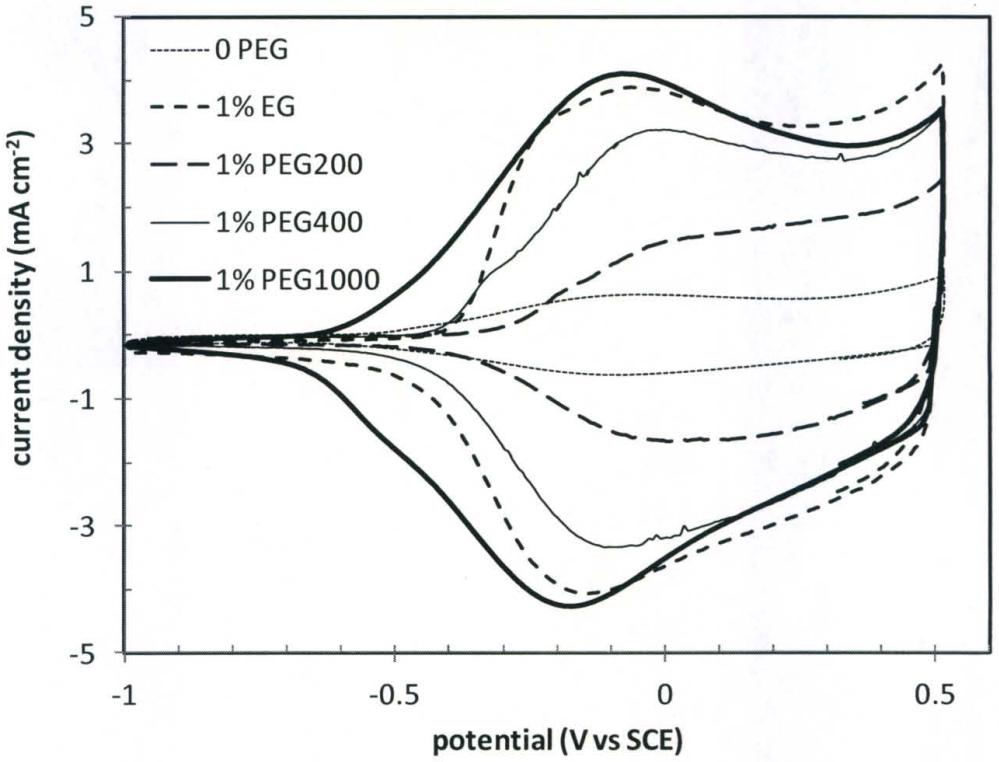

Fig. 4.23 Cyclic voltammograms of PPy films prepared with/out 1% of various steric stabilizers. The measurements were taken in 0.5 M $NaClO_4$ at 0.1 V s^{-1}. The polymer films were deposited on GC electrodes from 0.1 M Py, 20% BFEE in CH_3CN with different deposition charge of 0.018 C.

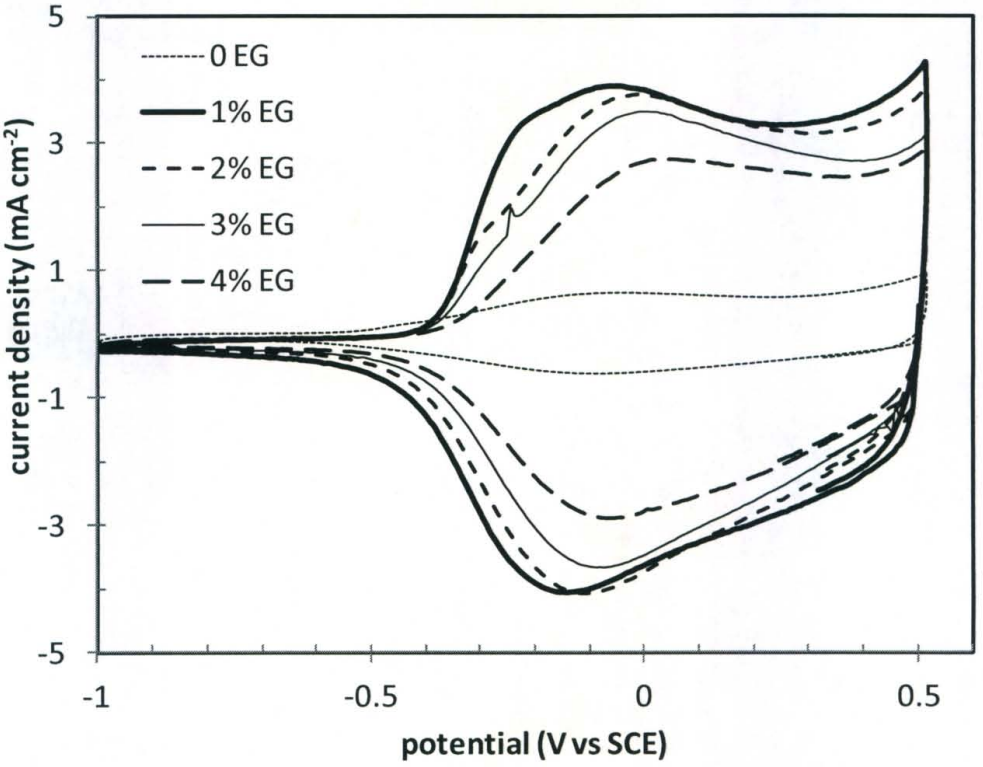

Fig. 4.24 Cyclic voltammograms of PPy films prepared with/out various concentrations of ethylene glycol (EG). The measurements were taken in 0.5 M $NaClO_4$ at 0.1 V s^{-1}. The polymer films were deposited on GC electrodes from 0.1 M Py, 20% BFEE, the indicated amount of EG, in CH_3CN with deposition charge of 0.018 C.

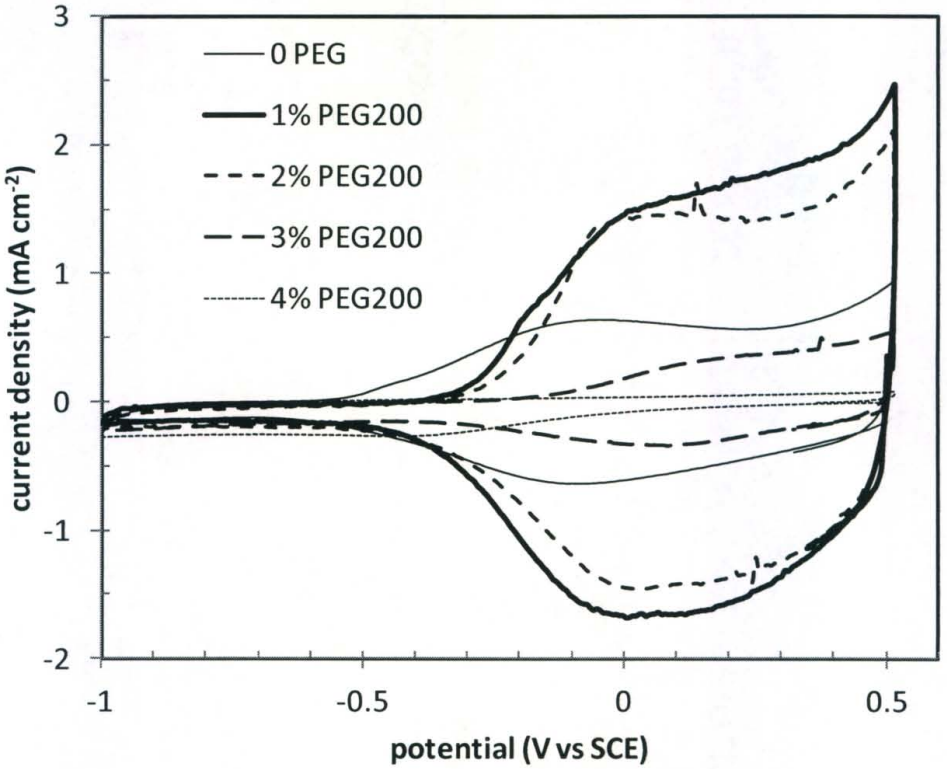

Fig. 4.25 Cyclic voltammograms of PPy films prepared with/out various concentrations of polyethylene glycol 200 (PEG-200). The measurements were taken in 0.5 M $NaClO_4$ at 0.1 V s^{-1}. The polymer films were deposited on GC electrodes from 0.1 M Py, 20% BFEE, the indicated amount of PEG-200 in CH_3CN with deposition charges of 0.018 C.

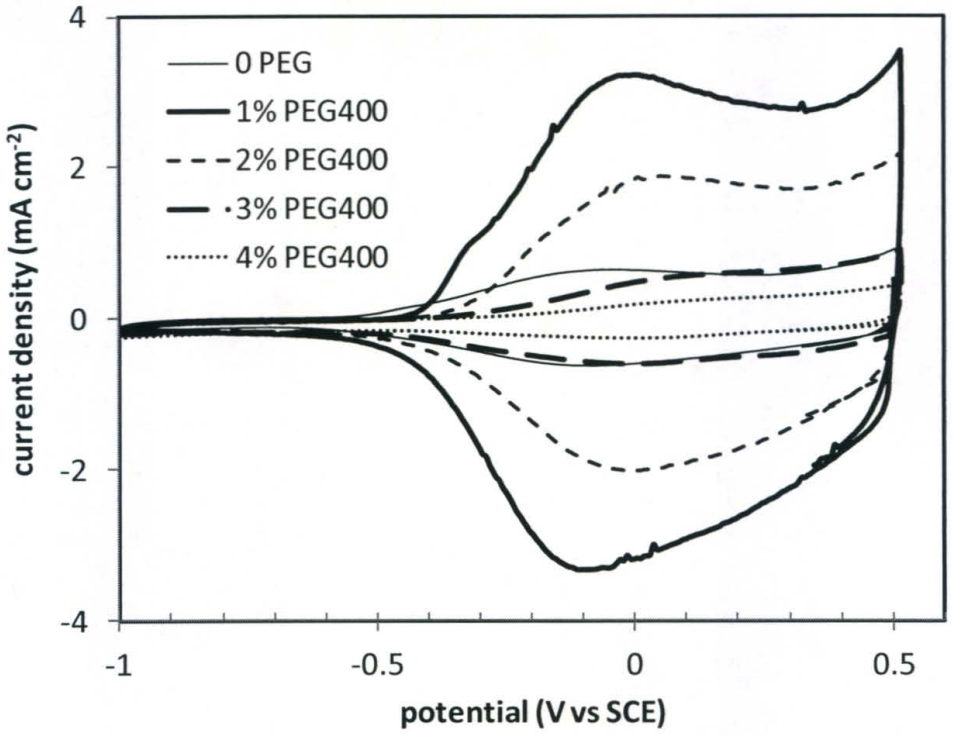

Fig. 4.26 Cyclic voltammograms of PPy films prepared with/out various concentrations of polyethylene glycol 400 (PEG-400) in 0.5 M $NaClO_4$ at 0.1 V s^{-1}. The polymer films were deposited on GC electrodes from 0.1 M Py, 20% BFEE, PEG-400 in CH_3CN with deposition charges of 0.018 C.

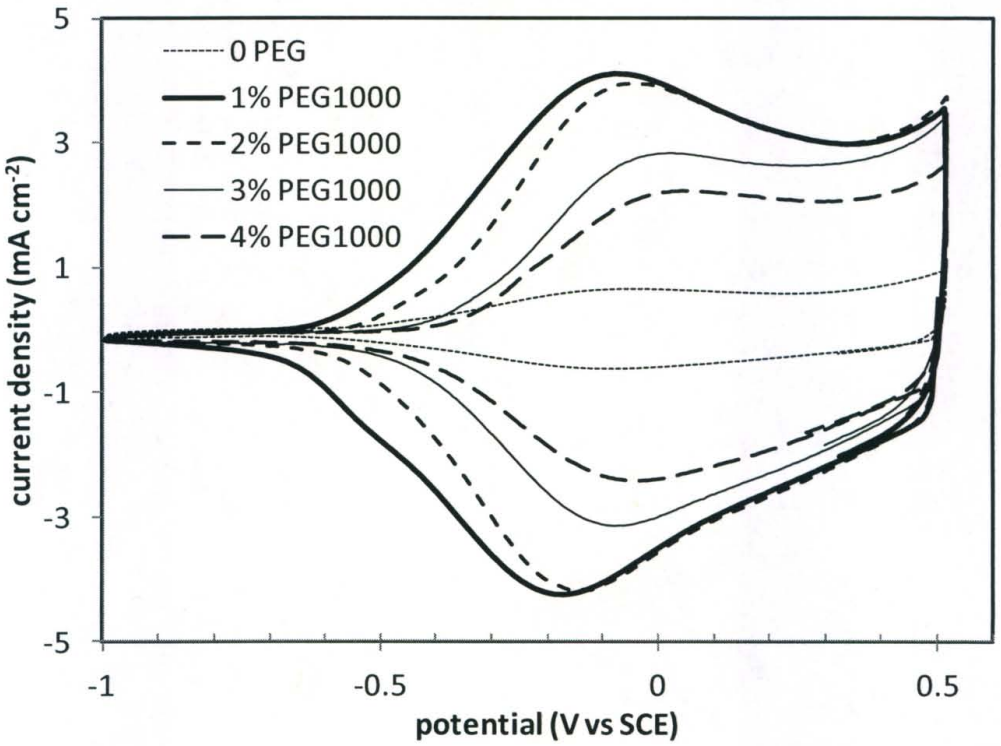

Fig. 4.27 Cyclic voltammograms of PPy films prepared with/out various concentrations of polyethylene glycol 1000 (PEG-1000) in 0.5 M $NaClO_4$ at 0.1 V s^{-1}. The polymer films were deposited on GC electrodes from 0.1 M Py, 20% BFEE, PEG-1000 in CH_3CN with deposition charges of 0.018 C.

concentrations above 1%. The activity of the polymer films did not change significantly with increasing the concentration of EG and PEG-1000. In contrast, a significant drop in the activity was observed at high concentrations (3% and 4%) of PEG-200 and PEG-400. Since the PEGs uptake should not be related to PEG concentration in the deposition solution, the origin of these effects must be related to variations in the polymerization efficiency. However, the extent of the activity decrease with each modifier length is not fully understood. The intermolecular interactions that each modifier can have with the counterions and polymer chains might have some effect. Table 4.5 summarizes the main aspects of the redox waves of the polymer films.

Figure 4.28 shows series capacitance plots (C_s versus Z_{re}) for the polymer films prepared with various concentrations of PEG-400 and compared with an unmodified PPy film. It can be seen that the capacitance was significantly enhanced for the polymer film with 1% PEG-400. The capacitance decreased after PEG-400 addition above 1% and returned to its original value for the PPy unmodified film for 4% PEG-400. This can be attributed, as discussed above, to the polymerization efficiency which is optimal at 1% of the steric stabilizer. The enhanced polymerization efficiency at 1% PEG is partially due the ionic complex formed between PEG and BF_3, however, high concentrations of PEG can reduce the deposition charge due to its consumption in the hydroxyl group oxidation, presumably to ketones.

Table 4.5 Redox waves properties of the polymer films in 0.5 M $NaClO_4$

polymer film	oxidation offset (V)	i_{pa} (mA cm^{-2})[a]	E_{pa} (V)[b]	i_{pc} (mA cm^{-2})[a]	E_{pc} (V)[b]
PPy	-0.58	0.64	-0.10	-0.64	-0.10
PPy-Fc	-0.47	0.66	-0.06	-0.70	-0.06
PPy-Fc-PEG400(1%)	-0.42	1.34	-0.03	-1.43	-0.04
PPy-Fc-PEG400(2%)	-0.30	0.94	0.00	-1.18	0.00
PPy-Fc-PEG400(3%)	-0.23	0.85	0.06	-0.82	0.04
PPy-Fc-PEG400(4%)	-0.23	0.10	0.09	-0.11	0.07
PPy-EG(1%)	-0.40	3.89	-0.07	-4.06	-0.14
PPy-EG(2%)	-0.40	3.72	-0.04	-4.06	-0.09
PPy-EG(3%)	-0.38	3.48	0.00	-3.64	-0.09
PPy-EG(4%)	-0.35	2.74	0.02	-2.89	-0.07
PPy-PEG200(1%)	-0.37	1.65	0.16	-1.66	0.05
PPy-PEG200(2%)	-0.27	1.43	0.16	-1.44	0.07
PPy-PEG200(3%)	-0.11	0.21	0.36	-0.32	0.17
PPy-PEG200(4%)	---[c]	---	---	---	---
PPy-PEG400(1%)	-0.47	3.19	-0.04	-3.32	-0.10
PPy-PEG400(2%)	-0.36	1.87	0.07	-2.04	0.03
PPy-PEG400(3%)	-0.30	0.60	0.15	-0.57	0.12
PPy-PEG400(4%)	-0.24	0.24	0.16	-0.27	0.12
PPy-PEG1000(1%)	**-0.61**	4.08	-0.09	-4.26	-0.18
PPy-PEG1000(2%)	-0.51	3.93	-0.05	-4.15	-0.17
PPy-PEG1000(3%)	-0.39	2.82	0.01	-3.15	-0.06
PPy-PEG1000(4%)	-0.33	2.21	0.09	-2.43	-0.02

[a] anodic peak and cathodic peak currents in mA cm^{-2}

[b] anodic peak and cathodic peak potentials in V

[c] no clear peak

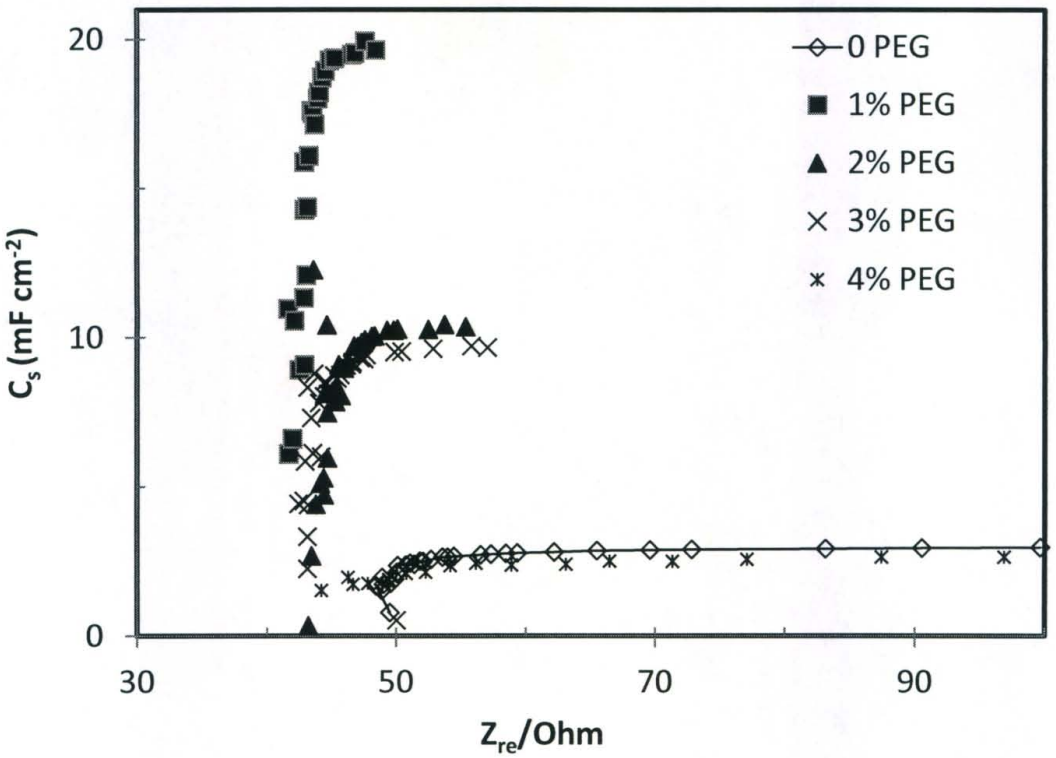

Fig. 4.28 Series capacitance plots for PPy films prepared with/out various concentrations of PEG-400 measured in 0.5 M $NaClO_4$ at 0.2 V. The films were deposited on GC electrodes from 0.1 M Py, the indicated amount of PEG-400, 20% BFEE in CH_3CN with deposition charges of 0.018 C. The frequency scan range was from 1 kHz to 1 Hz (to 0.1 Hz for 1% PEG).

The theoretical charge under a CV for $(\text{-PPy-})_3^+$ was calculated by using Equation 4.2.

$$Q_{cv}/Q_{pol} = n_{cv}/(2+n_{cv}) \qquad [4.2]$$

where Q_{cv} is the charge under the oxidation peak, Q_{pol} is the polymerization charge, and n_{cv} is the number of electrons consumed per pyrrole unit for partial oxidation (i.e. doping), which has a typical value between 0.25 and 0.33 (i.e. one positive charge for four and three Py units, respectively). The theoretical charge under the CV for Q_{pol} = 250 mC cm^{-2} was found to be between 28 mC cm^{-2} and 35 mC cm^{-2} for n_{cv} 0.25 and 0.33, respectively. The experimental charges under the CVs in Figures 4.22 and 4.26 were calculated by integration of the anodic peak up to 0.4 V. Table 4.6 summarizes the charge properties together with the film capacitance of some polymer films.

The polymerization efficiency (the charge of the polymer calculated from the area under oxidation peak over the charge consumed to form the polymer) was calculated by using Equation 4.3.

$$\text{pol. eff.} = (Q_{cv}/Q_{pol})\,(n_{pol}/n_{cv})\,100 \qquad [4.3]$$

where n_{pol} is the number of electrons consumed per Py unit during the polymerization. The factor (n_{pol}/n_{cv}) is used to normalize both Q_{cv} and Q_{pol} to be per one electron (n_{pol} = 2.3, n_{cv} = 0.3). The low polymerization efficiency of the unmodified PPy film can be understood because of the low ion concentration used for the polymerization, i.e. BEFF/CH_3CN. However, enhanced polymerization efficiency was observed with 1% PEG-400 added to the polymerization solution. This can be attributed to the ionic complex

formation between the hydroxyl group of PEG and BFEE, i.e. $[OH:BF_3]^-$, which increased the ionicity of the system. However, the polymerization efficiency decreased at higher PEG concentrations due to inefficiency of the deposition, i.e. some charge is used to oxidize the hydroxyl groups. It can also be seen that as the polymerization charge (Q_{pol}) increased polymerization efficiency decreased due to lower charge under the peak (Q_{cv}) of the produced thicker polymer. The low charge (Q_{cv}) for the thicker polymer can be attributed to the lower accessibility of counterions into inner polymer chains.

Table 4.6 Charge properties of PPy films

Film[a]	Q_{pol}[b]	Q_{cv}[c]	pol. eff.[d]	C_{film}[e]
PPy	250	5.72	18	2.9
PPy-1% PEG400	250	19.6	60	19.9
PPy-1% PEG400	507	30.5	46	--
PPy-1% PEG400	760	36.3	37	--
PPy-2% PEG400	250	11.0	34	9.7
PPy-3% PEG400	250	3.30	10	9.6
PPy-4% PEG400	250	1.33	4	2.5

[a] polymer film deposited from $BFEE/CH_3CN$ and corresponding concentration of PEG-400
[b] polymerization charge in mC cm^{-2}
[c] charge under the CV peak in mC cm^{-2} integrated up to 0.4 V
[d] polymerization efficiency calculated according to eq. 4.3
[e] film capacitance in mF cm^{-2} taken from Figure 4.28

4.4 Conclusions

Polypyrrole films have been modified by an electroactive ferrocene derivative (FcOH) using a novel method in which ionic ferrocene moieties are generated in situ with BF_3. They show an interesting electrochemical behaviour with enhanced charge capacity due to the redox of the FcOH complex. Polypyrrole was also modified with non-electroactive steric stabilizers which enhance its electrochemical activity by dispersing the polymer chains and decreasing agglomeration. The incorporation process of both species is believed to take place after complex formation between the hydroxyl group and the Lewis acid to gain a negative charge. Both types of modifier have a significant influence on the ion transport properties of the conducting polymer. Modifications with electroactive species lead to increase of the charge capacitance of the polymer film, while modifications with steric stabilizers lead to increase in the electrochemical activity of the polymer film.

The modifier incorporation process was successful using three electrochemical techniques: potentiodynamic, potentiostatic, and galvanostatic. The incorporation of the electroactive species can be monitored by the potentiodynamic technique during electrodeposition. However, attempts to expel the FcOH modifier by many different treatments were not successful, which indicates deep trapping of the molecule and/or complex formation with the conjugated system. In addition, electrochemical polymerization of pyrrole in the presence of modifiers was found to be very sensitive to the electropolymerization conditions.

4.5 Experimental

4.5.1 Electrochemistry and deposition of the polymer films

Electrochemical experiments were carried out in conventional three-compartment glass cells under a nitrogen atmosphere at 23 ± 2 °C. A glassy carbon (GC) disc working electrode of 0.071 cm^2, a Pt wire counter electrode, and a saturated calomel electrode (SCE) reference electrode were used. All potentials are quoted with respect to the SCE. All cyclic voltammograms and impedance measurements were taken under nitrogen gas.

In all cases, pyrrole (Py) was polymerized in non-aqueous solution and the cyclic voltammograms were measured in aqueous solution containing $NaClO_4$ as the supporting electrolyte or in non-aqueous solution of CH_3CN containing 0.1 M Et_4NClO_4 as the supporting electrolyte, unless otherwise stated. In a typical experiment, the polymer film was deposited from 0.1 M Py and 20% (v/v) BFEE in CH_3CN as the main solvent. In the case of incorporating a modifier into the polymer film, various concentrations of the modifier were also added to the polymerization solution, such as 10 mM of FcOH and 1% (v/v) PEG.

The polymer films were deposited on glassy carbon (GC) electrodes with surface area of 0.071 cm^2. The deposition charge was typically 0.018 C (0.25 C cm^{-2}) for galvanostatic polymerization. For potentiostatic and potentiodynamic polymerization, deposition conditions of holding potential at 1.0 V (for 1, 2, or 3 minutes) and scan rate of 0.1 V s^{-1} (between -0.2 V and 1.2 V) were used for deposition of the polymer film onto

the electrode surface, respectively. Unless otherwise stated, the potential scans started at +0.5 V.

4.5.2 Chemicals

Pyrrole (Py, Aldrich, 98%) was purified on a dry aluminum oxide column. Acetonitrile (CH_3CN, Aldrich, HPLC grade, 99.8%, water < 0.001), boron trifluoride ethyl etherate (BFEE, Aldrich, 46 % BF_3 basis, MW 141.93 g mol^{-1}), polyethylene glycol (PEG, Fluka, analytical grade, MW av. 200, 400, or 1000), sodium perchlorate ($NaClO_4$, Alfa Aesar, 98%), tetraethylammonium perchlorate (Et_4NClO_4, Alfa Aesar), 1-(ferrocenyl)ethanol (FcOH, Fluka, 97%, MW 230.08 g mol^{-1}), Alizarin Red S (ARS, synonym 3,4-dihydroxy-9,10-dioxo-2-anthracenesulfonic acid sodium salt, Sigma-Aldrich, $C_{14}H_7NaO_7S$, MW 342.26 g mol^{-1}), and sodium chloride (NaCl, ACP Chemicals, 99%), were used as received unless otherwise stated. The chemical structures of these chemicals are show in Figure 4.1. All aqueous solutions were prepared with deionized water.

4.5.3 Instrumentation

All electrochemical experiments were carried out using the same instruments described in Chapter 3. The UV-Vis spectra were recorded by an Agilent HP8453A UV-Visible diode array spectrophotometer, using tungsten and deuterium lamps for a 190 - 1100 nm spectral range. The instrument is precise within ± 0.5 nm. The flame atomic absorption instrument is a Varian SpectrAA 50 and an iron lamp was used.

References

1. W. Paik, I. Yeo, H. Suh, Y. Kim, E. Song, *Electrochim. Acta* 45 (2000) 3833.

2. M. Vorotyntsev, S. Vasilyeva, *Adv. Colloid Interface Sci.* 139 (2008) 97.

3. S. Radhakrishnan, S. Paul, *Sens. Actuators B* 125 (2007) 60.

4. H. Yang, W. Jiang, Y. Lu, *Mater. Lett.* 61 (2007) 1439.

5. J. Chen, J. Huang, G. Swiegers, C. Too, G. Wallace, *Chem. Commun.* (2004) 308.

6. J. Haccoun, B. Piro, V. Noel, M. Pham, *Bioelectrochem.* 68 (2006) 218.

7. M. Lee, Y. Hong, S. Rhee, *Synth. Met.* 69 (1995) 515.

8. M. Lee, S. Kim, *J. Kor. Phys. Soc.* 35 (1999) S299.

9. H. Eisazadeh, G. Wallace, G. Spinks, *Polymer* 35 (1994) 1754.

10. Y. Li, J. Ouyang, *Synth. Met.* 113 (2000) 23.

11. A. Galal, N. Atta, S. Darwish, A. Abdallah, *Bull. Chem. Soc. Jpn.* 70 (1997) 1769.

12. J. Xu, G. Shi, L. Qu, J. Zhang, *Synth. Met.* 135-136 (2003) 221.

13. S. Konwer, J. Maiti, S. Dolui, *Mater. Chem. Phys.* 128 (2011) 283.

14. A. Cihaner, S. Tirkes, A. Onal, *J. Electroanal. Chem.* 568 (2004) 151.

15. X. Ren, P. Pickup, *J. Phys. Chem.* 97 (1993) 5356.

16. X. Ren, P. Pickup, *Can. J. Chem.* 75 (1997) 1518.

Chapter 5

Ion Transport in Overoxidized Polypyrrole Films

5.1 Introduction

Overoxidation of conducting polymers occurs when they are exposed to high potentials beyond their normal electroactivity range causing formation of highly positive centers on the polymer backbone (1). Nucleophilic attack can then take place at these positive centers causing permanent modification to the polymer chains, i.e. covalent bond formation. The conjugated system of the conducting polymer can be distorted by the covalent bond formation between the nucleophile and the positive centers of the polymer chains, causing loss of the conductivity of the polymer film, and so the polymer can become electrochemically inactive. In some cases the conjugation system can be restored electrochemically by dehydrogenation (i.e. elimination of H_2) at high potentials in an electrolyte solution containing no nucleophile (2). After the revival of the conjugation, the polymer film possesses new electrochemical properties due to the effect of the substituent. The full process is known as electrochemically induced

substitution (3). The overoxidation process can be detected electrochemically by cyclic voltammetry as an irreversible anodic peak at high potentials.

Electrochemically induced halogenation reactions have been investigated due to their importance in electrosynthesis (3; 4; 5; 6). They are considered as safe reactions and environmentally friendly in which an electrochemical step (anodic oxidation) is followed by chemical reaction step (nucleophilic attack) at the electrode surface in an inert solvent. Bromide and chloride substitution reactions have been the subject of a considerable research effort (3; 4; 6). However, fluoride substitution (fluorination) was only recently discovered for macromolecules in ionic liquid (5).

Overoxidation of polypyrrole in aqueous solutions results in nucleophilic substitution of hydroxyl groups at the β positions followed by formation of carbonyl groups to form pyrrolinones, which have been detected by infrared and Raman spectroscopy (7). Further overoxidation can lead to a second hydroxyl substitution at the second β position to form 4-hydroxypyrrolinone. A proposed mechanism for the overoxidation of polypyrrole (8; 9) can be seen in Figure 5.1.

In contrast, overoxidation of conducting polymers in the presence of chloride ions results in Cl-substituted polymer chains due to a faster reaction between Cl^- and the positive centers of the polymer chains (3; 4). An elemental analysis for polypyrrole showed that the chlorination (Cl:N ratio) can be achieved up to 70% (3). The electrochemically induced chloride substitution results in electroactive polymer films with a small loss of electroactivity due to partial disruption of the conjugated structure.

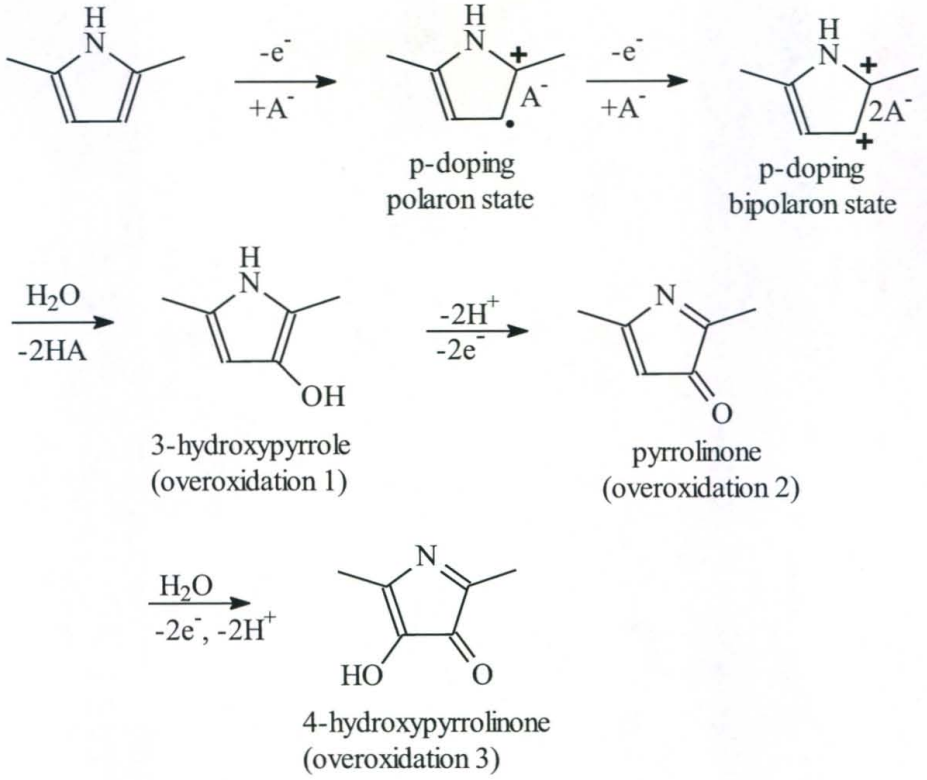

Fig. 5.1 Proposed overoxidation of polypyrrole in aqueous solutions (8; 9).

In some cases, overoxidation of conducting polymers results in degradation of the polymer film, and so restoring of the conductivity is impossible. Many efforts have been devoted to improve the overoxidation resistance limits (ORL) of conducting polymers to improve their stability at high potentials, and thus to avoid loss of their conductivity and electroactivity (10; 11; 12). On the other hand, some conducting polymers have been found to exhibit useful properties after overoxidation as electrode materials in electroanalysis, sensors, and being permselective toward specific ions (13; 14).

The aim of this chapter was to study the ion transport properties of polypyrrole films after exposure to various overoxidation potentials in different electrolyte solutions. Further implications are the possible modification of the polymer films by overoxidation.

5.2 Elemental and surface characterization of polymer films

The polypyrrole (PPy) films used here were characterized by scanning electron microscopy (SEM) for surface morphology and by energy dispersive X-ray emission (EDX) for elemental analysis. The measurements were taken before and after overoxidation of two types of polymer films (i.e. PPy and PPy-Fc), see Chapter 4 (section 4.2). The influence of modification with polyethylene glycol 400 (PEG-400) was also investigated for overoxidation. All polymer films were electrodeposited on Pt wire electrodes for SEM and EDX measurements, except for the ones used for film thickness measurements which were deposited on GC electrodes. The average film thickness on GC electrodes

was found to be ca. 0.3 μm for PPy films prepared from BFEE/CH_3CN with a deposition charge of 0.25 C cm^{-2}.

Figure 5.2 shows SEM images for PPy films on Pt wire electrodes deposited from BFEE/CH_3CN before and after overoxidation. The polymer film interface between the coated and uncoated areas can be seen before overoxidation in Figure 5.2-A. An enlarged image shows that the film had high surface area with various aggregate sizes, and can be described as a spongy structure (Figure 5.2-B). This morphology was significantly changed by overoxidation at ca. 1.5 V, which resulted in a smoother film without distinct aggregates (Figure 5.2-C and D). When PEG-400 was added to the polymerization solution, a smooth PPy film was produced with a few granules of various sizes (Figure 5.3-A and B). After exposing PPy-PEG to the overoxidation potentials, partial degradation of the film structure occurred with a few cracks appearing on the surface of the film. The overoxidized film on the Pt wire and an enlarged picture of a crack are shown in Figure 5.3-C and D, respectively.

Figure 5.4 shows SEM images for PPy-Fc films deposited in the presence of ferrocene derivative 1-(ferrocenyl)ethanol (FcOH). A significant difference can be noticed between the morphologies of the polymer films deposited with and without the ferrocene. The morphology of the PPy-Fc film can be described as relatively smooth with ridges before overoxidation (Figure 5.4-A and B). After exposing the film to overoxidation potentials, partial degradation can be seen where portions of the film

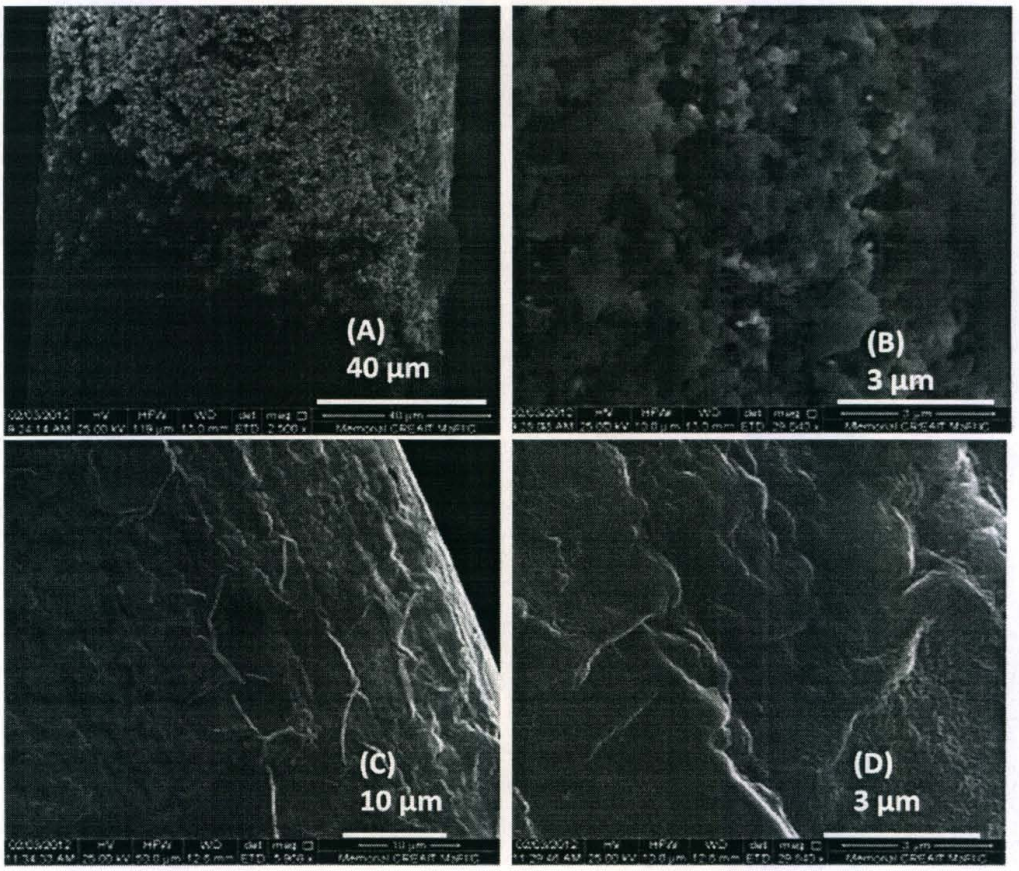

Fig. 5.2 SEM images for PPy films on Pt wire electrodes. The polymer films were deposited from 0.1 M Py, 20% BFEE in CH_3CN with deposition charges of 0.25 C cm^{-2}. **A** and **B** were measured as prepared (the same film with different magnifications). **C** and **D** were following overoxidation by potential scanning to 1.5 V in 0.5 M $NaClO_4$ (the same film with different magnifications).

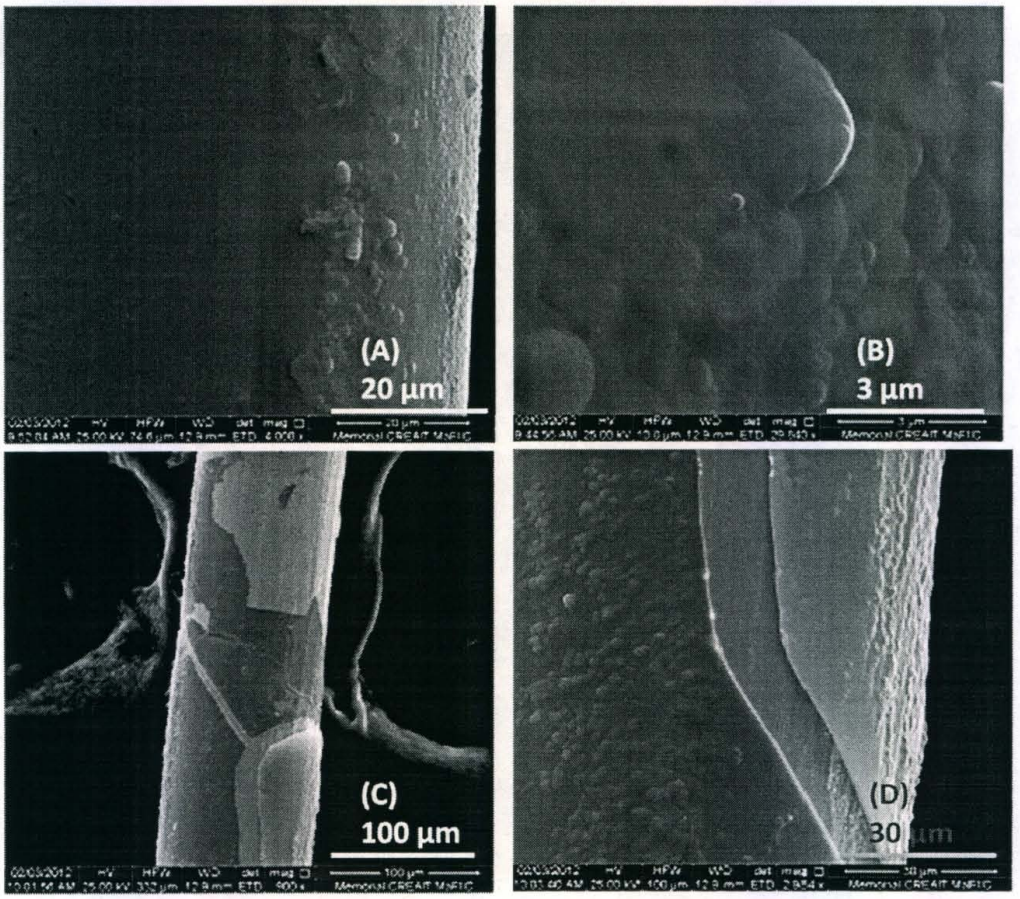

Fig. 5.3 SEM images for PPy films modified with PEG on Pt wire electrodes. The polymer films were deposited from 0.1 M Py, 1% PEG-400, 20% BFEE in CH_3CN with deposition charges of 0.25 C cm^{-2}. **A** and **B** were measured as prepared (the same film with different magnifications). **C** and **D** were following overoxidation by potential scanning to 1.5 V in 0.5 M $NaClO_4$ (the same film with different magnifications).

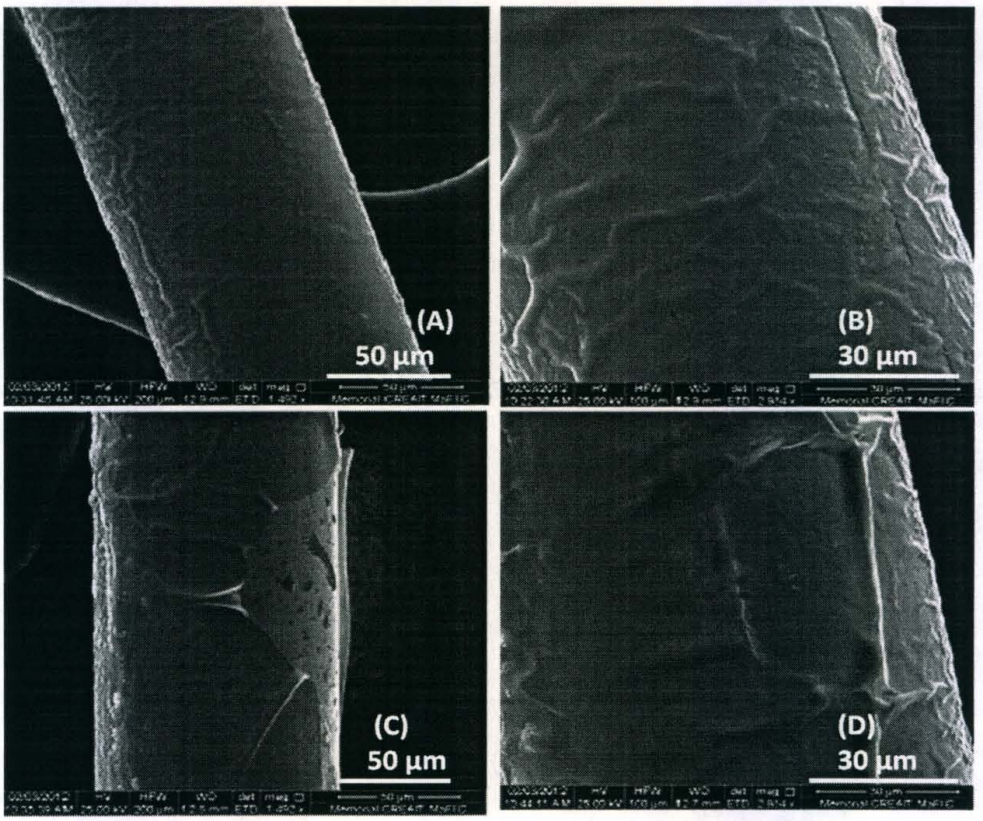

Fig. 5.4 SEM images for PPy-Fc films on Pt wire electrodes. The polymer films were deposited from 0.1 M Py, 10 mM FcOH, 20 % BFEE in CH_3CN with deposition charges of 0.25 C cm^{-2}. **A** and **B** were measured as prepared (the same film with different magnifications). **C** and **D** were following overoxidation by potential scanning to 1.5 V in 0.5 M $NaClO_4$ (the same film with different magnifications).

were lost (Figure 5.4-C and D). Modification of PPy-Fc films with PEG-400 during their deposition resulted in a smoother morphology with some ridges. Some aggregates but no cracks were observed after overoxidation (Figure 5.5-A to D).

Elemental compositions before and after overoxidation of the PPy and PPy-Fc films were probed by using EDX. The influence of PEG-400 modification on the elemental analysis of the PPy films can be seen in Figure 5.6-A. A significant amount of carbon and fluoride contents can be observed for the PPy film modified with PEG-400 compared with the film without PEG-400 modification. The increase in carbon content can be attributed to the increased amount of polymer deposited in the presence of PEG-400 (i.e. higher polymerization efficiency). The existence of fluoride in the film modified with PEG-400 is believed to be due to the existence of a negative charge complex of BFEE-PEG, see Chapter 4 (Fig. 4.2) for the structure.

Figure 5.6-B shows PPy-Fc before and after overoxidation. It can be seen that the film lost some of the carbon content after exposure to overoxidation potentials indicating partial degradation of the film. In addition, a loss of counterions (i.e. $FcO:BF_3^-$) can be observed after overoxidation. For both spectra, the Pt signal was high since the films were deposited on Pt wire electrodes. The peaks at ca. 1.7 keV and 2.4 keV are secondary peaks of Pt. The aluminum peak in Film 1 (A1) is due to Al_2O_3 used for cleaning the Pt electrodes. The absence of chloride for Film 4 (B4) is surprising since the film was doped in $NaClO_4$, however, expulsion of counterions during overoxidation is expected.

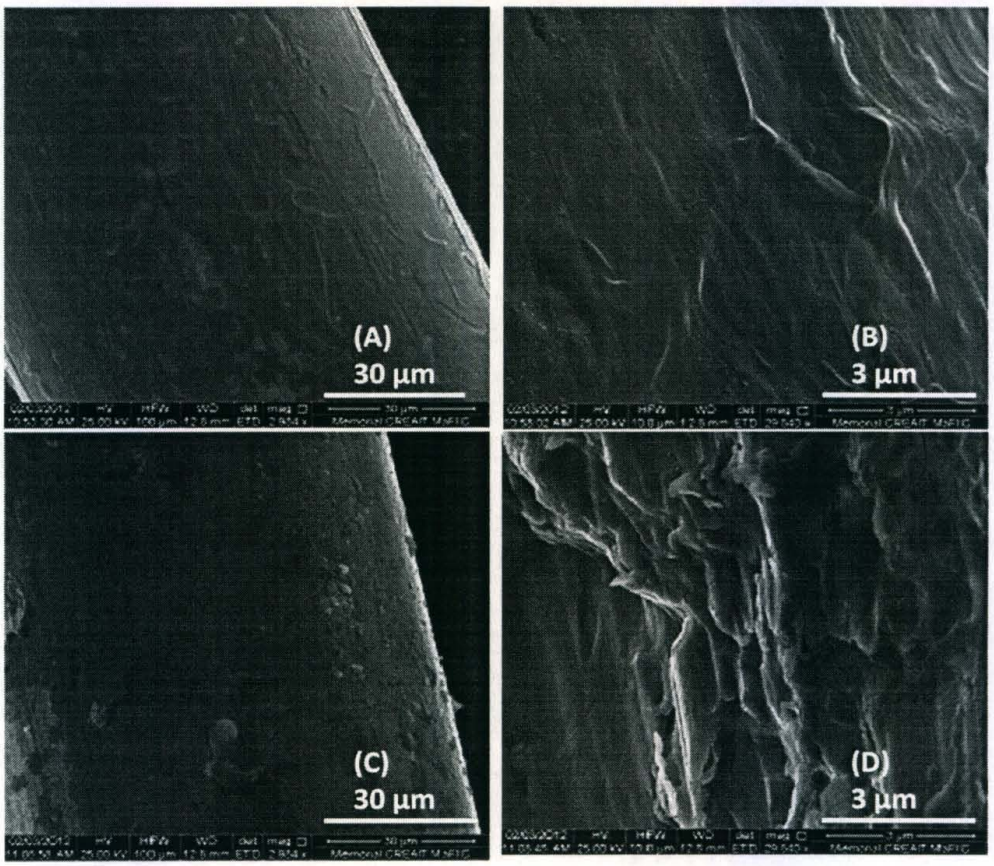

Fig. 5.5 SEM images for PPy-Fc films modified with PEG on Pt wire electrodes. The polymer films were deposited from 0.1 M Py, 10 mM FcOH, 1% PEG-400, 20% BFEE in CH_3CN with deposition charges of 0.25 C cm^{-2}. **A** and **B** were measured as prepared (the same film with different magnifications). **C** and **D** were following overoxidation by potential scanning to 1.5 V in 0.5 M $NaClO_4$ (the same film with different magnifications).

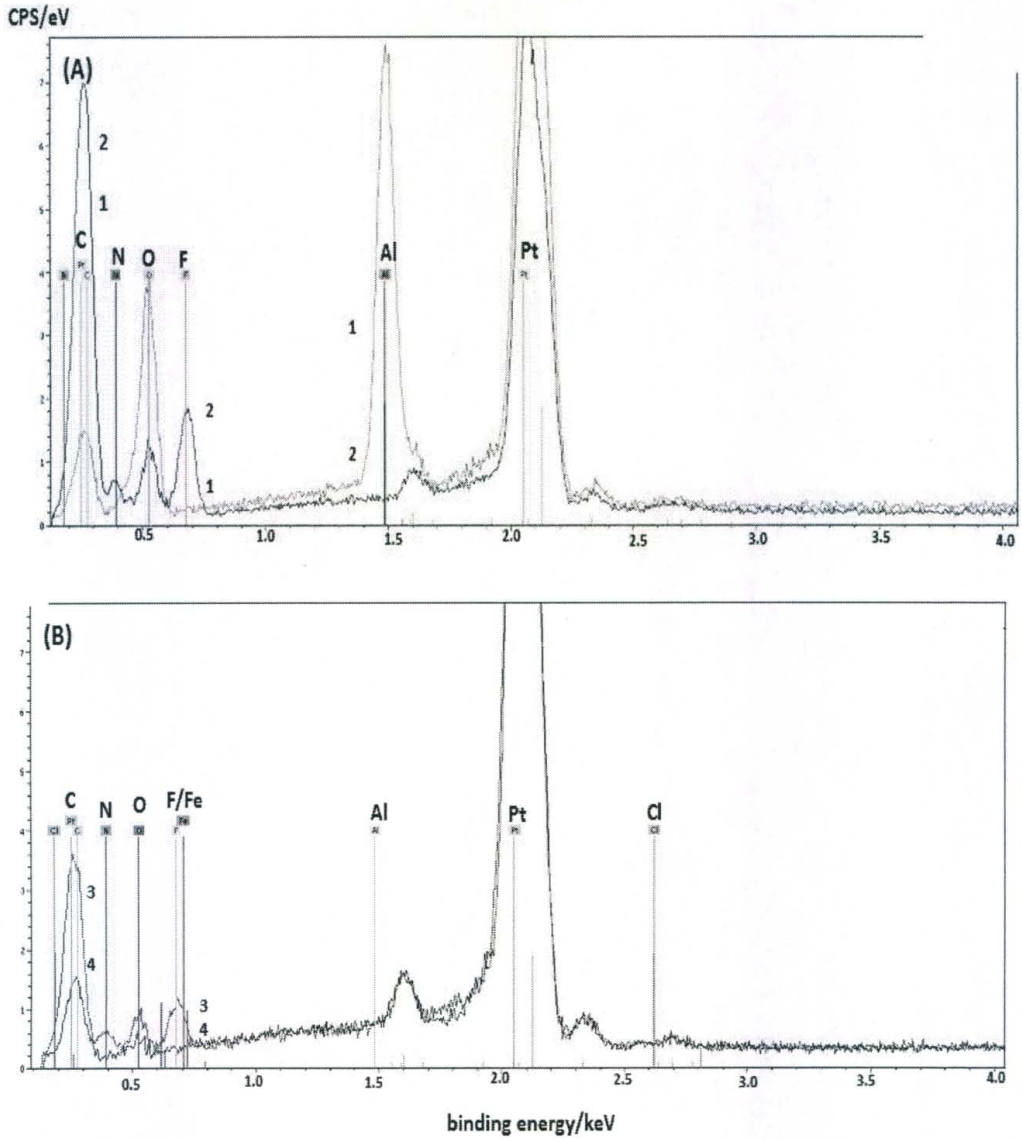

Fig. 5.6 EDX spectra for PPy films on Pt wire electrodes. The polymer films were deposited from 0.1 M Py, 20% BFEE in CH_3CN with deposition charges of 0.25 C cm^{-2}. **A.** Comparison of PPy films without (1) and with (2) PEG-400 modification; **B.** Comparison of PPy-Fc before (3) and after (4) overoxidation. 1% PEG-400 was added to the polymerization solution for Film 2; 10 mM FcOH was added to the polymerization solution for Films 3 and 4. All films were measured as prepared, except Film 4 which was overoxidized by potential scanning to 1.5 V in 0.5 M $NaClO_4$.

5.3 Electrochemical characterization by cyclic voltammetry

It was shown from SEM images and EDX spectra that polypyrrole (PPy) films exhibited different morphologies and were partially degraded after exposing to overoxidation potentials at ca. 1.5 V. However, no indication about the electrochemical activity of the polymer films can be inferred by using such characterization techniques. Cyclic voltammetry and impedance spectroscopy were used to probe the polymer films after overoxidation and compare them with the original films before overoxidation. It has been reported that conducting polymer films lose their electrochemical activities after overoxidation (12; 15), and so exposing the polymer films to high potentials beyond their normal electroactive windows is normally avoided. In addition, modifying the polymer films with various modifiers to increase their stabilities and resistance to overoxidation has been investigated (10; 11; 12). On the other hand, it has been shown that the polymer films can attain interesting electrochemical properties for many potential applications after exposure to overoxidation potentials under certain conditions (14). Thus, to exploit the overoxidized polymer films for such applications, electrochemical characterization was used to explore the effects of high potentials on the activity of the polymer films under various conditions.

Figure 5.7 shows cyclic voltammograms (CVs) before and after overoxidation in NaCl solution for a PPy film deposited from BFEE/isopropyl alcohol (IPA). The first cycle started at 0.5 V toward negative potentials and switched at -1.0 V and then at 1.1 V. A large irreversible anodic peak can be seen at ca. 0.9 V indicating the large amount of

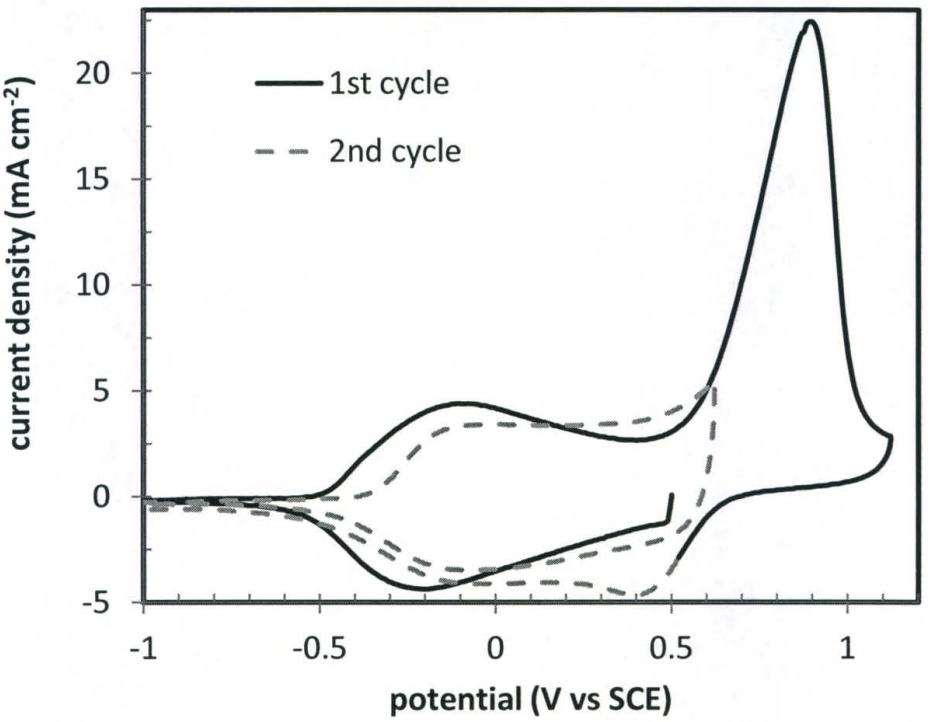

Fig. 5.7 Cyclic voltammograms of a PPy film in 0.5 M NaCl at 0.1 V s^{-1} before (1^{st} cycle) and after (2^{nd} cycle) overoxidation. The polymer film was deposited on a GC electrode from 0.1 M Py, 20% BFEE in IPA with a deposition charge of 0.25 C cm^{-2}.

charge associated with overoxidation. A typical redox wave of PPy can also be seen at ca. -0.2 V, but was shifted anodically to ca. 0.1 V after overoxidation. This shift could be due to electron withdrawing effect of the substituent. Both Cl-substitution and OH-substitution are possible, and so further elemental analysis is required to probe the nature of the substitution. The small loss of electroactivity after the substitution suggests that the conjugated structure was partially disrupted. A small reduction peak at ca. 0.4 V can be seen after the overoxidation peak which disappears in the subsequent cycle. This could be due to Cl_2 reduction following Cl^- oxidation (3).

Another substitution can also be detected electrochemically following the first substitution. Figure 5.8 shows (A) three overoxidation peaks at 0.9 V, 1.5 V, and 2.1 V; and (B) the CVs after each overoxidation peak (OP) in NaCl for a PPy film deposited from BFEE/CH_3CN. The CV before overoxidation is also shown for comparison and is designated as the first cycle. It was shown that Cl-substitution can readily occur at lower potentials (3), and so it can be assumed that Cl-substitution occurs first. Thus, the first two overoxidation peaks (OP1 and OP2) can be assigned to Cl-substitution followed by OH-substitution. However, it is very hard to judge which one occurred first based on electrochemical characterization. The third overoxidation peak (OP3) can be assigned to water electrolysis at high potentials and/or to oxidative degradation of the polymer film. The CV after OP1 exhibited a small loss of electroactivity and a small anodic shift for the oxidation peak. These can be attributed to the disruption of the conjugated structure

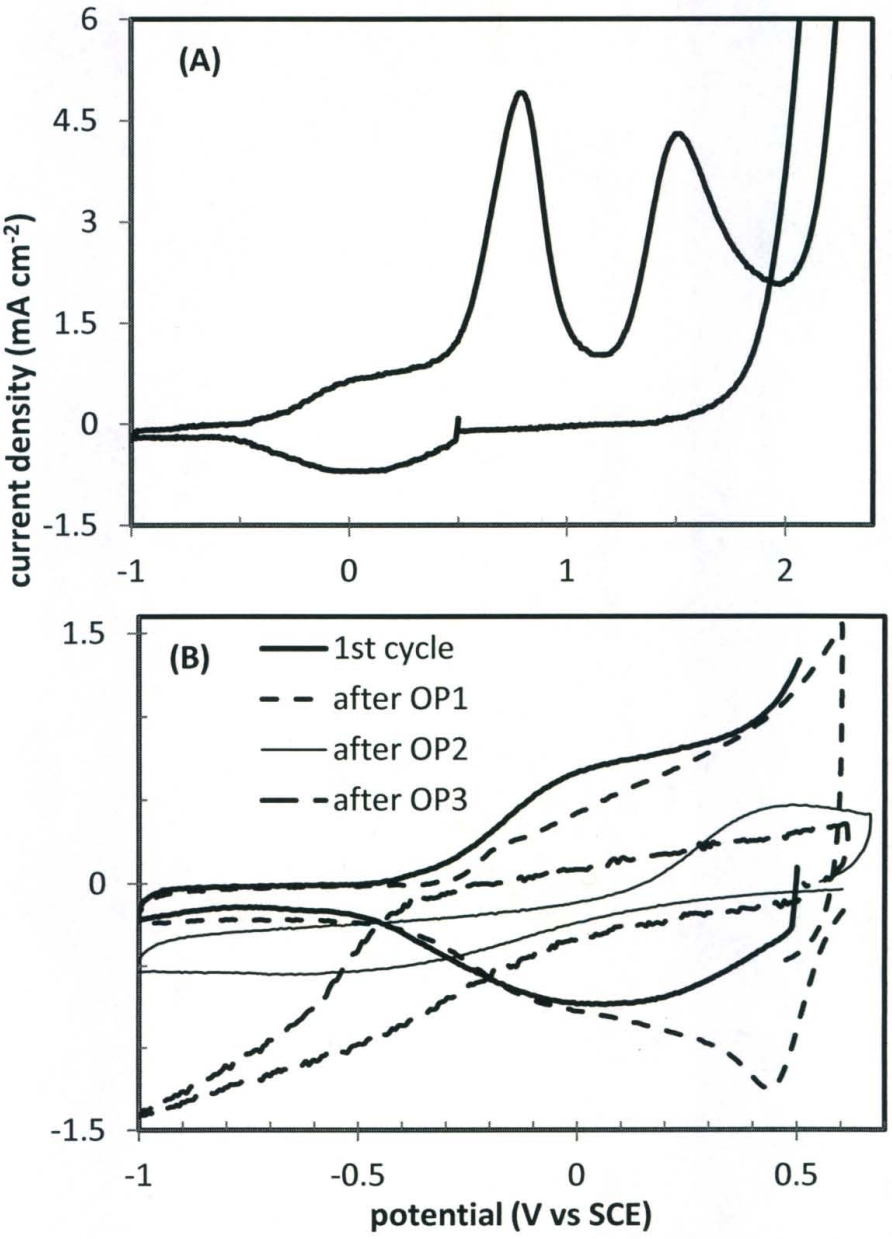

Fig. 5.8 Cyclic voltammograms of PPy films in 0.5 M NaCl at 0.1 V s^{-1} showing **A.** Three overoxidation peaks; **B.** CVs after each overoxidation peak (OP). The polymer films were deposited on GC electrodes from 0.1 M Py, 20% BFEE in CH_3CN with deposition charges of 0.25 C cm^{-2}.

and the Cl^- substitution, respectively. The reduction peak at 0.45 V can be attributed to Cl_2 reduction following Cl^- oxidation (3), i.e. $2Cl^- \rightleftharpoons Cl_2 + 2e^-$.

The CVs after OP2 and OP3 displayed a significant loss of electroactivity characterized by a large peak separation and reduction peak at low potentials, respectively. The large peak separation for the CV after OP2 is a characteristic of highly resistive film where the conjugated structure is expected to be largely disrupted after the second substitution. The reduction peak below -0.45 V can be attributed to O_2 reduction followed the water electrolysis at high potentials (OP3).

Table 5.1 compares overoxidation peaks (OP1 and OP2) for the polymer films prepared from BFEE/CH_3CN or BFEE/IPA and measured in NaCl or $NaClO_4$. Two electrochemically induced substitutions can be detected in NaCl (i.e. Cl^- and OH^-), but only one in $NaClO_4$ (i.e. OH^-).

A comparison of polymer films deposited from BFEE and CH_3CN, IPA, or an equal mixture of them can be seen in Figure 5.9. It can be seen that the film activity after overoxidation increases with the amount of IPA and the anodic peak offset decreases with increasing IPA content. The CVs were taken in NaCl after OP1 (ca. 1.1 V) for films deposited with same deposition charges (0.25 C cm^{-2}), and so Cl-substitution is expected. A significant activity difference can be clearly seen indicating that the solvent used for deposition of the polymer film plays a significant role in the polymerization efficiency.

Table 5.1 Potentials and currents for overoxidation peaks (OP1 and OP2) of PPy films

film[a]	OP1 (V)	OP2 (V)	OP1 (mA cm^{-2})	OP2 (mA cm^{-2})
BFEE/CH_3CN (in $NaClO_4$)	0.87	--	4.64	--
BFEE/CH_3CN (in NaCl)	0.78	1.53	4.91	4.29
BFEE/IPA (in $NaClO_4$)	1.24	--	49.6	--
BFEE/IPA (in NaCl)	1.07	1.51	39.0	4.39

[a] films were prepared from BFEE/CH_3CN or BFEE/IPA and measured in $NaClO_4$ or NaCl.

5.3.1 Overoxidation of polypyrrole films modified with ferrocene

Polypyrrole films prepared in the presence of FcOH (i.e. PPy-Fc) were found to be stable under cycling with no significant expulsion of ferrocene, indicating it is deeply trapped into the polymer chains, see section 4.2. However, exposing the film to overoxidation potentials causing chemical modifications of the polymer chains might result in expulsion of ferrocene. Figure 5.10 shows CVs of PPy-Fc before and after overoxidation in $NaClO_4$ and NaCl for films prepared from BFEE/CH_3CN and BFEE/IPA, respectively. It can be seen that the peak assigned to ferrocene at ca. 0.3 V disappeared after exposing the films to overoxidation potentials. This result was also supported by the EDX spectra which show FcOH loss with overoxidation, see Figure 5.6.

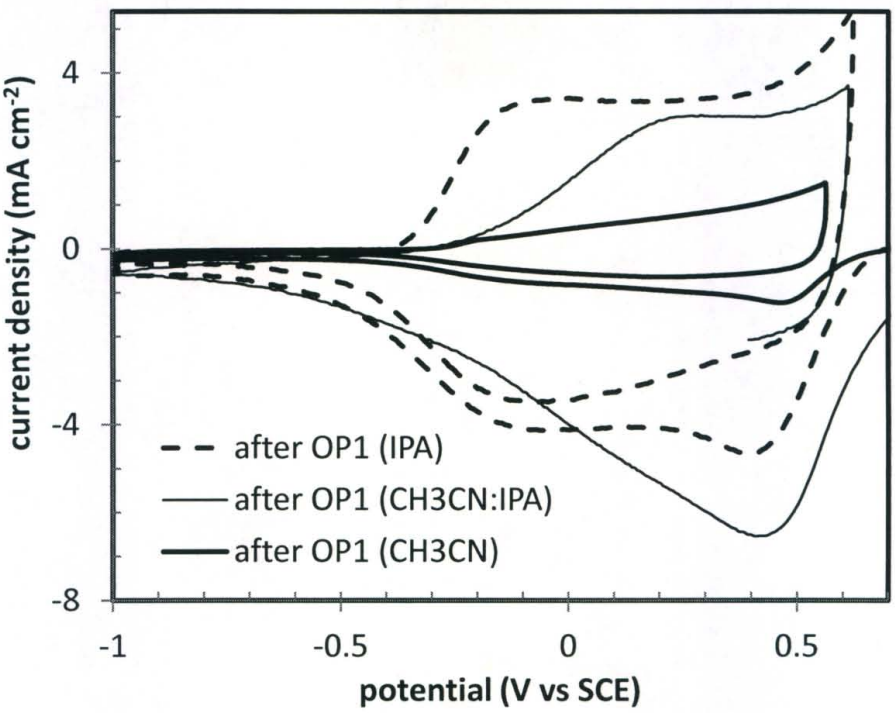

Fig. 5.9 Cyclic voltammograms of PPy films in 0.5 M NaCl at 0.1 V s^{-1} after the overoxidation peak one (OP1). The polymer films were deposited on GC electrodes from 0.1 M Py, 20% BFEE in CH_3CN, IPA, or an equal mixture of them with deposition charges of 0.25 C cm^{-2}.

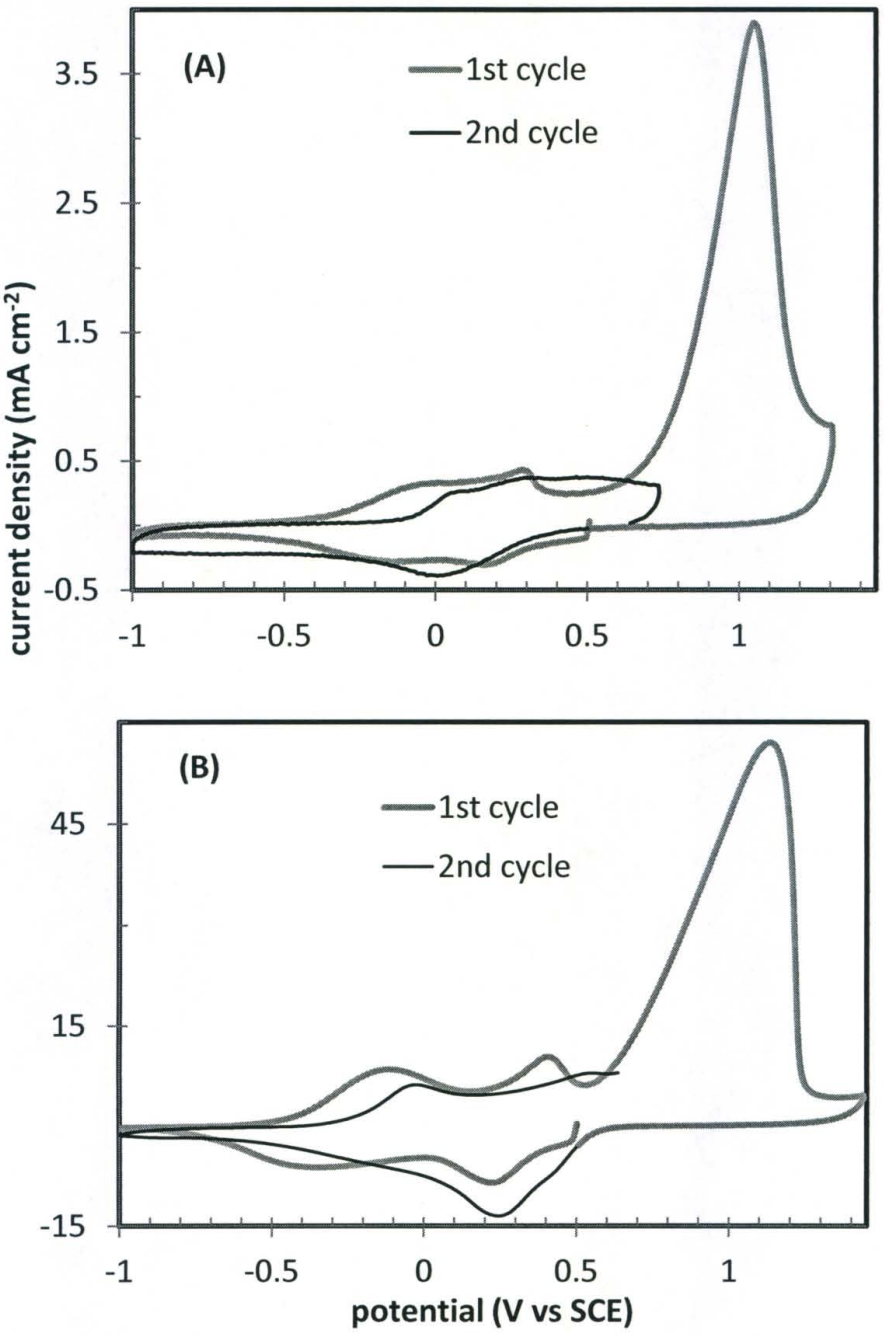

Fig. 5.10 Cyclic voltammograms of PPy-Fc films in 0.5 M **A.** $NaClO_4$; **B.** NaCl at 0.1 V s^{-1} before and after overoxidation. The polymer films were deposited on GC electrodes from 0.1 M Py, 10mM FcOH, 20% BFEE in CH_3CN (A) or IPA (B) at constant potential of 1.0 V for 60 seconds.

5.4 Kinetics characterization by impedance spectroscopy

Selected polymer films were characterized by impedance spectroscopy to investigate the kinetics of ion transport before and after overoxidation. The ion transport properties of the polymer film can be probed inside the polymer layer, at the solution/polymer interface, and in the electrolyte solution closed to the working electrode by measuring its ionic conductivity (R_i), charge transfer resistance (R_{CT}), and uncompensated solution resistance (R_s), respectively. A potential wave (E_{AC}) applied to the polymer film has a frequency scanned from high to low values. As the frequency decreases, the redox reaction grows into the polymer film from the outer to inner layers, and so at the lowest frequencies, the redox reaction encompasses all polymer layers (16). The result of an impedance experiment can be presented as imaginary impedance (Z_{im}) versus real impedance (Z_{re}) or, alternatively, series capacitance (C_s) versus real impedance (Z_{re}), where [$C_s = -1/(\omega Z_{im})$]; angular frequency ($\omega = 2\pi f$). Looking at these two plots at the same time is very useful in assessing the various kinetic parameters.

Figures 5.11, 5.12, and 5.13 show impedance (A) and capacitance (B) plots measured at 0.2 V in $NaClO_4$ before and after overoxidation for polymer films prepared from BFEE/CH_3CN, BFEE/IPA, and BFEE with an equal mixture of CH_3CN:IPA, respectively. Three conditions had been assessed for each film: as-prepared where the impedance was measured immediately after preparation, after OP1 where the impedance was measured after scanning to ca. 1.2 V, and after OP2 where the impedance was measured after scanning to ca. 2.4 V. The film resistance (R_f) consisting of its electronic

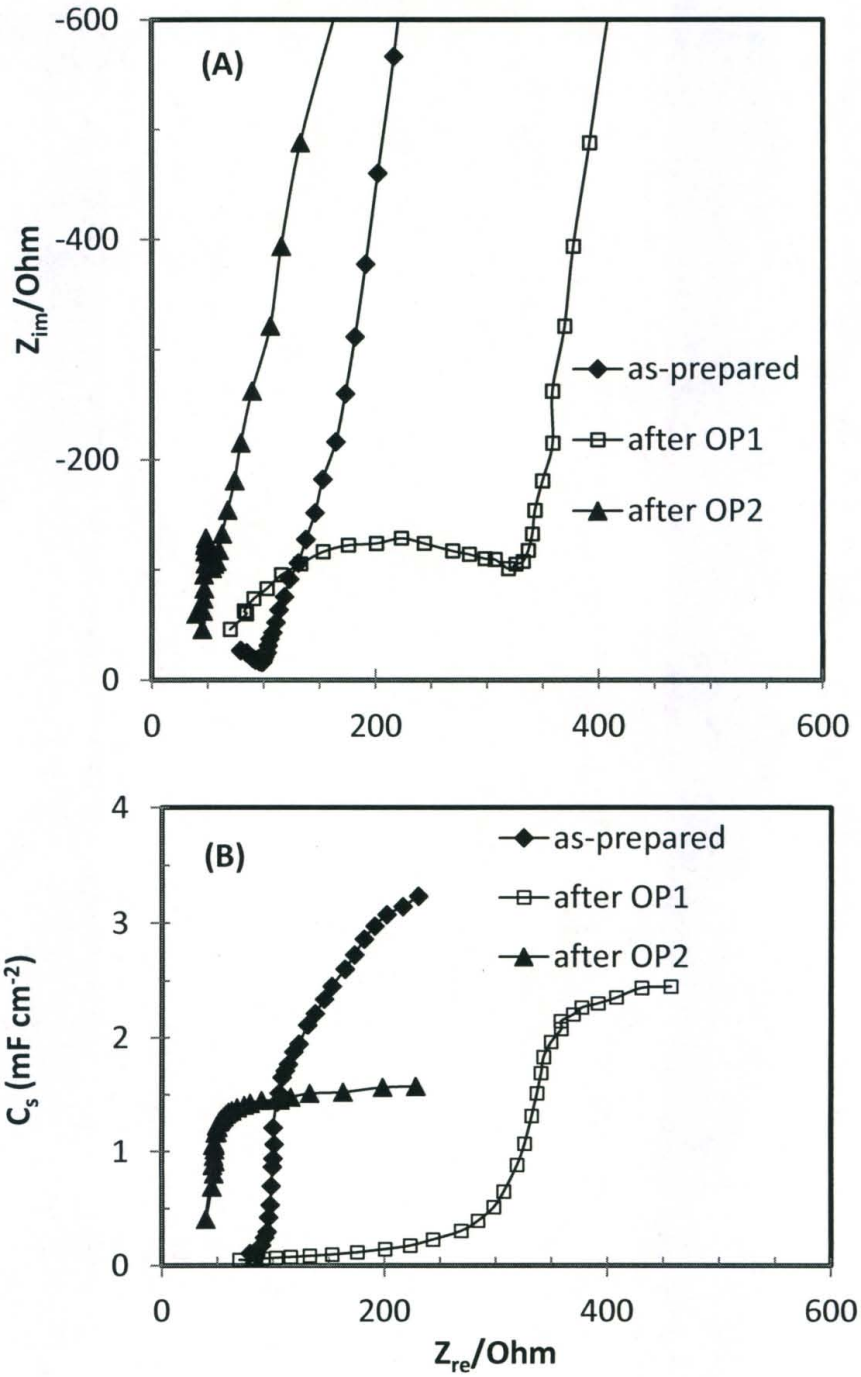

Fig. 5.11 A. Impedance and **B.** series capacitance plots before and after PPy overoxidation measured at 0.2 V in 0.5 M $NaClO_4$. The films were deposited on GC electrodes from 0.1 M Py, 20% BFEE in CH_3CN with deposition charges of 0.018 C (0.25 C cm^2). The frequency scan range was from 1 kHz to 1 Hz.

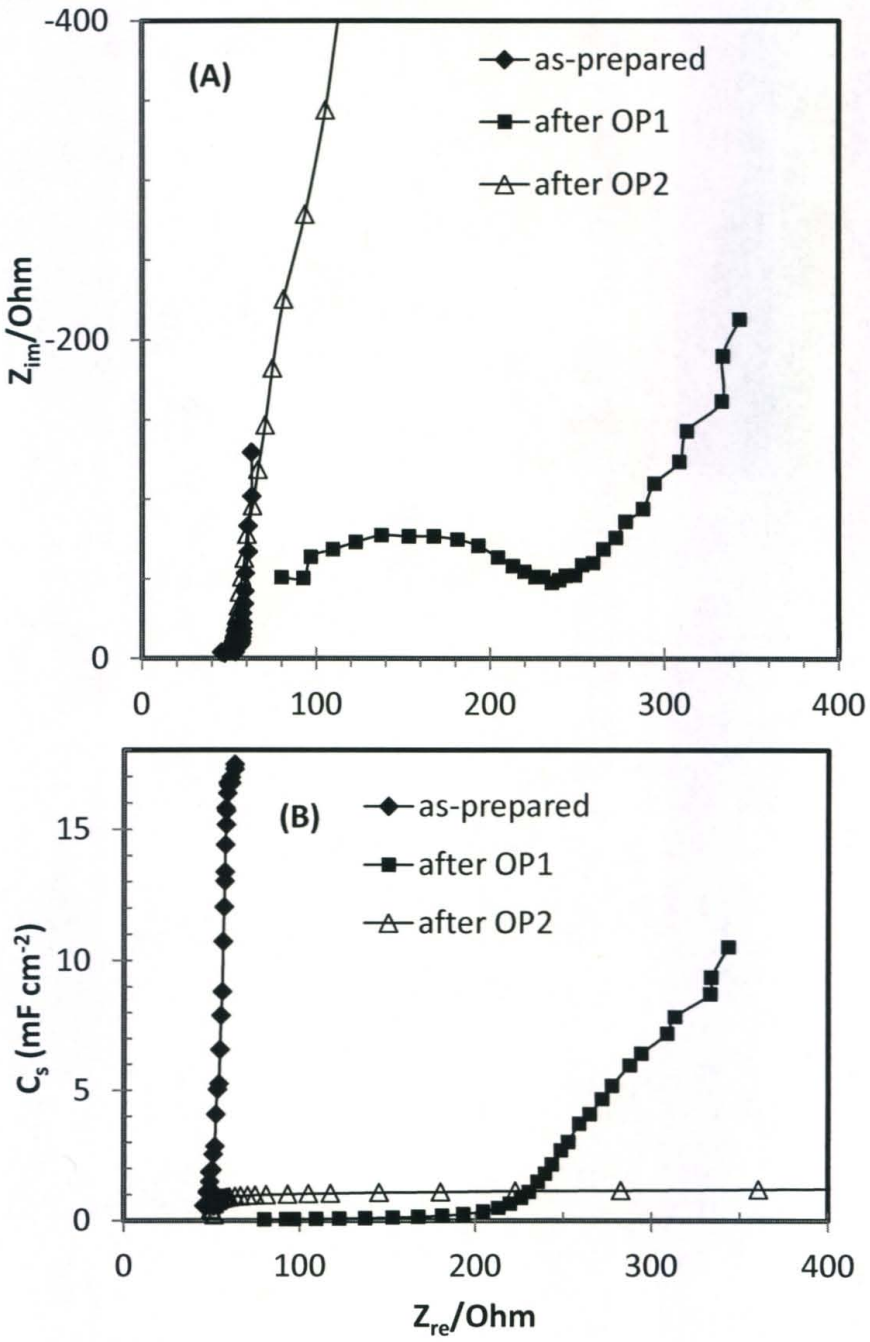

Fig. 5.12 A. Impedance and **B.** series capacitance plots before and after PPy overoxidation measured at 0.2 V in 0.5 M $NaClO_4$. The films were deposited on GC electrodes from 0.1 M Py, 20 % BFEE in IPA with deposition charges of 0.018 C (0.25 C cm^{-2}). The frequency scan range was from 1 kHz to 1 Hz.

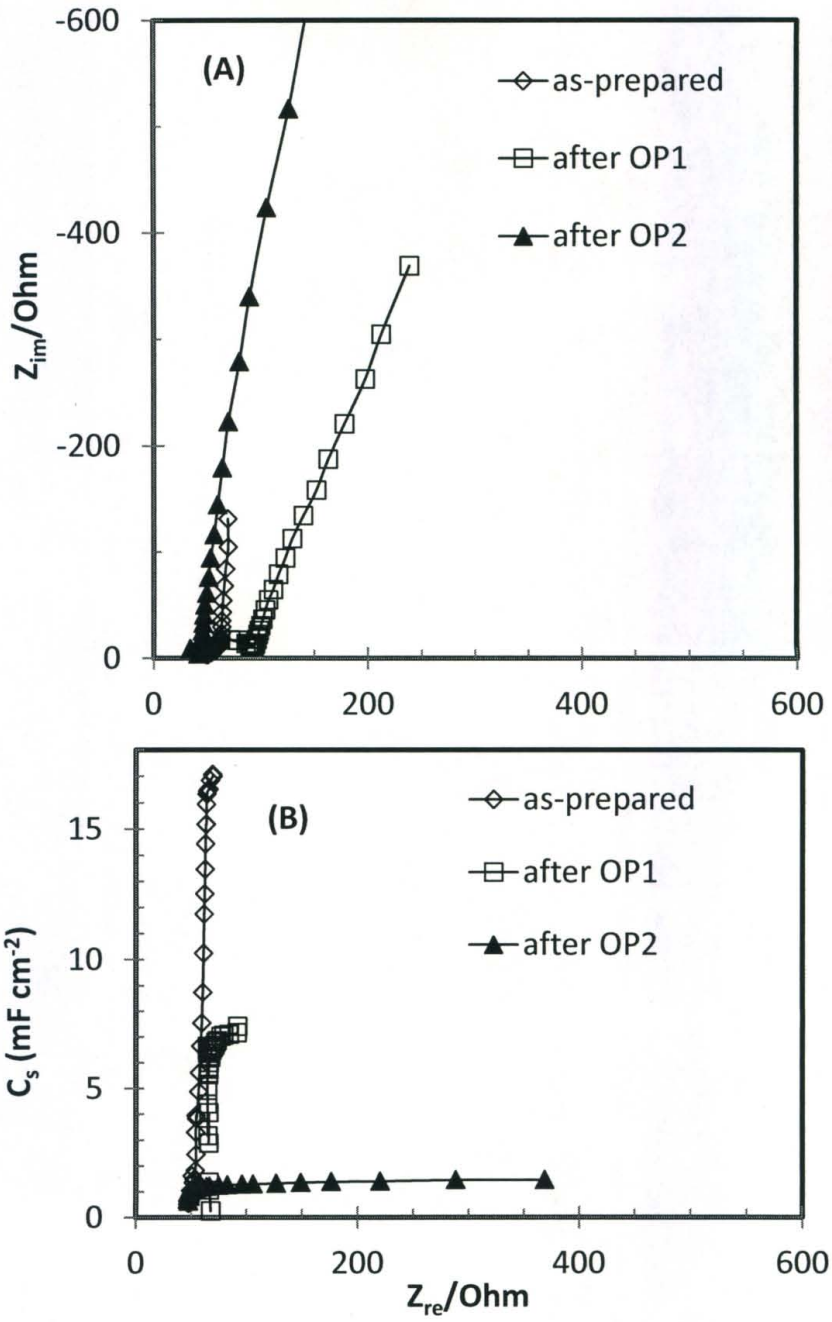

Fig. 5.13 A. Impedance and **B.** series capacitance plots before and after PPy overoxidation measured at 0.2 V in 0.5 M $NaClO_4$. The films were deposited on GC electrodes from 0.1 M Py, 20% BFEE in a mixture of CH_3CN:IPA (1 to 1 ratio) with deposition charges of 0.25 C cm^{-2}. The frequency scan range was from 1 kHz to 1 Hz.

resistance (R_e) and ionic resistance (R_i) can be measured from the impedance plot or capacitance plot (17). Because the measurements were conducted at 0.2 V where the polymer film is in its conducting state, the electronic resistance is very small (i.e. electron transport is very fast). By looking at the impedance plots, the film resistance (R_f) can be measured from the Warburg region of the plot where [$R_{Warburg} = R_f/3$]. The Warburg line at medium frequencies with about 45° slope was negligible for the as-prepared film and after OP2, and was very small for the polymer films after OP1. This indicates that the ion transport rates were high.

It can also be noticed from the impedance plots that the presence of a charge transfer resistance (R_{CT}) indicated by a high-frequency semicircle was significant after OP1. The origin of the semicircle and its presence or absence is not fully understood (18). By looking at the capacitance plots, the constant capacitance at high frequencies with almost zero slope represents the charge transfer resistance equivalent to the semicircle in the impedance plot, which can be noticed for the polymer film after OP1. The slope of the rising portion represents the conductivity of the polymer film and is dominated by the smaller of the electronic or ionic conductivity; high slope reflects high conductivity. The constant capacitance at low frequencies with almost zero slope represents the limiting capacitance (C_{lim}) of the polymer film. In the cases where the slope of the rising portion is low, C_{lim} cannot be observed and the highest capacitance reached at the lowest frequencies is designated as the low frequency capacitance (C_{lf}). In these cases, a lower frequency range is required to observe C_{lim}.

As a general trend for all polymer films, the capacitance of the polymer films decreases with exposure to overoxidation potentials. This can be attributed to polymer film degradation at high potentials which destroys some of the electroactive centers.

For the polymer films prepared from BFEE/CH_3CN and BFEE/IPA, the film resistance increased after OP1 and decreased after OP2 compared with the as-prepared resistance. This can also be seen from the slopes of rising portions of the capacitance plots where OP1 had a lower slope compared with the other the two cases. It can be concluded that the film conductivity decreases after OP1 due to the nucleophilic substitution disturbing the conjugated system, but after OP2 the conductivity increases due to dehydrogenation, which restores the conjugation system.

In contrast, the film prepared from BFEE with an equal mixture of CH_3CN:IPA showed only a small R_{CT} and only after OP1. Further, the film conductivity did not change with overoxidation potential as can be seen from the slopes of the rising portion in the capacitance plot. This may indicate superior properties of the film prepared from the mixture solution.

A further comparison was conducted to investigate the effect of electrolyte ions on each oxidation state (i.e. as-prepared, OP1, and OP2) for PPy films prepared from BFEE/CH_3CN and BFEE/IPA. Figures 5.14, 5.15, and 5.16 show impedance (A) and capacitance (B) plots for PPy films at three conditions: as-prepared, after OP1, and after OP2, respectively.

It is clear from the data in Figure 5.14 that the as-prepared films measured in NaCl had lower film resistances than those measured in $NaClO_4$, and this can be attributed to the higher anion mobility of the former. Furthermore, it can be noticed for the films after OP1 that the appearance of R_{CT} indicated by high-frequency semicircles was associated with the large electrolyte anion, i.e. ClO_4^-, rather than the solvent used to prepare the film (Figure 5.15). It can also be noticed that the films prepared from BFEE/IPA had much higher capacitances than those prepared from BFEE/CH_3CN. This can be attributed to a higher polymerization efficiency that can be achieved using a protic solvent, e.g. with hydroxyl groups, in the presence of a Lewis acid, i.e. BFEE. In contrast, Figure 5.16 shows that the films exposed to overoxidation potentials (after OP2) in $NaClO_4$ had higher capacitances and conductivities than those measured in NaCl exposed to the same potentials. This can be attributed to chemical modifications of the polymer structure caused by overoxidation change ion transport properties of the polymer film significantly. Table 5.2 summarizes the properties of PPy films prepared from BFEE/CH_3CN and BFEE/IPA for impedance and capacitance measurements in NaCl and $NaClO_4$.

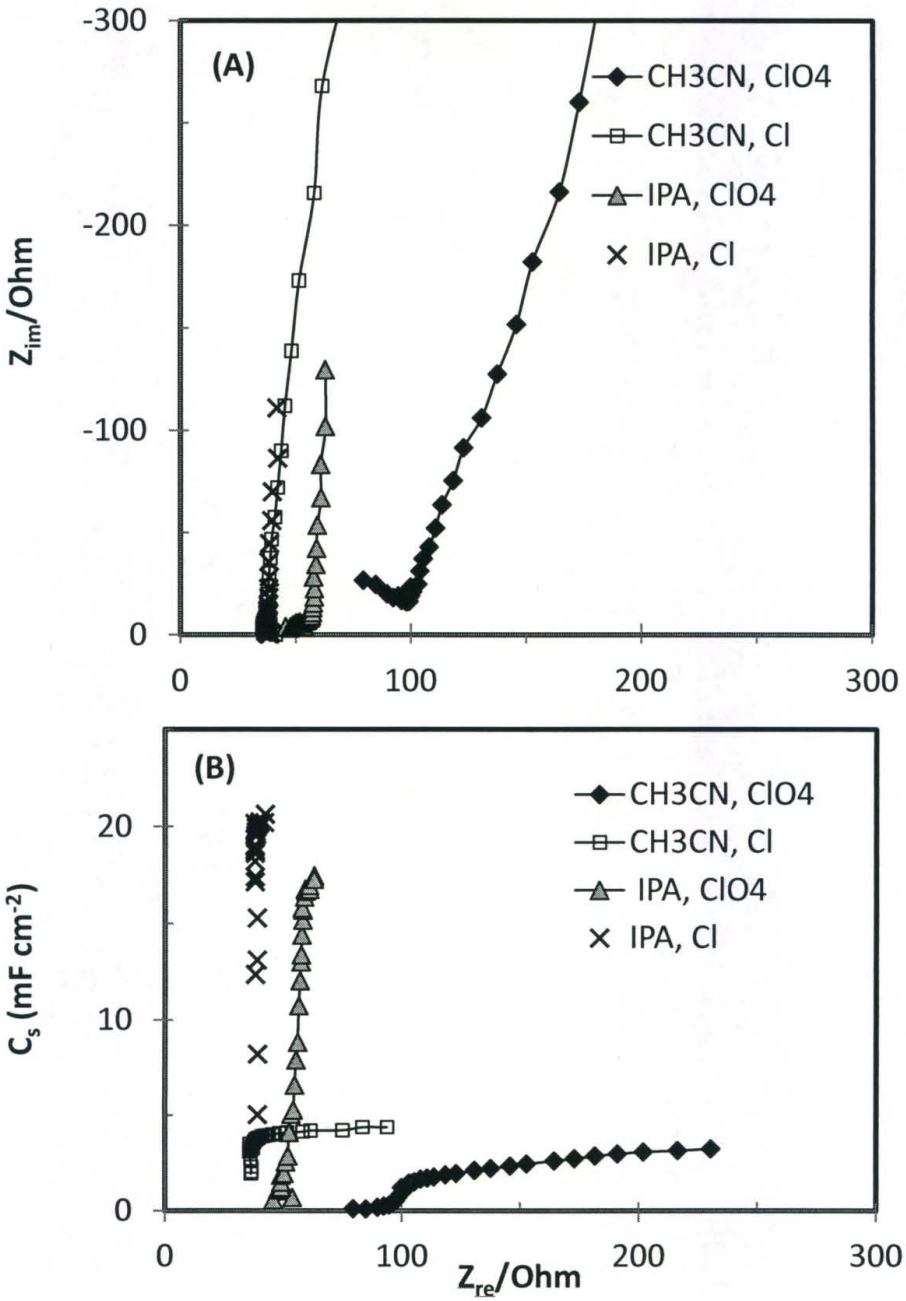

Fig. 5.14 A. Impedance and **B.** series capacitance plots for as-prepared PPy films measured at 0.2 V in 0.5 M $NaClO_4$ (ClO_4) or NaCl (Cl). The films were deposited on GC electrodes from 0.1 M Py, 20% BFEE in CH_3CN or IPA with deposition charges of 0.018 C (0.25 C cm^{-2}). The frequency scan range was from 1 kHz to 1 Hz.

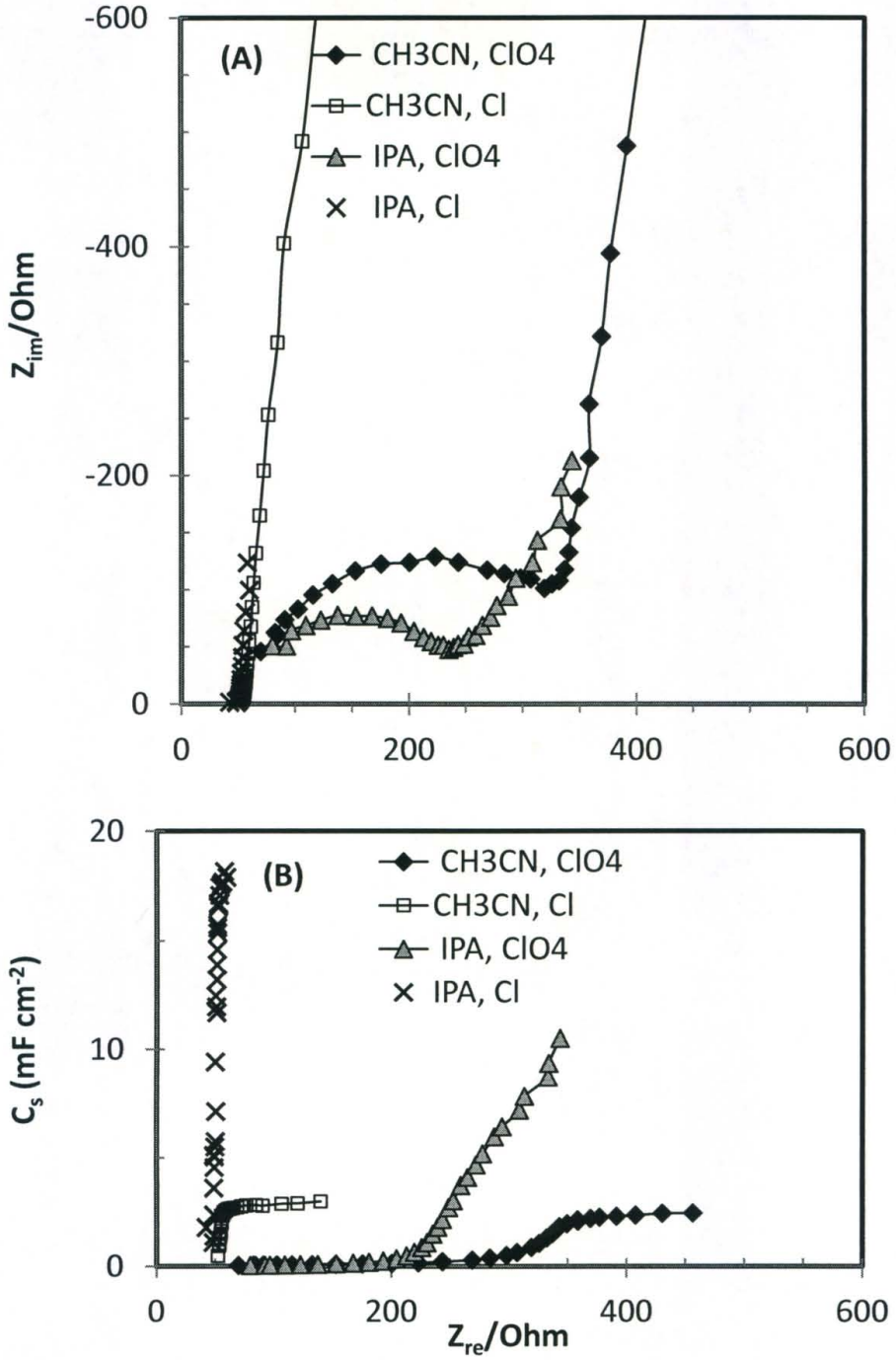

Fig. 5.15 A. Impedance and **B.** series capacitance plots of PPy films after OP1 measured at 0.2 V in 0.5 M $NaClO_4$ (ClO_4) or NaCl (Cl). The films were deposited on GC electrodes from 0.1 M Py, 20% BFEE in CH_3CN or IPA with deposition charges of 0.018 C (0.25 C cm^{-2}). The frequency scan range was from 1 kHz to 1 Hz.

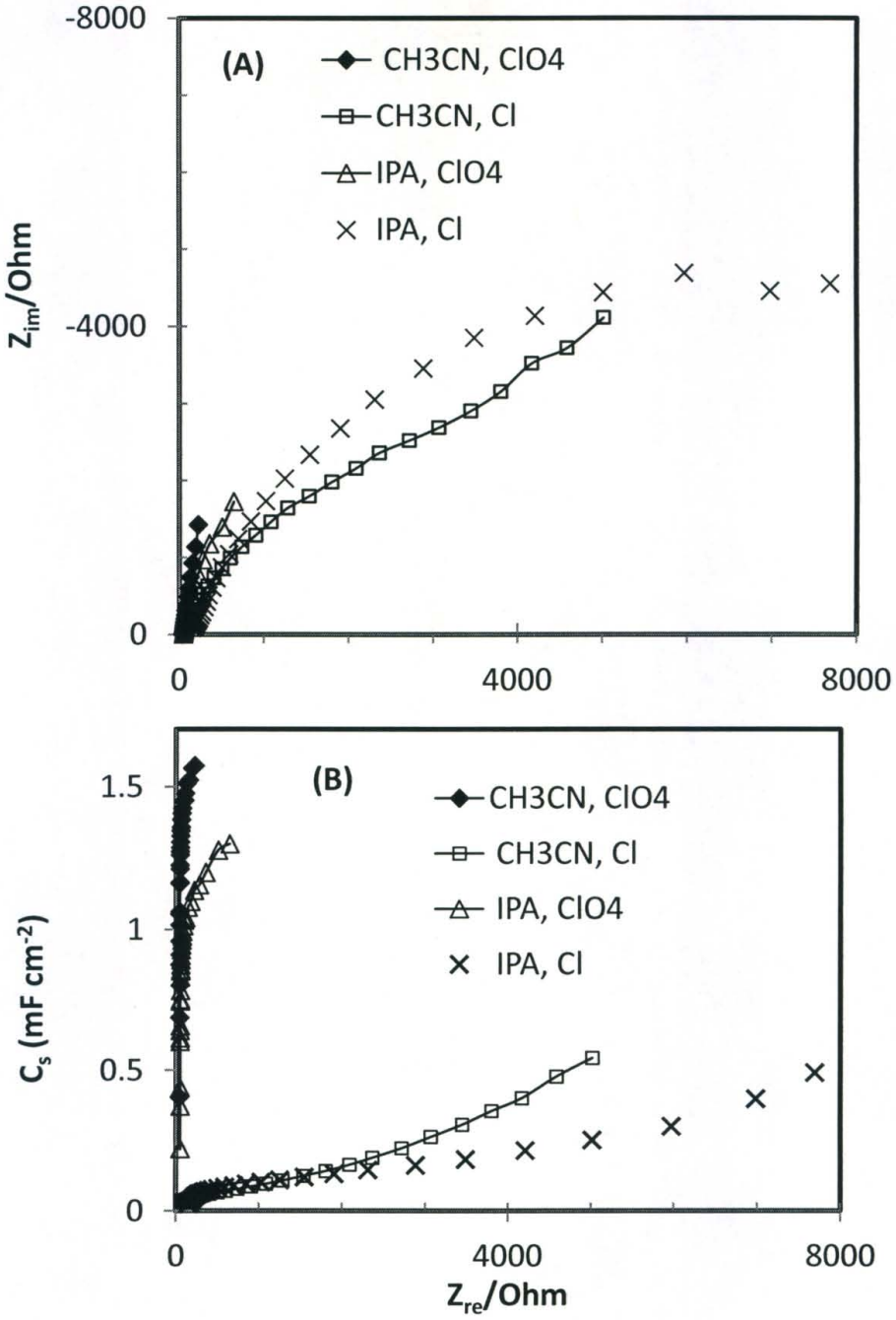

Fig. 5.16 A. Impedance and **B.** series capacitance plots of PPy films after OP2 measured at 0.2 V in 0.5 M $NaClO_4$ (ClO_4) or NaCl (Cl). The films were deposited on GC electrodes from 0.1 M Py, 20% BFEE in CH_3CN or IPA with deposition charges of 0.018 C (0.25 C cm^{-2}). The frequency scan range was from 1 kHz to 1 Hz.

Table 5.2 Properties of polypyrrole films measured in 0.5 M $NaClO_4$ and NaCl at 0.2 V

System[a]	R_s[b]	R_s'[c]	R_{low}[d]	R_{high}[e]	R_{CT}[f]	R_i[g]	C_{lf} (mF cm^{-2})[h]
BFEE/CH_3CN (in $NaClO_4$)	70	97	150	100	27	150	3.2
BFEE/CH_3CN (in $NaClO_4$, OP1)	70	340	330	250	270	240	2.5
BFEE/CH_3CN (in $NaClO_4$, OP2)	50	NA	84	CBD	CBC	CBC	1.6
BFEE/CH_3CN (in NaCl)	36	NA	49	CBD	CBC	CBC	4.4
BFEE/CH_3CN (in NaCl, OP1)	48	NA	52	CBD	CBC	CBC	3.0
BFEE/CH_3CN (in NaCl, OP2)	84	7000	NA	CBD	6916	CBC	0.5
BFEE/CH_3CN (in NaCl, OP3)	88	NA	NA	CBD	CBC	CBC	0.5
BFEE/IPA (in $NaClO_4$)	48	NA	54	CBD	CBC	CBC	17.5
BFEE/IPA (in $NaClO_4$, OP1)	80	240	300	220	160	240	10.5
BFEE/IPA (in $NaClO_4$, OP2)	50	NA	NA	CBD	CBC	CBC	1.3
BFEE/IPA (in NaCl)	38	NA	38	CBD	CBC	CBC	20.6
BFEE/IPA (in NaCl, OP1)	48	NA	53	CBD	CBC	CBC	17.9
BFEE/IPA (in NaCl, OP2)	151	12000	NA	CBD	11849	CBC	0.5

NA: not available; CBD: cannot be determined; CBC: cannot be calculated; OP: overoxidation peak

[a] polymer films were deposited on GC electrodes with deposition charges of 0.25 C cm^{-2} from BFEE/CH_3CN and BFEE/IPA.

[b] uncompensated solution resistance (all resistances were measured in Ohm)

[c] real axis intercept (Z_{re}) of low-frequency semi-circle ($R_s' = R_s + R_{CT}$)

[d] real axis intercept (Z_{re}) of low-frequency Warburg line

[e] real axis intercept (Z_{re}) of high-frequency Warburg line

[f] charge transfer resistance ($R_{CT} = R_s' - R_s$)

[g] ionic resistance, $R_i = 3\ (R_{low} - R_{high})$

[h] capacitance taken at the lowest frequency correspond to limiting capacitance if steady state values are reached

5.4.1 Overoxidation of modified polypyrrole films

Polypyrrole films were prepared in the presence of ferrocenyl ethanol (FcOH) and polyethylene glycol (PEG) in order to investigate their ion transport properties after overoxidation. These modifications introduce new properties into the polymer films. In addition, they can change the overoxidation limits of the polymer film (11). Thus, the ion transport properties of modified polymer films were studied to examine the modification effect after overoxidation.

Figure 5.17 shows impedance and capacitance plots for overoxidized PPy-Fc and PPy-Fc-PEG400 along with an unmodified PPy film. These results show that PPy-Fc exhibited very high resistance and low capacitance. However, reasonable resistance and enhanced capacitance were achieved after 1% addition of PEG-400 to the pyrrole solution. It can also be noticed that the appearance of R_{CT} was associated with polymer film modification with PEG-400, but the origin of R_{CT} is not fully understood. It can be concluded that the low ion mobility in overoxidized films caused by additional ion-polymer interactions due to FcOH insertion can be increased by a steric stabilizer, e.g. PEG-400.

5.5 Conclusions

The ion transport properties of overoxidized polymer films were studied in various solvents and electrolytes by using cyclic voltammetry and impedance spectroscopy. Overoxidation of polypyrrole films leads to both Cl-substitution and OH-

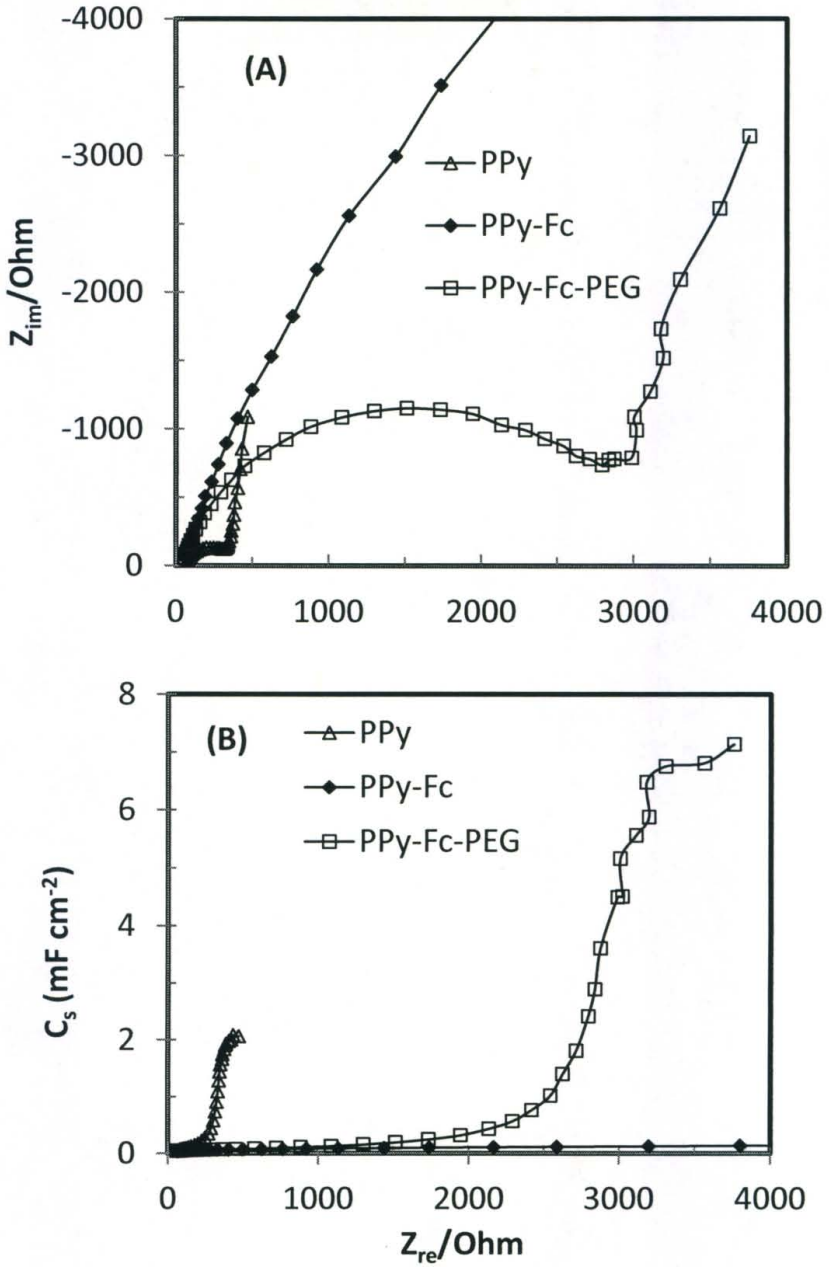

Fig. 5.17 A. Impedance and **B.** series capacitance plots for overoxidized PPy, PPy-Fc, and PPy-Fc-PEG400 films measured in 0.5 M $NaClO_4$ at 0.2 V. The polymer films were exposed to overoxidation potentials ca. 1.5 V by potential scanning at 0.1 V s^{-1} in $NaClO_4$ before measurements. The films were deposited on GC electrodes from 0.1 M Py, 20% BFEE in CH_3CN (10 mM FcOH, 1% PEG400 for corresponding films) with deposition charges of 0.018 C (0.25 C cm^{-2}). The frequency scan range was between 1 kHz to 0.1 Hz (to 1 Hz for PPy).

substitution in NaCl(aq), but further elemental analysis is required to assign which one occurs first. However, in the absence of Cl^- ions only OH-substitution can be detected. Further oxidation can lead to degradation of the polymer and possibly CO_2 formation (19). It has been shown that the polymer film maintain their conjugation to different levels after overoxidation based on the working parameters, such as solvent, electrolyte, and applied potential.

The morphology of the polymer film was also found to be significantly altered at high potentials below degradation due to overoxidation. The morphology alterations and the permanent modification of the polymer backbone lead to new ion transport properties which can be exploited in various applications, such as sensors and ion selective electrode. In addition, overoxidation may lead to a novel way of electrochemical substitutions in the presence of electroactive nucleophiles.

5.6 Experimental

Isopropyl alcohol (IPA, Sigma-Aldrich, 99.5%) was used as received. All other chemicals were described in the previous chapters.

The polymer films were deposited on GC electrodes (0.071 cm^2) from 0.1 M Py, 20 % BFEE in CH_3CN and/or IPA at a constant current of 0.3 mA with deposition charges of 0.018 C (0.25 C cm^{-2}). Overoxidized polymer films were scanned to 1.2 V for overoxidation peak 1 (OP1) and scanned to 2.4 V for overoxidation peak 2 (OP2).

The impedance spectra were measured at 0.2 V where the polymer film is in a conducting state. All potentials are versus SCE. All impedance results were scanned from 1 kHz to 1 Hz, unless otherwise stated. When the plots did not show limiting capacitance behaviour at low frequencies, the frequency was scanned to 0.1 Hz. A logarithmic scale was chosen over 30 points from high to low frequency. The impedance plots were drawn as imaginary impedance (Z_{im}) versus real impedance (Z_{re}); capacitance plots were drawn as series capacitance (C_s) versus real impedance (Z_{re}). This type of plot is useful to determine the limiting capacitance (C_{lim}) if the capacitance at low frequencies reaches a constant value, but in some cases the capacitance of the film continued to increase beyond the lowest frequency point, and hence the highest value was designated as the low frequency capacitance (C_{lf}). This plot gives an easy way to estimate the conductivity of the film from the slope of rising portion, i.e. high slopes indicate high conductivities (20).

References

1. P. Pickup, In Modern Aspects of Electrochemistry, ed. B. Conway, J. Bockris, R. White, Plenum, New York 33 (1999) 549.

2. Z. Qi, P. Pickup, *J. Chem. Soc. Chem. Commun.* (1992) 1675.

3. Z. Qi, N. Rees, P. Pickup, *Chem. Mater.* 8 (1996) 701.

4. S. Hayashi, S. Inagi, T. Fuchigami, *Polym. Chem.* 2 (2011) 1632.

5. T. Fuchigami, S. Inagi, *Chem. Commun.* 47 (2011) 10211.

6. S. Inagi, K. Hosaka, S. Hayashi, T. Fuchigami, *J. Electrochem. Soc.* 157 (2010) E88.

7. S. Ghosh, G. Bowmaker, R. Cooney, J. Seakins, *Synth. Met.* 95 (1998) 63.

8. F. Beck, P. Braun, M. Oberst, *Bunsen-Ges. Phys. Chem. Chem. Phys.* 91 (1987) 967.

9. F. Beck, P. Braun, F. Schloten, *J. Electroanal. Chem.* 267 (1989) 141.

10. S. Gentil, E. Crespo, I. Rojo, A. Friang, C. Vinas, F. Teixidor, B. Gruner, D. Gabel, *Polymer* 46 (2005) 12218.

11. E. Crespo, S. Gentil, C. Vinas, and F. Teixidor, *J. Phys. Chem. C* 111 (2007) 18381.

12. C. Debiemme-Chouvy, T. Tran, *Electrochem. Commun.* 10 (2008) 947.

13. Y. Sahin, B. Ercan, M. Sahin, *Talanta* 75 (2008) 369.

14. L. Ozcan, Y. Sahin, H. Turk, *Biosens. Bioelectron.* 24 (2008) 512.

15. B. Krische, M. Zagorska, *Synth. Met.* 28 (1989) 257.

16. X. Ren, P. Pickup, *J. Phys. Chem.* 97 (1993) 5356.

17. R. Moghaddam, P. Pickup, *Electrochim. Acta* 56 (2011) 7666.

18. G. Duffitt, P. Pickup, *J. Chem. Soc. Faraday Trans.* 88 (1992) 1417.

19. P. Christensen, A. Hamnett, *Electrochim. Acta* 36 (1991) 1263.

20. R. Moghaddam, P. Pickup, *Phys. Chem. Chem. Phys.* 12 (2010) 4733.

Chapter 6

Ion Transport in Polyfluorenone Films

6.1 Introduction

Conducting polymers, such as polypyrrole (PPy), polythiophene (PTh), and polyaniline (PAn), are electron rich conjugated polymers and have been extensively studied in their oxidized or p-doped forms, due to their ability to stabilize the inserted positive charge (1; 2; 3). Furthermore, most conducting polymers can be considered as p-type conductors due to their ability to delocalize the positive charge over their conjugated system. In contrast, electron deficient conducting polymers are much less studied and have received much less attention in research due to the limited number of stable n-type materials that have been discovered. The ability to stabilize a negative charge, n-type conductors, is governed by the existence of electron withdrawing functionality in the polymer unit structure. There are many potential applications for this type of conductor in supercapacitors, electronic devices, and organic light emitting diodes (OLEDs) (4). As such, there is a demand to develop new materials with n-type

properties and to facilitate their use as cathodic materials, and so understanding their conduction mechanism is a crucial point.

In contrast to p-type conductors with high-lying valence bands, n-type conductors possess low-lying conduction bands with high electron affinity. As such, the mechanism of conduction is different in each type where p-type conduction involves hole transport along the polymer chains and n-type conduction involves electron hopping between localized sites (5). The two mechanisms can also exist in one polymer by copolymerization of donor and acceptor units which produces low band gap polymers (5; 6). This type of conductor generally has low conductivities due to poor matching of orbital energies (5).

Fluoren-9-one (FO) is an excellent candidate to produce an n-type conducting polymer (polyfluorenone) due to the existence of an electron withdrawing group (i.e. carbonyl group) in its molecular structure at the 9-positon and its ability to stabilize/accept a negative charge, see Figure 6.1. Polyfluorenone (PFO) has high electron affinity and a low-lying conduction band. In addition, the carbonyl group at the 9-position can stabilize the inserted negative charge and substantially decrease the reduction potential of the polymer (7). Although there are very few reports on the polymerization of FO as a polymer-coated electrode, it can be electropolymerized on a Pt electrode surface by oxidative coupling polymerization in CH_2Cl_2 or boron trifluoride ethyl etherate (BFEE) as reported in reference (7) and (8), respectively. Modifications of

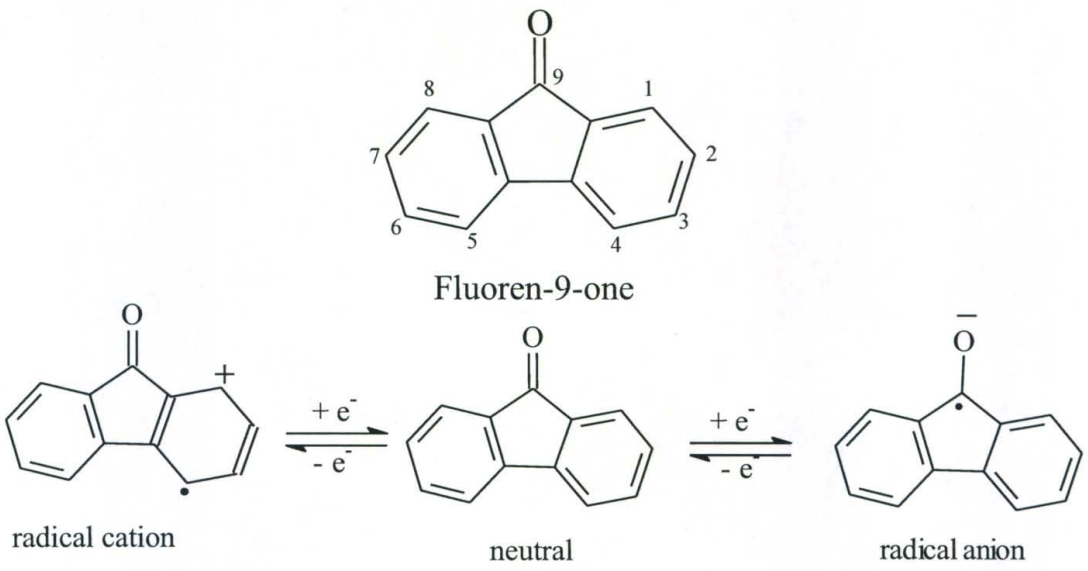

Fig. 6.1 Chemical structure of fluoren-9-one; oxidation and reduction of fluoren-9-one.

these polymer films are required to get more stable films. In addition, the electrochemical and ion transport properties of PFO are not fully understood.

Thus, the aim of the work in this chapter was to produce stable PFO films that can be electrochemically characterized and used as cathodic materials. In addition, it is important to understand the n-doping process in the presence of various electrolyte ions, which is kinetically difficult due to restricted cation mobility inside the polymer matrix.

6.2 Electrochemical polymerization of fluoren-9-one

Polyfluorenone (PFO) can be deposited from two different systems; dichloromethane (CH_2Cl_2) containing a supporting electrolyte (e.g. Bu_4NBF_4) or pure boron trifluoride ethyl etherate (BFEE). BFEE is generally a conducting solvent due to its reaction with water from the environment which can form a complex anion according to Equation 6.1.

$$H_2O + BF_3\text{-}EE \rightleftharpoons EE + H^+ + (BF_3{:}OH)^- \qquad [6.1]$$

The ionic complex $(BF_3{:}OH)^-$ eliminates the need for a supporting electrolyte, and thus BFEE can serve as an ionic solvent.

Figure 6.2 shows the electrochemical polymerization of FO on Pt electrodes in (A) CH_2Cl_2 containing Bu_4NBF_4 and (B) BFEE. Five cycles can be seen for each system in which the electrodeposition of PFO was increasing with cycling where the current increase is an indication of more polymeric material deposited on the electrode surface. It can also be noticed that PFO was deposited over two different potential windows; (A) between 1.0 V and 2.8 V in CH_2Cl_2 and (B) between 0.7 V and 2.0 V in BFEE. The starting potential was just before the redox wave of FO in each solvent and the switching potential was just on the tail of the redox wave and before overoxidation starts. The electrocatalytic ability of BFEE to polymerize FO over a lower potential window can be observed from the first cycle of the polymerization (Figure 6.3). The oxidation onset potential of FO in BFEE was 1.6 V (vs SCE) which is much lower than 2.0 V (vs SCE) for FO in CH_2Cl_2/Bu_4NBF_4. The catalytic ability of BFEE to oxidize FO is not fully understood, but

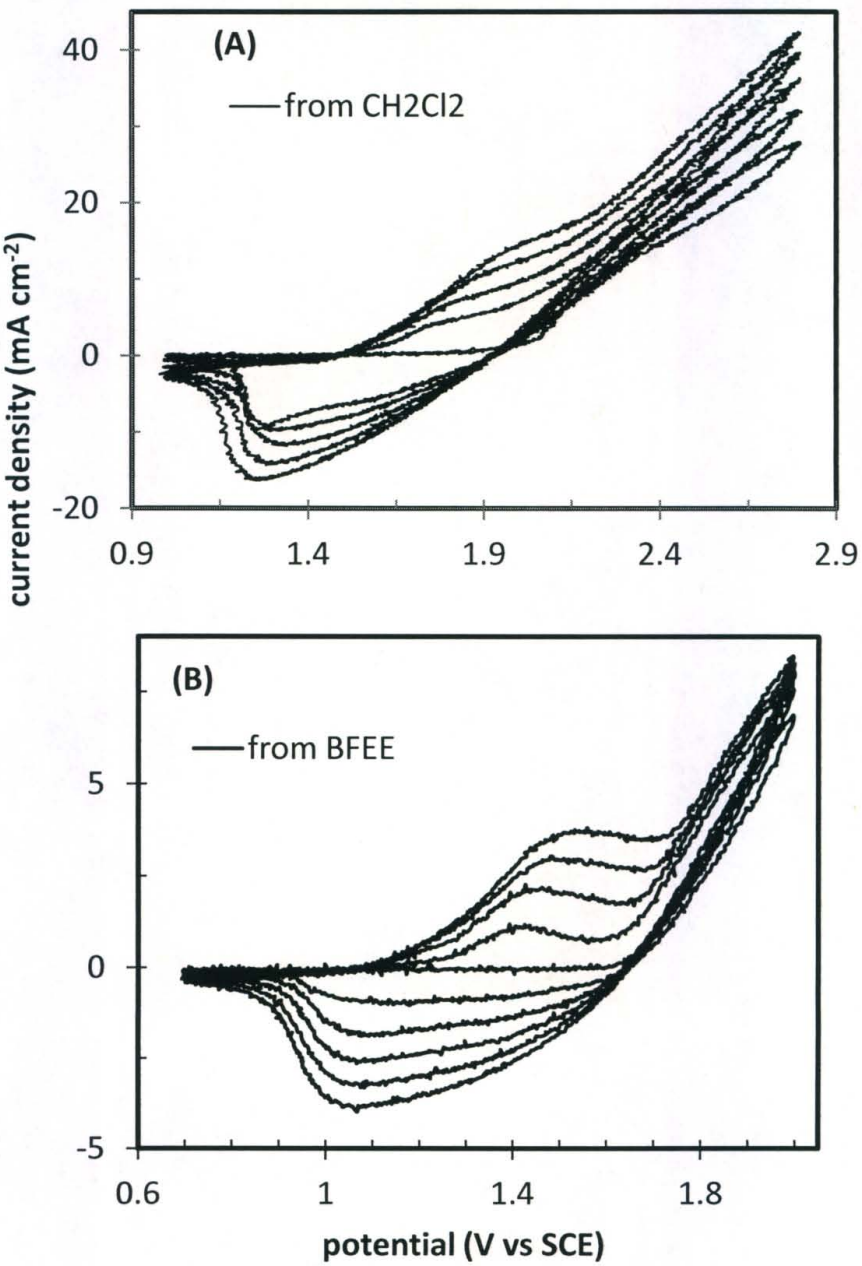

Fig. 6.2 Electropolymerization of fluoren-9-one (FO) on Pt electrodes (0.0045 cm^2) from two different systems; **A.** 0.1 M FO in CH_2Cl_2 containing 0.1 M Bu_4NBF_4, **B.** 30 mM FO in pure BFEE. The scan rate was 0.1 V s^{-1}.

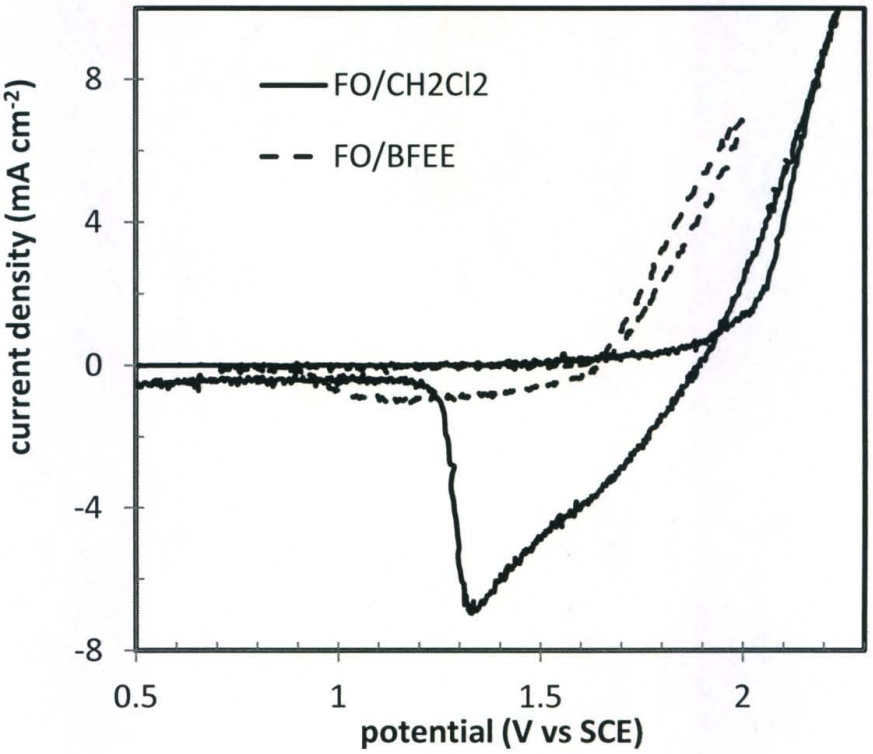

Fig. 6.3 First cycle voltammograms for fluoren-9-one polymerization in BFEE and CH_2Cl_2 containing Bu_4NBF_4.

might be attributed to the interaction between the vacant orbital of the Lewis acid (BF_3) and the aromatic monomer units of FO (8). The increased current for the FO/CH_2Cl_2/Bu_4NBF_4 system compared with FO/BFEE is due to the excess of supporting electrolyte used for the former system. A nucleation loop can also be observed for FO/CH_2Cl_2/Bu_4NBF_4 on the first cycle indicating initiation of the deposition on the electrode surface. The polymerization of FO ring occurs at 2,7-position which was proven by structural studies, e.g. ^{1}H NMR (8).

In addition to potentiodynamic polymerization, FO can also be polymerized by potentiostatic and galvanostatic techniques. Figure 6.4 show cyclic voltammograms (CVs) of PFO in CH_3CN containing 0.1 M Et_4NClO_4 (TEAP) in which PFO was deposited from FO/BFEE by using the three different techniques. The depositions were achieved at various conditions as follows; at constant current of 0.01 mA for 1 minute (GS), at 1.6 V for 1 minute (PS), and by cycling between 0.7 V and 2.0 V three times at 0.1 V s^{-1} (PD). As a result, the three PFO films have different deposition charges during the polymerization processes, and so they cannot be compared quantitatively with respect to the amount of deposited material. It can be noticed that the formal potential of the n-doping processes occurs at ca. -1.3 V for all films indicating similar thermodynamic conditions during switching between the doped (reduction) and undoped (oxidation) states. It can also be noticed that the cathodic peak is always bigger than the anodic peak. This is discussed in the following sections of this chapter. The small cathodic peak at -1.0 V for the GS film is

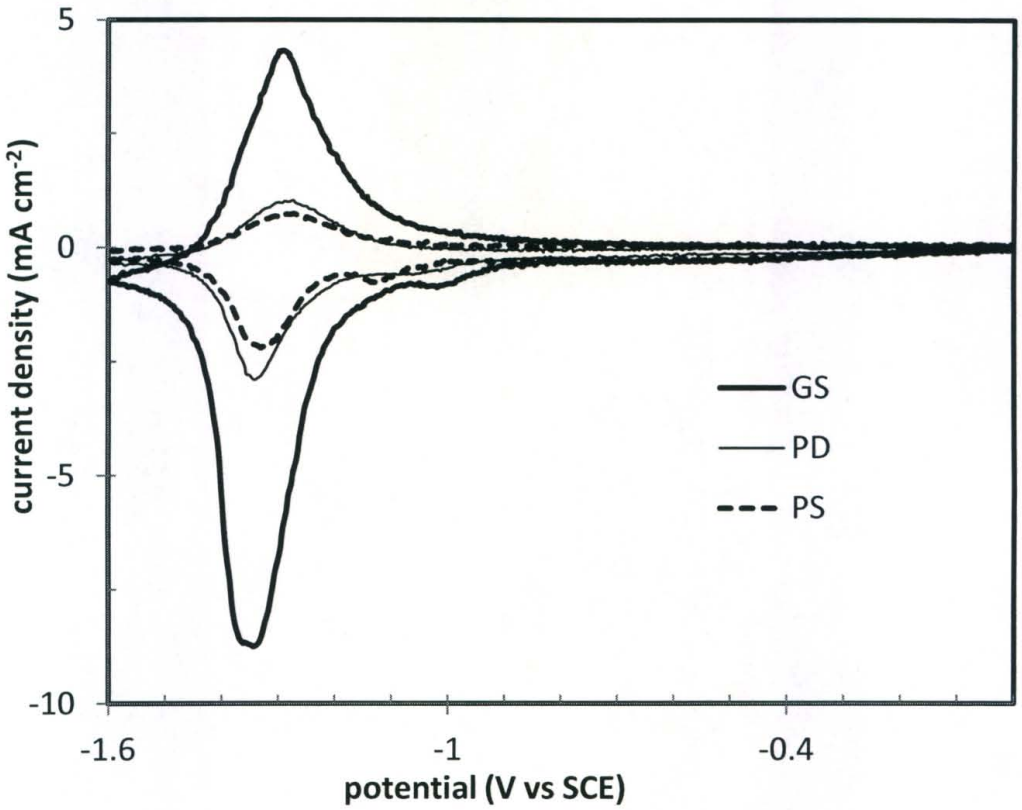

Fig. 6.4 Cyclic voltammograms for PFO films in 0.1 M TEAP/CH_3CN at 0.1 V s^{-1}. The polymer films were deposited on Pt electrodes from 30 mM FO in BFEE potentiodynamically (PD, 3 cycles between 0.7 V and 2.0 V at 0.1 V s^{-1}), potentiostatically (PS, 1.6 V for 1 min), or galvanostatically (GS, 0.01 mA for 1 min, 0.6 mC, 0.133 C cm^{-2}).

believed to be due to irreversible oxygen reduction where atmospheric oxygen was incompletely purged from the electrochemical cell prior to that measurement.

6.3 Electrochemistry of polyfluorenone

The electrochemical switching of conducting polymers between doped and undoped states is generally accompanied by anion and cation transport during the p-doping and n-doping processes, respectively. PFO can be oxidized (p-doped) and reduced (n-doped) according to Equations 6.2 and 6.3, respectively.

$$\mathbf{PFO + A^- \rightleftharpoons PFO^+/A^- + e^-} \qquad \mathbf{[6.2]}$$

$$\mathbf{PFO + e^- + C^+ \rightleftharpoons PFO^-/C^+} \qquad \mathbf{[6.3]}$$

Where $\mathbf{e^-}$ is an electron; $\mathbf{A^-}$ and $\mathbf{C^+}$ are anions and cations from the external electrolyte solution, respectively. Equations 6.2 and 6.3 represent simple ion transport in conducting polymers in which anions or cations move into/out of the film during the redox process to preserve the electroneutrality of the film. However, more complicated ion transport often occurs during oxidation and reduction in which both anions and cations contribute in the charge compensation process.

Figure 6.5 shows CVs for PFO films in CH_3CN containing 0.1 M TEAP in which the films were deposited from the two solvents (CH_2Cl_2 and BFEE) described above. Addition of 1% polyethylene glycol (PEG-400) to the polymerization solution of BFEE was employed to produce a more stable film on the electrode surface, which will be described later in this chapter.

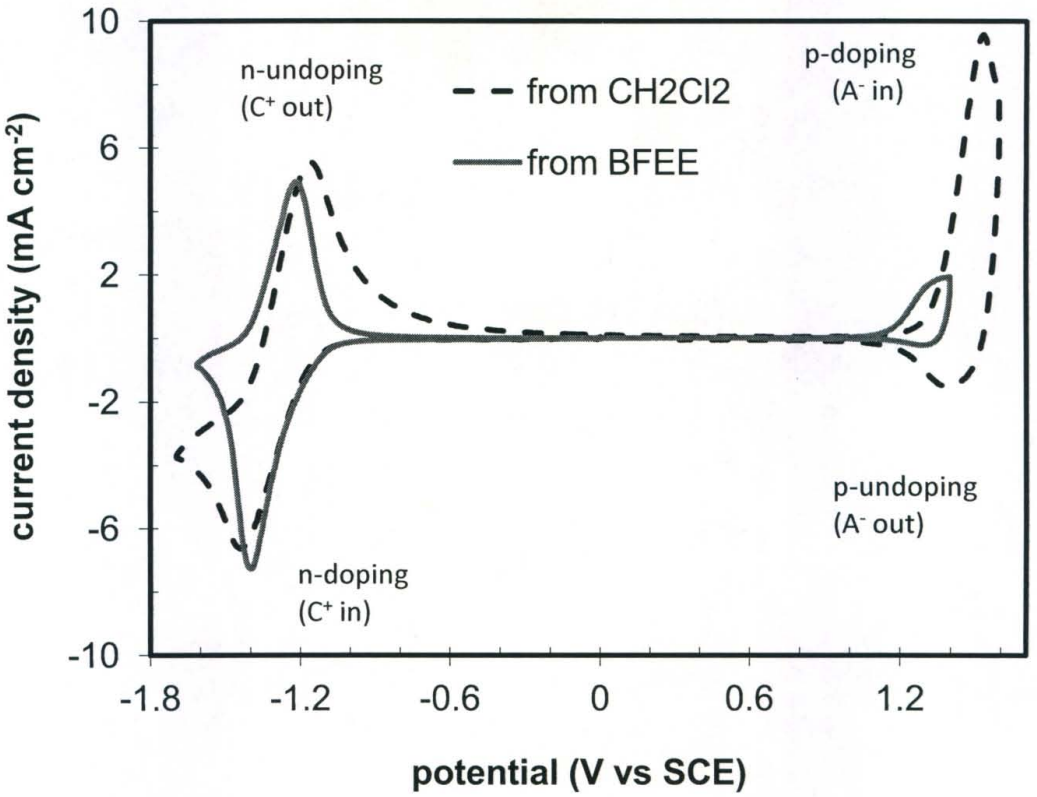

Fig. 6.5 Cyclic voltammograms for PFO in CH_3CN containing 0.1 M TEAP at 0.1 V s^{-1}. The scans started at 0 V to negative potentials first. The films were deposited on Pt wire electrodes from 30 mM FO, 1% PEG-400 in BFEE by cycling between 0.7 V and 2.0 V (5 cycles at 0.05 V s^{-1}) or 0.1 M FO, 0.1 M $TBAPF_6$ in CH_2Cl_2 by cycling between 0.5 V and 2.8 V (5 cycles at 0.1 V s^{-1}). Ion transport is indicated on each peak (C^+: cation, A^-: anion).

The scans started at 0 V toward negative potentials switching at ca. -1.7 V, then continued toward positive potentials switching at 1.3 V (BFEE film) and at 1.4 V (CH_2Cl_2 film). High positive potentials were avoided to protect the films from overoxidation. Two distinct doping processes (conducting states for n- and p-doping) can be distinguished in the scanned potential region for the two CVs. The two doping processes were separated by a zero-current nonconducting state. The difference between the two onset potentials is the electrochemical band gap (4) which was found to have a value of ca. 2.5 V. This value is equivalent to 2.5 eV which is a typical band gap for organic semiconductors (1).

Well defined redox peaks for the n-doping process can be observed for both CVs. This can be attributed to the existence of an electron withdrawing group (carbonyl group) which enhances the reduction process. The formal potentials for the n-doping processes were very similar for both films at ca. -1.3 V. However, p-doping exhibited different formal potentials at ca. 1.25 V and ca. 1.35 V for the BFEE film and CH_2Cl_2 film, respectively. It can also be noticed that the film prepared in CH_2Cl_2 exhibited broader redox peaks than the film prepared in BFEE for the n-doping process and larger redox peaks for the p-doping process. These behaviours can be attributed to the existence of dimer units in the CH_2Cl_2 film (8). The oxidation onset for the shorter conjugated lengths (e.g. dimer or trimer units) is higher than for the longer ones, which is consistent with higher p-doping formal potential of the film prepared in CH_2Cl_2.

6.4 Scan rate dependence of cyclic voltammetry

The scan rate dependence was investigated for CVs of various PFO films to explore any kinetics limitation during n-doping. Figures 6.6 and 6.7 show CVs of PFO films prepared from CH_2Cl_2 and BFEE, respectively, in 0.1 M TEAP/CH_3CN at various scan speeds. Increasing peak separations (ΔE_p) and peak currents (i_{pa} and i_{pc}) can be observed with increasing scan rate for both films. Plots of peak separation versus total current ($i_a - i_c$) are shown in Figures 6.8-A and 6.9-A. There are significant peak separations with increasing current where both anodic and cathodic peaks (equally) shifted away from each other. This can be attributed to the resistance of the system and the increasing currents at higher scan rates. The peak separation (ΔE_p) can be described by Equation 6.4.

$$\mathbf{\Delta E_p = 59/n + iR} \qquad \mathbf{[6.4]}$$

Where $\mathbf{\Delta E_p}$ is in mV, **n** is the number of electron transferred, and **iR** is the ohmic potential drop due to the solution resistance. The iR factor can be minimised by decreasing the distance between the working and reference electrodes. However, even for a reversible system there is increase in ΔE_p with increasing scan rate due to the solution (uncompensated) resistance which cannot be removed completely. Increasing ΔE_p with increasing scan rate can also indicate the presence of electrochemical irreversibility. The electrochemical irreversibility (or quasi-reversibility) arises due to slow electron kinetic transfer. On the other hand, the peak currents increased almost linearly as a function of scan rate indicating the absence of any kinetic limitation due to electron transfer.

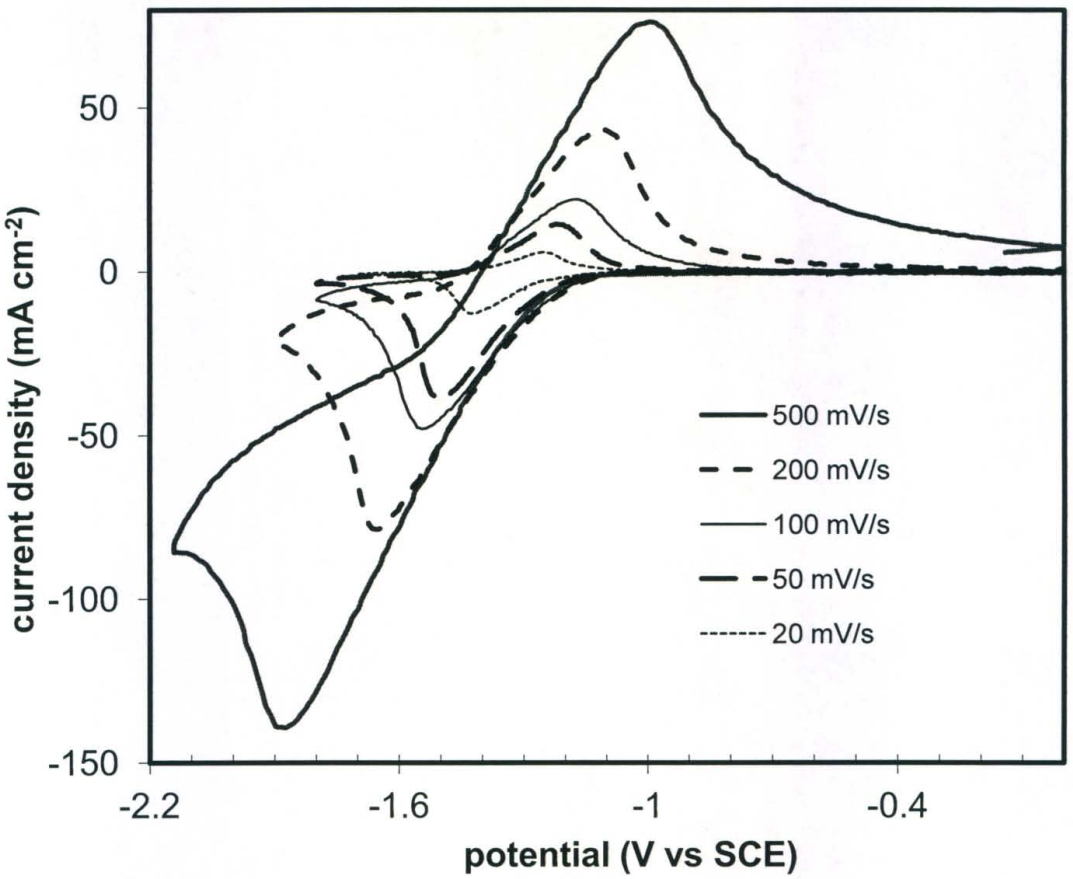

Fig 6.6 Cyclic voltammograms for a PFO film in 0.1 M TEAP/CH_3CN at various scan rates as indicated. The polymer film was deposited on a Pt wire from 0.1 M FO, 0.1 M Bu_4NPF_6 in CH_2Cl_2 with a deposition charge of 3 mC.

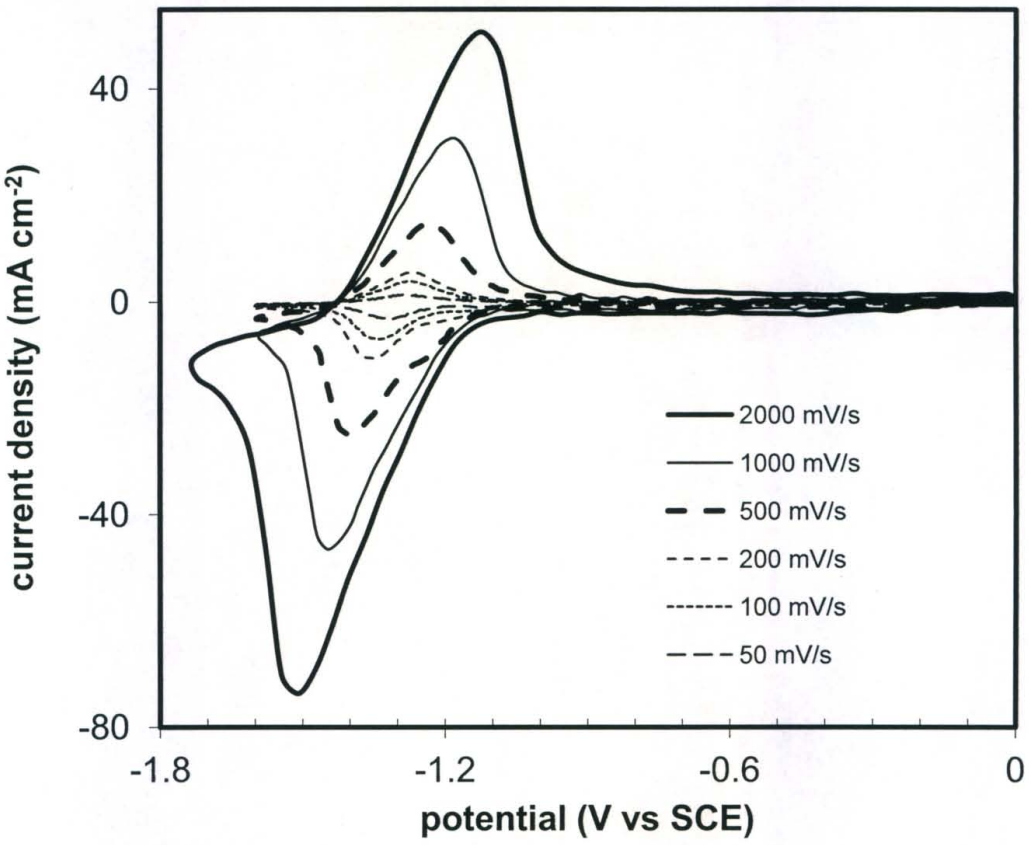

Fig 6.7 Cyclic voltammograms for a PFO film in 0.1 M TEAP/CH_3CN at various scan rates as indicated. The polymer film was deposited on a Pt wire from 30 mM FO in BFEE with a deposition charge of 0.6 mC.

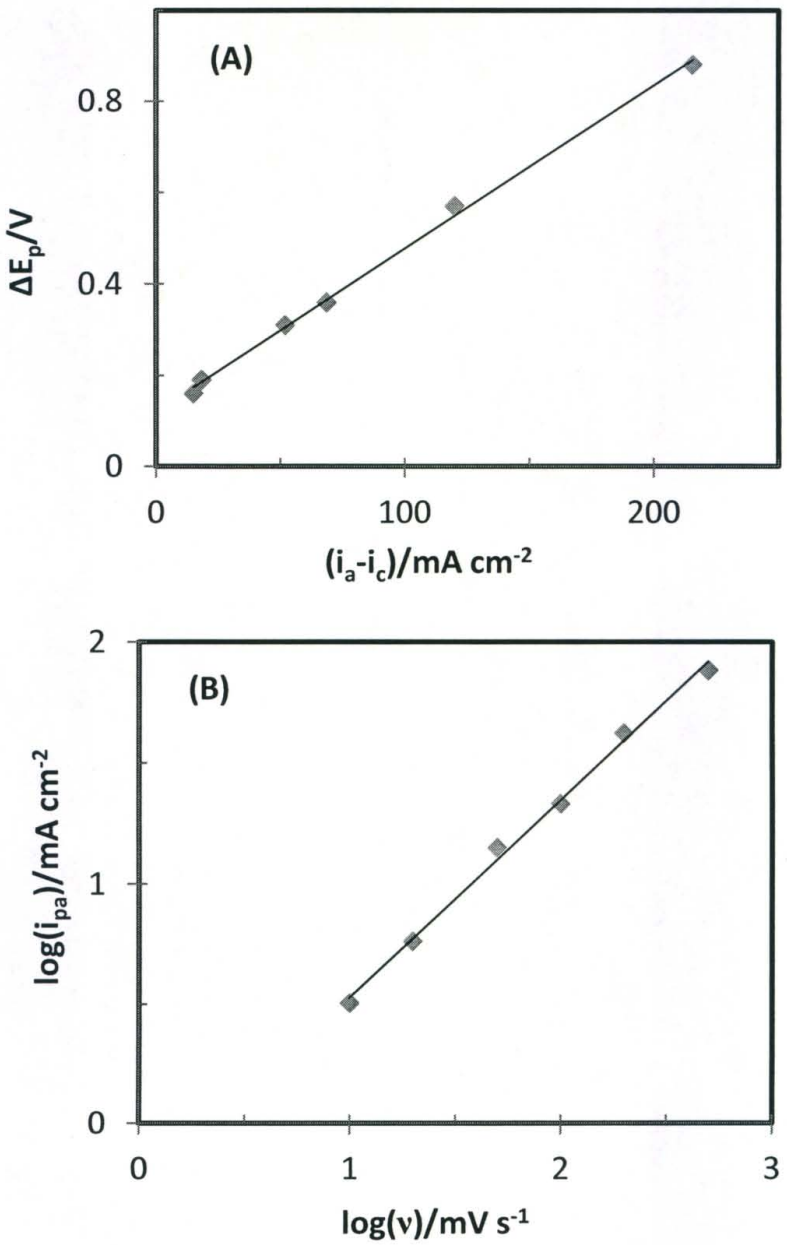

Fig. 6.8 **A.** Plot of peak potential separation vs total current; **B.** Log plot of anodic current vs scan rate for the PFO film prepared from Bu_4NPF_6/CH_2Cl_2.

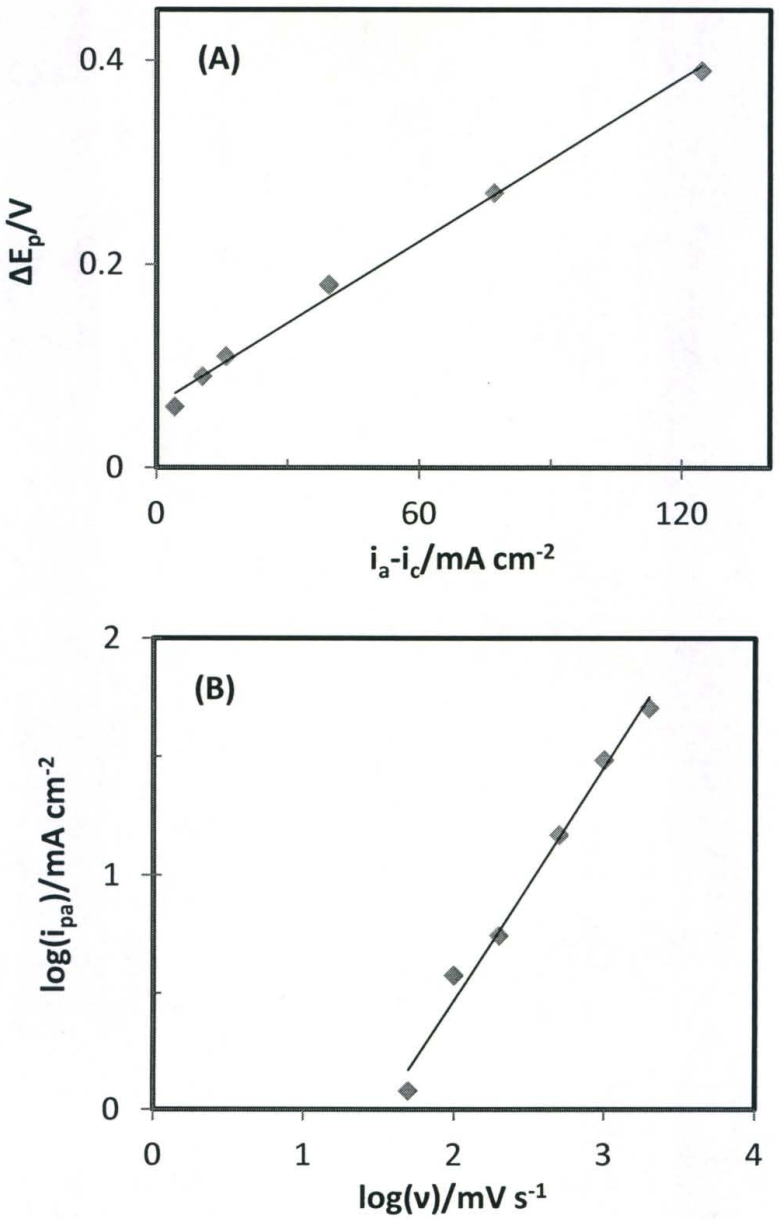

Fig. 6.9 A. Plot of peak potential separation vs total current; **B.** Log plot of anodic current vs scan rate for the PFO film prepared from BFEE.

Figures 6.8-B and 6.9-B show log plots of peak current versus scan rate. This behaviour has similar response as a redox couple which is governed by the Randles-Sevcik equation (Equation 6.5) for reversible electron transfer:

$$\mathbf{i_p = (2.69 \times 10^5)\, n^{3/2}\, A\, D^{1/2}\, C\, \nu^{1/2}} \qquad \mathbf{[6.5]}$$

Where $\mathbf{i_p}$ is the peak current (ampere), **n** is the electron stoichiometry, **A** is the electrode area (cm^2), **D** is the diffusion coefficient ($cm^2\ s^{-1}$), **C** is the concentration of a redox species (mol cm^{-3}), and **ν** is the scan rate ($V\ s^{-1}$). Both plots gave almost linear relationship between the peak currents and scan rate indicating reversible electron transfer. The low slope for the CH_2Cl_2 film can be attributed to higher iR effect.

6.5 Potential dependence of impedance spectroscopy

Impedance spectroscopy was used to measure the film resistance ($R_e + R_i$) for a PFO film in Et_4NBF_4/CH_3CN as a function of its oxidation level. The impedance measurements were taken at negative potentials between 0 V and -1.6 V to investigate ion and electron transport during n-doping. When PFO is reduced at negative potentials, it behaves as a redox polymer where an electron hopping model can be applied to the n-type conduction. The conductivity of redox polymers involves electron transport between localized sites which is governed by Equation 6.6 (9).

$$\mathbf{D_e = k_{ex}\, \lambda^2\, (C_{ox} + C_{red})} \qquad \mathbf{[6.6]}$$

Where $\mathbf{D_e}$ is the electron diffusion coefficient, $\mathbf{k_{ex}}$ is the rate constant for electron exchange between the fixed oxidized and reduced sites in the polymer, λ is the average

distance of electron hops, and $\mathbf{C_{ox}}$ and $\mathbf{C_{red}}$ are the concentrations of oxidized and reduced sites ($C_{total} = C_{ox} + C_{red}$). The electronic ($R_e$) and ionic ($R_i$) resistances can be obtained by using Equations 6.7 and 6.8.

$$\mathbf{R_\infty^{-1} = R_e^{-1} + R_i^{-1}} \qquad \mathbf{[6.7]}$$

$$\mathbf{R_\Sigma = R_e + R_i} \qquad \mathbf{[6.8]}$$

Where $\mathbf{R_\infty}$ is the intercept of the real axis at high frequencies in the impedance plot minus solution resistance (i.e. $R_\infty = R_{high} - R_s$), and $\mathbf{R_\Sigma}$ is given by extrapolation of the linear portion at low frequencies to the real axis (i.e. $R_\Sigma = 3(R_{low} - R_s)$). R_e and R_i can be equal to each other either coincidently or due to coupling of electron and counterion motions. In cases where they are not equal, the two resistances cannot be assigned to R_e and R_i, and so additional information is required to assign each resistance (10).

Figure 6.10 shows impedance (A) and capacitance plots for a PFO film prepared from BFEE and measured in Et_4NBF_4/CH_3CN at negative potentials between 0 V and -1.6 V. The measurements were taken in the order of decreasing potential which reflect the neutral and n-doped states. The behaviour of the film at 0 V and -0.5 V is not clear from the impedance plots where the film is at its neutral (undoped) state and high resistance is expected. This behaviour is clear from the capacitance plots where very low capacitances are shown indicating that there was no oxidation or reduction of the film at these potentials. Under these conditions, R_f cannot be determined. The behaviour at -1.1 V, -1.2 V, and -1.3 V can be explained by examining both impedance and capacitance

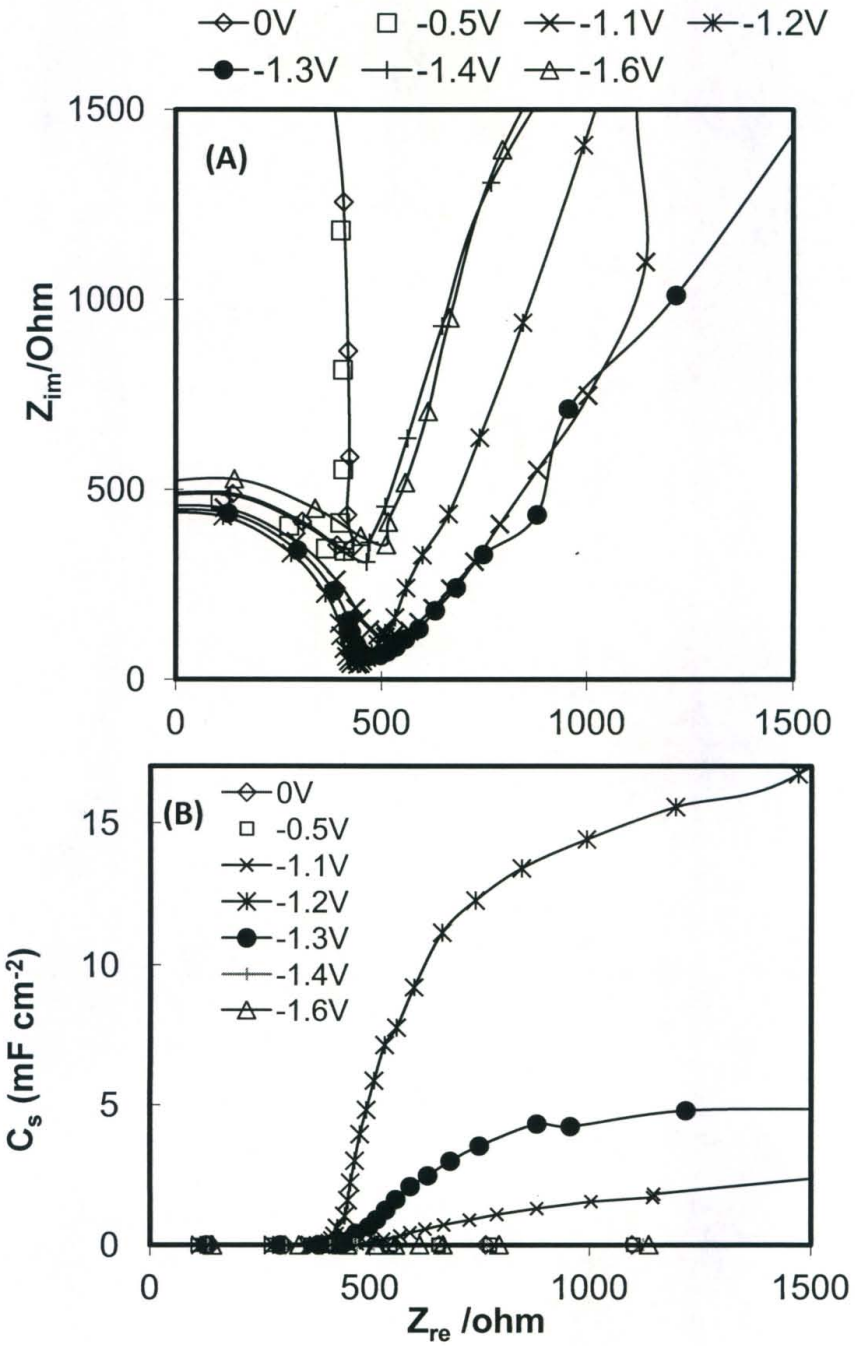

Fig. 6.10 **A.** Impedance and **B.** Capacitance plots for a PFO film in 0.1 M Et_4NBF_4/CH_3CN at various potentials recorded in the order of decreasing potential. Frequency was scanned from 100 kHz to 1 Hz. The polymer film was deposited on a Pt electrode from 30 mM FO in BFEE potentiodynamically (10 cycles between 0.7 V and 2.0 V at 0.05 V s^{-1}).

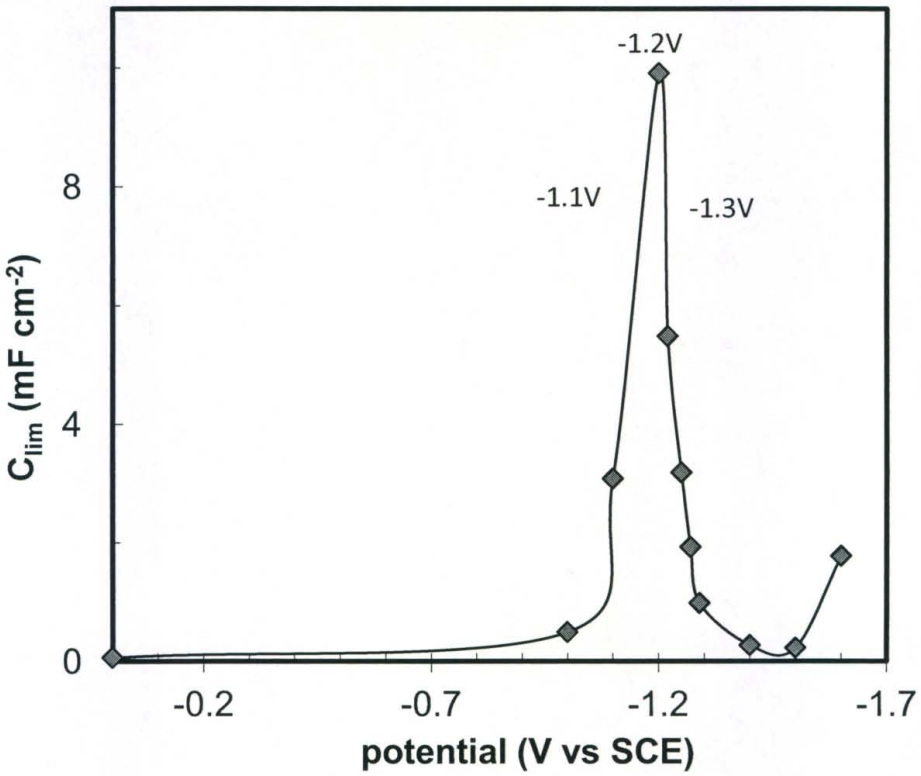

Fig. 6.11 Limiting capacitance (measured at 0.1 Hz) versus electrode potential for a PFO film in 0.1 M Et_4NBF_4/CH_3CN recorded in the order of decreasing potential. The polymer film was deposited on a Pt electrode from 30 mM FO in BFEE potentiodynamically (3 cycles between 0.7 V and 2.0 V at 0.05 V s^{-1}).

plots. It can be seen that the film exhibited higher resistance at -1.1 V and -1.3 V compared with the value at -1.2 V. This can be explained by their capacitance behaviours where at -1.2 V the film exhibited the highest capacitance. The resistance can be attributed to the electron diffusion (proportional with conductivity) which has its maximum value at the formal potential (Equation 6.6) and is lower before and after its optimum value. This behaviour can be seen clearly by plotting limiting capacitance (C_{lim}) versus potential (Figure 6.11). Figure 6.11 also shows an increase in capacitance behaviour at -1.6 V, suggesting an irreversible second reduction at low potentials, or overreduction. The impedance plots show semicircles at high frequencies due to the geometric capacitance of the cell. This is not to be confused with the charge transfer resistance (R_{CT}) often observed for conducting polymers.

6.6 Influence of electrolyte cation size

The influence of cation size was investigated during n-doping between 0 V and -1.6 V in various electrolyte solutions. Figure 6.12 shows CVs for a PFO film prepared from BFEE and measured in the sequence of Et_4NClO_4, Et_4NBF_4, Bu_4NClO_4, and Bu_4NPF_6. It can be seen that the currents (both anodic and cathodic) decreased with each run in the sequence and the larger cations (Bu_4N^+) caused irreversibility, i.e. $i_{pa} << i_{pc}$. The decreased current with each run can be attributed to an electroactivity decrease with cycling (i.e. deactivation), which is described in the next section. In addition, bigger cations exhibit lower ion mobility causing lower activity. The wave irreversibility for the

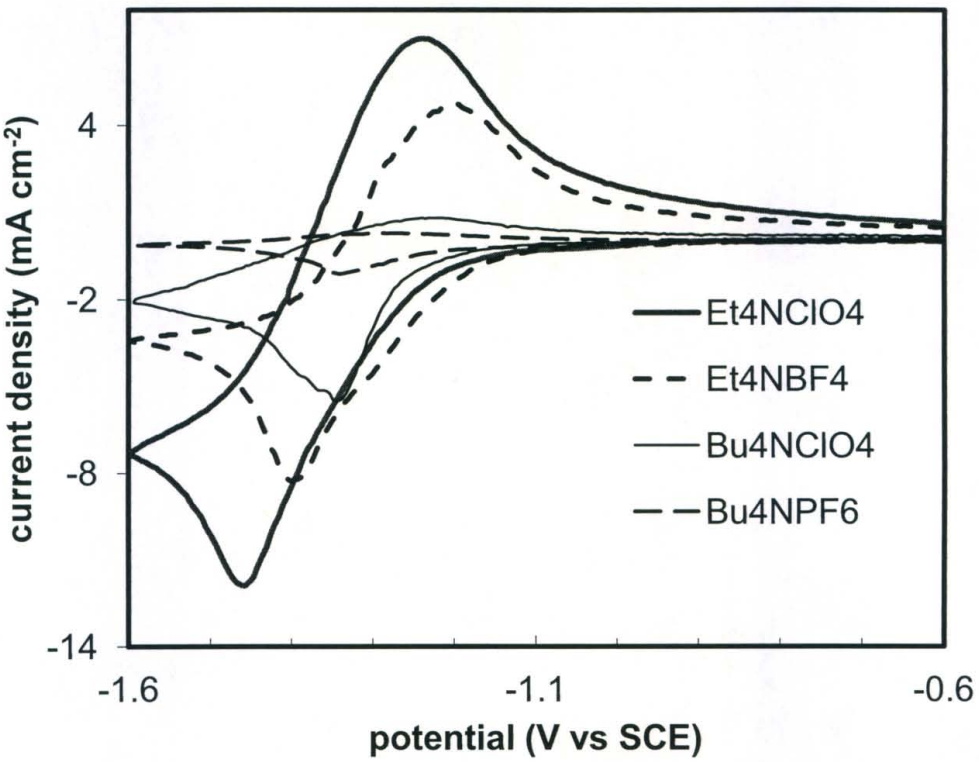

Fig. 6.12 Cyclic voltammograms for a PFO film in various electrolytes (0.1 M) in CH_3CN at 0.1 V s^{-1}. The polymer film was deposited on a Pt electrode from 30 mM FO in BFEE potentiodynamically (12 cycles between 0.7 V and 2.0 V at 0.05 V s^{-1}). The CVs were recorded in the order shown in the legend.

larger cation indicates kinetics limitation in which large cations cannot freely move within the polymer matrix, and so they were trapped following their insertion.

6.7 Deactivation/reactivation processes

Deactivation and reactivation phenomena in conducting polymer have been studied due to their importance in the understanding of ion transport mechanisms (11; 12; 13; 14). A decrease in or loss of electrochemical activity in conducting polymers can occur for a variety reasons, such as overoxidation, use of bulky electrolyte ions, and irreversible chemical processes due to reactions with the solvent, electrolyte, or impurities such as trace oxygen. It is shown here that deactivation can also take place during n-doping of PFO due to cation trapping caused by continuous cycling. A reactivation process can be achieved in some cases to partially restore the electrochemical activity of the polymer.

The polymer film deactivation process was investigated by consecutive cycling in TEAP/CN_3CN for various film preparation conditions. Figure 6.13 shows consecutive CVs in TEAP/CH_3CN for a PFO film prepared from BFEE (three cycles between 0.7 V and 2.0 V). The first cycle shows a reasonably reversible wave at a formal potential of ca. -1.3 V. However, both the reduction (n-doping) and re-oxidation (undoping) waves continuously decreased with cycling, and the film became electrochemically inactive within 12 cycles, i.e. full deactivation.

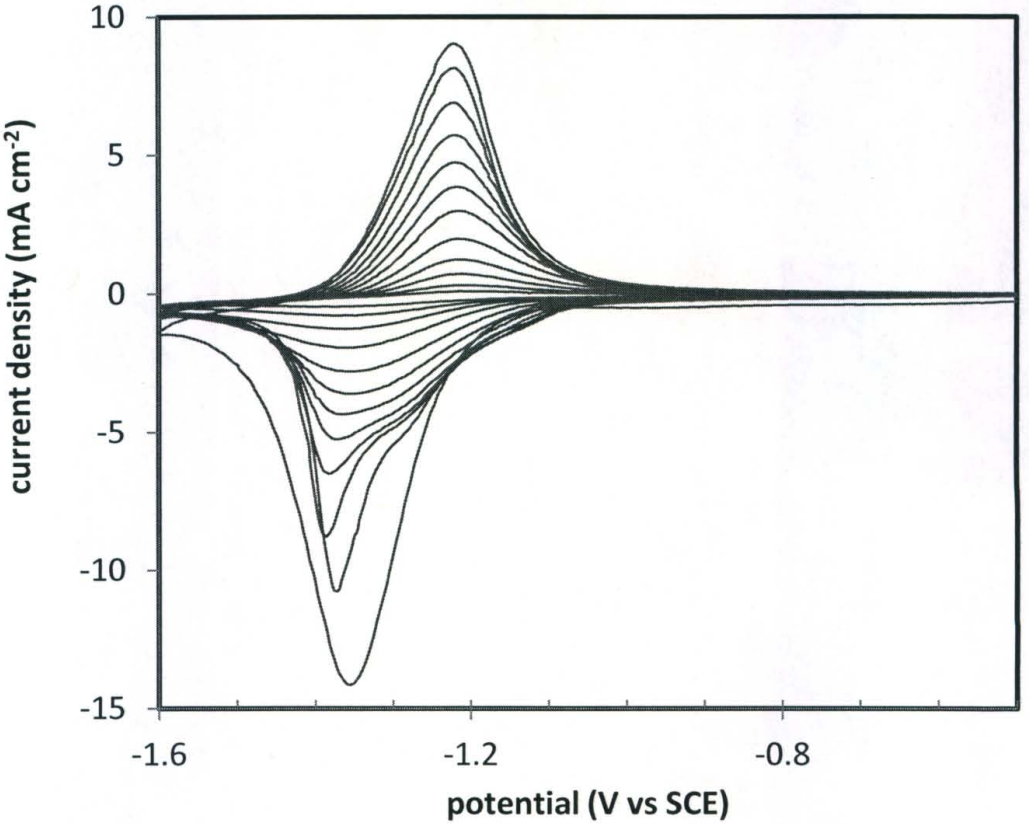

Fig. 6.13 Cyclic voltammograms for a PFO film in 0.1 M TEAP/CH_3CN at 0.1 V s^{-1}. The polymer film was deposited on a Pt electrode from 30 mM FO in BFEE potentiodynamically (3 cycles between 0.7 V and 2.0 V at 0.05 V s^{-1}).

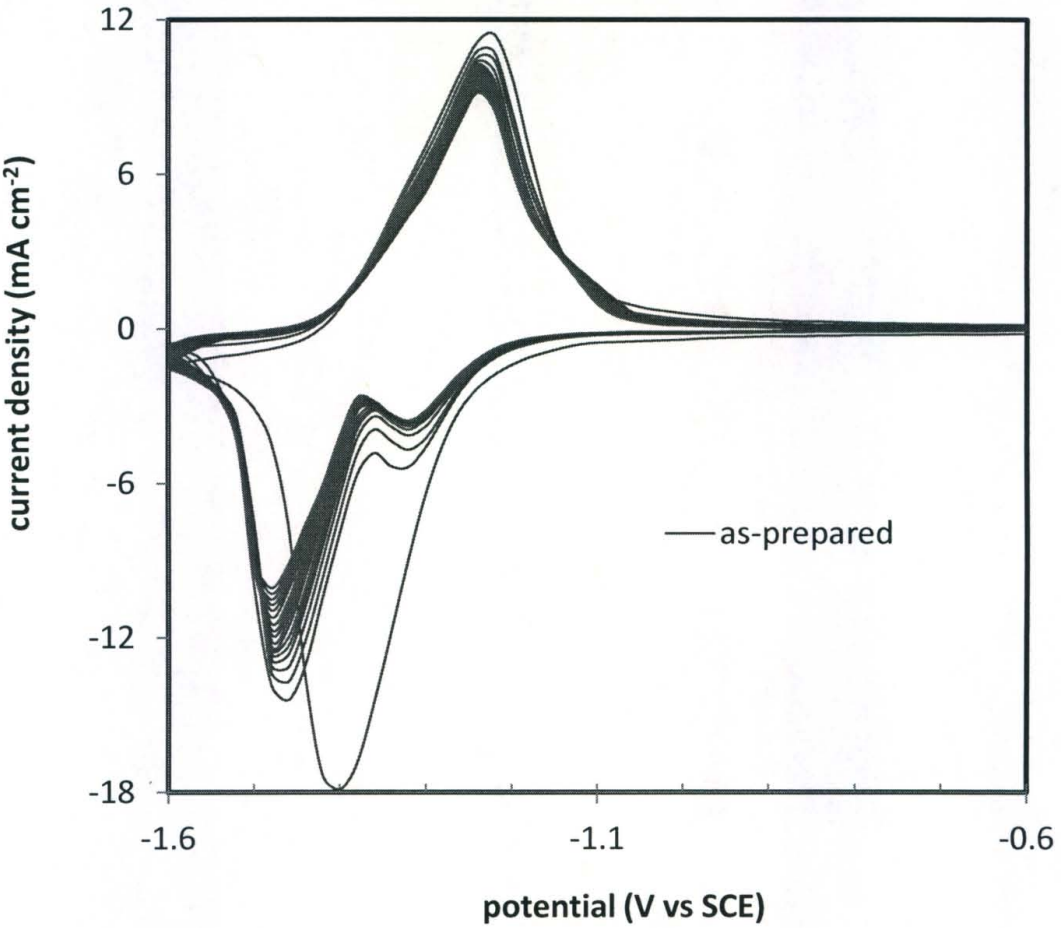

Fig. 6.14 Cyclic voltammograms for a PFO film in 0.1 M TEAP/CH_3CN at 0.1 V s^{-1}. The polymer film was deposited on a Pt electrode from 30 mM FO in BFEE potentiodynamically (5 cycles between 0.7 V and 2.0 V at 0.05 V s^{-1}).

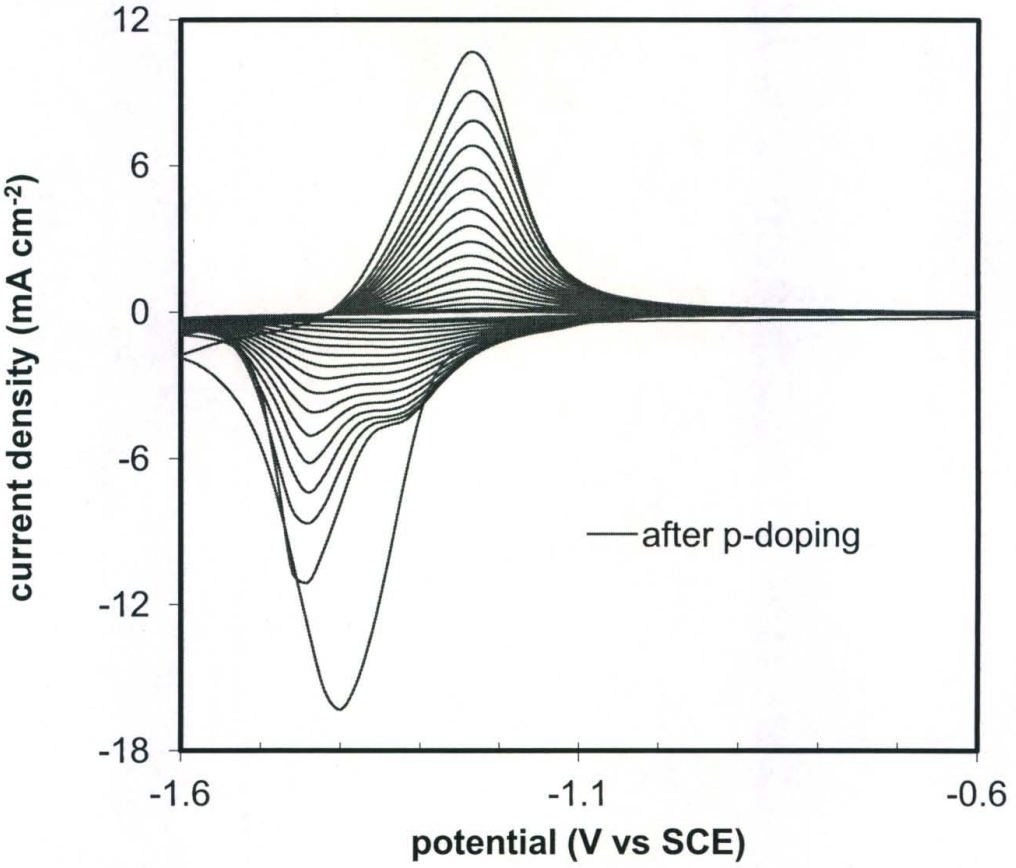

Fig. 6.15 Cyclic voltammograms for a p-doped PFO film in 0.1 M TEAP/CH_3CN at 0.1 V s^{-1}. The polymer film was deposited on a Pt electrode from 30 mM FO in BFEE potentiodynamically (5 cycles between 0.7 V and 2.0 V at 0.05 V s^{-1}).

The loss of electrochemical activity was also investigated for thicker films in TEAP/CH_3CN. Figure 6.14 and 6.15 show consecutive CVs in TEAP/CH_3CN for PFO films prepared from BFEE (five cycles between 0.7 V and 2.0 V). The continuous cycling was performed either directly after preparation (as-prepared) for Figure 6.14 or after p-doping (scanning between 0 V and +1.4 V in TEAP/CH_3CN) for Figure 6.15. The first cycles show a reasonably reversible wave at a formal potential ca. -1.35 V. The first reduction wave shows a higher current compared with the subsequent waves due the influence from the previous history of the film (i.e. film deposition). Only a partial loss of electrochemical activity was observed for the as-prepared film over 20 cycles. However, a complete loss of electrochemical activity was observed within 20 cycles for the film deactivated after p-doping.

The loss of electrochemical activity (partially or fully) with continuous cycling in these films is believed to be due to variety of reasons as follows. Structure changes during the doping/undoping processes can cause the pore size of the polymer matrix to decrease during the undoping process so that some cations can be inserted but cannot be ejected. An irreversible reduction process, which is shown in the capacitance plot at -1.6 V, destroys electroactive sites (see Figure 6.11). Existence of residual anions after film deposition or after p-doping causes ion pair formation which inhibits cation release.

The influence of film thickness indicates a facile deactivation for the thin film, while the insertion of extra anions is required in order to fully deactivate the thicker

film. The change in cathodic waves with continuous cycling indicates complicated ion transport behaviour.

Partial reactivation of the deactivated films was accomplished by polarization at positive potentials, but was entirely not successful due to instability of the films during polarization at positive potentials. However, it was found that modification of PFO films with a steric stabilizer (e.g. PEG-400) makes the deactivated films more stable at positive potential, and so a successful reactivation was obtained, as described in the next section.

6.8 Modification of polyfluorenone by steric stabilizer

The use of polyethylene glycol 400 (PEG-400) as a steric stabilizer during film deposition can enhance the mechanical properties of polypyrrole films (15), see Chapter 4. In addition, it was found that the use of 1% PEG-400 during PFO deposition can enhance the stability of the deactivated film at positive potentials. Figure 6.16 shows consecutive CVs in TEAP/CH_3CN for a PFO film prepared from BFEE/PEG-400 (five cycles between 0.7 V and 2.0 V). The first cycle shows a reasonably reversible wave at a formal potential of ca. -1.35 V. It can be seen that the electrochemical activity continuously decreased with cycling, and that the film became almost inactive within ca. 30 cycles.

The film reactivation process is shown in Figure 6.17 in which the film was cycled to positive potentials up to 1.4 V. Two cycles to each of three upper limits for reactivation in TEAP/CH_3CN were employed. It can be seen that the first cycle of each

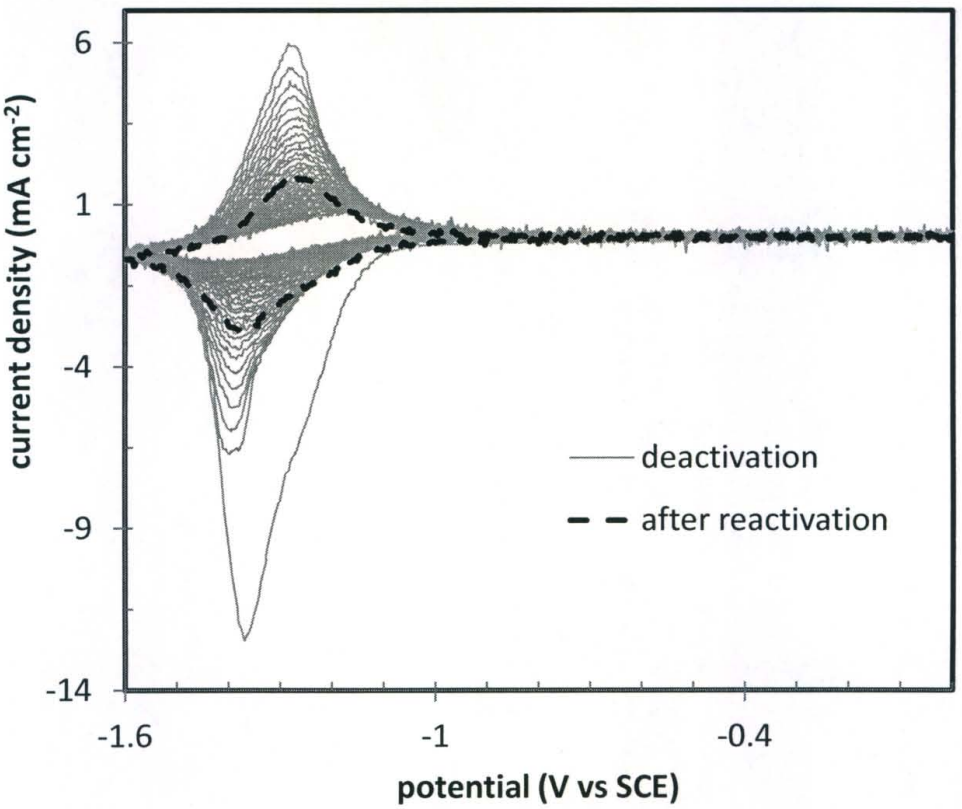

Fig. 6.16 Cyclic voltammograms for deactivation and after reactivation of PFO in CH_3CN containing 0.1 M TEAP at 0.1 V s^{-1}. The film was deposited on a Pt electrode from 30 mM FO, 1% PEG-400 in BFEE by cycling between 0.7 V and 2.0 V (5 cycles at 0.1 V s^{-1}).

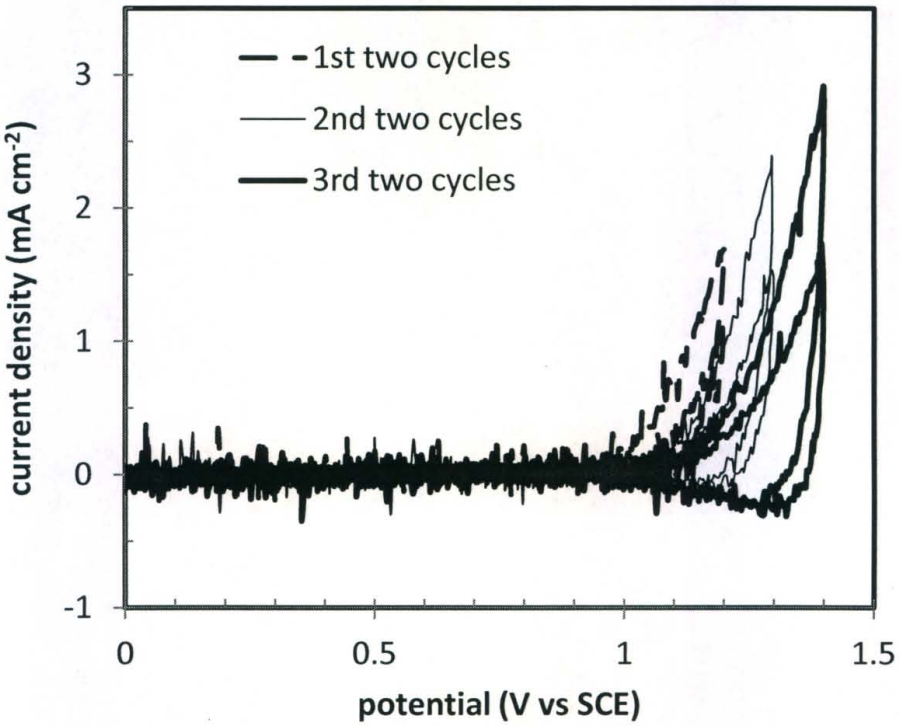

Fig. 6.17 Cyclic voltammograms for reactivation of a PFO film (deactivated in Fig. 6.17) in CH_3CN containing 0.1 M TEAP at 0.1 V s^{-1}. The film was deposited on a Pt electrode from 30 mM FO, 1% PEG-400 in BFEE by cycling between 0.7 V and 2.0 V (5 cycles at 0.1 V s^{-1}).

reactivation exhibited more current (i_{pa}) than the second cycle, and as the potential was increased for each reactivation cycle, the current increased. This might be attributed to cation expulsion occurring faster at higher potentials.

A CV after reactivation is shown in Figure 6.16 in which about 50 % of the film's original activity had been restored. This indicates that the loss of electrochemical activity is not due entirely to irreversible damage to the electronic structure of the polymer since the activity can be partially restored by p-doping of the film.

The reactivation process can also be achieved by using constant potential polarization. Figure 6.18 shows consecutive CVs in TEAP/CH_3CN for a PFO film prepared from BFEE/PEG. CVs after reactivation are also shown in which the reactivation processes were achieved at a constant potential of 1.15 V hold for one and two hours. It can be seen that electrochemical activity was partially restored after one hour of polarization, but the longer time polarization was not effective and resulted in a lower activity.

6.9 Scanning electron microscopy of polyfluorenone

The surface morphology of polyfluorenone was investigated by SEM after deposition on Pt wires, Figure 6.19 and 6.20. Figure 6.19 shows SEM images of PFO films deposited on Pt wires at various conditions; **A** and **B** show an as-prepared film and some

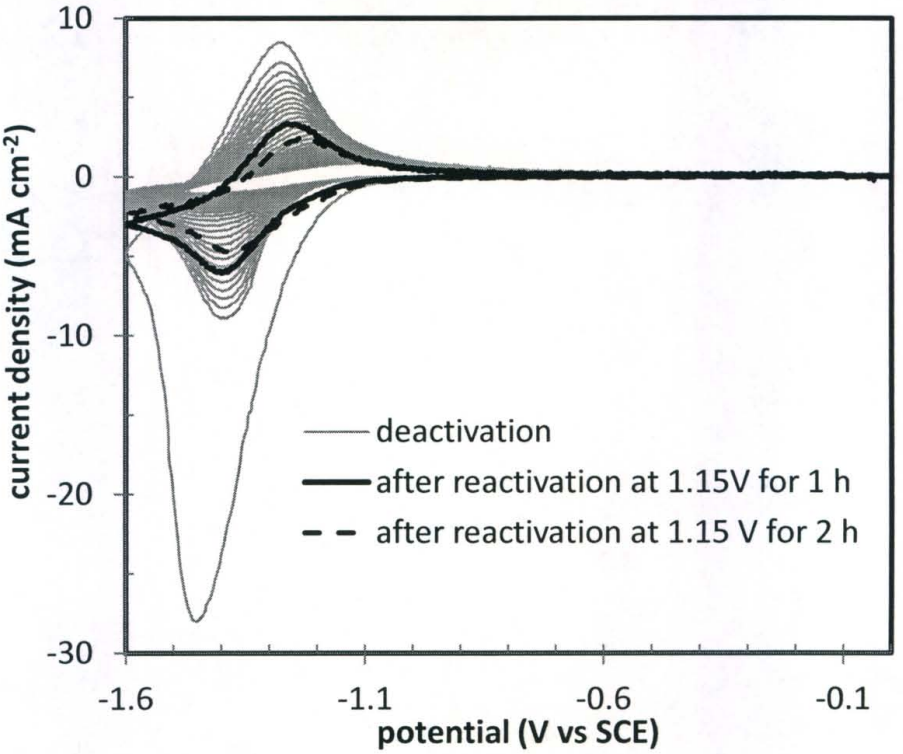

Fig. 6.18 Cyclic voltammograms for deactivation and after reactivation of PFO in CH_3CN containing 0.1 M TEAP at 0.1 V s^{-1}. The film was deposited on a Pt electrode from 30 mM FO, 2% PEG-400 in BFEE by cycling between 0.7 V and 2.0 V (5 cycles at 0.1 V s^{-1}). The film reactivation was achieved at a constant potential of 1.15 V for the indicated time.

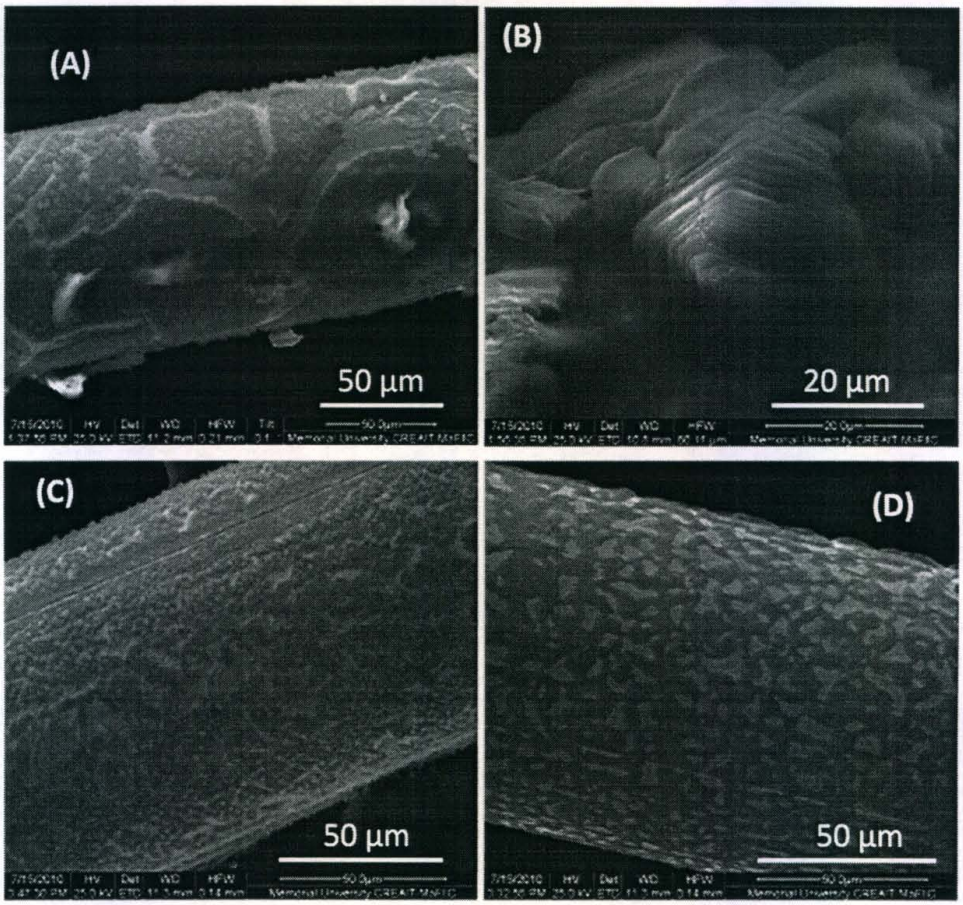

Fig. 6.19 SEM images for PFO films on Pt wires at various conditions; **A.** and **B.** As-prepared film (some crystals of flouren-9-one on the polymer film surface before washing (B)), **C.** p-Doped film (scanned between 0 V and 1.4 V for 1 cycle in 0.1 M TEAP/CH_3CN), and **D.** deactivated (10 cycles between 0 V and -1.6 V in 0.1 M TEAP/CH_3CN) then reactivated (2 cycles between 0 V and 1.4 V). The polymer films were deposited on Pt wires by potentiodynamic polymerization from 30 mM FO, 1% PEG-400, 20% BFEE in CH_3CN (scan range between 0.7 V and 2.0 V at 0.1 V s^{-1} for 5 cycles (10 cycles for A and B)).

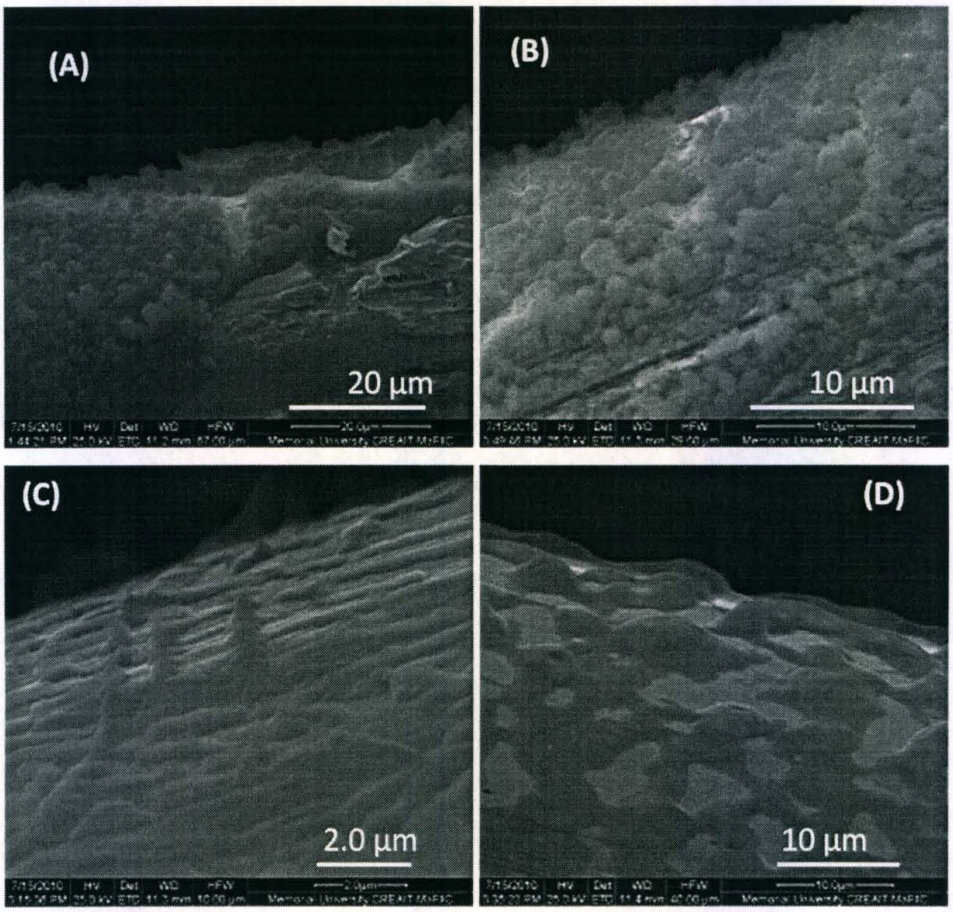

Fig. 6.20 SEM images for PFO films on Pt wires at various conditions; **A.** As-prepared, **B.** p-doped (cycled between 0 V and 1.4 V for 1 cycle in 0.1 M TEAP/CH_3CN), **C.** n-doped (cycled between 0 V and -1.6 V for 10 cycles in 0.1 M TEAP/CH_3CN), and **D.** reactivated (after deactivation) between 0 V and 1.4 V for 2 cycles in 0.1 M TEAP/CH_3CN. The polymer films were deposited on Pt wires by potentiodynamic polymerization from 30 mM FO, 1% PEG-400, 20% BFEE in CH_3CN (scan range between 0.7 V and 2.0 V at 0.1 Vs^{-1} for 5 cycles (10 cycles for A)).

FO crystals can be seen (B) on the surface of the polymer film before washing. **C** and **D** show the surface of the film after CV scanning in CH_3CN containing 0.1 M Et_4NClO_4 (TEAP) at positive potentials between 0 V and 1.4 V (C). The film (D) was reactivated (two cycles between 0 V and 1.4 V) following deactivation (10 cycles between 0 V and -1.6 V). Changes in the surface morphology can be observed following CV scanning in CH_3CN containing 0.1 M TEAP.

Enlarged images can be seen in Figure 6.20. The as-prepared film (A) and the p-doped film (B) show small granules of various sizes indicating a high surface area. The deactivated film (C) shows a much smoother surface indicating a lower surface area. The reactivated film (D) shows a smooth morphology that makes it look as if the polymer had been melted onto the Pt surface. This indicates that there had been major restructuring of the polymer to a more compact form.

6.10 Conclusions

Fluoren-9-one has been polymerized and deposited electrochemically from CH_3CN and BFEE. However, a more stable film results from the use of a steric stabilizer (e.g. PEG-400) during film deposition from BFEE. This modification enhances the film stability after deactivation, and so reactivation can be achieved and probed by cyclic voltammetry.

A decrease in or loss of electrochemical activity during n-doping for PFO occurs as a result of continuous cycling due to factors that affect the electrochemical

reversibility. Structure changes during doping and undoping, irreversible reduction destroying electroactive sites, and ion pair formation between cations and anions are possible factors that can cause deactivation. Partial reactivation of the polymer film was achieved by cycling or polarizing the film at positive potentials.

Further characterization using electrochemical impedance spectroscopy revealed that polyfluorenone (PFO) behaves as a redox polymer in its reduced state. Electron diffusion for a reduced PFO film is potential dependent and has its maximum value close to -1.2 V.

6.11 Experimental

6.11.1 Chemicals

Acetonitrile (CH_3CN, Aldrich, HPLC grade, 99.8%), dichloromethane (CH_2Cl_2, ACP Chemicals INC.), boron trifluoride diethyl etherate (BFEE; Aldrich, 46% BF_3 basis), tetrabutylammonium hexafluorophosphate (Bu_4NPF_6; Fluka, electrochemical grade), tetrabutylammonium perchlorate (Bu_4NClO_4; Fluka), tetraethylammonium tetrafluoroborate ($TEABF_4$; Alfa Aesar), and tetraethylammonium perchlorate (TEAP; Alfa Aesar), were used as received. Fluoren-9-one (FO, Aldrich, 98%) was recrystallized from n-hexanes and dried under vacuum overnight.

6.11.2 Instrumentation

Cyclic voltammetry and impedance spectroscopy measurements were carried out using a computerized potentiostat–galvanostat Model 273A EG&G

Potentiostat/Galvanostat and Model 5210 Lock-in Amplifier with Power-Suite commercial software. The measurnments were performed over the range of 100 kHz to 1 Hz with an ac amplitude of 10 mV at various dc potentials. A logarithmic scale was chosen over 20 points from high to low frequencies.

PFO films were deposited electrochemically on platinum working electrodes (0.0045 cm^2 Pt disc sealed in glass). Nitrogen gas was used to degas all solutions before measurements in a standard three-compartment glass cell. A Pt wire was used as counter electrode, and a saturated calomel electrode (SCE) was used as a reference electrode.

Due to limitations in the microbalance available and the very small masses of the deposited materials, the masses of the films could not be determined precisely enough to calculate the doping level of the PFO.

References

1. P. Pickup, In Modern Aspects of Electrochemistry, ed. B. Conway, J. Bockris, R. White, Plenum, New York 33 (1999) 549.

2. X. Ren, P. Pickup, *J. Phys. Chem.* 97 (1993) 5356.

3. W. Chen, G. Xue, *Prog. Polym. Sci.* 30 (2005) 783.

4. K. Loganathan, F. Huang, P. Pickup, *Electrochim. Acta* 52 (2006) 15.

5. K. Loganathan, P. Pickup, *Electrochim. Acta* 52 (2007) 4685.

6. M. Levi, R. Demadrille, E. Markevich, Y. Gofer, A. Pron, D. Aurbach, *Electrochem. Commun.* 8 (2006) 993.

7. A. Cihaner, S. Tirkes, A. Onal, *J. Electroanal. Chem.* 568 (2004) 151.

8. S. Zhang, G. Nie, X. Han, J. Xu, M. Li, T. Cai, *Electrochim. Acta* 51 (2006) 5738.

9. T. Skothiem, R. Elsenbaumer, Hand Book of Conducting Polymers, ed. J. Reynolds, Marcel Dekker: New York, 1989.

10. P. Pickup, J. Chem. Soc. *Faraday Trans.* 86(1990) 3631.

11. Z. Qi, P. Pickup, *J. Chem. Soc. Chem. Commun.* (1992) 1675.

12. S. Refaey, G. Schwitzgebel, O. Schneider, *Synth. Met.* 98 (1999) 183.

13. Z. Ezerskis, Z. Jusys, *J. Appl. Electrochem.* 31 (2001) 1117.

14. H. Harada, T. Fuchigami, T. Nonaka, *J. Electroanal. Chem.* 303 (1991) 139.

15. J. Xu, G. Shi, L. Qu, J. Zhang, *Synth. Met.* 135-136 (2003) 221.

Chapter 7

Summary and Future Work

This thesis reports a study on the electrochemistry of two conducting polymers, namely polypyrrole (PPy) and polyfluorenone (PFO). Both polymers have been prepared electrochemically by oxidative coupling using various techniques, namely potentiodynamic, potentiostatic, and galvanostatic. High quality films of both polymers were obtained under optimized conditions. Both p-doping and n-doping were investigated to achieve better understanding of ion and charge transport for PPy and PFO, respectively. The ion transport properties and the accompanied charge compensation mechanisms were found to be very sensitive to the polymerization conditions. Both cyclic voltammetry and impedance spectroscopy were used to probe the electrochemical properties of the polymer films. Scanning electron microscopy and energy dispersive X-ray emission were used for surface morphology and elemental analysis characterizations, respectively.

Chapters 3, 4, and 5 focus on ion transport and electrochemistry of PPy in aqueous and non-aqueous solutions. The dependence of ion transport on the size and

charge of the dopant anions incorporated during polymerization was investigated in Chapter 3. PPy films doped with a large univalent anion (i.e. Alizarin Red S) showed enhanced anion transport in NaCl due to the porous morphology caused by the dopant anion, which was probed by scanning electron microscopy. Whereas composite PPy films (i.e. PPy doped with polystyrene sulfonate) showed enhanced cation transport in NaCl due to the high mobility of the co-ion (i.e. Na^+).

The ion transport properties of modified PPy films were investigated in Chapter 4. The modification was achieved with electroactive (i.e. 1-(ferrocenyl)ethanol) and non-electroactive (i.e. polyethylene glycol, PEG) modifiers using a novel method in which an ionic complex was generated in situ with a Lewis acid (boron trifluoride ethyl etherate, BFEE). These modifications influence the ion transport properties of PPy causing enhanced charge capacity and electroactivity. In contrast, overoxidation of PPy leads to Cl-substitution and OH-substitution on the PPy chains in $NaCl_{(aq)}$ (Chapter 5). However, further elemental analysis is required to identify each substitution and to confirm which one occurs first.

The ion transport properties and electrochemistry of PFO were investigated in Chapter 6. PFO films have been deposited from CH_2Cl_2 and BFEE, but a better film quality was achieved using 1% or 2% PEG in BFEE during film deposition. The high quality of PFO films after using PEG is believed to be due to the influence of the steric stabilizer (i.e. PEG) in which decreased repulsion between radical cations and a lower acidity of BFEE can be achieved. A decrease or loss of electroactivity during n-doping for PFO

occurs as a result of continuous cycling due to factors that affect the electrochemical reversibility. Structure changes, irreversible reduction, and ion pair formation are possible factors that can cause deactivation. However, reactivation was achieved for PFO modified with PEG by polarizing the film at positive potentials. Further characterization using impedance spectroscopy revealed that PFO behaves as a redox polymer in its reduced state.

An interesting study to investigate for future work is incorporation of various electroactive molecules, such as anthraquinone derivatives, into polymer films using the method described in Chapter 4. Two anthraquinone derivatives, i.e. 2,6-dihydroxyanthraquinone and 1,2,4-trihydoxyanthraquinone, were attempted to be incorporated into PPy matrices, but their electroactivities were very weak inside the PPy film indicating low incorporation levels. The incorporation levels can be enhanced by optimizing the polymerization conditions, such as the solvent, electrolyte, and potential used for film deposition.